Forschungszentrum Karlsruhe
Technik und Umwelt

Wissenschaftliche Berichte
FZKA 6322

On the Gradient Plasticity Approach to Size Effects Part II: Applications

**T. Malmberg, I. Tsagrakis,
I. Eleftheriadis, E.C. Aifantis**

**Institut für Reaktorsicherheit
Programm Nukleare Sicherheitsforschung**

März 2001

Forschungszentrum Karlsruhe

Technik und Umwelt

Wissenschaftliche Berichte

FZKA 6322

On the Gradient Plasticity Approach to Size Effects

Part II: Applications

T. Malmberg, I. Tsagrakis[(1)], I. Eleftheriadis[(1)], E.C. Aifantis[(1), (2)]

Institut für Reaktorsicherheit

Programm Nukleare Sicherheitsforschung

(1) Laboratory of Mechanics and Materials
Aristotle University of Thessaloniki
GR-54006 Thessaloniki, Greece

(2) Center for Mechanics of Materials and Instabilities
Michigan Technological University
Houghton, MI 49931, USA

Forschungszentrum Karlsruhe GmbH, Karlsruhe

2001

Als Manuskript gedruckt

Forschungszentrum Karlsruhe GmbH
Postfach 3640, 76021 Karlsruhe

Mitglied der Hermann von Helmholtz-Gemeinschaft
Deutscher Forschungszentren (HGF)

ISSN 0947-8620

On the Gradient Plasticity Approach to Size Effects Part II: Applications

Abstract

The size effect in deformation and failure of structures is presently a subject of increasing interest. It has been observed frequently for a variety of conditions and specimen types (Part I 'Reviews' of this report). Evidently, the assessment of its significance is important for the validity of the transfer of small-scale model testing results to full-scale structures and also for the computational modeling of large scale components when the material parameters of the used constitutive model are obtained from small scale laboratory type test results. Different explanations have been proposed in the past but only recently non-classical continuum mechanics theories have provided a means to interpret size effects; for example, by incorporating higher order spatial strain gradients into classical plasticity theories. These extensions implicate additional material parameters which relate to internal length scales of the material. In spite of the increased complexity of such extended material models, a relatively easy theoretical treatment may be possible in cases of simple loading configurations and under simplifying assumptions.

In this study deformation theories of plasticity, extended by spatial first and/or second order strain gradients, are used. On this basis, solutions are obtained for different types of idealized specimens to determine the extent at which strain gradient models describe size influences on the deformation behavior. This assessment is accomplished by

(a) fitting simple elastic-plastic 1^{st} and 2^{nd} order strain gradient models to available experimental data of geometrically similar specimens revealing a decrease of the yield stress with size under non-uniform stresses (pure torsion and pure bending),
(b) performing systematic parameter variations (in particular the size or an internal length) to determine the relative influence of the non-classical 2^{nd} order strain gradient generalization; the constitutive part describing homogeneous deformations is given by a Hollomon type strain hardening power law and the analyses are performed for geometrically scaled specimens of the same material (tension of tapered rods and three-point-bending of smooth beams).

The first group of tasks requires only the solution of some algebraic equations and a least squares fitting. A comforting agreement of the fitted models with the mean yield stresses of the torsion and bending experiments of two different structural steels is obtained, without making a particular effort for a careful physical interpretation of the gradient terms.

The second group of tasks leads to one-dimensional, generally non-linear, 2^{nd} order differential equations for the strain or curvature distribution supplemented by non-classical boundary conditions. For small internal length scales relative to the size of the specimen they represent singularly perturbed boundary value problems. Upon linearization (linear hardening and small deformations) exact solutions are obtained. For the non-linear problems and relatively small internal length scales the method of multiple scales is used to obtain approximate analytical solutions for the singular perturbation problems of boundary layer type. An extensive evaluation of the results is provided, yielding a direct understanding of the effects of the strain gradient terms. Close form expressions and graphical representations are obtained which allow an immediate quantitative estimate of the relative influence of various parameters, particularly the size of geometrically similar specimens or the internal length. A

comparison with experimental results is not possible since corresponding experimental data are presently not available.

Über den Ansatz der Gradientenplastizität zur Beschreibung von Größeneffekten Teil II: Anwendungen

Zusammenfassung

Der Größeneinfluss auf das Deformations- und Versagensverhalten von Strukturen erfährt gegenwärtig ein wachsendes Interesse. Unter verschiedenen Bedingungen und für verschiedene Probentypen ist er häufig beobachtet worden (Teil I: "Überblicke" dieses Berichts). Ganz offensichtlich ist eine Überprüfung seiner Bedeutung wichtig für die Übertragbarkeit der Ergebnisse von verkleinerten Modellversuchen auf das (1:1)-Strukturverhalten und auch für die rechnerische Modellierung von Großkomponenten, wenn die in den Stoffmodellen benutzten Materialparameter auf kleinen, labortypischen Versuchsergebnisse beruhen. Verschiedene Erklärungen sind in der Vergangenheit bisher vorgeschlagen worden, aber erst seit kurzem werden nicht-klassische, kontinuumsmechanische Theorien eingesetzt, um Größeneffekte zu interpretieren; beispielsweise Gradientenkonzepte, die klassische Plastizitätstheorien um höhere räumliche Verzerrungsgradienten erweitern. Diese Erweiterungen beinhalten auch zusätzliche Materialparameter, die im Zusammenhang mit materialtypischen, inneren Längenskalen stehen. Trotz der erhöhten Komplexität solcher erweiterter Materialmodelle, kann eine relativ leichte theoretische Behandlung für einfache Belastungsfälle und unter vereinfachenden Annahmen möglich sein.

In dieser Studie werden Deformationstheorien der Plastizität eingesetzt, die durch räumliche Verzerrungsgradienten erster und/oder zweiter Ordnung ergänzt sind. Auf dieser Basis werden Lösungen für verschiedene idealisierte Proben entwickelt, um zu ermitteln, in welchem Ausmaß Verzerrungsgradientenmodelle den Größeneinfluss auf das Deformationsverhalten beschreiben können. Diese Überprüfung wird erreicht, indem

(a) einfache, elastisch-plastische Modelle, die um Verzerrungsgradienten 1. und 2. Ordnung erweitert sind, an verfügbare experimentelle Daten geometrisch ähnlicher Proben angepasst werden, welche eine Abnahme der Fließspannung mit der Probengröße bei ungleichförmiger Spannungsverteilung (reine Torsion und reine Biegung) zeigen;

(b) systematische Parametervariationen (insbesondere die Größe oder eine innere Länge) durchgeführt werden, um den relativen Einfluss der Ergänzung durch den nicht-klassischen Verzerrungsgradienten 2. Ordnung zu bestimmen; der konstitutive Teil, der homogene Deformationen beschreibt, wird durch einen Potenzansatz (nach Hollomon) für die Dehnungsverfestigung gegeben und die Analysen werden durchgeführt für geometrisch skalierte Proben aus demselben Material (Zugbeanspruchung von sich verjüngenden Rundproben und Drei-Punkt-Biegung glatter Balken).

Die erste Aufgabengruppe erfordert nur die Lösung einiger algebraischer Gleichungen und eine Anpassung mit der Fehlerquadratmethode. Eine ermutigende Übereinstimmung des angepassten Modells mit den Mittelwerten der Fließspannung der Torsions- und Biegeversuche zweier Baustähle wird erzielt, wenn auch ohne eine besondere Bemühung um eine sorgfältige physikalische Interpretation der Gradiententerme.

Die zweite Aufgabengruppe führt auf eindimensionale, im allgemeinen nicht-lineare Differentialgleichungen 2. Ordnung für die Dehnungs- oder Krümmungsverteilung, ergänzt

durch nicht-klassische Randbedingungen. Für kleine innere Längen relativ zur Größe der Proben stellen sie singulär gestörte Randwertprobleme dar. Bei Linearisierung (lineare Verfestigung und kleine Deformationen) werden exakte Lösungen erhalten. Für die nicht-linearen Probleme und relativ kleine innere Längen wird die Methode der Mehrfachskalen eingesetzt, um approximative, analytische Lösungen für die singulären Störungsprobleme vom Grenzschichttyp zu erhalten.

Eine ausführliche Auswertung der Ergebnisse wird durchgeführt, die ein direktes Verständnis der Einflüsse der Verzerrungsgradienten liefern. Geschlossene Ausdrücke und graphische Darstellungen werden erhalten, die eine unmittelbare Abschätzung des Einflusses verschiedener Parameter, insbesondere der Größe geometrisch ähnlicher Proben oder der inneren Länge, liefern. Ein Vergleich mit experimentellen Daten ist nicht möglich, da entsprechende experimentelle Daten gegenwärtig fehlen.

Contents (Part II "Applications")

1. Introduction

The objective of Part I "Reviews" [1.1] of this report was to provide a limited survey of scaled experiments of geometrically similar specimens of metallic materials and to examine briefly several pertinent gradient plasticity theories. The purpose of the present report Part II "Applications" exemplifies to what extent strain gradient models can describe the size influence on the deformation behavior.

Strain gradient models in elasticity and plasticity are not just straightforward modifications of the standard models. The extensions consist of an enrichment of the classical constitutive equations by gradient terms of the strains or other variables, which increase the order of the governing differential equations and this implies also the definition of additional boundary conditions; in some cases even extra balance equations are introduced. Thus, in general, they lead to three-dimensional boundary value problems of a system of coupled partial differential equations with a higher order structure than the classical models.

However, depending on the complexity of the gradient model, in cases of simple loading configurations and under simplifying assumptions, relatively easy theoretical treatments may be possible. For example, when the equilibrium equations can be trivially satisfied and the strain distribution is assumed as in classical treatments (e.g. torsion and pure bending), the gradient theory may not even require the solution of any boundary value problem.

In other cases, the equilibrium equations can be solved independently of the constitutive relations (e.g. tension of a thin rod with non-uniform cross-section). This 'uncoupling' often allows a direct integration of the constitutive equations, which now take the form of differential equations for the strain. Thus, a grossly simplified boundary value problem is obtained.

It is well known that the classical mathematical theories of plasticity can be divided roughly into two types: deformation theories and flow theories. The deformation theories are characterized by constitutive equations that relate the instantaneous strain to the stress in a uniquely determined way or vice versa. Flow theories, however, are characterized by relations between increments or rates of stress and strain, which are homogeneous of degree one in the rate terms and thus are independent of the time scale. Although flow theories describe better plastic deformation phenomena involving loading and unloading, gradient enhanced generalizations of deformation type plasticity models are used in this report because deformation plasticity is mathematically more convenient and also sufficient for proportional loading configurations. Furthermore, the applications of these strain gradient theories to be treated in this study belong to the two aforementioned simplified problem groups.

The assessment of the size influence on the deformation behavior is accomplished by fitting the strain gradient model to some available experimental data and also by performing systematic parameter variations (size or internal length) to determine the relative influence of the non-classical part of the constitutive equations.

To this end, Part II is organized as follows. In Section 2, size effects for yield initiation under non-uniform stress distributions are discussed. Two characteristic examples are considered which do not require the solution of a boundary value problem. The first example, considered in Section 2.1, pertains to the yield behavior of cylindrical bars in torsion. Experiments have shown that the apparent yield stress increases with decreasing specimen diameter [1.2]. The second example, considered in Section 2.2, pertains to the yield behavior of beams with rectangular cross-section in pure bending. In this case, experiments [1.3] have shown that the apparent yield stress increases with decreasing specimen depth. A simple strain gradient dependent strength of materials approach, which does not require the solution of a

boundary value problem, is employed for interpreting the results. The respective gradient coefficients are assigned a purely phenomenological meaning and are treated as fitted parameters without being calculated from independent tests.

In Section 3, the tensile behavior of tapered rods is discussed using a linear version of a 2^{nd} order gradient dependent constitutive equation for a uniaxial state of stress. The assumption of a uniaxial state of stress allows an independent solution of the equilibrium equation. Thus, the problem reduces to the integration of the gradient enhanced constitutive equation to obtain the strains. This one-dimensional boundary value problem is considered for an exponentially tapered rod, as well as for an idealized U-notched rod. Due to the assumed linearity in the stress-strain relation (without also taking into account the cross-section area reduction), an exact solution of the resultant 2^{nd} order differential equation is obtained. These solutions are used to demonstrate the influence of the gradient term on the deformation and failure behavior.

In Section 4, a conventional deformation plasticity model with a non-linear power law for the strain hardening is extended by a 2^{nd} order strain gradient term but also the cross-section reduction due to the plastic deformation is allowed for. The tensile behavior of an exponentially tapered rod is considered again. In this case, an exact solution of the governing differential equation can not be deduced. However, provided the internal length parameter associated with the 2^{nd} order strain gradient term is small compared to the dimensions of the specimen, a singularly perturbed boundary value problem is obtained. Using a singular perturbation method for ordinary differential equations, an approximate analytical solution is derived.

Section 5 pertains to the size dependent strength of a beam with a uniform cross-section subjected to a three-point bending test. A 2^{nd} order strain gradient term and a power law for the strain hardening is adopted again. An ordinary 2^{nd} order differential equation for the curvature is derived which allows an analogous approximate solution procedure for this one-dimensional boundary value problem as for the previous tension problem.

Both the tension problem in Section 4 and the bending problem in Section 5 reflect, to a limited extent, test conditions as investigated in the experimental part of Task 5 in the REVISA project ([1.4, 1.5]).

The conclusions of the present report Part II are discussed in Section 6 and detailed calculations concerning various elaborate portions of the work are provided in Appendices (2)-(10). In addition, Appendix (1) contains a discussion of the non-classical boundary condition of a 2^{nd} order strain gradient model by comparing the gradient model with a simple non-local (integral) model.

2. Size Effects in Yielding (Yield Initiation)

In this section a strength of materials approach based on the gradient dependent constitutive equation

$$\sigma = k\varepsilon^n - c_1(\nabla\varepsilon \cdot \nabla\varepsilon)^{m/2} - c_2\nabla^2\varepsilon \tag{2.1}$$

is used for the interpretation of the size effects observed by Morrison (1939, [1.2]) and Richards (1958, [1.3]). Morrison carefully performed a series of tension, torsion, bending, and combined tension-torsion tests on the yield behavior of cylindrical plain carbon steel specimens of different size. The specimens were geometrically similar with varying diameter. A scale factor up to 3.55 was used for the tension tests. The results of these tests showed that

the yield stress and the ultimate stress are *size invariant* for homogeneous states of tensile or compressive stresses. On the other hand, Morrison's torsion and bending tests indicated an increase in the apparent yield stress with decreasing specimen size. A scale factor up to 8.67 and up to 5.2 was used for the torsion tests and the bending tests, respectively. The value of yield stress increases by about 15,5 % and 8 % respectively, when the size is decreased from the largest to the smallest (diameter 2.586 mm) specimen.

Richards (1958, [1.3]) performed a series of pure bending tests for geometrically similar mild steel beam specimens of different size. In these tests a scale factor up to 6.31 was used and the value of yield stress increases by about 41.7 % as the specimen size is decreased from the largest to the smallest (depth 4.026 mm) specimen. In our analysis, the results concerning the smallest specimen are not taken into account because of the doubts that Richards has about their validity.

For the interpretation of these size effects, Hooke's law for the elastic region and Eq.(2.1) for the plastic region are adopted and a simplified strength of materials analysis is used.

It is noteworthy that also recent dynamic and quasistatic scaled bending tests with austenitic stainless steel specimens (scale factor 10, minimum diameter 1mm) showed a size influence on the initial yield stress with a similar trend (Stach (1997,[2.1]), Jordan and Malmberg (1998, [2.2])). However, also recent tension tests with the same material show a significant size influence with the same trend as the bending specimens (Malmberg, Aktaa, Schlossmacher (1999, [2.3]), see Part I). This implies that the macroscopic non-uniformity of the stress or strain distribution is not responsible for the size effect in this case.

2.1 Torsion Problem

In the elastic region the shear stress τ is given by the standard elastic relation $\tau = G\gamma$, where γ denotes the shear strain and G the shear modulus.

Carbon steel may be considered as perfectly plastic for homogeneous deformations beyond the elastic limit. Therefore, n is zero in Eq.(2.1), where k now denotes the tensile yield stress σ_0. For the present shear deformation problem, the effective axial stress σ equals to τ / Λ and the effective axial strain ε is $\gamma\Lambda$, where Λ is the ratio of the shear yield stress τ_0 over the tensile yield stress σ_0 ($\Lambda = 0.5$ for the Tresca yield criterion and $\Lambda = 1/\sqrt{3} = 0.577$ for the von Mises yield criterion). By also assuming that the coefficient m is unity, Eq.(2.1) takes the form

$$\tau = \tau_0 - \bar{c}_1 \left| \nabla\gamma \right| - \bar{c}_2 \nabla^2\gamma \quad , \tag{2.2}$$

where $\bar{c}_1 = c_1\Lambda^2$ and $\bar{c}_2 = c_2\Lambda^2$.

In polar coordinates we have that $\gamma = \varphi r$, where φ denotes the angle of twist per unit length of the bar and r is the radial coordinate measured from the rod axis. We assume that yielding first occurs when the stress at the outer surface of the specimen ($r = \alpha$) becomes equal to the yield stress value Y in shear. Therefore,

$$Y = G\varphi\alpha = \tau_0 - \bar{c}_1\varphi - \bar{c}_2\varphi / \alpha \ , \tag{2.3}$$

since $\nabla\gamma = \varphi$ and $\nabla^2\gamma = \varphi / r$. On eliminating φ from the system of Eqs.(2.3), we obtain the following relation for the dependence of the yield stress Y on the specimen radius α

$$Y(\alpha) = \tau_0 \left(\frac{\alpha^2}{\alpha^2 + (\bar{c}_2 / G) + (\bar{c}_1 / G)\alpha} \right) . \qquad (2.4)$$

According to the experimental results of Morrison, $Y(\alpha)$ must be a decreasing function of α. This implies that the admissible values of $\bar{c}_1$ and $\bar{c}_2$ are those which satisfy the inequality $\bar{c}_1\alpha + 2\bar{c}_2 < 0$. This relation holds true for all positive values of radius α, provided that both $\bar{c}_1$ and $\bar{c}_2$ are negative. However, restricting the validity of this inequality to the range of radii where experimental results are available, positive values are also allowed for only one of them. Then two internal length scales may be defined as $l_1 = |\bar{c}_1| / G$ and $l_2 = \sqrt{|\bar{c}_2| / G}$, respectively.

Using the least squares method, Morrison's torsion experimental results are fitted and the values of the alternative internal lengths $\ell_1 = |c_1| / G$ $(= l_1 / \Lambda^2)$ and $\ell_2 = \sqrt{|c_2| / G}$ $(= l_2 / \Lambda)$ are calculated as shown in Fig.2.1. It is noted that c_1 (and therefore $\bar{c}_1$) is negative, while c_2 (and therefore $\bar{c}_2$) is positive having a value such that $Y(\alpha)$ is a decreasing function in the range of α of the fitted data. The ratio Λ of the shear yield stress τ_0 to the tensile yield stress σ_0 is also calculated by the aforementioned fitting and is found to be equal to 0.516. This value is between 0.577 obtained by the Von Mises yield criterion and 0.5 obtained by the Tresca yield criterion and it is comparable to the values found in the literature on carbon steel.

Another approach related to an integral yield condition involving an internal length scale has been used by Malmberg (1995, [2.4]) for the interpretation of Morrison's torsion results. This treatment, which corresponds approximately to the enhancement of the classical local yield condition by stress gradients, gives the right trend to the observed behavior but does not fit adequately the experimental data. This is partly due to the fact that only one parameter was available for the fitting procedure.

2.2 Bending Problem

In the elastic region the axial stress σ in the beam axis is given by Hooke's law $\sigma = E\varepsilon$, where E is the Young's modulus and $\varepsilon = \kappa y$ is the axial strain; this corresponds to Bernoulli's hypothesis, where κ denotes the curvature of the beam and y is the coordinate along the depth of the beam measured from the neutral axis.

Mild steel behaves as a perfectly plastic material for homogeneous deformations beyond the elastic limit. Therefore, n is zero in Eq.(2.1) and k is equal to the tensile yield stress σ_0. Furthermore, assuming that the coefficient m is unity, Eq.(2.1) in tension takes the form

$$\sigma = \sigma_0 - c_1 |\nabla\varepsilon| - c_2 \nabla^2\varepsilon \quad . \qquad (2.5)$$

We assume that yielding first occurs when the stress at the outer surface of the specimen ($y = \pm h / 2$) becomes equal to the yield stress value Y. Therefore,

$$Y = E\kappa h/2 = \sigma_0 - c_1\kappa , \qquad (2.6)$$

since $\nabla\varepsilon = \kappa$ and $\nabla^2\varepsilon = 0$ for the case of pure bending. On eliminating κ from the system of Eqs.(2.6), we obtain the following relation for the dependence of the yield stress Y on the specimen depth h

$$Y(h) = \sigma_0 \left(\frac{h/2}{(h/2) + (c_1 / E)} \right) . \qquad (2.7)$$

Observing Richards' results (1958, [1.3]), $Y(h)$ must be a decreasing function, which implies that the value of c_1 must be negative. Also, $Y(h)$ must be greater than zero. This indicates that Eq.(2.7) is valid for depth values $h/2$ greater than an internal characteristic length $l = -c_1 / E$.

Using the least squares method, Richards' bending experimental data are fitted, as shown in Fig.2.2, and the value of the internal length l is calculated. With this value of l we can compute an alternative internal characteristic length $\ell_1 = -c_1 / G = 2.64l$, where the value $\nu = 0.32$ for the Poisson ratio was used. It is noted that this internal length is two times larger than the one obtained for the torsion data. This difference may be attributed to the fact that the two steels used have different microstructure and composition. Because of the lack of data for the tension behavior of the material used, the tensile yield stress is also calculated by the aforementioned fitting and is found to be equal to 225.6 MPa. This value is comparable to the value 250 MPa found in the literature on mild steel.

3. The Tapered Tensile Rod: Two Linear Problems

3.1 Exact Solution for an Exponentially Tapered Rod

3.1.1 Statement of the Problem

Restricting the problem to a uniaxial state of stress and infinitesimal deformations, the uniaxial linear stress-strain relation is taken to be

$$\sigma = K\,\varepsilon - K\,l_i^2 \frac{d^2\varepsilon}{dx^2} \qquad (3.1)$$

with the two material constants:
K : constitutive modulus[1]
l_i : internal length scale.

The uniaxial stress, which is in fact the average stress in a cross-section, is given by

$$\sigma = \frac{P}{A_R(x)} \qquad (3.2)$$

P : prescribed longitudinal force
A_R : undeformed cross-section of tapered rod

which simply follows from the static equilibrium in the rod. Here the exponentially tapered rod as shown in Fig.3.1 is considered.

[1] In the elastic case K corresponds to Young modulus E

$$A_R(x) = A_o\,\rho^2\,, \quad \rho^2 = [\alpha + (1-\alpha)\,e^{-x/L^*}]^{-1}$$
$$\alpha = \frac{A_o}{A_\infty} < 1 \qquad \Big\} \qquad (3.3)$$

A_o: minimum cross-section area
A_∞: largest cross-section area at infinity
L^*: characteristic length of the exponential profile.

In Fig.3.2 various profiles are shown to illustrate the influence of the geometry parameters α and L^*. Introducing dimensionless quantities

$$\xi = \frac{x}{L^*}, \qquad \beta = \frac{l_i}{L^*} \qquad (3.4)$$

and combining the constitutive relation (3.1) and the equilibrium condition (3.2), the following 2nd order differential equation for the strain ε,

$$\varepsilon = \frac{du}{dx} \qquad (3.5)$$

u: displacement function,

is obtained

$$\beta^2 \frac{d^2\varepsilon}{d\xi^2} - \varepsilon = -r(\xi)\,; \qquad (3.6)$$

the right-hand side

$$r(\xi) = \frac{P}{A_o}\frac{1}{K}\rho^{-2}(\xi) \qquad (3.7)$$

does not involve the parameter β.

Two boundary conditions are required for the solution of this differential equation. They are motivated by the following considerations. Ignoring the strain gradient influence by setting β=0 in Eq.(3.6), we obtain the classical solution for the strain distribution

$$\varepsilon = \varepsilon_c = r(\xi). \qquad (3.8)$$

For the present exponential cross-section variation the strain ε_c is almost uniform at large values of ξ. Thus, it is reasonable to assume that the non-classical solution, including the strain gradient effect, behaves similarly for large ξ. This provides the first boundary condition (B.C.I):

$$\text{B.C. I}: \quad \lim_{\xi\to\infty} \varepsilon = \varepsilon_\infty = \frac{P}{A_\infty}\frac{1}{K}. \tag{3.9}$$

At the minimum cross-section (ξ=0) the classical strain ε_c has its absolute maximum but its first order spatial derivative is discontinuous. If the variation of the cross-section would allow the classical strain gradient to be continuous, then

$$\frac{d\varepsilon_c}{d\xi} = 0 \text{ at } \xi=0$$

for symmetry reasons and this would also apply to the non-classical strain distribution. However, for the present cross-section distribution this is not so obvious. For purely mathematical reasons one could choose either the value of the strain or its first order derivative or a combination of both of them. The prescription of the strain at ξ=0 is physically unreasonable; a combination of ε and $d\varepsilon/d\xi$ is not immediately obvious but such a boundary condition can be derived if the gradient model is interpreted as an approximation to a certain non-local (integral) constitutive model (Appendix (1)). We do not follow this motivation but assume that the gradient model renders a continuous gradient[2]. Then the second boundary condition follows from symmetry:

$$\text{B.C. II}: \quad \left(\frac{d\varepsilon}{d\xi}\right)_{\xi=0} = 0. \tag{3.10}$$

We consider now geometrically similar specimens scaled up by the geometric scaling factor λ>1. Then the geometrical data are changed as follows

$$\overline{A}_o = A_o\,\lambda^2\,,\ \overline{A}_\infty = A_\infty\,\lambda^2\,,\ \overline{L^*} = L^*\lambda\,,\ \overline{\alpha} = \alpha = \text{constant}. \tag{3.11}$$

According to similarity theory (Malmberg (1995, [2.4])) the strain at homologous points $\bar{x}$= $x\lambda$ will be the same $\bar{\varepsilon}(\bar{x})$=$\varepsilon(x)$ if the dimensionless characteristic parameters of the governing differential equation and boundary conditions are the same, i.e.

$$\left.\begin{array}{lll} \overline{\beta} = \beta & \text{and} & \dfrac{\overline{P}}{\overline{A}_o}\dfrac{1}{\overline{K}} = \dfrac{P}{A_o}\dfrac{1}{K} \\ \text{or} & & \\ \dfrac{\overline{l}_i}{l_i} = \lambda & \text{and} & \dfrac{\overline{P}}{P}\dfrac{K}{\overline{K}} = \lambda^2\,. \end{array}\right\} \tag{3.12}$$

These are the general similarity conditions for this simple gradient problem. They imply that the ratio of the constitutive internal lengths $\bar{l}_i/l_i$ equals the macroscopic geometric scale factor λ; also the ratio of the stresses at the minimum cross-section is required to correspond to the modulus ratio, i.e.

[2] This assumption needs motivation from a physically based model which, under certain restriction, gives rise to the gradient model.

$$\frac{\bar{P}/\bar{A}_o}{P/A_o}=\frac{\bar{K}}{K}.$$

In principle these conditions can be satisfied if different materials are used for the small and the large scale specimen. However, if the same material is used, then

$$\frac{\bar{l}_i}{l_i}=1\,,\qquad \frac{\bar{K}}{K}=1$$

and according to Eq.$(3.12)_1$ similarity in differently sized specimens cannot be achieved. This implies a size effect when testing of scaled specimens of the same model material is done. When the gradient effect is not present, then $\bar{l}_i=l_i=0$ and condition $(3.12)_1$ is identically satisfied and $(3.12)_2$ yields

$$\frac{\bar{P}}{\bar{A}_o}=\frac{P}{A_o}\quad\text{or}\quad \bar{P}=P\lambda^2$$

that is, the stresses at the minimum cross-section (and at any homologous section) are required to be the same; correspondingly, the scaling of the tensile force P is governed by the ratio of the cross-sections $\bar{A}_o/A_o=\lambda^2$.

3.1.2 Qualitative Estimate of the Strain-Gradient Influence

Without solving the above simple boundary value problem a qualitative estimate of the gradient effect on the maximum strain, as obtained by the classical model, is determined.

The classical strain distribution is given by Eq.(3.8); its absolute maximum is at $\xi=0$ with a discontinuity of the gradient $d\varepsilon_c/d\xi$. For large values of ξ

$$\frac{d\varepsilon_c}{d\xi}<0\quad\text{and}\quad\lim_{\xi\to\infty}\frac{d\varepsilon_c}{d\xi}=0$$

and $$\frac{d^2\varepsilon_c}{d\xi^2}>0.$$

The non-classical solution ε, including the 2nd order gradient effect, will also have these properties for large values of ξ, especially

$$\left(\frac{d^2\varepsilon}{d\xi^2}\right)_{\xi\to\text{large}}>0.$$

At $\xi=0$ the non-classical strain distribution $\varepsilon(\xi)$ will have a vanishing first derivative (B.C. II) and it is reasonable to expect that there is no other relative extremum at some finite value of ξ. Therefore, the function $\varepsilon(\xi)$ has a turning point at some finite value of ξ; a saddle point at $\xi=0$ contradicts the symmetry condition at $\xi=0$. Consequently,

$$\frac{d^2\varepsilon}{d\xi^2} < 0$$

in some neighborhood of ξ=0. Therefore, at ξ=0 the gradient term in the constitutive equation (3.1) is additive. Comparing the classical and the non-classical solutions ε_c and ε, respectively, for the same stress level σ at ξ=0 shows, that the non-classical solution yields a smaller maximum strain:

The inclusion of a 2nd order strain-gradient in the constitutive model together with the non-classical boundary condition yields a smoothing-out of strain peaks (discontinuities in the first order strain gradient) and a reduction in their maxima. This qualitative finding is not restricted to a classical part of the constitutive equation, which is linear in the strain, it applies also for the non-linear case e.g., power law strain dependence.

The importance of the non-classical boundary condition may also be illustrated. Naively one may suggest that to a first approximation the gradient term in the constitutive equation (3.1) can be approximated by the classical solution ε_c. Then with (3.8)

$$\frac{d^2\varepsilon_c}{d\xi^2} > 0 \text{ at } \xi = 0$$

and the gradient term in (3.1) is subtractive and the non-classical strain is approximated by

$$\varepsilon = [\frac{\sigma}{K} + \beta^2 \frac{d^2\varepsilon_c}{d\xi^2}] = [\frac{\sigma}{K} + \beta^2 \frac{d^2(\sigma/K)}{d\xi^2}] \text{ at } \xi = 0.$$

This estimate is larger than the classical value

$$\varepsilon_c = [\frac{\sigma}{K}] \text{ at } \xi=0$$

which is clearly in conflict with the previous result. The essential deficiency of this estimate is the neglect of the non-classical boundary condition at ξ=0.

3.1.3 The Exact Solution

The 2nd order differential equation (3.6) is linear and thus allows an exact solution. For reasons of convenience we introduce the coordinate transformation

$$\zeta = \frac{\xi}{\beta} = \frac{x}{l_i} \tag{3.13}$$

and the DEQ simplifies to

$$\frac{d^2\varepsilon}{d\zeta^2} - \varepsilon = -\bar{r}(\zeta) \tag{3.14}$$

with

$$\tilde{r}(\zeta) = r(\beta\zeta) = \frac{P}{A_o}\frac{1}{K}\left[\alpha+(1-\alpha)e^{-\beta\zeta}\right] \tag{3.15}$$

and the boundary conditions are

$$\left.\begin{aligned} &\text{B.C. I}: \lim_{\zeta\to\infty}\varepsilon = \varepsilon_\infty , \\ &\text{B.C. II}: \left(\frac{d\varepsilon}{d\zeta}\right)_{\zeta=0} = 0. \end{aligned}\right\} \tag{3.16}$$

In the following we restrict attention to the case $\beta<1$. The cases $\beta\geq 1$ do not make physical sense since the internal constitutive length l_i is somehow related to the microstructure of the material and the minimum dimension of the specimen should certainly be larger than l_i. On the other hand for $\beta=1$ the particular solution of (3.14) needs special attention.

For $\beta<1$ the solution of (3.14) ÷ (3.16) is easily obtained (Appendix (2)) and reads

$$\varepsilon(\xi) = \varepsilon_{co}\left\{\left[\alpha+\frac{1-\alpha}{1-\beta^2}e^{-\xi}\right] - \frac{1-\alpha}{1-\beta^2}\beta e^{-\frac{\xi}{\beta}}\right\} \tag{3.17}$$

where

$$\varepsilon_{co} = \frac{P}{A_o}\frac{1}{K} \tag{3.18}$$

is the maximum strain of the classical solution at the minimum cross-section. On the other hand, the classical solution is

$$\varepsilon_c(\xi) = r(\xi) = \varepsilon_{co}\left[\alpha+(1-\alpha)\,e^{-\xi}\right]. \tag{3.19}$$

The displacement distribution $u(\xi)$ in the non-classical case is simply

$$\begin{aligned} u(\xi) &= L^* \int_0^\xi \varepsilon(\xi')\mathrm{d}\xi' \\ &= L^*\,\varepsilon_{co}\left\{\alpha\xi+\frac{1-\alpha}{1-\beta^2}(1-e^{-\xi}) - \frac{1-\alpha}{1-\beta^2}\beta^2\,(1-e^{-\frac{\xi}{\beta}})\right\} \end{aligned} \tag{3.20}$$

and for the classical case ($\beta=0$)

$$u_c(\xi) = L^*\,\varepsilon_{co}\left\{\alpha\xi+(1-\alpha)(1-e^{-\xi})\right\}. \tag{3.21}$$

3.1.4 Discussion

3.1.4.1 General Observations

It is noted that the non-classical solution, Eq.(3.17), consists of two parts: a part

$$\varepsilon_{co}\left[\alpha+\frac{1-\alpha}{1-\beta^2}e^{-\xi}\right]$$

which essentially represents the classical solution Eq.(3.19) for small values of β and which is determined by the variation of the cross-section along the length of the rod and another part

$$\varepsilon_{co}\left[\frac{1-\alpha}{1-\beta^2}\beta\, e^{-\frac{\xi}{\beta}}\right]$$

which for small values of β is a fast decaying contribution close to the boundary ξ=0; in fact, it represents for β<<1 a boundary layer effect. This is also the region where the first and the second order derivative of the classical solution ε_c are largest. Obviously, the 2nd order strain gradient influence is largest where the classical solution shows a large variation, i.e. inhomogeneity.

This boundary layer effect is demonstrated in Fig.3.3 and 3.4 for different values $0\leq\beta\leq0.4$ and two different cross-section ratios

$$\alpha = A_o/A_\infty = 0.0625 \;\&\; 0.5625$$

$$\sqrt{\alpha} = r_o/r_\infty = 0.25 \;\&\; 0.75$$

where r_o and r_∞ are the minimum and maximum radii of the cylindrical rod. It is seen that the 2nd order strain gradient effect reduces the maximum strain of the classical solution at the minimum cross-section which was already qualitatively demonstrated in section (3.1.2). This reduction can be formulated mathematically in very simple terms. Using the result (3.17) one gets

$$\frac{(\varepsilon)_o}{\varepsilon_{co}}=\frac{1+\alpha\beta}{1+\beta} \qquad (3.22)$$

and this is illustrated in Fig.3.5. It is seen that the qualitative influence of the gradient effect is moderate: e.g., for a very small cross-section ratio α=0.0625 the strain reduction is less than 20% if β is less than 0.2.

We note that a variation in β is obtained by either changing the internal length scale l_i that is, by changing the material or by changing the characteristic length L^*. The latter can be done in two very different ways:

- Either by scaling up (or down) all dimensions of the specimen such that the new cross-sections are

$$\overline{A}_o = A_o\,\lambda^2\,,\ \overline{A}_\infty = A_\infty\,\lambda^2\,,\ \overline{\alpha} = \alpha = \text{const.}$$

and the characteristic length is

$$\bar{L}^* = L^* \lambda ,$$

where λ is the geometrical scaling factor

- or by keeping the cross-sections A_o and A_∞ the same and again α=const. but changing the characteristic length L^* alone. This corresponds to a partial change of the specimen shape.

Whatever choice is made, the diagram Fig.3.5 will be the same. The first approach will reveal a size dependence of the specimen response.

3.1.4.2 On the Size-Effect in Deformation and Failure

The size dependence of the above linear model manifests itself in two different aspects:

- Size dependence of the deformation behavior
- Size dependence of failure.

Deformation Behavior

Classical elasticity - linear or non-linear - as well as classical rate-independent plasticity do not involve an internal length scale. Thus, it may be shown using similitude theory (Malmberg 1995, [2.4])) that geometrical similar structures of different sizes but made from the same elastic or rate-independent plastic material are subject not only to the same strain but also to the same stress distribution if the loading is quasistatic and if the stress and displacement boundary condition are the same or are properly scaled.[3] Thus, complete similarity, geometrical and physical, is obtained whatever shapes of the structure are chosen and no size dependence can be observed. If such a classical material model is enriched by a 2nd order strain gradient dependence, complete similarity is also obtained if the material parameters are constant everywhere and if the geometry and the external loading or constraint conditions are such that no 2nd order gradients will occur. In the present context this is the tensile rod with a uniform cross-section and under quasistatic loading at the ends and with homogeneous material properties. However, even under these conditions a non-similarity or size dependence may show up if large deformations are considered and the response becomes unstable together with a localization of the deformation, for example necking of the rod. Furthermore, in the dynamic case longitudinal wave propagation induces an inhomogeneous strain field that triggers the 2nd order strain gradient influence and thus may induce non-similarity. These more complex problems are excluded from the following discussion.

We will demonstrate this size dependence for the above model first by constructing a dimensionless force-displacement graph of the tapered tensile rod. Clearly, this graph will

[3] Gravitational forces are ignored. In the dynamic case also the characteristic velocities, e.g. impact velocities have to be the same (Malmberg (1995, [2.4])).

depend on the reference length of the rod. Here the characteristic length L^* is chosen. For ξ=1 Eq.(3.20) gives the displacement u^* at x=L^* or equivalently the average strain

$$\tilde{\varepsilon}^* = u^*/L^* = \varepsilon_{co}\left[1+\frac{1-\alpha}{1-\beta^2}\ (\beta^2 e^{-\frac{1}{\beta}} - e^{-1})\right]. \tag{3.23}$$

The dimensionless force $\tilde{P}$ is obtained by dividing P by a force like quantity such as A_oK; thus

$$\tilde{P} = \frac{P}{A_o}\frac{1}{K} = \varepsilon_{co}. \tag{3.24}$$

With (3.23) the dimensionless force-displacement graph is given by the linear relation

$$\tilde{P} = C(\alpha,\beta)\ \tilde{\varepsilon}^* \tag{3.25}$$

where the stiffness C is defined by

$$C(\alpha,\beta) = \left[1+\frac{1-\alpha}{1-\beta^2}\ (\beta^2 e^{-\frac{1}{\beta}} - e^{-1})\right]^{-1}. \tag{3.26}$$

If the gradient dependence is not present at all or if the characteristic length L^* is very large compared to the internal length l_i, then β=0 and Eq.(3.25) reduces to

$$\tilde{P} = C_o(\alpha)\ \tilde{\varepsilon}^* \tag{3.27}$$

with

$$C_o(\alpha) = \left[1-(1-\alpha)e^{-1}\right]^{-1}. \tag{3.28}$$

On the other hand, if $\beta\to 1$, one obtains from (3.26) in the limit

$$C_{1-}(\alpha) = \lim_{\beta\to 1} C(\alpha,\beta) = \left[1-(1-\alpha)\frac{3}{2}e^{-1}\right]^{-1}. \tag{3.29}$$

These values give an idea of the stiffness variation with a change in β

$$C_o(\alpha) \le C(\alpha,\beta) \le C_{1-}(\alpha) \tag{3.30}$$

$$0 \le \beta = \frac{l_i}{L^*} < 1.$$

We consider now geometrical similar specimens of different size but made from the same material and subject to scaled loading. The small scale specimen is denoted by the subscript m and the large scale by p. Then

$$\left.\begin{aligned} &\alpha_p = \alpha_m = \alpha\,,\ L_p^* = L_m^* \lambda,\ \tilde{P}_p = \tilde{P}_m \\ &\text{and} \\ &\beta_p = \beta_m \frac{1}{\lambda} \end{aligned}\right\} \qquad (3.31)$$

where $\lambda \geq 1$ is the geometric scale factor. If the scale factor λ is very large, then $\beta_p \rightarrow 0$ and the lower bound of the stiffness, Eq.(3.30), defines the dimensionless force-displacement graph. Thus, the relation (3.27) applies to specimens which are very large compared to the internal length l_i. For geometrical similar specimens that are very small, theoretically one gets $\beta \rightarrow 1$ and the upper bound in (3.30) applies. The corresponding dimensionless force-displacement graphs are shown in Fig.3.6(a) for two values of the cross-section ratio α=0.0625 and 0.5625. It is obvious that the smaller specimens are stiffer than the larger.

It is noted that the upper limit of β ($\rightarrow 1$) is certainly exaggerated. In any case it should also be assured that the minimum diameter $2r_o$ is not smaller than the internal length l_i. Therefore, the upper limit of β should be

$$\beta < \text{Min}\,[1, \frac{2r_o}{L^*}]. \qquad (3.32)$$

It is instructive to visualize the size dependence of the deformation by using another dimensionless force-deformation graph. With the dimensionless force $\tilde{P}$, Eq.(3.24), which corresponds to the dimensionless stress at the minimum cross-section, the strain ratio (3.22) yields

$$\tilde{P} = \varepsilon_{co} = \frac{1+\beta}{1+\alpha\beta} (\varepsilon)_o\ , \qquad (3.33)$$

a linear relation between the dimensionless force $\tilde{P}$ and the local strain at the minimum cross-section. The corresponding graphs for very small ($\beta \rightarrow 1$) and very large ($\beta \rightarrow 0$) specimens are plotted in Fig.3.6(b) for the two cross section ratios α=0.0625 & 0.5625. Note that for very large specimens

$$\tilde{P} = (\varepsilon)_o$$

which is independent of the cross-section ration α, in fact a trivial result.

A comparison of Figs. 3.6(a) and 3.6(b) demonstrates a fairly obvious fact: The size influence is more readily detectable in dimensionless force-deformation graphs when local strains – from regions of intensive strain-nonuniformities – are used as a deformation measure than approaches which use an average on extended spatial domains.

Failure Behavior

Only two very simple cases are considered which are common in engineering. In addition to the deformation law an extra failure criterion is introduced e.g.,

- a critical local stress σ_c
- or a critical local strain ε_c .

They are considered to be local fracture criteria characteristic for the material and they are assumed to be size independent.

Critical stress criterion

The maximum stress in the tensile rod is at the minimum cross-section. Thus, prescribing a size invariant critical stress σ_c yields a critical normalized load

$$\tilde{P}_{c\sigma} = \frac{\sigma_{\max}}{K} = \frac{\sigma_c}{K}.$$

Therefore, by inverting Eq.(3.25) we can compute the corresponding average strain $\tilde{\varepsilon}^*_{c\sigma}$ at fracture,

$$\tilde{\varepsilon}^*_{c\sigma} = C^{-1}(\alpha,\beta)\ \tilde{P}_{c\sigma}, \tag{3.34}$$

which is a size dependent quantity. From Fig.3.6(a) it is obvious that proportionally scaled-up tensile specimens have larger average strains at fracture. Trivially this is also true for the critical strain $(\varepsilon)_{oc\sigma}$ at the minimum cross-section. With (3.22) and (3.24) we obtain

$$(\varepsilon)_{oc\sigma} = \frac{1+\alpha\beta}{1+\beta}\,\tilde{P}_{c\sigma}. \tag{3.35}$$

Thus, for a size invariant critical stress (i.e. critical normalized load $\tilde{P}_{c\sigma}$) the associated local failure strain is determined as shown in Fig.3.6(b). From the graphs of this figure we see that the scaled-up specimens have larger local failure strains. It is noted that this qualitative trend is not in agreement with the trends observed experimentally (e.g. Brown et al. (1947, [3.1])).

Critical strain criterion

The maximum strain in the tensile rod is at the minimum cross-section and at the initiation of fracture we may assume that

$$(\varepsilon)_o = \varepsilon_c .$$

The associated normalized failure load $\tilde{P}_{c\varepsilon}$ is given by

$$\tilde{P}_{c\varepsilon} = \frac{1+\beta}{1+\alpha\beta}\,\varepsilon_c . \tag{3.36}$$

This result is sketched in Fig.3.6(b) for a size invariant critical local strain. It is obvious that smaller specimens ($\beta \to 1$) are characterized by larger normalized fracture loads. This is a qualitative trend that is in accordance with experimental observations (e.g. [3.1]).

With the notation (3.31) the ratio of the fracture loads for a large and a small specimen is given by

$$\frac{(\tilde{P}_{c\varepsilon})_p}{(\tilde{P}_{c\varepsilon})_m} = \frac{1+\alpha\beta_p\lambda}{1+\beta_p\lambda}\frac{1+\beta_p}{1+\alpha\beta_p} = \frac{\lambda+\beta_m}{\lambda+\alpha\beta_m}\frac{1+\alpha\beta_m}{1+\beta_m} < 1. \tag{3.37}$$

It is evident that this ratio does not only depend on the geometrical scale factor λ but also on the absolute size via β_m or β_p. Therefore, keeping λ=const. but increasing the size of the small (m) and the large specimen (p) proportionally will increase this ratio towards "one" such that this size effect dies out with an increase of the absolute size.

From the knowledge of the normalized failure load $\tilde{P}_{c\varepsilon}$ one may determine the associated average strains $\tilde{\varepsilon}^*_{c\varepsilon}$ for various specimen sizes. Note that although the maximum local strains are assumed to be the same at fracture, the average strains are not equal. This may be seen from Fig.3.6(a). In fact, the average strains at failure are larger for the small specimen than for the large one. This is again a manifestation of the size dependent response of this model.

3.2 Exact Solution for a U-Notched Rod

3.2.1 Statement of the Problem

The linear 2nd order gradient model is now applied to another uniaxial stress problem which differs from the previous one by the choice of the cross-section variation $A_R(x)$ along the axis (Fig.3.7):

$$A_R(x) = A_0\rho^2, \quad \rho^2 = \begin{cases} \left(\cos\left(\frac{\pi}{2}\frac{x}{L}\right)\right)^{-2}, & |x| < L \\ \\ \infty & L \le |x| \end{cases} \tag{3.38}$$

A_o : minimum cross-section area
$2L$: length of notched region.

The applied tensile force is P and the uniaxial stress varies in the notched region but is vanishing for $L \le |x|$. Therefore, approaching the boundaries of the notch, the axial strain will vanish.

With the dimensionless quantities

$$\xi = \frac{x}{L}, \qquad \beta = \frac{l_i}{L} \tag{3.39}$$

the governing differential equation, corresponding to (3.6), is

$$\beta^2 \frac{d^2\varepsilon}{d\xi^2} - \varepsilon = -r(\xi)\,; \tag{3.40}$$

$$r(\xi) = \frac{P}{A_o}\frac{1}{K}\left(\cos(\frac{\pi}{2}\xi)\right)^2. \tag{3.41}$$

The associated boundary conditions are

$$\left.\begin{aligned} &\text{B.C. I}: \ (\varepsilon)_{\xi=1} = 0 \\ &\text{B.C. II}: \left(\frac{d\varepsilon}{d\xi}\right)_{\xi=0} = 0. \end{aligned}\right\} \tag{3.42}$$

Here the B.C. II follows from the smooth distribution of the cross-section area within the notch and the symmetry at ξ=0.

3.2.2 The Exact Solution

We introduce the coordinate transformation

$$\zeta = \frac{\xi}{\beta} = \frac{x}{l_i}\,; \tag{3.43}$$

then Eq.(3.40) simplifies to

$$\frac{d^2\varepsilon}{d\zeta^2} - \varepsilon = -\tilde{r}(\zeta) \tag{3.44}$$

with

$$\tilde{r}(\zeta) = r(\beta\zeta) = \frac{P}{A_o}\frac{1}{K}\left(\cos(\frac{\pi}{2}\beta\zeta)\right)^2. \tag{3.45}$$

The homogeneous solution is

$$\varepsilon_{\text{hom}} = C_1\,\varepsilon_1(\zeta) + C_2\,\varepsilon_2(\zeta) \tag{3.46}$$

$$\varepsilon_1(\zeta) = e^{\zeta}, \qquad \varepsilon_2(\zeta) = e^{-\zeta}.$$

A particular solution is obtained by using the method of "variation of parameters" (e.g. Hildebrand (1962, [3.2])). For this 2nd order differential equation we obtain:

$$\varepsilon_{part} = \alpha_1(\zeta)\,\varepsilon_1(\zeta) + \alpha_2(\zeta)\,\varepsilon_2(\zeta)$$

with

$$\left.\begin{aligned} \alpha_1(\zeta) &= -\frac{1}{2}\int \varepsilon_2(\zeta)\tilde{r}(\zeta)\mathrm{d}\zeta \\ \alpha_2(\zeta) &= \frac{1}{2}\int \varepsilon_1(\zeta)\tilde{r}(\zeta)\mathrm{d}\zeta \quad . \end{aligned}\right\} \tag{3.47}$$

The choice of the cross-section distribution was such that a closed-form integration of (3.47) is possible by using integral tables. One obtains (e.g. Dwight (1967, [3.3]))

$$\left.\begin{aligned} \alpha_1(\zeta) &= -\frac{P}{A_0}\frac{1}{K}\frac{1}{\pi\beta}\frac{e^{-\zeta}}{\left(\frac{2}{\pi\beta}\right)^2+4}\left(-\frac{\cos^2(\frac{\pi}{2}\beta\zeta)}{\frac{\pi}{2}\beta}+\sin(\pi\beta\zeta)-\pi\beta\right) \\ \alpha_2(\zeta) &= \frac{P}{A_0}\frac{1}{K}\frac{1}{\pi\beta}\frac{e^{\zeta}}{\left(\frac{2}{\pi\beta}\right)^2+4}\left(\frac{\cos^2(\frac{\pi}{2}\beta\zeta)}{\frac{\pi}{2}\beta}+\sin(\pi\beta\zeta)+\pi\beta\right) \quad . \end{aligned}\right\} \tag{3.48}$$

The complete solution

$$\varepsilon(\zeta) = \varepsilon_{hom}+\varepsilon_{part}$$

is then found by accounting for the boundary conditions (3.42)

$$\varepsilon(\xi) = \varepsilon_{co}\,\frac{1}{1+(\pi\beta)^2}\left\{\cos^2(\frac{\pi}{2}\xi)+\frac{1}{2}(\pi\beta)^2\left(1-\frac{\cosh(\xi/\beta)}{\cosh(1/\beta)}\right)\right\}, \tag{3.49}$$

where the coordinate ξ has been reintroduced and with

$$\varepsilon_{co} = \frac{P}{A_o}\frac{1}{K}\,, \tag{3.50}$$

which is the strain at the minimum cross-section of the classical solution. For $\beta\to 0$ the non-classical solution (3.49) approaches the classical one

$$\varepsilon_c(\xi) = \varepsilon_{co}\cos^2(\frac{\pi}{2}\xi). \tag{3.51}$$

The displacement $u(\xi)$ in the region $0\le\xi\le 1$ is obtained from (3.49) by integration with the boundary condition $u(0)=0$:

$$u(\xi) = L\,\varepsilon_{co}\left\{\frac{1}{2}\xi + \frac{1}{1+(\pi\beta)^2}\frac{\sin(\pi\xi)}{2\pi} - \frac{(\pi\beta)^2}{2[1+(\pi\beta)^2]}\frac{\beta\sinh(\xi/\beta)}{\cosh(1/\beta)}\right\}; \tag{3.52}$$

for the classical case (β=0) we get

$$u_C(\xi) = L\,\varepsilon_{co}\left\{\frac{1}{2}\xi + \frac{\sin(\pi\xi)}{2\pi}\right\}. \tag{3.53}$$

3.2.3 Discussion

We will not repeat the extensive discussion performed in Section 3.1.4 but we will mention only a few corresponding facts.

The maximum strain is found at ξ=0:

$$\varepsilon(0) = \varepsilon_{co}\left\{1 - \frac{(\pi\beta)^2}{2[1+(\pi\beta)^2]}\left(1 + \frac{1}{\cosh(1/\beta)}\right)\right\}. \tag{3.54}$$

Here the first term is the classical part and the second term is the non-classical contribution due to the gradient influence. Evidently, the 2nd order strain gradient contribution in the enriched constitutive equation reduces the maximum value ε_{co} of the classical solution. For small values of β<<1 this reduction is only quadratic in β and thus rather small, as demonstrated in Fig.3.8.

Introducing the dimensionless force $\tilde{P}$

$$\tilde{P} = \frac{P}{A_o}\frac{1}{K} = \varepsilon_{co},$$

which corresponds to the dimensionless stress at the minimum cross-section, we can invert Eq.(3.54) to give the relation between $\tilde{P}$ and maximum local strain at the minimum cross-section:

$$\tilde{P} = C(\beta)\,\varepsilon(0) \tag{3.55}$$

with

$$C(\beta) = \left[1 - \frac{(\pi\beta)^2}{2[1+(\pi\beta)^2]}\left(1 + \frac{1}{\cosh(1/\beta)}\right)\right]^{-1}. \tag{3.56}$$

The stiffness $C(\beta)$ reflects the size influence if β is varied between β=0 (very large specimens) and $\beta\to$1 (very small specimens). For β<<1 the influence of β on the stiffness C is only quadratic. This is in contrast to the previous example, the exponentially tapered rod, where, according to Eq.(3.33), the influence is linear. This difference will be analysed more deeply in section 4.4.

The displacement at ξ=1 is obtained from (3.52)

$$u(1) = L\,\varepsilon_{co}\,\frac{1}{2}\left\{1-\frac{(\pi\beta)^2}{1+(\pi\beta)^2}\,\beta\,\mathrm{tgh}(1/\beta)\right\}$$

and the corresponding classical solution yields

$$u_C(1) = L\,\varepsilon_{co}\,\frac{1}{2}.$$

They determine the average strains in the notch region

$$\tilde{\varepsilon} = u(1)/L\,, \quad \tilde{\varepsilon}_c = u_C(1)/L$$

and their ratio is

$$\tilde{\varepsilon}/\tilde{\varepsilon}_c = 1-\frac{(\pi\beta)^2}{1+(\pi\beta)^2}\,\beta\,\mathrm{tgh}(1/\beta)\,.$$

For $\beta<<1$ this ratio shows a 3rd order dependence on β (Fig.3.9) which is even more difficult to detect than the ratio of local strains obtained from (3.54).

4. The Exponentially Tapered Tensile Rod: A Non-Linear Problem due to Power Law Hardening and Cross-Section Reduction

4.1 Statement of the Problem

Assuming a uniaxial state of stress as previously, the uniaxial non-linear stress-strain relation is taken to be of the following form

$$\sigma = K f(\varepsilon) - K\,l_i^2\,\frac{d^2\varepsilon}{dX^2} \tag{4.1}$$

where σ is the true (Cauchy) stress and ε is the logarithmic strain; the derivative is defined with respect to the Lagrangian coordinate X along the axis of the rod. For the uniaxial case considered the two conjugated variables σ and ε are defined as follows

$$\left.\begin{aligned}\sigma &= \frac{P}{A(X)}\\ \varepsilon &= \ln(1+\varepsilon_R)\\ \varepsilon_R &= \frac{du}{dX}\end{aligned}\right\} \tag{4.2}$$

where:
P : longitudinal force
$A(X)$: instant cross-section of rod
ε_R : engineering strain
u : displacement along the rod.

The uniaxial stress σ given by $(4.2)_1$ is the average in a deformed cross-section and it follows simply from the quasistatic equilibrium in the rod.

For the case of power law hardening the non-linear function $f(\varepsilon)$ takes the form[4]

$$f(\varepsilon)=\varepsilon^n ; \quad 0<n\leq 1 \tag{4.3}$$

Three material constants are involved
n: hardening exponent
K: power law modulus
l_i: internal length scale.

The restricted range of the hardening exponent assures that the plastic modulus $d\sigma/d\varepsilon$ is a decreasing function of strain as observed in a tensile test of a uniform specimen. The initial undeformed geometry of the tapered rod is defined by the cross-section distribution $A_R(X)$ along the axis of the rod. Here an exponentially tapered rod as shown in Fig.3.1 is considered:

$$\left.\begin{aligned} &A_R(X) = A_o\,\rho^2 , \qquad \rho^2 = [\alpha+(1-\alpha)\,e^{-X/L^*}]^{-1} \\ &\alpha=\frac{A_o}{A_\infty}<1 \end{aligned}\right\} \tag{4.4}$$

A_o : minimum cross-section
A_∞ : large cross-section at infinity
L^* : characteristic length of the exponential cross-section.

The change of the cross-section with the deformation is assumed to be controlled by the volume conserving plastic deformation, ignoring the elastic part of the deformation. Volume conservation of a material element yields

$$A_R(X)dX \qquad = \qquad A(X)\left(1+\frac{du}{dX}\right)dX$$

Reference configuration Instantaneous configuration

such that

$$A(X) = \frac{A_R(X)}{1+\varepsilon_R} = A_R(X)\,\mathrm{e}^{-\varepsilon} . \tag{4.5}$$

[4] This corresponds to a Hollomon (1949, [4.1]) finite strain deformation law for plasticity where the elastic strains and a distinct yield point are ignored.

Introducing dimensionless quantities

$$\xi = \frac{X}{L^*}, \qquad \beta = \frac{l_i}{L^*} \tag{4.6}$$

and combining the constitutive relation (4.1), the equilibrium condition (4.2), and the condition of volume conservation (4.5), the following 2nd order differential equation for the logarithmic strain ε is obtained

$$\beta^2 \frac{d^2\varepsilon}{d\xi^2} - \varepsilon^n = -r_R(\xi)\, e^{\varepsilon} \tag{4.7}$$

where

$$r_R(\xi) = \frac{\sigma_R(\xi)}{K}, \qquad \sigma_R(\xi) = \frac{P}{A_R(\xi)} = \frac{P}{A_o}\rho^{-2}(\xi)\,; \tag{4.8}$$

here σ_R represents the engineering stress. As previously for the linear case and small deformations, the boundary conditions are

$$\left.\begin{array}{lll} \text{B.C.I} & \xi \to \infty & \lim\limits_{\xi\to\infty} \varepsilon = \varepsilon_\infty \\ \text{B.C. II} & \xi = 0 & \dfrac{d\varepsilon}{d\xi} = 0\,. \end{array}\right\} \tag{4.9}$$

Here ε_∞ is the solution of (4.7) at infinity where the gradient influence has vanished.

Corresponding to section (3.1.1), geometrically similar specimens are considered which are scaled up by the geometrical scaling factor $\lambda > 1$. The geometrical data take the values

$$\overline{A}_o = A_o\,\lambda^2\,,\ \overline{A}_\infty = A_\infty\,\lambda^2\,,\ \overline{L}^* = L^*\,\lambda\,,\ \overline{\alpha} = \alpha = \text{constant.} \tag{4.10}$$

If geometrical and physical similarity is required, then the dimensionless characteristic parameters of the determining differential equation and the boundary conditions must be the same, i.e.

$$\left.\begin{array}{l} \overline{\beta} = \beta \quad \text{or} \quad \dfrac{\overline{l}_i}{l_i} = \lambda \\ \overline{n} = n \\ \dfrac{\overline{P}}{\overline{A}_o}\dfrac{1}{\overline{K}} = \dfrac{P}{A_o}\dfrac{1}{K} \quad \text{or} \quad \dfrac{\overline{P}}{P}\dfrac{K}{\overline{K}} = \lambda^2\,. \end{array}\right\} \tag{4.11}$$

These are the similarity conditions for this gradient problem. Compared to (3.12) the equality of the hardening exponents is added to the list. Again, in principle these conditions can be satisfied, provided the hardening exponents are the same. Then

$$\lambda = \frac{\bar{l}_i}{l_i} \quad \text{and} \quad \frac{\overline{P}}{P} = \frac{\overline{K}}{K}\left(\frac{\bar{l}_i}{l_i}\right)^2 . \tag{4.12}$$

However, due to the gradient term similarity cannot be achieved if the material is the same, i.e. $\bar{l}_i = l_i$ among others, in the small and the large-scale specimen.

4.2 Solutions without Gradient Effect

4.2.1 Uniform Cross-Section

For a uniform cross-section, A_R = const., gradient effects are not introduced. Thus, Eq.(4.7) reduces to a non-linear algebraic equation for ε :

$$\varepsilon^n = \frac{\sigma_R}{K}\, \mathrm{e}^{\varepsilon} \tag{4.13}$$

where

$$\sigma_R = \frac{P}{A_R} = \text{const.} \tag{4.14}$$

is the engineering stress. In terms of σ_R and the engineering strain ε_R, Eq.(4.13) corresponds to the following stress-strain relation

$$\sigma_R = K\,\varepsilon^n e^{-\varepsilon} = K\,\frac{\left(\ln(1+\varepsilon_R)\right)^n}{1+\varepsilon_R} . \tag{4.15}$$

The slope of the graph σ_R vs. ε_R is given by

$$\frac{d\sigma_R}{d\varepsilon_R} = K\frac{\left(\ln(1+\varepsilon_R)\right)^n}{(1+\varepsilon_R)^2}\left(\frac{n}{\ln(1+\varepsilon_R)} - 1\right) \tag{4.16}$$

which yields a maximum value for the engineering stress when

$$\ln(1+\varepsilon_R) = n$$

or

$$\left.\begin{aligned} \varepsilon_R &= \mathrm{e}^{\,n} - 1 \\ \varepsilon &= n \end{aligned}\right\} \qquad (4.17)$$

and

$$(\sigma_R)_{\max} = K\frac{n^n}{\mathrm{e}^n}. \qquad (4.18)$$

At this instant the increase in load P or stress σ_R due to hardening is balanced by the "geometric softening" due to cross-section reduction. Introducing the inverse of the hardening exponent

$$m = \frac{1}{n}, \qquad (4.19)$$

the associated strain limits are given in Table 4.1.

These critical strains suggest that the following analysis is restricted to strain values less than the critical ones, i.e.

$$\varepsilon < n. \qquad (4.20)$$

The non-linear equation (4.13) allows a simple solution for the logarithmic strain ε if the cross-section reduction is ignored. Then

$$\varepsilon = \left(\frac{\sigma_R}{K}\right)^{1/n}. \qquad (4.21)$$

In the general case, however, an exact solution is not possible. Approximations can be found as follows. Using the inverse m, Eq.(4.13) reads

$$\varepsilon = \left(\frac{\sigma_R}{K}\right)^m \mathrm{e}^{\,m\varepsilon}. \qquad (4.22)$$

With

$$\bar{\varepsilon} = m\,\varepsilon, \qquad \bar{\sigma} = m\left(\frac{\sigma_R}{K}\right)^m \qquad (4.23)$$

Eq.(4.22) takes the simple form

$$\bar{\varepsilon} = \bar{\sigma}\,\mathrm{e}^{\,\bar{\varepsilon}}. \qquad (4.24)$$

We note that for $\bar{\sigma} \geq 1$ a real solution certainly does not exist. Also, according to (4.20), $\bar{\varepsilon}$ is restricted to

$$\bar{\varepsilon} < 1 \tag{4.25}$$

which implies

$$\bar{\sigma} < \frac{1}{e} = 0.3679. \tag{4.26}$$

Moreover, Eq.(4.24) implies $\bar{\sigma} < \bar{\varepsilon}$. For $\bar{\varepsilon} << 1$ the exponential function can be approximated by its Taylor series approximation at $\bar{\varepsilon} = 0$:

$$e^{\bar{\varepsilon}} = 1 + \bar{\varepsilon} + \frac{1}{2}\bar{\varepsilon}^2 + \ldots .$$

Thus, Eq.(4.24) yields with $\bar{\sigma} < \bar{\varepsilon} << 1$

$$\bar{\varepsilon} \cong \frac{1-\bar{\sigma}}{\bar{\sigma}} \pm \sqrt{\left(\frac{1-\bar{\sigma}}{\bar{\sigma}}\right)^2 - 2} \tag{4.27}$$

provided the radicand is non-negative, i.e

$$\bar{\sigma} \le \frac{1}{\sqrt{2}+1} \approx 0.4142 \tag{4.28}$$

which is assured since the more stringent condition (4.26) applies.

With $\bar{\varepsilon} = 1 - \omega$, $\omega << 1$ an expansion at $\bar{\varepsilon} = 1$ can be used

$$e^{\bar{\varepsilon}} = e\,(1 - \omega + \frac{1}{2}\omega^2 + \ldots) = e\,\frac{1}{2}(1 + \bar{\varepsilon}^2)$$

which yields

$$\bar{\varepsilon} = \frac{1}{e\,\bar{\sigma}} \pm \sqrt{\left(\frac{1}{e\,\bar{\sigma}}\right)^2 - 1} \tag{4.29}$$

From (4.27) and (4.29) we easily obtain, observing (4.23), the explicit relation between ε or ε_R and σ_R.

4.2.2 Non-Uniform Cross-Section

If one considers a non-uniform cross-section but ignores the non-classical part of the constitutive equation, then the above results are also valid with the engineering stress σ_R being a function of X:

$$\sigma_R = \hat{\sigma}_R(X) = \frac{P}{A_R(X)} .$$

A solution of (4.13), its two approximations given by (4.27) and (4.29), is called a classical solution ε_c for the tapered rod problem. A few peculiar properties of the logarithmic strain distribution $\varepsilon_c(\xi)$ are found as follows. Derivation of (4.13) with respect to ξ yields

$$\varepsilon_c' = (\varepsilon_c)_\xi = \frac{\sigma_R'}{\sigma_R} \frac{\varepsilon_c}{n - \varepsilon_c}$$

where $(\,)' = \dfrac{\mathrm{d}}{\mathrm{d}\xi}(\,)$ and

$$\frac{\sigma_R'}{\sigma_R} = (\ln \sigma_R)' = \frac{r_R'}{r_R} = -\frac{A_R'}{A_R} .$$

For the second derivative we obtain

$$\varepsilon_c'' = (\varepsilon_c)_{\xi\xi} = (\ln \sigma_R)'' \frac{\varepsilon_c}{n - \varepsilon_c} + (\ln \sigma_R)' \frac{n(\varepsilon_c)_\xi}{(n - \varepsilon_c)^2} =$$

$$= \frac{\varepsilon_c}{(n - \varepsilon_c)^3} \{(\ln \sigma_R)''(n - \varepsilon_c)^2 + [(\ln \sigma_R)']^2 n\}.$$

Thus, for the strain ε_c approaching the critical value n, the two derivatives are unbounded

$$\varepsilon_c \to n, \qquad (\varepsilon_c)_\xi \to \infty, \qquad (\varepsilon_c)_{\xi\xi} \to \infty.$$

However, the curvature of the function $\varepsilon_c(\xi)$

$$k = \frac{(\varepsilon_c)_{\xi\xi}}{[1 + [(\varepsilon_c)_\xi]^2]^{3/2}}$$

approaches a finite value

$$\lim_{\varepsilon_c \to n} k = \frac{\sigma_R}{\sigma_R'} \frac{1}{n}$$

provided $\sigma_R' \neq 0$.

With (4.5) the first derivative of the instantaneous cross-section is

$$\frac{A'}{A} = 2\frac{d'}{d} = \left(\frac{A_R'}{A_R} + (\varepsilon_c)_\xi \right), \qquad A = \pi \frac{d^2}{4}$$

where d is the instantaneous diameter of the section. Therefore, a tensile rod with a sharp circumferential notch having initially a finite-opening angle at the tip will deform such that the notch angle will decrease and will shrink to zero, i.e. the notch becomes sharper when the strain reaches the critical value. This is a peculiar property of this simplified uniaxial model.

4.3 Approximate Analytical Solution by the Method of Multiple Scales

4.3.1 The Governing System of Perturbation Equations

For n=1 and ignoring the cross-section reduction, i.e.

$$A(X)=A_R(X)\,,$$

the problem described in section (4.1) reduces to the linear case for which an exact solution was derived. However, for the more general case n<1, with or without consideration of the cross-section deformation, the differential equation for the logarithmic strain is non-linear and an exact solution appears not to be possible. But assuming that

$$\beta=\frac{l_i}{L^*}<<1\,, \tag{4.30}$$

then the first term in the differential equation (4.7) is small (provided $d^2\varepsilon/d\xi^2$ is bounded) for $\beta\to 0$ and it represents a "perturbation" in the equation. Ignoring it entirely, the differential equation (4.7) reduces to a non-linear algebraic equation for the logarithmic strain, which was discussed in section (4.2). Its solution does not satisfy the boundary condition at the minimum cross-section. This suggests that the influence of the perturbing term $\beta^2 d^2\varepsilon/d\xi^2$ is operative over a boundary layer at ξ=0, as observed in the exact linear solution. The linear solution consists of two parts:

- a first part which essentially represents the classical solution and which is determined by the variation of the cross-section along the length of the bar
- a second part which is controlled by the parameters β and which dies out exponentially with ξ/β (boundary layer term).

Thus, there are essentially two types of spatial dependencies involved. According to perturbation theory (e.g. O'Malley (1991, [4.2])), the above problem is a singular perturbation problem. For this problem an approximate asymptotic solution for a small parameter β appears possible using an analytic approach, e.g. the method of matched asymptotics or the multiple scale method (e.g. Nayfeh (1973, [4.3]; 1981, [4.4]), Kervorkian & Cole (1981, [4.5]), Holmes (1995, [4.6])). Compared to a purely numerical approach, analytic approximations often reveal the essential influence of the small parameter on the exact solution more satisfying.

The method of multiple scales introduces new spatial coordinates for each dependency, which are considered to be independent of one another. As a consequence, starting with an

ordinary differential equation, its transformation leads initially to a partial differential equation.

It is assumed that the logarithmic strain distribution can be represented in the form

$$\varepsilon = \hat{\varepsilon}(\xi;\beta) = \tilde{\varepsilon}(\xi,\eta;\beta) \tag{4.31}$$

where

$$\left.\begin{aligned} &\xi = \frac{X}{L^*} \text{ is the "slow" variable} \\ &\text{and} \\ &\eta = \frac{\mu(\xi)}{\beta} \text{ is the "fast" variable .} \end{aligned}\right\} \tag{4.32}$$

The function $\mu(\xi)$ remains to be determined. Observing the linear case Eq.(3.17), the "fast" variable is

$$\eta = \frac{\xi}{\beta};$$

Thus $\mu = \xi$. In the nonlinear case one may show that this choice is too restrictive. The introduction of the function $\mu(\xi)$ follows a generalized version of the method of multiple scales by Nayfeh (1973, [4.3]). This method, as applied to the present problem, proceeds in the following steps.

The derivatives in the ordinary differential equation and in the boundary conditions are developed in terms of the two-scale representation of the strain distribution $\varepsilon = \tilde{\varepsilon}(\xi,\eta;\beta)$. This gives

$$\left.\begin{aligned} &\frac{d\hat{\varepsilon}}{d\xi} = \tilde{\varepsilon}_\xi + \tilde{\varepsilon}_\eta \frac{\mu'}{\beta} \\ &\frac{d^2\hat{\varepsilon}}{d\xi^2} = \tilde{\varepsilon}_{\xi\xi} + 2\,\tilde{\varepsilon}_{\xi\eta} \frac{\mu'}{\beta} + \tilde{\varepsilon}_{\eta\eta} \left(\frac{\mu'}{\beta}\right)^2 + \tilde{\varepsilon}_\eta \frac{\mu''}{\beta} \end{aligned}\right\} \tag{4.33}$$

where

$$\mu' = \frac{d\mu}{d\xi} \tag{4.34}$$

and

$$\tilde{\varepsilon}_\xi = \frac{\partial\tilde{\varepsilon}}{\partial\xi}, \qquad \tilde{\varepsilon}_\eta = \frac{\partial\tilde{\varepsilon}}{\partial\eta}, \qquad \tilde{\varepsilon}_{\xi\xi} = \frac{\partial^2\tilde{\varepsilon}}{\partial\xi^2} \text{ etc.}$$

are partial derivatives of the two-scale function $\tilde{\varepsilon}$. Then the differential equation (4.7) and the boundary conditions take the following form

$$\beta^2\left\{\tilde{\varepsilon}_{\xi\xi}+2\tilde{\varepsilon}_{\xi\eta}\frac{\mu'}{\beta}+\tilde{\varepsilon}_{\eta\eta}\left(\frac{\mu'}{\beta}\right)^2+\tilde{\varepsilon}_{\eta}\frac{\mu''}{\beta}\right\}-\tilde{\varepsilon}^{\,n}=-r_R(\xi)\,e^{\tilde{\varepsilon}} \tag{4.35}$$

$$\left.\begin{array}{lll} \text{B.C. I} & \xi,\ \eta\to\infty & \lim\limits_{\xi,\eta\to\infty}\tilde{\varepsilon}=\varepsilon_\infty \\ \text{B.C. II} & \xi,\ \eta=0 & \tilde{\varepsilon}_{\xi}+\tilde{\varepsilon}_{\eta}\frac{\mu'}{\beta}=0\,. \end{array}\right\} \tag{4.36}$$

It is assumed that the two-scale function $\tilde{\varepsilon}\,(\xi,\eta;\beta)$ admits a uniformly valid expansion in terms of the small parameter β, i.e.

$$\tilde{\varepsilon}\,(\xi,\eta;\beta)=\overset{0}{\varepsilon}\,(\xi,\eta)+\beta\,\overset{1}{\varepsilon}\,(\xi,\eta)+\beta^2\,\overset{2}{\varepsilon}\,(\xi,\eta)+\beta^3\,\overset{3}{\varepsilon}\,(\xi,\eta)\,. \tag{4.37}$$

As demonstrated later, the inclusion of the cubic term is necessary if the approximation should be accurate up to and including the quadratic term.

The partial derivatives in Eq.(4.35) and (4.36) are expressed in terms of the polynomial presentation (4.37) (Appendix (3)). Further, the power law term $\tilde{\varepsilon}^{\,n}$ and the exponential term $e^{\tilde{\varepsilon}}$ are approximated in terms of powers of β. Finally all terms in the differential equation (4.35) are collected according to powers of β which yields (Appendix (3))

$$\beta^0 D_0+\beta^1 D_1+\beta^2 D_2+\beta^3 D_3=0.$$

Following the "Fundamental Theorem of Perturbation Theory" (Simmonds & Mann (1986, [4.7])), for small and positive but otherwise arbitrary values of β the terms D_i must vanish identically. This yields the following system of differential equations:

$$\left.\begin{array}{l} \beta^0:\text{DEQ(0)}\Rightarrow \overset{0}{\varepsilon}_{\eta\eta}-\dfrac{\overset{0}{\varepsilon}{}^{n}}{(\mu')^2}=-\dfrac{r_R(\xi)e^{\overset{0}{\varepsilon}}}{(\mu')^2} \\ \beta^1:\text{DEQ(1)}\Rightarrow \overset{1}{\varepsilon}_{\eta\eta}-\Omega^2(\xi)\,\overset{1}{\varepsilon}=R_1(\overset{0}{\varepsilon},\mu) \\ \beta^2:\text{DEQ(2)}\Rightarrow \overset{2}{\varepsilon}_{\eta\eta}-\Omega^2(\xi)\,\overset{2}{\varepsilon}=R_2(\overset{0}{\varepsilon},\overset{1}{\varepsilon},\mu,r_R) \\ \beta^3:\text{DEQ(3)}\Rightarrow \overset{3}{\varepsilon}_{\eta\eta}-\Omega^2(\xi)\,\overset{3}{\varepsilon}=R_3(\overset{0}{\varepsilon},\overset{1}{\varepsilon},\overset{2}{\varepsilon},\mu,r_R) \end{array}\right\} \tag{4.38}$$

where

$$\left.\begin{aligned} \Omega^2(\xi) &= \Omega_R^2(\xi) - \underline{\frac{\overset{0}{(\varepsilon)}^n}{(\mu')^2}} \\ \Omega_R^2(\xi) &= \frac{n}{\overset{0}{\varepsilon}} \frac{\overset{0}{(\varepsilon)}^n}{(\mu')^2} \end{aligned}\right\} \qquad (4.39)$$

such that

$$\Omega^2(\xi) = \frac{1}{(\mu')^2}\left(\frac{n}{\overset{0}{\varepsilon}} - 1 \right)\overset{0}{\varepsilon}^n, \qquad 0<n\leq 1. \qquad (4.40)$$

The right sides R_i, i=1,2,3, are differential operators defined as follows:

$$\left.\begin{aligned} R_1 &= -\frac{1}{(\mu')^2}(2\,\mu'\,\overset{0}{\varepsilon}_{\xi\eta} + \mu''\,\overset{0}{\varepsilon}_{\eta}) \\ R_2 &= R_{R2} - \underline{\frac{r_R \overset{0}{e^{\varepsilon}}}{(\mu')^2}\frac{1}{2}\overset{1}{(\varepsilon)}^2} \\ R_{R2} &= -\frac{1}{(\mu')^2}(2\,\mu'\,\overset{1}{\varepsilon}_{\xi\eta} + \mu''\,\overset{1}{\varepsilon}_{\eta} + \overset{0}{\varepsilon}_{\xi\xi}) - \Omega_R^2\,\frac{1}{2}(1-n)\,\frac{1}{\overset{0}{\varepsilon}}\left(\overset{1}{\varepsilon}\right)^2 \\ R_3 &= R_{R3} - \underline{\frac{r_R \overset{0}{e^{\varepsilon}}}{(\mu')^2}\left(\overset{1}{\varepsilon}\,\overset{2}{\varepsilon} + \frac{1}{6}\left(\overset{1}{\varepsilon}\right)^3\right)} \\ R_{R3} &= -\frac{1}{(\mu')^2}(2\,\mu'\,\overset{2}{\varepsilon}_{\xi\eta} + \mu''\,\overset{2}{\varepsilon}_{\eta} + \overset{1}{\varepsilon}_{\xi\xi}) - \\ &\quad -\Omega_R^2\,\frac{1}{2}(1-n)\,2\frac{\overset{1}{\varepsilon}\,\overset{2}{\varepsilon}}{\overset{0}{\varepsilon}} + \Omega_R^2\,\frac{1}{6}(1-n)(2-n)\,\frac{\left(\overset{1}{\varepsilon}\right)^3}{\left(\overset{0}{\varepsilon}\right)^2}. \end{aligned}\right\} \qquad (4.41)$$

We show in Appendix (3) that the underlined terms in (4.39)-(4.41) represent the contribution due to the cross-section reduction. A similar procedure, applied to the two boundary conditions (4.36), gives

$$
\begin{array}{lll}
 & \text{B.C. I } (\xi,\ \eta \to \infty) & \text{B.C. II } (\xi,\ \eta = 0) \\
\beta^{-1}: & - & \overset{0}{\mu'}\ \overset{0}{\varepsilon}_{\eta} = 0 \\
\beta^{0}: & \overset{0}{\varepsilon} \to \varepsilon_{\infty} & \overset{0}{\varepsilon}_{\xi} + \overset{0}{\mu'}\ \overset{1}{\varepsilon}_{\eta} = 0 \\
\beta^{1}: & \overset{1}{\varepsilon} \to 0 & \overset{1}{\varepsilon}_{\xi} + \overset{1}{\mu'}\ \overset{2}{\varepsilon}_{\eta} = 0 \\
\beta^{2}: & \overset{2}{\varepsilon} \to 0 & \overset{2}{\varepsilon}_{\xi} + \overset{2}{\mu'}\ \overset{3}{\varepsilon}_{\eta} = 0 \\
\beta^{3}: & \overset{3}{\varepsilon} \to 0 & (\overset{3}{\varepsilon}_{\xi} = 0).
\end{array}
\qquad (4.42)
$$

Note that the condition B.C.II for β^3 is not accurate since 4th order terms in the development of $\tilde{\varepsilon}$ are not included; it will be seen that this condition is not required.

Several comments concerning the structure of this system of differential equations are in place:

- The equations of this system are ordinary differential equations in the η variable. With respect to their integration the ξ-variable is silent. This implies that the integration constants of these 2nd order differential equations will be functions of ξ which need to be determined like $\mu(\xi)$. For their determination, additional conditions have to be set up.

- This system appears to be almost completely uncoupled, however, it must be solved in successive steps since the right side of the kth equation depends on the solution of the previous differential equations.

- The non-linearity is restricted to the very first equation governing the 0th approximation $\overset{0}{\varepsilon}$. A solution for this differential equation DEQ(0) and its boundary conditions is obtained if one sets

$$\overset{0}{\varepsilon}_{\eta} \equiv 0\,, \quad \forall \eta\,; \qquad (4.43)$$

then $$\overset{0}{\varepsilon}^{n} = r_R(\xi)\ \mathrm{e}^{\overset{0}{\varepsilon}} \qquad (4.44)$$

which implies that $\overset{0}{\varepsilon}$ is simply the classical solution without gradient effects

$$\overset{0}{\varepsilon} = \varepsilon_c\,(\xi) \qquad (4.45)$$

with $$\lim_{\xi \to \infty} \varepsilon_c = \varepsilon_{\infty}\,. \qquad (4.46)$$

The results (4.44) and (4.45) imply that the differential operators R_i simplify to

$$
\left.
\begin{aligned}
& R_1(\overset{0}{\varepsilon},\mu) \equiv 0 \\
& R_2(\overset{0}{\varepsilon},\overset{1}{\varepsilon},\mu, r_R) = \tilde{R}_2(\overset{0}{\varepsilon},\overset{1}{\varepsilon},\mu) = R_{R2}(\overset{0}{\varepsilon},\overset{1}{\varepsilon},\mu) - \underline{\frac{(\overset{0}{\varepsilon})^n}{(\mu')^2}\frac{1}{2}(\overset{1}{\varepsilon})^2} \\
& R_3(\overset{0}{\varepsilon},\overset{1}{\varepsilon},\overset{2}{\varepsilon},\mu, r_R) = \tilde{R}_3(\overset{0}{\varepsilon},\overset{1}{\varepsilon},\overset{2}{\varepsilon},\mu) = \\
& \qquad = R_{R3}(\overset{0}{\varepsilon},\overset{1}{\varepsilon},\overset{2}{\varepsilon},\mu) - \underline{\frac{(\overset{0}{\varepsilon})^n}{(\mu')^2}\left(\overset{1}{\varepsilon}\,\overset{2}{\varepsilon} + \frac{1}{6}(\overset{1}{\varepsilon})^3\right)}.
\end{aligned}
\right\} \qquad (4.47)
$$

- From the structure of the differential equations $(4.38)_{2+4}$ a peculiar property becomes evident: as long as

  $$\Omega^2(\xi) > 0,$$

  the homogeneous solutions for $\overset{1}{\varepsilon}$, $\overset{2}{\varepsilon}$, $\overset{3}{\varepsilon}$ are exponential functions in ξ which reflects the result of the linear small strain result, section (3.1.3). With (4.40), i.e.

  $$\Omega^2(\xi) = \frac{1}{(\mu')^2}\left(\frac{n}{\overset{0}{\varepsilon}} - 1\right)\overset{0}{\varepsilon}{}^n, \qquad 0<n\leq 1,$$

  Ω^2 may vanish if the limiting condition (4.17) is reached, i.e. $\overset{0}{\varepsilon} = n$, and the yet unknown function μ' is non-zero. If $\overset{0}{\varepsilon} > n$, the stress and strain state is in the descending branch of the engineering stress-strain curve where the geometric softening exceeds the strain hardening; here possibly $\Omega^2 < 0$ provided $(\mu')^2 > 0$. This would imply that the homogeneous solutions for the perturbations $\overset{1}{\varepsilon}$, $\overset{2}{\varepsilon}$, $\overset{3}{\varepsilon}$ become oscillatory. In the following, the analysis is restricted to the ascending branch of the stress-strain curve, $\overset{0}{\varepsilon} < n$.

- A corresponding set of equations can be formulated when the cross-section reduction is entirely ignored. This simplified problem is discussed in section (4.3.3).

4.3.2 Solution of the Perturbation Equations in the Ascending Stress-Strain Branch ($d\sigma_R/d\varepsilon_R > 0$)

As shown above, the 0th approximation $\overset{0}{\varepsilon}(\xi)$ is equivalent to the classical solution

$$\overset{0}{\varepsilon}(\xi) = \varepsilon_c(\xi). \qquad (4.48)$$

As a consequence, the right-hand side R_1 of the DEQ(1) vanishes identically

$$R_1(\overset{0}{\varepsilon},\mu)\equiv 0$$

and the DEQ(1) takes the simple form

$$\overset{1}{\varepsilon}_{\eta\eta} - \Omega^2(\xi)\,\overset{1}{\varepsilon} = 0 \tag{4.49}$$

with $\Omega^2 > 0$. Its general solution is

$$\overset{1}{\varepsilon}(\xi,\eta) = A_1(\xi)\,e^{\Omega(\xi)\eta} + B_1(\xi)\,e^{-\Omega(\xi)\eta} \tag{4.50}$$

with

$$\Omega(\xi) = \left[\frac{1}{(\mu')^2}\left(\frac{n}{\overset{0}{\varepsilon}} - 1\right)\overset{0}{\varepsilon}^{\,n}\right]^{1/2}. \tag{4.51}$$

The associated boundary condition for $\eta \to \infty$ requires

$$A_1(\xi)\equiv 0 \tag{4.52}$$

and (4.50) reduces to

$$\overset{1}{\varepsilon}(\xi,\eta) = B_1(\xi)\,e^{-\Omega(\xi)\eta} \tag{4.53}$$

where the functions $B_1(\xi)$ and $\Omega(\xi)$ remain to be determined. With

$$\left.\begin{aligned} \overset{1}{\varepsilon}_{\eta} &= -\Omega B_1 e^{-\Omega\eta} \\ \overset{1}{\varepsilon}_{\xi\eta} &= \overset{1}{\varepsilon}_{\eta\xi} = -(\Omega B_1)'\,e^{-\Omega\eta} + \eta\Omega'(\Omega B_1)\,e^{-\Omega\eta} \end{aligned}\right\} \tag{4.54}$$

the right-hand side R_2, Eq.$(4.47)_2$, is given by

$$R_2 = -\frac{1}{(\mu')^2}(2\mu'\overset{1}{\varepsilon}_{\xi\eta} + \mu''\overset{1}{\varepsilon}_{\eta} + \overset{0}{\varepsilon}_{\xi\xi}) - \Omega_R^2\frac{1}{2}(1-n)\frac{1}{\overset{0}{\varepsilon}}\left(\overset{1}{\varepsilon}\right)^2 - \underline{\frac{(\overset{0}{\varepsilon})^n}{(\mu')^2}\frac{1}{2}(\overset{1}{\varepsilon})^2} =$$

$$= \alpha_0 + (\alpha_1 + \overline{\alpha}_1\eta)\,e^{-\Omega\eta} + \left(\alpha_2 - \underline{\frac{(\overset{0}{\varepsilon})^n}{(\mu')^2}\frac{1}{2}B_1^2}\right)e^{-2\Omega\eta} \tag{4.55}$$

where α_o, α_1, $\bar{\alpha}_1$, α_2 as well as Ω and Ω_R are functions of ξ:

$$\left.\begin{aligned}
\alpha_o(\xi) &= -\frac{1}{(\mu')^2}\overset{0}{\varepsilon}_{\xi\xi} \\
\alpha_1(\xi) &= \left(\frac{2}{\mu'}(\Omega B_1)' + \frac{\mu''}{(\mu')^2}(\Omega B_1)\right) \\
\bar{\alpha}_1(\xi) &= -\frac{2}{\mu'}\Omega'(\Omega B_1) \\
\alpha_2(\xi) &= -\Omega_R^2 \frac{1}{2}(1-n)\frac{1}{\overset{0}{\varepsilon}} B_1^2 \,.
\end{aligned}\right\} \qquad (4.56)$$

With

$$\alpha_2^*(\xi) = \alpha_2 - \underline{\underline{\frac{(\overset{0}{\varepsilon})^n}{(\mu')^2}\frac{1}{2}B_1^2}} = -\left[n(1-n)\frac{1}{(\overset{0}{\varepsilon})^2} + \underline{\underline{1}}\right]\frac{\overset{0}{\varepsilon}^n}{(\mu')^2}\frac{1}{2}B_1^2$$

$$= -\left[\frac{(1-n)}{\overset{0}{\varepsilon}} + \underline{\frac{\overset{0}{\varepsilon}}{n}}\right]\frac{1}{2}\Omega_R^2 B_1^2 \qquad (4.57)$$

we get the compact formulation

$$R_2 = \alpha_0 + (\alpha_1 + \eta\bar{\alpha}_1)\, e^{-\Omega\eta} + \alpha_2^*\, e^{-2\Omega\eta}. \qquad (4.58)$$

The solution of the DEQ(2), Eq.$(4.38)_3$, consists of a homogeneous and a particular solution

$$\overset{2}{\varepsilon}(\xi,\eta) = \overset{2}{\varepsilon}_{\text{hom}}(\xi,\eta) + \overset{2}{\varepsilon}_{\text{part}}(\xi,\eta). \qquad (4.59)$$

The homogeneous part is

$$\overset{2}{\varepsilon}_{\text{hom}} = A_2(\xi)\, e^{\Omega(\xi)\eta} + B_2(\xi)\, e^{-\Omega(\xi)\eta}. \qquad (4.60)$$

For the particular solution the following formulation is used

$$\overset{2}{\varepsilon}_{\text{part}} = -\frac{\alpha_o(\xi)}{\Omega^2(\xi)} + f(\xi,\eta)\, e^{-\Omega(\xi)\eta} + h(\xi,\eta)\, e^{-2\Omega(\xi)\eta} \qquad (4.61)$$

where f and h have to be determined. The details are given in Appendix (4) and the result is

$$\overset{2}{\varepsilon}_{\text{part}} = -\frac{\alpha_o}{\Omega^2} + (f_1\eta + f_2\,\eta^2)\ \mathrm{e}^{-\Omega\eta} + h_o\mathrm{e}^{-2\Omega\eta} \tag{4.62}$$

with

$$\left.\begin{aligned} f_1(\xi) &= -\left(\frac{\alpha_1}{2\Omega} + \frac{\overline{\alpha}_1}{4\Omega^2}\right) \\ f_2(\xi) &= -\frac{\overline{\alpha}_1}{4\Omega} \\ h_o(\xi) &= \frac{\alpha_2{}^*}{3\Omega^2}. \end{aligned}\right\} \tag{4.63}$$

Combining the homogeneous and the particular solution and observing the boundary condition for $\eta\to\infty$, Eq.(4.42)$_4$, the exponential terms vanish since

$$\lim_{\eta\to\infty} \eta\mathrm{e}^{-\Omega\eta} = 0\,, \qquad \lim_{\eta\to\infty} \eta^2\mathrm{e}^{-\Omega\eta} = 0$$

except $A_2(\xi)\ \mathrm{e}^{\Omega\eta}$; thus, it is required that

$$A_2(\xi)\equiv 0 \tag{4.64}$$

and the solution (4.59) reduces to

$$\overset{2}{\varepsilon}(\xi,\eta) = B_2\mathrm{e}^{-\Omega\eta} - \frac{\alpha_o}{\Omega^2} + (f_1\eta + f_2\,\eta^2)\ \mathrm{e}^{-\Omega\eta} + h_o\mathrm{e}^{-2\Omega\eta}. \tag{4.65}$$

It is now required that the various perturbation functions $\overset{k}{\varepsilon}$, k=0,1,2,... are restricted by the condition (Nayfeh (1973, [4.3]))

$$\frac{\left(\overset{k}{\varepsilon}\right)}{\left(\overset{k-1}{\varepsilon}\right)} < \infty \tag{4.66}$$

for all ξ and η. This condition expresses the fact that the series expansion (4.37) is regular. Otherwise there may be ξ, η - regimes where the higher order perturbation terms become larger than the smaller order terms, even for small values of β. In order that $\overset{2}{\varepsilon}/\overset{1}{\varepsilon}$ be bounded for all η, the coefficients of $\eta\mathrm{e}^{-\Omega\eta}$ and $\eta^2\mathrm{e}^{-2\Omega\eta}$ must vanish (removal of secular terms, Holmes (1995, [4.6])); this yields

$$\left.\begin{aligned} f_1 &= -\left(\frac{\alpha_1}{2\Omega} + \frac{\overline{\alpha}_1}{4\Omega^2}\right) = 0 \\ f_2 &= -\frac{\overline{\alpha}_1}{4\Omega} = 0. \end{aligned}\right\} \tag{4.67}$$

Further, the ratio $\overset{2}{\varepsilon} / \overset{1}{\varepsilon}$ gives also the term $(\alpha_o / \Omega^2 B_1)\, e^{\Omega\eta}$ which must be bounded :

$$\lim_{\xi\to\infty} \frac{\alpha_o}{\Omega^2 B_1} = 0. \tag{4.68}$$

We come to this condition later. From Eq.(4.67) we have

$$\left.\begin{aligned} \alpha_1(\xi) &= \frac{2}{\mu'}(\Omega B_1)' + \frac{\mu''}{(\mu')^2}(\Omega B_1) = 0 \\ \bar{\alpha}_1(\xi) &= -\frac{2}{\mu'}\Omega'(\Omega B_1) = 0\,. \end{aligned}\right\} \tag{4.69}$$

This is a set of differential equations for B_1 and μ where Ω is defined by (4.40). Since only $\Omega B_1 \neq 0$ is of interest, $(4.69)_2$ gives

$$\Omega' = 0\,. \tag{4.70}$$

Thus

$$\Omega = \pm\sqrt{\varphi} = \text{const.} \neq 0\,; \tag{4.71}$$

the constant φ has to be suitably adjusted. Observing (4.39), the function $\mu(\xi)$ is then the integral of

$$\mu' = \pm\left[\frac{1}{\varphi}\left(\frac{n}{0}-1\right)\overset{0}{\varepsilon}{}^{n}\right]^{1/2} \tag{4.72}$$

$$\mu = \int_0^{\xi}\left[\frac{1}{\varphi}\left(\frac{n}{0}-1\right)\overset{0}{\varepsilon}{}^{n}\right]^{1/2} d\tau = \int_0^{\xi}\left[\frac{1}{\varphi}\frac{(n-\overset{0}{\varepsilon})}{\overset{0}{\varepsilon}{}^{1-n}}\right]^{1/2} d\tau \tag{4.73}$$

where the conditions

$$\mu(0) = 0 \quad \text{and} \quad \mu \geq 0 \tag{4.74}$$

are implied. From $(4.69)_1$ one gets

$$B_1' + \frac{1}{2}\frac{\mu''}{\mu'} B_1 = 0. \tag{4.75}$$

The general solution, derived in Appendix (5), is

$$B_1(\xi) = \frac{c}{(\mu')^{1/2}} \tag{4.76}$$

and the integration constant c is determined from the boundary condition for $\overset{1}{\varepsilon}$ at $\xi,\eta=0$, Eq.(4.42). This yields

$$B_1(\xi) = D\left(\frac{\overset{0}{\varepsilon}(\xi)^{1-n}}{n-\overset{0}{\varepsilon}(\xi)}\right)^{1/4} \tag{4.77}$$

where

$$D = c\varphi^{1/4} = \left(\frac{\overset{0}{\varepsilon}{}^{1-n}}{n-\overset{0}{\varepsilon}}\right)_0^{1/4} (\overset{0}{\varepsilon}_\xi)_0 \ . \tag{4.78}$$

Thus, the first order perturbation function $\overset{1}{\varepsilon}(\xi,\eta)$ is

$$\overset{1}{\varepsilon}(\xi,\eta) = B_1(\xi)\ \mathrm{e}^{-\sqrt{\varphi}\eta} = D\left(\frac{\overset{0}{\varepsilon}(\xi)^{1-n}}{n-\overset{0}{\varepsilon}(\xi)}\right)^{1/4} \mathrm{e}^{-\sqrt{\varphi}\eta} =$$

$$= (\overset{0}{\varepsilon}_\xi)_0 \left(\frac{\overset{0}{\varepsilon}{}^{1-n}}{n-\overset{0}{\varepsilon}}\right)_0^{1/4} \left(\frac{\overset{0}{\varepsilon}(\xi)^{1-n}}{n-\overset{0}{\varepsilon}(\xi)}\right)^{1/4} \mathrm{e}^{-\sqrt{\varphi}\eta} . \tag{4.79}$$

Since

$$\lim_{\xi\to\infty} \overset{0}{\varepsilon} = \varepsilon_\infty \ ,$$

the function $B_1(\xi)$ is bounded everywhere and $\overset{1}{\varepsilon}(\xi,\eta)$ satisfies the boundary condition at $\xi,\eta\to\infty$, Eq.(4.42). Further, the condition (4.68), observing $(4.56)_1$, (4.72), and (4.76), is satisfied since

$$\lim_{\xi\to\infty} \overset{0}{\varepsilon}_{\xi\xi} = 0.$$

This completes the determination of $\overset{1}{\varepsilon}(\xi,\eta)$, except that the constant φ, which effects $\mu(\xi)$ and thus $\eta=\mu/\beta$, has to be defined. However, an explicit determination is not yet necessary since $\sqrt{\varphi}$ cancels in the exponential term of (4.79) when (4.73) is accounted for:

$$\sqrt{\varphi}\eta = \sqrt{\varphi}\frac{\mu(\xi)}{\beta} = \frac{1}{\beta}\int_0^{\xi}\left[\left(\frac{n}{\overset{0}{\varepsilon}}-1\right)\overset{0}{\varepsilon}^{n}\right]^{1/2} d\tau . \tag{4.80}$$

As an intermediate result we note the reduced form of the perturbation function $\overset{2}{\varepsilon}(\xi,\eta)$

$$\overset{2}{\varepsilon}(\xi,\eta) = B_2(\xi)e^{-\sqrt{\varphi}\eta} - \frac{\alpha_o(\xi)}{\varphi} + \frac{\alpha_2^*(\xi)}{3\varphi}e^{-2\sqrt{\varphi}\eta} . \tag{4.81}$$

For a complete description of the logarithmic strain distribution

$$\tilde{\varepsilon} = \overset{0}{\varepsilon}(\xi) + \beta\overset{1}{\varepsilon}(\xi,\eta) + \beta^2\overset{2}{\varepsilon}(\xi,\eta)$$

up to terms quadratic in β the function $B_2(\xi)$ remains to be determined. This is done analogously to the determination of $B_1(\xi)$, i.e. we suppress the secular terms in the perturbation solution $\overset{3}{\varepsilon}(\xi,\eta)$. Therefore, the general solution of DEQ(3), Eq.$(4.38)_4$, is derived in Appendix (6):

$$\left.\begin{aligned}\overset{3}{\varepsilon}(\xi,\eta) &= B_3(\xi)e^{-\sqrt{\varphi}\eta} + \overset{3}{\varepsilon}_{part}\\ \overset{3}{\varepsilon}_{part}(\xi,\eta) &= u_1(\xi)\eta\, e^{-\sqrt{\varphi}\eta} + v_o(\xi)\, e^{-2\sqrt{\varphi}\eta} + w_o(\xi)\, e^{-3\sqrt{\varphi}\eta}\end{aligned}\right\} \tag{4.82}$$

with

$$u_1(\xi) = -\gamma_1(\xi)/(2\sqrt{\varphi}), \qquad v_o(\xi) = \gamma_2(\xi)/(3\varphi), \qquad w_o(\xi) = \gamma_3(\xi)/(8\varphi) \tag{4.83}$$

and γ_i, i=1,2,3 given by (A6.12). Requiring

$$\frac{\left(\overset{3}{\varepsilon}\right)}{\left(\overset{2}{\varepsilon}\right)} < \infty \qquad \forall\xi,\eta , \tag{4.84}$$

gives $u_1(\xi)\equiv 0$ or

$$\begin{aligned}\gamma_1(\xi) = {} & \frac{2\sqrt{\varphi}}{\mu'}B_2' + \frac{\mu''}{(\mu')^2}\sqrt{\varphi}\, B_2\\ & - \frac{1}{(\mu')^2}B_1'' + \frac{\overset{0}{\varepsilon}^{n}}{(\mu')^2}\left(\frac{n(1-n)}{\left(\overset{0}{\varepsilon}\right)^2} + \frac{1}{=}\right)\frac{\alpha_0}{\varphi}\, B_1 \equiv 0.\end{aligned} \tag{4.85}$$

This is a linear first order differential equation for $B_2(\xi)$ which takes the following lucid form

$$B_2' + \frac{1}{2}\frac{\mu''}{\mu'} B_2 = S \tag{4.86}$$

where the right-hand side is a known function given by

$$S(\xi) = \frac{1}{2}\frac{1}{\sqrt{\varphi}}\frac{1}{\mu'} B_1'' - \frac{1}{2}\frac{1}{\sqrt{\varphi}}\frac{\overset{0}{\varepsilon}{}^{n}}{\mu'}\left(\frac{n(1-n)}{(\overset{0}{\varepsilon})^2} + 1\right)\frac{\alpha_0}{\varphi} B_1. \tag{4.87}$$

Note that this is the inhomogeneous counterpart of the differential equation for B_1, Eq.(4.75), and a similar integration technique as in Appendix (5) can be applied. This is done in Appendix (7). The solution of (4.86) is, in general terms,

$$B_2(\xi) = \frac{1}{\nu}\int_0^{\xi} \nu S \, d\tau + \frac{(\nu)_0}{\nu}(B_2)_0 \tag{4.88}$$

where

$$\nu = (\mu')^{1/2} = \left(\frac{1}{\varphi}\frac{n-\overset{0}{\varepsilon}}{(\overset{0}{\varepsilon})^{1-n}}\right)^{1/4}, \qquad (\nu)_0 = (\mu')_0^{1/2} \tag{4.89}$$

and

$$(B_2)_0 = B_2(0) = \frac{1}{4}\frac{1}{\left(n - \underset{===}{(\overset{0}{\varepsilon})_0}\right)^2}\frac{1}{(\overset{0}{\varepsilon})_0^{n}}\left[\frac{7}{3}n(1-n) + n\underset{====}{(\overset{0}{\varepsilon})_0} + \frac{4}{3}\underset{====}{(\overset{0}{\varepsilon})_0^2}\right](\overset{0}{\varepsilon}_{\xi})_0^2 \tag{4.90}$$

is the boundary value of B_2 at ξ=0 which is determined from the boundary condition B.C.II, Eq.(4.42)$_3$ (see Appendix(7)). Note that the parameter φ is not contained in (4.90) and inspection of the other terms on the right-hand side of (4.88) shows that φ cancels out.

The integration of the integral in (4.88) requires $\overset{0}{\varepsilon}$, which is equivalent to the classical solution ε_c, to be known explicitly. Only approximate analytical solutions, limited to either small or large strains have been obtained (section 4.2). Provided a solution was available, it appears that an integration can be done only numerically.

The approximate perturbation solution for the logarithmic strain takes now the following form

$$\varepsilon = \tilde{\varepsilon}\ (\xi,\eta;\beta) = \overset{0}{\varepsilon}(\xi) + \beta\overset{1}{\varepsilon}(\xi,\eta) + \beta^2\overset{2}{\varepsilon}(\xi,\eta) =$$

$$= \overset{0}{\varepsilon}(\xi) + \beta B_1(\xi)\, e^{-\sqrt{\varphi}\eta} + \beta^2\left[B_2(\xi)e^{-\sqrt{\varphi}\eta} - \frac{\alpha_o(\xi)}{\varphi} + \frac{\alpha_2{}^*(\xi)}{3\varphi}e^{-2\sqrt{\varphi}\eta}\right] \tag{4.91}$$

with

$$\sqrt{\varphi}\eta = \sqrt{\varphi}\frac{\mu(\xi)}{\beta} = \frac{1}{\beta}\int_0^{\xi}\left[\frac{n-\overset{0}{\varepsilon}}{\overset{0}{\varepsilon}^{1-n}}\right]^{1/2} \mathrm{d}\tau. \tag{4.92}$$

The parameter φ cancels out in (4.91).

It should be pointed out that the derived approximate solution for the logarithmic strain distribution does not explicitly depend on the distribution of the cross-section area; this is solely contained in the function $\overset{0}{\varepsilon}=\varepsilon_c$ and the obtained solution is applicable to any smooth cross-section variation in the region $0<\xi<\infty$ satisfying the appropriate properties ($\xi\to\infty$).

Without solving Eq.(4.13) for $\varepsilon_c=\overset{0}{\varepsilon}$ and determining the integral in (4.88), an important result can be obtained from (4.91). This is the maximum strain at the minimum cross-section. This analysis and its discussion are postponed to Section 4.4.2.

In comparison to the linear problem analyzed in section (3) further insight is obtained by reducing the non-linear problem to small strains, i.e. ignoring the cross-section reduction. This allows to obtain explicit solutions, which are derived in the following section.

4.3.3 Solution for Power Law Hardening without Cross-Section Reduction

The restriction to small strains implies that the cross-section reduction due to the volume conserving plastic deformation is ignored. Then the Cauchy stress and the logarithmic strain are approximated by the engineering stress and engineering strain, σ_R and ε_R, respectively. For reasons of simplicity the subscript (R) of the engineering strain is dropped in the following.

The classical solution, denoted by ε_c, follows from (4.13)

$$\varepsilon_c = \left(\frac{\sigma_R(\xi)}{K}\right)^{1/n} = (\varepsilon_c)_0\, g(\xi)^{1/n} \tag{4.93}$$

where

$$(\varepsilon_c)_0 = \left(\frac{\sigma_R}{K}\right)_{\xi=0}^{1/n} \tag{4.94}$$

is the strain at the minimum cross-section and

$$g(\xi) = \alpha + (1-\alpha)\,\mathrm{e}^{-\xi} \tag{4.95}$$

is related to the inverse of the cross-section area variation along the axis of the rod. Naturally, the geometric instability cannot be described by this simplified model.

The differential equation (4.7) reduces to

$$\beta^2 \frac{d^2\varepsilon}{dX^2} - \varepsilon^n = -r_R(\xi). \tag{4.96}$$

The boundary conditions are given by (4.9) with

$$\varepsilon_\infty = \left(\frac{(\sigma_R)_\infty}{K} \right)^{1/n}, \qquad (\sigma_R)_\infty = \frac{P}{A_\infty} = \frac{P}{A_o}\alpha. \tag{4.97}$$

An analytical solution is not feasible, but again the method of multiple scales can be used to obtain an asymptotic solution for small values of β. In fact, this small strain case is contained in the previous analysis and, clearly, advantage is taken from this property by *ignoring all underlined terms*, which are due to the exponential term e^{ε}. An abridged description is given in the following.

The system of perturbation equations (4.38) reduces to

$$\left.\begin{aligned}
&\beta^0 : \mathrm{DEQ}(0) \Rightarrow \overset{0}{\varepsilon}_{\eta\eta} - \frac{\overset{0}{\varepsilon}^n}{(\mu_R')^2} = -\frac{r_R(\xi)}{(\mu_R')^2} \\
&\beta^1 : \mathrm{DEQ}(1) \Rightarrow \overset{1}{\varepsilon}_{\eta\eta} - \Omega_R^2(\xi)\,\overset{1}{\varepsilon} = R_1(\overset{0}{\varepsilon}, \mu_R) \\
&\beta^2 : \mathrm{DEQ}(2) \Rightarrow \overset{2}{\varepsilon}_{\eta\eta} - \Omega_R^2(\xi)\,\overset{2}{\varepsilon} = R_{R2}(\overset{0}{\varepsilon}, \overset{1}{\varepsilon}, \mu_R) \\
&\beta^3 : \mathrm{DEQ}(3) \Rightarrow \overset{3}{\varepsilon}_{\eta\eta} - \Omega_R^2(\xi)\,\overset{3}{\varepsilon} = R_{R3}(\overset{0}{\varepsilon}, \overset{1}{\varepsilon}, \overset{2}{\varepsilon}, \mu_R)
\end{aligned}\right\} \tag{4.98}$$

where Ω_R^2 is given by $(4.39)_2$ and the differential operators R_1, R_{R2}, R_{R3} are defined by (4.41). Also we use the notation μ_R instead of μ.

Evidently, the corresponding boundary conditions are given by (4.42). The 0^{th} approximation $\overset{0}{\varepsilon}$ is now

$$\overset{0}{\varepsilon}(\xi) = \varepsilon_c(\xi) = (\varepsilon_c)_0\, g(\xi)^{1/n}. \tag{4.99}$$

For later purposes the first and second derivative are cited here

$$\left.\begin{aligned}
&\overset{0}{\varepsilon}_\xi = (\varepsilon_c)_0 \frac{1}{n} g^{\frac{1-n}{n}} g_\xi = (\varepsilon_c)_0 \frac{1}{n} g^{\frac{1-n}{n}} (\alpha - g) \\
&\overset{0}{\varepsilon}_{\xi\xi} = (\varepsilon_c)_0 \frac{1}{n} \left\{ \frac{1-n}{n} g^{\frac{1-2n}{n}} (\alpha - g)^2 - g^{\frac{1-n}{n}} (\alpha - g) \right\}
\end{aligned}\right\} \tag{4.100}$$

where the property of the derivative g_ξ,

$$g_\xi = \frac{dg}{d\xi} = (\alpha - g), \tag{4.101}$$

is accounted for. Further, the first order perturbation function $\overset{1}{\varepsilon}(\xi,\eta)$ is

$$\overset{1}{\varepsilon}(\xi,\eta) = B_1(\xi)\, \mathrm{e}^{-2\Omega_R(\xi)\eta} \,. \tag{4.102}$$

Following the procedure in section (4.3.2), the removal of secular terms of the particular solution of the 2nd order perturbation function $\overset{2}{\varepsilon}$ yields now

$$\Omega_R = +\sqrt{\varphi} = \text{const.} \tag{4.103}$$

which implies, observing $(4.39)_2$,

$$\left.\begin{aligned} \mu_R{}' &= +\left[\frac{1}{\varphi}\frac{n}{\overset{0}{\varepsilon}{}^{1-n}}\right]^{1/2} \\ \text{and} \\ \mu_R &= +\int_0^{\xi}\left[\frac{1}{\varphi}\frac{n}{\overset{0}{\varepsilon}{}^{1-n}}\right]^{1/2} \mathrm{d}\tau \,. \end{aligned}\right\} \tag{4.104}$$

Further, as previously with the integration constant c,

$$B_1(\xi) = \frac{c}{(\mu_R{}')^{1/2}} \tag{4.105}$$

and explicitly

$$B_1(\xi) = D\left(\frac{\overset{0}{\varepsilon}{}^{1-n}}{n}\right)^{1/4} , \tag{4.106}$$

where

$$D = c\varphi^{1/4} = \left(\frac{\overset{0}{\varepsilon}{}^{1-n}}{n}\right)_0^{1/4} \overset{0}{(\varepsilon_\xi)}_0 \,; \tag{4.107}$$

here the boundary condition for $\overset{1}{\varepsilon}$ at $\xi,\eta = 0$, Eq.(4.42), is accounted for. Thus, the general result (4.79) for the first order perturbation function $\overset{1}{\varepsilon}(\xi,\eta)$ simplifies to

$$\overset{1}{\varepsilon}(\xi,\eta) = B_1(\xi)\ \mathrm{e}^{-\sqrt{\varphi}\eta} = (\overset{0}{\varepsilon}_\xi)_0 \left(\frac{\overset{0}{\varepsilon}{}^{1-n}}{n} \right)_0^{1/4} \left(\frac{\overset{0}{\varepsilon}(\xi)^{1-n}}{n} \right)^{1/4} \mathrm{e}^{-\sqrt{\varphi}\eta}\,. \tag{4.108}$$

Observing (4.99), $(4.100)_1$, and

$$(\overset{0}{\varepsilon}_\xi)_0 = -(\varepsilon_c)_0\ \frac{1-\alpha}{n}, \tag{4.109}$$

Eq.(4.108) takes the following explicit form

$$\overset{1}{\varepsilon}(\xi,\eta) = -(1-\alpha) \left(\frac{(\varepsilon_c)_0^{3-n}}{n} \right)^{1/2} g(\xi)^{\frac{1-n}{4n}}\, \mathrm{e}^{-\sqrt{\varphi}\eta}\ . \tag{4.110}$$

The intermediate result for the 2nd order perturbation function $\overset{2}{\varepsilon}(\xi,\eta)$, Eq.(4.81), reads now

$$\overset{2}{\varepsilon}(\xi,\eta) = B_2(\xi)\mathrm{e}^{-\sqrt{\varphi}\eta} - \frac{\alpha_o(\xi)}{\varphi} + \frac{\alpha_2(\xi)}{3\varphi}\mathrm{e}^{-2\sqrt{\varphi}\eta}\,, \tag{4.111}$$

where $\alpha_o(\xi)$ and $\alpha_2(\xi)$ are given by $(4.56)_{1\&4}$. The suppression of the secular term in the particular solution of $\overset{3}{\varepsilon}(\xi,\eta)$ yields a differential equation for B_2, formally the same as (4.86):

$$B_2{}' + \frac{1}{2}\frac{\mu_R{}''}{\mu_R{}'} B_2 = S_R\,; \tag{4.112}$$

here the right-hand side (S_R) is slightly different from (4.87) in the second term

$$S_R(\xi) = \frac{1}{2}\frac{1}{\sqrt{\varphi}}\frac{1}{\mu_R{}'}\ B_1{}'' - \frac{1}{2}\frac{1}{\sqrt{\varphi}}\frac{\overset{0}{\varepsilon}{}^n}{\mu_R{}'} \left(\frac{n(1-n)}{(\overset{0}{\varepsilon})^2} \right) \frac{\alpha_o}{\varphi} B_1\,. \tag{4.113}$$

Recalling Eq.(4.88), the solution of (4.112) is

$$B_2(\xi) = \frac{1}{\nu_R}\int_0^\xi \nu_R S_R\, \mathrm{d}\tau + \frac{(\nu_R)_0}{\nu_R}(B_2)_0 \tag{4.114}$$

where the ν_R is now defined by

$$\nu_R = (\mu_R{}')^{1/2} = \left(\frac{1}{\varphi}\frac{n}{\overset{0}{\varepsilon}{}^{1-n}} \right)^{1/4}, \quad (\nu_R)_0 = (\mu_R{}')_0^{1/2} \tag{4.115}$$

and with (4.90) (see also Appendix (7), Eq.(A7.12))

$$(B_2)_0 = B_2(0) = \frac{1}{4}\left(\frac{1}{n}\right)^2 \frac{1}{\overset{0}{(\varepsilon)}_0^n}\left[\frac{7}{3}n(1-n)\right]\left(\overset{0}{\varepsilon}_\xi\right)_0^2 \quad . \tag{4.116}$$

The explicit determination of $\mu_R(\xi)$ and $B_2(\xi)$ requires definite knowledge of $\overset{0}{\varepsilon}(\xi) = \varepsilon_c(\xi)$. For the exponential cross-section distribution (4.4) and odd integer values of $m=1/n$ analytical solutions for $\mu_R(\xi)$ are obtained as shown in Appendix (8). The result is

$$\mu_R(\xi) = \left(\frac{n}{\varphi}\right)^{1/2} (\varepsilon_c)_0^{-\frac{1-n}{2}}\, G(g(\xi);p) \tag{4.117}$$

with

$$p=\frac{1}{2}(m-1) = \frac{1-n}{2n} = 0,\ 1,\ 2,\ \ldots\ .$$

The integral functions $G(g(\xi);p)$ are listed in Table A8.2; they are valid only for the specific cross-section variation (4.95).

The determination of the function $B_2(\xi)$, according to the integral representation (4.114), can be done analytically for arbitrary hardening exponents n and for the exponentially tapered rod when the cross-section area varies according to $g(\xi)^{-1}$. The essential steps of this lengthy procedure are contained in Appendix (9). The result is for $n\neq 1/3$ (otherwise see Appendix 9)

$$B_2(\xi) = (\varepsilon_c)_0^{2-n}(1-\alpha)\,\frac{1-n}{n^3}\, g(\xi)^{\frac{1-n}{4n}} \left\{ \frac{1}{16}\left[\alpha\frac{17-21n}{1-3n}\left(1-g(\xi)^{\frac{1-3n}{2n}}\right)-\right.\right.$$

$$\left.\left.-\frac{17-n}{1-n}\left(1-g(\xi)^{\frac{1-n}{2n}}\right)\right] + \frac{7}{12}(1-\alpha)\right\}. \tag{4.118}$$

With $B_2(\xi)$ given by (4.118) the intermediate result for the 2nd order perturbation function $\overset{2}{\varepsilon}(\xi,\eta)$, Eq.(4.111), is almost completely defined when α_o/φ and $\alpha_2/3\varphi$ are given. With $(4.56)_{1\&4}$, (4.99), and $(4.100)_2$ one obtains

$$\frac{\alpha_o(\xi)}{\varphi} = -\frac{1}{\varphi}\left(\mu_R'\right)^{-2}\overset{0}{\varepsilon}_{\xi\xi} = -\frac{\overset{0}{\varepsilon}(\xi)^{1-n}}{n}\overset{0}{\varepsilon}_{\xi\xi} =$$

$$= -(\varepsilon_c)_0^{2-n}\frac{1}{n^3}\, g^{\frac{2-3n}{n}}(g-\alpha)(g-\alpha+n\alpha) \tag{4.119}$$

and

$$\frac{\alpha_2(\xi)}{3\varphi} = -\frac{1}{3\varphi}\,\Omega_R^2\,\frac{1}{2}(1-n)\frac{1}{\overset{0}{\varepsilon}(\xi)}B_1^2(\xi) = -(\varepsilon_c)_0^{2-n}\,\frac{1-n}{n^3}\,\frac{1}{6}(1-\alpha)^2\; g^{-\frac{1+n}{2n}}\,. \tag{4.120}$$

Finally we note, accounting for (4.117),

$$\sqrt{\varphi}\eta = \sqrt{\varphi}\,\frac{\mu_R(\xi)}{\beta} = \frac{1}{\beta}\left(\frac{n}{(\varepsilon_c)_0^{1-n}}\right)^{1/2} G(g(\xi);p). \tag{4.121}$$

Eq. (4.99), (4.108) or (4.110) and (4.111) together with (4.118) to (4.121) define the asymptotic perturbation solution

$$\varepsilon = \hat{\varepsilon}(\xi;\beta) = \tilde{\varepsilon}(\xi,\eta;\beta) = \overset{0}{\varepsilon}(\xi) + \beta\,\overset{1}{\varepsilon}(\xi,\eta) + \beta^2\,\overset{2}{\varepsilon}(\xi,\eta) \tag{4.122}$$

for the strain distribution in the exponentially tapered tensile rod. It is noted again that the integration constant φ cancels out in all terms. Thus, any finite value, preferably the value "one", may be attributed to φ.

For the special case n=1 we obtain

$$\left.\begin{aligned}
&\overset{0}{\varepsilon}(\xi) = (\varepsilon_c)_0\, g(\xi)\,, \quad (\varepsilon_c)_0 = \left(\frac{\sigma_R}{K}\right)_{\xi=0}\\
&\overset{1}{\varepsilon}(\xi,\eta) = -(1-\alpha)\,(\varepsilon_c)_0\, e^{-\sqrt{\varphi}\eta}\\
&\overset{2}{\varepsilon}(\xi,\eta) = -\frac{\alpha_o(\xi)}{\varphi} = (\varepsilon_c)_0(g-\alpha)\\
&\sqrt{\varphi}\eta = \frac{1}{\beta}\,\xi\,.
\end{aligned}\right\} \tag{4.123}$$

Thus

$$\varepsilon = (\varepsilon_c)_0\,[g(\xi) - \beta(1-\alpha)\,e^{-\xi/\beta} + \beta^2(g(\xi)-\alpha)] =$$

$$= (\varepsilon_c)_0\,[\alpha + (1-\alpha)\,e^{-\xi} - \beta(1-\alpha)\,e^{-\xi/\beta} + \beta^2(1-\alpha)\,e^{-\xi}]. \tag{4.124}$$

For the linear case (n=1) we can benefit from the luxury of the existence of the exact solution, Eq.(3.17). It is found that the asymptotic solution (4.124) and the exact solution agree exactly up to and including terms quadratic in β.

4.4 Evaluation

4.4.1 Second Order Perturbation Solution for Power Law Hardening without Cross-Section Reduction

To begin with attention is put to that part of the exponentially tapered rod where the non-classical 2nd order gradient term will have the largest effect, i.e. at the minimum cross-section where the maximum axial strain is produced and where gradients are largest. At $\xi = 0$, $\eta = 0$ the perturbation solution (4.122) reads

$$\varepsilon(0,0) = \overset{0}{\varepsilon}(0) + \beta \overset{1}{\varepsilon}(0,0) + \beta^2 \overset{2}{\varepsilon}(0,0) = \varepsilon_o \,. \tag{4.125}$$

With (4.99), (4.108) and (4.111) as well as (4.103), (4.106), (4.116), (4.119) and (4.120) we have

$$\left.\begin{aligned}
&\overset{0}{\varepsilon}(0) = \varepsilon_c(0) = \varepsilon_{co} \\
&\overset{1}{\varepsilon}(0,0) = B_1(0) = \left(\frac{\overset{0}{\varepsilon}{}^{1-n}}{n}\right)_0^{1/2} \left(\overset{0}{\varepsilon}_\xi\right)_0 \\
&\overset{2}{\varepsilon}(\xi,\eta) = B_2(0) - \frac{\alpha_o(0)}{\varphi} + \frac{\alpha_2(0)}{3\varphi} \\
&\quad = \frac{1}{4}\left(\frac{1}{n}\right)^2 \frac{1}{\left(\overset{0}{\varepsilon}\right)_0^n}\left[\frac{7}{3}n(1-n)\right]\left(\overset{0}{\varepsilon}_\xi\right)_0^2 + \frac{\left(\overset{0}{\varepsilon}\right)_0^{1-n}}{n}\left(\overset{0}{\varepsilon}_{\xi\xi}\right)_0 - \\
&\qquad - \frac{1}{6}(1-n)\frac{1}{\left(\overset{0}{\varepsilon}\right)_0} \frac{\left(\overset{0}{\varepsilon}\right)_0^{1-n}}{n}\left(\overset{0}{\varepsilon}_\xi\right)_0^2 \\
&\quad = \frac{\left(\overset{0}{\varepsilon}\right)_0^{1-n}}{n}\left(\overset{0}{\varepsilon}_{\xi\xi}\right)_0 + \frac{5}{12}\frac{1-n}{n}\frac{1}{\left(\overset{0}{\varepsilon}\right)_0^n}\left(\overset{0}{\varepsilon}_\xi\right)_0^2 \,.
\end{aligned}\right\} \tag{4.126}$$

Then the relative strain at the minimum cross-section is defined by the strain ratio $\varepsilon(0,0)/\,\varepsilon_{co}$ and is given by

$$\begin{aligned}
\frac{\varepsilon_o}{\varepsilon_{co}} = \frac{\varepsilon(0,0)}{\varepsilon_{co}} = 1 + \beta\left[\frac{1}{n\left(\overset{0}{\varepsilon}\right)_0^{1+n}}\right]^{1/2}\left(\overset{0}{\varepsilon}_\xi\right)_0 + \\
+ \beta^2\left[\frac{1}{n\left(\overset{0}{\varepsilon}\right)_0^{1+n}}\right]\left\{\left(\overset{0}{\varepsilon}_{\xi\xi}\right)_0\left(\overset{0}{\varepsilon}\right)_0 + \frac{5}{12}(1-n)\left(\overset{0}{\varepsilon}_\xi\right)_0^2\right\} \,.
\end{aligned} \tag{4.127}$$

Here it should be recalled that the 0th order approximation $\overset{0}{\varepsilon}(\xi)$ is equal to the classical solution $\varepsilon_c(\xi)$, i.e.

$$\overset{0}{\varepsilon}(\xi) = \varepsilon_c(\xi) = \left(\frac{\sigma_R(\xi)}{K} \right)^{1/n}, \qquad \sigma_R(\xi) = \frac{P}{A_R(\xi)} . \tag{4.128}$$

Recalling the analysis, it is noted that the result (4.127) is generally valid independent of the specific cross-section variation along the rod, except obeying the symmetry with respect to ξ=0 and uniformity for $X \to \infty$.

It is noteworthy that the relative strain is determined, among others, by the 1st and not only by the 2nd order spatial derivative of the classical solution $\varepsilon_c(\xi)$ at ξ=0. If the cross-section variation $A_R(\xi)$ is smooth at ξ=0, i.e.

$$(A_R')_{\xi=0} = 0 , \tag{4.129}$$

then

$$\left(\varepsilon_{c\xi}\right)_{\xi=0} = \left(\overset{0}{\varepsilon}_{\xi} \right)_0 = 0 \tag{4.130}$$

and the term linear in the parameter β drops out in Eq.(4.127). Thus, the relative strain and the 2nd order strain gradient contribution is only quadratically depending on the length ratio β:

$$\frac{\varepsilon_o}{\varepsilon_{co}} = \frac{\varepsilon(0,0)}{\varepsilon_{co}} = 1 + \beta^2 \left[\frac{1}{n\left(\overset{0}{\varepsilon}\right)_0^{1+n}} \right] \left\{ \left(\overset{0}{\varepsilon}_{\xi\xi} \right)_0 \left(\overset{0}{\varepsilon}\right)_0 \right\}$$

$$= 1 + \beta^2 \frac{\left(\overset{0}{\varepsilon}_{\xi\xi} \right)_0}{n\left(\overset{0}{\varepsilon}\right)_0^{n}} . \tag{4.131}$$

This reflects the quadratic dependence of the constitutive equation (4.1) on the internal length l_i. Thus, a 1st order dependence of the relative strain on β is induced only by the non-smoothness of the stress-distribution. For the case of a smoothly tapered rod with a neck at ξ=0, the classical strain distribution $\varepsilon_c(\xi) = \overset{0}{\varepsilon}(\xi)$ has a relative maximum at ξ=0 such that

$$\left(\overset{0}{\varepsilon}_{\xi} \right)_0 = 0 , \qquad \left(\overset{0}{\varepsilon}_{\xi\xi} \right)_0 < 0 .$$

Thus, Eq.(4.131) reads

$$\frac{\varepsilon_o}{\varepsilon_{co}} = \frac{\varepsilon(0,0)}{\varepsilon_{co}} = 1 - \beta^2 \frac{\left|\left(\varepsilon_{c\xi\xi}\right)_0\right|}{n\varepsilon_{co}^n} ; \tag{4.132}$$

obviously the 2nd order strain gradient term implies a reduction of the maximum strain $\varepsilon(0,0)$ of the non-classical solution.

The expression (4.132) can be put in a more lucid form, which allows further interpretation and easy determination of the internal length scale l_i using two scaled thought-experiments with smoothly necked specimens.

With (4.128) one obtains

$$\overset{0}{\varepsilon}_{\xi} = -\left(\frac{P}{K}\right)^{1/n} \frac{1}{n} A_R^{-(1+n)/n} A_R' = -\left(\frac{\sigma_R}{K}\right)^{1/n} \frac{1}{n} \frac{A_R'}{A_R} , \tag{4.133}$$

where

$$\left.\begin{aligned} A_R &= \frac{\pi}{4}[D(\xi)]^2 \\ A_R' &= \frac{dA_R}{d\xi} = \frac{\pi}{2} DD' ; \end{aligned}\right\} \tag{4.134}$$

then

$$\begin{aligned} \overset{0}{\varepsilon}_{\xi\xi} &= -\left(\frac{P}{K}\right)^{1/n} \frac{1}{n}\left\{A_R^{-(1+n)/n} A_R'' - \frac{1+n}{n} A_R^{-(1+2n)/n} (A_R')^2\right\} \\ &= -\left(\frac{\sigma_R}{K}\right)^{1/n} \frac{1}{n}\left\{\frac{A_R''}{A_R} - \frac{1+n}{n}\left(\frac{A_R'}{A_R}\right)^2\right\}, \end{aligned} \tag{4.135}$$

where

$$A_R'' = \frac{\pi}{2}\left[DD'' + (D')^2\right] .$$

With (4.129) one gets

$$(A_R'')_0 = \frac{\pi}{2}(DD'')_0 = 2\pi\left(\frac{D}{2}\right)_0\left(\frac{D''}{2}\right)_0 , \tag{4.136}$$

where $D/2$ is the radius of the circular rod.

The radius R_o of curvature of the meridional profile at the minimum section (ξ=0) is given by

$$R_o = \frac{1}{\left(\frac{d^2(D/2)}{dX^2}\right)} = \frac{(L^*)^2}{\left(\frac{D''}{2}\right)_0} \tag{4.137}$$

where (4.6) is observed. Thus

$$(A_R'')_0 = \pi D_o \frac{(L^*)^2}{R_o}$$

and with (4.128), (4.134) and (4.135)

$$\left(\overset{0}{\varepsilon}_{\xi\xi}\right)_0 = -\left(\frac{\sigma_{Ro}}{K}\right)^{1/n} \frac{4}{n} \frac{(L^*)^2}{D_o R_o}. \tag{4.138}$$

Finally (4.132) takes the form

$$\frac{\varepsilon(0,0)}{\varepsilon_{co}} = 1 - \beta^2 \frac{1}{n(\sigma_{R0}/K)} \left(\frac{\sigma_{Ro}}{K}\right)^{1/n} \frac{4}{n} \frac{(L^*)^2}{D_o R_o}$$

$$= 1 - (l_i)^2 \left(\frac{\sigma_{Ro}}{K}\right)^{\frac{1-n}{n}} \frac{4}{n^2} \frac{1}{D_o R_o}\ ; \tag{4.139}$$

here σ_{Ro} is the stress at the minimum cross-section. Eq.(4.139) shows that the relative strain reduction due to the 2nd order strain gradient plasticity, given by

$$\frac{\varepsilon_{co} - \varepsilon(0,0)}{\varepsilon_{co}} = \left(\frac{\sigma_{Ro}}{K}\right)^{\frac{1-n}{n}} \frac{4}{n^2} \left(\frac{l_i}{D_o}\right)\left(\frac{l_i}{R_o}\right)$$

$$= (\varepsilon_{co})^{1-n} \frac{4}{n^2} \left(\frac{l_i}{D_o}\right)\left(\frac{l_i}{R_o}\right), \tag{4.140}$$

depends non-linearly on the stress level σ_{Ro} or the classical strain level ε_{co} and is proportional to the length ratios l_i/D_o and l_i/R_o. D_o and R_o represent the minimum characteristic dimensions of the rod. Thus, the result (4.140) demonstrates that the internal length scale l_i in relation to the minimum geometrical length scales determines the gradient effect. Here the ratio l_i/R_o is of special importance since for very uniform necks, i.e. R_o/D_o very large, the gradient effect vanishes.

From Eq.(4.140) the influence of the increasing non-linearity, i.e. $n \to 0$, can be derived under different assumptions. Decreasing the hardening exponent n but holding all other parameters constant, especially the intermediate variable 'non-classical strain' ε_{co} = const., implies that the normalized stress σ_{Ro}/K increases according to

$$\frac{\sigma_{Ro}}{K} = \varepsilon_{co}^{n}\ , \qquad \varepsilon_{co} = \text{const.}$$

With this assumption and depending on the strain level ε_{co}, the relative strain reduction $(4.140)_2$ decreases and after passing through a minimum increases beyond bounds when the hardening exponent approaches very small values.

On the other hand, if not the strain ε_{co} but the nominal stress σ_{Ro} is held constant, i.e. σ_{Ro}=const., a quantity which really can be controlled, then Eq.(4.140)$_1$ applies. Fig.4.1 shows the relative strain reduction versus n; it demonstrates the presence of a maximum for the relative strain reduction (or minimum for the relative strain) which suggests the interaction of two opposing effects. An interpretation can be given as follows. Eq.(4.132) can be transformed to read

$$\frac{\varepsilon(0,0)}{\varepsilon_{co}} = 1 - \beta^2 \frac{1}{n} \varepsilon_{co}^{1-n} \left| \frac{\left(\varepsilon_{c\xi\xi}\right)_0}{\varepsilon_{co}} \right|$$

$$= 1 - \beta^2 \frac{1}{n} \left(\frac{\sigma_{Ro}}{K} \right)^{\frac{1-n}{n}} \left| \frac{\left(\varepsilon_{c\xi\xi}\right)_0}{\varepsilon_{co}} \right| ; \qquad (4.141)$$

With (4.128) and (4.135) the magnitude of normalized 2nd order derivative of the classical strain for a smooth neck is defined as

$$\left| \frac{\left(\varepsilon_{c\xi\xi}\right)_0}{\varepsilon_{co}} \right| = \frac{1}{n} \left\{ \frac{A_R''}{A_R} \right\}_0 . \qquad (4.142)$$

This quantity is a relative measure for the non-uniformity of the classical strain distribution around $\xi = 0$; it depends only on the local geometry and the hardening exponent n but not on the strain or load level. For decreasing n-value it increases monotonously beyond bounds at $n = 0$. This implies that a 'relative localization' of the plastic deformation occurs with decreasing hardening exponent.

The term $1/n$ in Eq.(4.141) has a similar dependence on n as the normalized 2nd order strain gradient $\left|\left(\varepsilon_{c\xi\xi}\right)_0 / \varepsilon_{co}\right|$. The strain or stress dependence is solely contained in the term

$$\varepsilon_{co}^{1-n} = \left(\frac{\sigma_{Ro}}{K} \right)^{\frac{1-n}{n}} , \qquad \frac{\sigma_{Ro}}{K} < 1;$$

its dependence on the hardening exponent n is determined whether the strain ε_{co} is held constant or whether the normalized stress σ_{Ro}/K is fixed. In the first case it decreases monotonously with decreasing n and it remains between the finite bounds 1 and ε_{co}. In the second case the term

$$\left(\frac{\sigma_{Ro}}{K} \right)^{\frac{1-n}{n}} = \varepsilon_{co} \Big/ \left(\frac{\sigma_{Ro}}{K} \right) \qquad \frac{\sigma_{Ro}}{K} = \text{const.} < 1$$

also decreases monotonously with decreasing n within the bounds 1 and 0. This is contrary to the dependency of the other terms in Eq.(4.141) and explains the existence of an extremum in the relative strain reduction when the hardening exponent n is changed. Under the constant strain assumption a minimum for the relative strain reduction is obtained but for the constant stress case a maximum is found.

We consider two geometrically similar specimens of different sizes made of the same material under scaled loading. The large specimen is denoted by the subscript p (prototype) and the small specimen by m (model). The geometric scale factor is

$$\lambda = \frac{(D_o)_p}{(D_o)_m} = \frac{(R_o)_p}{(R_o)_m} > 1$$

and the scaling of the loading implies

$$(\sigma_{Ro})_p = (\sigma_{Ro})_m = \sigma_{Ro} \,. \tag{4.143}$$

Then, taking the ratio of (4.139) for specimen p and m, this yields

$$\frac{[\varepsilon(0,0)]_p}{[\varepsilon(0,0)]_m} = \frac{1-\left(\frac{\sigma_{Ro}}{K}\right)^{\frac{1-n}{n}} \frac{4}{n^2} \frac{(l_i)^2}{(D_o R_o)_p}}{1-\left(\frac{\sigma_{Ro}}{K}\right)^{\frac{1-n}{n}} \frac{4}{n^2} \frac{(l_i)^2}{(D_o R_o)_m}} \,. \tag{4.144}$$

We consider the quantities $[\varepsilon(0,0)]_p$ and $[\varepsilon(0,0)]_m$ to be measured with the property

$$[\varepsilon(0,0)]_p > [\varepsilon(0,0)]_m \,.$$

Solving (4.142) for $(l_i)^2$, one gets

$$(l_i)^2 = \frac{\frac{[\varepsilon(0,0)]_p}{[\varepsilon(0,0)]_m} - 1}{\frac{[\varepsilon(0,0)]_p}{[\varepsilon(0,0)]_m} - \frac{1}{\lambda^2}} \frac{n^2}{4} \frac{(D_o R_o)_m}{\left(\frac{\sigma_{Ro}}{K}\right)^{\frac{1-n}{n}}} \,. \tag{4.145}$$

In principle this equation represents a possibility to determine the internal length l_i using two scaled tension experiments of smoothly necked specimens in the range of small strains when the cross-section reduction due to plastic deformation is still small. If this gradient theory is truly the appropriate model to describe the observed size effect, then another pair of differently sized tension specimens of the same material should yield the same internal length l_i. This is a necessary check of the usefulness of the model.

Returning to the exponentially tapered rod with a sharp neck, the classical solution for the strain distribution is given by (4.93) where (4.95) defines $g(\xi)$. With (4.99), (4.100) and $g(0)=1$ one gets

$$\left.\begin{aligned}
\left(\overset{0}{\varepsilon}\right)_0 &= \varepsilon_{co} = \left(\frac{\sigma_{Ro}}{K}\right)^{1/n} \\
\left(\overset{0}{\varepsilon_\xi}\right)_0 &= -\frac{\varepsilon_{co}}{n}(1-\alpha) \\
\left(\overset{0}{\varepsilon_{\xi\xi}}\right)_0 &= \frac{\varepsilon_{co}}{n}\left\{\frac{1-n}{n}(1-\alpha)^2 + (1-\alpha)\right\}
\end{aligned}\right\} \qquad (4.146)$$

and (4.127) takes the following explicit form

$$\frac{\varepsilon_o}{\varepsilon_{co}} = \frac{\varepsilon(0,0)}{\varepsilon_{co}} = 1 - \beta\left(\frac{\varepsilon_{co}^{1-n}}{n}\right)^{1/2}\frac{1-\alpha}{n} + \\ + \beta^2\left(\frac{\varepsilon_{co}^{1-n}}{n}\right)\left(\frac{1-\alpha}{n}\right)^2\left[\frac{17}{12}(1-n) + \frac{n}{1-\alpha}\right]. \qquad (4.147)$$

For the linear case n=1 the relative strain (4.147) simplifies considerably:

$$\frac{\varepsilon_o}{\varepsilon_{co}} = 1 - \beta(1-\alpha) + \beta^2(1-\alpha). \qquad (4.148)$$

The exact ratio for n=1 is given by (3.22)

$$\frac{\varepsilon_o}{\varepsilon_{co}} = \frac{1+\alpha\beta}{1+\beta}, \qquad (4.149)$$

which is, in contrast to the perturbation solution (4.148), a monotonously decreasing function of β for all values $\beta < 1$. The graphs of the approximate and the exact solution for n=1 are shown in Fig.4.2 for the three values of α = 0.0625, 0.25 and 0.5625. Agreement within less than 10% overestimation is found up to β = 0.275. For larger values of β the parabolic character of the asymptotic solution becomes dominant and strongly erroneous: after passing a minimum at β = 0.5 the relative strain of the asymptotic solution increases with β.

It is evident that for sufficiently small values of β the dominant term in (4.147) and (4.148) is linear in β. Its negative sign signals a decrease of the maximum strain at ξ=0. This implies an apparent strengthening of a specimen when its size is reduced: for large sizes β tends to 'zero' and the maximum strain $\varepsilon(0,0)$ approaches ε_{co}, the classical solution; for a reduced size, such that β is finite but small, $\varepsilon(0,0)$ becomes less than ε_{co}. It is noteworthy that the relative strain $\varepsilon(0,0)/\varepsilon_{co}$ of the fully linear problem, Eq.(4.148) or (4.149), does not depend on the load level or equivalently on the classical strain level ε_{co} whereas the consideration of the power law strain hardening (n<1) induces a strong dependence on the loading level σ_{Ro}, possibly defined by ε_{co}, Eq.(4.128), and on the power law exponent n, Eq.(4.147).

The influence of increasing non-linearity, i.e. $n \to 0$, on the relative strain $\varepsilon(0,0)/\varepsilon_{co}$ can be made evident as follows. The general perturbation solution (4.127) shows that this ratio

does not only depend on the classical strain level ε_{co} but also on the 1st and 2nd order spatial derivatives $(\varepsilon_{c\xi})_0$ and $(\varepsilon_{c\xi\xi})_0$ at ξ=0. Increasing the degree of non-linearity by decreasing n to small values but simultaneously increasing the load level σ_{Ro} such that

$$\varepsilon_{co} = \left(\overset{0}{\varepsilon}\right)_0 = \left(\frac{\sigma_{Ro}}{K}\right)^{1/n} = \text{const.} \qquad \frac{\sigma_{Ro}}{K} < 1 ,$$

yields an increase of the magnitude of the 1st and 2nd order derivative, Eq.$(4.133)_2$ and $(4.135)_2$. This corresponds to a shift of the plastic deformation distribution towards the center of the tension rod at ξ=0. This localization of the deformation, generated by a decreased hardening exponent n and an increased stress σ_{Ro}/K such that ε_{co}=const., increases the non-uniformity of the strain distribution which enhances the strain gradient influence. The localization as well as the intensified gradient effect are illustrated in Fig.4.3a & b. The influence of the gradient term is more readily seen in Fig.4.4a & b; obviously it is restricted to a boundary layer at ξ=0 for small values of β. These graphs are based on the full perturbation solution Eq.(4.122) together with the integral function $G(g(\xi); p)$ (Table A8.2).

To illustrate the influence of the various quantities, the relative strain $\varepsilon(0,0)/\varepsilon_{co}$ is plotted versus the normalized strain gradient coefficient β ($\beta \le 0.15$) for the exponents n=1, 1/3, 1/5, 1/9, 1/13 and for fixed values of the classical strain level, i.e. ε_{co}=0.01, 0.05, 0.1, 0.15, 0.3 and α = 0.81, 0.64, 0.5625, 0.25, the initial cross section ratio $A_{Ro}/A_{R\infty}$ (Fig.4.5a & b). For the variation of β in the interval $0 \le \beta \le 0.15$ the parabolic character of the curves is seen for some of the parameters and here the 2nd order approximate perturbation solution is clearly not sufficiently accurate. Therefore, expanded graphs with β restricted to smaller values in the interval $0 \le \beta \le 0.04$ are also shown (Fig.4.6a & b). Fig.4.5 & 4.6 also reveal that the increase of the parameters ε_{co}, n and α reduce the range of β-values where the quadratic perturbation solution is an acceptable approximation.

From these figures the following trends are obvious: increasing the degree of non-linearity (decrease of n), with the strain ε_{co} and parameters held constant or with an increase of the strain level ε_{co} as well as the degree of tapering (decrease of α), the sensitivity 'S' of the strain ratio $\varepsilon(0,0)/\varepsilon_{co}$ with respect to β rises. Mathematically 'S' is simply given by the magnitude of the derivative

$$S := \left|\frac{d[\varepsilon(0,0)/\varepsilon_{co}]}{d\beta}\right|_{\beta\to 0} = \left|\left[\frac{1}{n\left(\overset{0}{\varepsilon}\right)_0^{1+n}}\right]^{1/2}\left(\overset{0}{\varepsilon}_{\xi}\right)_0\right|$$

$$= \frac{1}{n^{1/2}}\left[\left(\overset{0}{\varepsilon}\right)_0\right]^{\frac{1-n}{2}}\left|\frac{\left(\overset{0}{\varepsilon}_{\xi}\right)_0}{\left(\overset{0}{\varepsilon}\right)_0}\right| = \frac{1}{n^{1/2}}\left(\frac{\sigma_{Ro}}{K}\right)^{\frac{1-n}{2n}}\left|\frac{\left(\overset{0}{\varepsilon}_{\xi}\right)_0}{\left(\overset{0}{\varepsilon}\right)_0}\right|$$

$$= \frac{1}{n^{1/2}}\left[\left(\overset{0}{\varepsilon}\right)_0\right]^{\frac{1-n}{2}}\frac{(1-\alpha)}{n} = \frac{1}{n^{1/2}}\left(\frac{\sigma_{Ro}}{K}\right)^{\frac{1-n}{2n}}\frac{(1-\alpha)}{n} , \qquad (4.150)$$

where the right-hand sides follow from Eq.(4.127) and (4.147). A more detailed analysis laid open that for small constant values of ε_{co} in Eq.(4.150)$_4$ the sensitivity S first decreases, passes through a minimum, and then increases beyond bounds for small n-values when the hardening exponent n is decreased. If, however, n is decreased and the stress level σ_{Ro}/K and the tapering α are held constant, then Eq.(4.150)$_5$ applies. Fig.4.7 shows a plot of S versus n ($\sigma_{Ro}/K = 0.3$, 0.5, 0.7 and $\alpha = 0.0625$) revealing a maximum of the sensitivity; this is qualitatively similar to n-dependence of the relative strain reduction of a tensile specimen with a smooth neck (Fig.4.1). Also the explanation, relating this to two opposing effects, is similar: the normalized strain gradient, obtained from Eq.(4.133),

$$\left|\frac{\left(\overset{0}{\varepsilon_\xi}\right)_0}{\left(\overset{0}{\varepsilon}\right)_0}\right| = \left|\frac{\left(\varepsilon_{c\xi}\right)_0}{\varepsilon_{co}}\right| = \frac{1}{n}\left\{\frac{A_R'}{A_R}\right\}_0 = \frac{1-\alpha}{n},$$

is independent of the strain or stress level and increases with decreasing hardening exponent n. This increase represents a 'relative localization' of the plastic deformation. On the other hand the term

$$\left(\frac{\sigma_{Ro}}{K}\right)^{\frac{1-n}{2n}} = \left[\varepsilon_{co}\Big/\left(\frac{\sigma_{Ro}}{K}\right)\right]^{1/2}, \qquad \frac{\sigma_{Ro}}{K} = \text{const.} < 1$$

decreases with decreasing n under constant normalized stress σ_{Ro}/K since ε_{co} diminishes towards zero. These opposing effects are responsible for the maximum of the sensitivity. Since βS is the dominant term determining the relative strain, this peculiar behavior is also seen in the dependence of the relative strain on the hardening exponent for $\sigma_{Ro}/K = \text{const}$.

The validity of the graphs in Fig.4.5, 4.6 & 4.7 is actually restricted to small stress levels or strains ε_{co} since the geometric non-linearity due to the reduction of the cross-section by the plastic deformation is not accounted for. Therefore, the graphs for ε_{co}=0.15 and 0.3, which correspond to 15% and 30% strain at ξ=0 of the classical strain distribution, have a rather limited validity and require an improved model.

It should be recalled that the normalized strain gradient parameter $\beta = l_i/L^*$ is inversely proportional to a characteristic geometric dimension L^*, the transition length of the specimen. For geometrically similar specimens this is a measure for the specimen size. Thus, Fig.4.5 & 4.6 map the size influence on the relative strain: very large specimens correspond to $\beta \approx 0$ and thus $\varepsilon(0,0)/\varepsilon_{co} \approx 1$; decreasing the size considerably, a noticeable decrease of the relative strain is seen. For example, if α=0.5625[5], n=1/9[6], β=0.004 and ε_{co}=0.05 one gets from Fig.4.6b about $\varepsilon(0,0)/\varepsilon_{co}$=0.9883; decreasing the specimen size in all dimensions by a factor of 10 and scaling the loading such that the stress σ_{Ro} remains constant (or equivalently holding ε_{co} constant), one obtains $\beta = 0.04$ and the corresponding relative strain is $\varepsilon(0,0)/\varepsilon_{co}$=0.898. Thus, the maximum strain, which is affected by 2nd order gradient plasticity, reduces by about

$$\frac{0.9883 - 0.898}{0.9883} 100 = 9.1\%.$$

[5] $\alpha = 0.64$ corresponds to a 20% difference between the maximum and minimum diameter of the specimen.

[6] n=1/9 corresponds roughly to the hardening exponent of the ferritic reactor vessel steel A533-B at 93^{0}C (see Table 5.2).

The 1st order approximation $S\beta$, based on the sensitivity S, Eq.(4.148), yields a value of 11.37%.

Obviously, larger effects can be obtained by an increase of the stress σ_{Ro} or the strain ε_{co}, respectively and by reducing α. From Fig.4.5a & b one estimates that the difference in the maximum strains may possibly become about 20%.

4.4.2 Second Order Perturbation Solution for Power Law Hardening with Cross-Section Reduction: The Fully Non-Linear Problem

We recall that the distribution of the classical logarithmic strain $\varepsilon_c(\xi)$ is the solution of Eq.(4.13), i.e.

$$[\varepsilon_c(\xi)]^n = \frac{\sigma_R(\xi)}{K} e^{\varepsilon_c(\xi)} \quad ; \tag{4.151}$$

it corresponds to the 0th order approximation of the perturbation solution:

$$\varepsilon_c(\xi) = \overset{0}{\varepsilon}(\xi) . \tag{4.152}$$

However, an explicit analytical representation of $\varepsilon_c(\xi)$ in terms of $\sigma_R(\xi)$ is not available. The approximate perturbation solution for the non-classical logarithmic strain distribution is given by (4.91) which requires the integration of Eq.(4.73) and (4.88) to get the $\mu(\xi)$-function and the $B_2(\xi)$-function. In general this can be done only numerically. It is not the intention in this report to get involved into this numerical analysis to obtain the actual strain distribution in the boundary layer. Instead, attention is put to the most important question, i.e. the gradient effect on the maximum strain at $\xi=0$ in relation to the maximum classical strain ε_{co}. This information can be obtained from the results of Section 4.3.2 without the mentioned integrations as follows.

From (4.91) one gets at $\xi=0$, $\eta=0$

$$\varepsilon(0,0) = \overset{0}{\varepsilon}(0) + \beta \overset{1}{\varepsilon}(0,0) + \beta^2 \overset{2}{\varepsilon}(0,0) = \varepsilon_o . \tag{4.153}$$

With (4.79) and (4.81) one obtains

$$\left.\begin{aligned} &\overset{0}{\varepsilon}(0) = \varepsilon_c(0) = \varepsilon_{co} \\ &\overset{1}{\varepsilon}(0,0) = B_1(0) = \left(\frac{\overset{0}{\varepsilon}{}^{1-n}}{n - \overset{0}{\underset{=}{\varepsilon}}} \right)_0^{1/2} \left(\overset{0}{\varepsilon}_\xi \right)_0 \\ &\overset{2}{\varepsilon}(0,0) = B_2(0) - \frac{\alpha_o(0)}{\varphi} + \frac{\alpha_2^*(0)}{3\varphi} \end{aligned}\right\} \tag{4.154}$$

where, observing (4.90), $(4.56)_1$ (4.57) and (4.72),

$$
\left.
\begin{aligned}
B_2(0) &= \frac{1}{4}\left(n-\underset{===}{\overset{0}{(\varepsilon)}_0}\right)^{-2}\left(\overset{0}{\varepsilon}\right)_0^{-n}\left[\frac{7}{3}n(1-n)+\underset{====}{n\left(\overset{0}{\varepsilon}\right)_0}+\underset{====}{\frac{4}{3}\left(\overset{0}{\varepsilon}\right)_0^2}\right]\left(\overset{0}{\varepsilon}_\xi\right)_0^2 \\
\frac{\alpha_o(0)}{\varphi} &= -\frac{1}{\varphi}(\mu')_0^{-2}\left(\overset{0}{\varepsilon}_{\xi\xi}\right)_0 = -\frac{\overset{0}{(\varepsilon)}_0^{1-n}}{n-\underset{====}{\overset{0}{(\varepsilon)}_0}}\left(\overset{0}{\varepsilon}_{\xi\xi}\right)_0 \\
\frac{\alpha_2^*(0)}{3\varphi} &= -\frac{1}{3\varphi}\left[\frac{(1-n)}{\overset{0}{\varepsilon}}+\underset{=}{\frac{\overset{0}{\varepsilon}}{n}}\right]_0\frac{1}{2}\left(\Omega_R^2 B_1^2\right)_0
\end{aligned}
\right\} \quad (4.155)
$$

and with $(4.39)_2$ and (4.72) one finds

$$
\left(\Omega_R^2\right)_0 = \left[\frac{n}{\overset{0}{\varepsilon}}\frac{\overset{0}{(\varepsilon)^n}}{(\mu')^2}\right]_0 = \left[\frac{n}{\overset{0}{\varepsilon}^{1-n}}\frac{\overset{0}{\varepsilon}^{1-n}}{n-\underset{=}{\overset{0}{\varepsilon}}}\varphi\right]_0 = \frac{n\varphi}{n-\underset{===}{\overset{0}{(\varepsilon)}_0}} . \qquad (4.156)
$$

Inserting (4.155) and (4.156) into $(4.154)_3$ yields

$$
\overset{2}{\varepsilon}(0,0) = \frac{\overset{0}{(\varepsilon)}_0^{1-n}}{n-\underset{====}{\overset{0}{(\varepsilon)}_0}}\left(\overset{0}{\varepsilon}_{\xi\xi}\right)_0 + \left(n-\underset{===}{\overset{0}{(\varepsilon)}_0}\right)^{-2}\left(\overset{0}{\varepsilon}\right)_0^{-n}\left(\overset{0}{\varepsilon}_\xi\right)_0^2\left[\frac{5}{12}n(1-n)+\underset{=====}{\frac{n}{4}\overset{0}{(\varepsilon)}_0}+\underset{=====}{\frac{1}{6}\overset{0}{(\varepsilon)}_0^2}\right] \qquad (4.157)
$$

and the relative strain is

$$
\begin{aligned}
\frac{\varepsilon_o}{\varepsilon_{co}} &= 1+\beta\left\{\left[n-\underset{===}{\overset{0}{(\varepsilon)}_0}\right]\overset{0}{(\varepsilon)}_0^{1+n}\right\}^{-1/2}\left(\overset{0}{\varepsilon}_\xi\right)_0 + \\
&+\beta^2\left(\left[n-\underset{===}{\overset{0}{(\varepsilon)}_0}\right]\overset{0}{(\varepsilon)}_0^{1+n}\right)^{-1}\left\{\left(\overset{0}{\varepsilon}_{\xi\xi}\right)_0\overset{0}{(\varepsilon)}_0 + \right. \\
&\left. +\left(\overset{0}{\varepsilon}_\xi\right)_0^2\left(n-\underset{===}{\overset{0}{(\varepsilon)}_0}\right)^{-1}\left[\frac{5}{12}n(1-n)+\underset{=====}{\frac{n}{4}\overset{0}{(\varepsilon)}_0}+\underset{=====}{\frac{1}{6}\overset{0}{(\varepsilon)}_0^2}\right]\right\} .
\end{aligned} \qquad (4.158)
$$

The underlined terms in the above equations are due to the allowance for the cross-section reduction. If they are set equal to zero in Eq.(4.154) to (4.157) and especially (4.158), the small strain results of Section 4.4.1 are obtained again.

It is noted that the expression $[n-(\overset{0}{\varepsilon})_0]$ instead of n appears in the denominator. Recalling the analysis in Section 4.2, the logarithmic strain $\varepsilon_{co}=(\overset{0}{\varepsilon})_o$ is approaching the value n, the point of instability, with increasing engineering stress σ_{Ro} and the derivatives

$$(\varepsilon_{c\xi})_0 = \left(\overset{0}{\varepsilon}_{\xi}\right)_0 , \qquad (\varepsilon_{c\xi\xi})_0 = \left(\overset{0}{\varepsilon}_{\xi\xi}\right)_0 \tag{4.159}$$

become unbounded (Section 4.2.2). Therefore, the 1st and 2nd order terms $\overset{1}{\varepsilon}(0,0)$ and $\overset{2}{\varepsilon}(0,0)$, Eq.(4.154)$_2$ and (4.157), and thus (4.158) grow beyond limits when instability is approached. Consequently, this perturbation solution is not valid close to the critical state $\varepsilon_{co} = n$.

With Section 4.2.2 one has

$$\left.\begin{aligned} \left(\overset{0}{\varepsilon}_{\xi}\right)_0 &= (\varepsilon_{c\xi})_0 = \frac{(\sigma'_R)_0}{\sigma_{Ro}} \underline{\underline{\frac{\varepsilon_{co}}{n-\varepsilon_{co}}}} \\ \left(\overset{0}{\varepsilon}_{\xi\xi}\right)_0 &= (\varepsilon_{c\xi\xi})_0 = \underline{\underline{\frac{\varepsilon_{co}}{(n-\varepsilon_{co})^3}}} \left\{ \underline{\underline{\left[(\ln\sigma_R)''\right]_0 (n-\varepsilon_{co})^2}} + \left[(\ln\sigma_R)'\right]_0^2 n \right\} , \end{aligned}\right\} \tag{4.160}$$

where

$$\left.\begin{aligned} \left(\frac{\sigma'_R}{\sigma_R}\right)_0 &= \left[(\ln\sigma_R)'\right]_0 = -\left(\frac{A'_R}{A_R}\right)_0 \\ \left[(\ln\sigma_R)''\right]_0 &= -\left(\frac{A''_R}{A_R} - \frac{(A'_R)^2}{A_R^2}\right)_0 . \end{aligned}\right\} \tag{4.161}$$

With (4.161) the derivatives (4.160) are determined by the initial geometry of the rod at ξ=0, the strain level ε_{co}, and especially the difference $(n-\varepsilon_{co})$. Then this applies also to the relative strain (4.158). Thus, it follows that the consideration of geometric non-linearity by accounting for the cross-section reduction intensifies the gradient effect.

For the exponentially tapered tensile rod the above expressions are now put in an explicit form. The undeformed cross-section $A_R(\xi)$ is given by

$$A_R(\xi) = A_o[g(\xi)]^{-1} = A_o[\alpha + (1-\alpha)\ e^{-\xi}]^{-1}, \tag{4.162}$$

such that

$$\left.\begin{aligned} A_R' &= A_o(1-\alpha)e^{-\xi}[\alpha+(1-\alpha)\ e^{-\xi}]^{-2} \\ A_R'' &= -A_o(1-\alpha)e^{-\xi}[\alpha-(1-\alpha)\ e^{-\xi}][\alpha+(1-\alpha)\ e^{-\xi}]^{-3} \end{aligned}\right\} \quad (4.163)$$

and thus

$$\left.\begin{aligned} \left(\frac{\sigma_R'}{\sigma_R}\right)_0 &= \left[(\ln\sigma_R)'\right]_0 = -(1-\alpha) \\ \left[(\ln\sigma_R)''\right]_0 &= \alpha(1-\alpha)\,. \end{aligned}\right\} \quad (4.164)$$

With (4.152) and results of Section 4.2.2 one gets for the spatial derivatives of $\overset{0}{\varepsilon}(\xi)$

$$\left.\begin{aligned} \left(\overset{0}{\varepsilon}_{\xi}\right)_0 &= -(1-\alpha)\frac{(\overset{0}{\varepsilon})_0}{n-(\overset{0}{\varepsilon})_0} \\ &\quad ===\\ \left(\overset{0}{\varepsilon}_{\xi\xi}\right)_0 &= \frac{(\overset{0}{\varepsilon})_0}{(n-(\overset{0}{\varepsilon})_0)^3}\left\{(1-\alpha)\alpha\left(n-(\overset{0}{\varepsilon})_0\right)^2 + (1-\alpha)^2\ n\right\}. \\ &\quad == \quad == \end{aligned}\right\} \quad (4.165)$$

Dropping the underlined terms, which are induced by the cross-section reduction, yields the previous result (4.146). Inserting (4.165) into (4.158) gives finally

$$\frac{\varepsilon_o}{\varepsilon_{co}} = 1-\beta\left[\frac{(\overset{0}{\varepsilon})_0^{1-n}}{n-(\overset{0}{\varepsilon})_0}\right]^{1/2}\frac{1-\alpha}{n-(\overset{0}{\varepsilon})_0} + \\ == \quad ==$$

$$+\beta^2\frac{(\overset{0}{\varepsilon})_0^{1-n}}{n-(\overset{0}{\varepsilon})_0}\left[\frac{1-\alpha}{n-(\overset{0}{\varepsilon})_0}\right]^2\frac{1}{n-(\overset{0}{\varepsilon})_0}\left\{\frac{\alpha}{1-\alpha}\left(n-(\overset{0}{\varepsilon})_0\right)^2+n\right. \\ == \quad == \quad ==$$

$$\left.+\frac{5}{12}n(1-n)+\underline{\frac{n}{4}(\overset{0}{\varepsilon})_0}+\underline{\frac{1}{6}(\overset{0}{\varepsilon})_0^2}\right\}. \quad (4.166) \\ ===== \quad =====$$

Of course, deleting the underlined terms again gives the relation (4.147) after some rearrangement. Eq.(4.166) allows to define the sensitivity 'S' of the β-dependence of the relative logarithmic strain analogous to Eq.$(4.150)_1$:

$$S = \left| \frac{d[\varepsilon(0,0)/\varepsilon_{co}]}{d\beta} \right|_{\beta \to 0} = \left(\frac{\varepsilon_{co}^{1-n}}{n - \varepsilon_{co}} \right)^{1/2} \frac{1-\alpha}{n-\varepsilon_{co}} \,. \tag{4.167}$$

It is recalled that the strain level ε_{co} should be definitely less than the critical strain, the hardening exponent n, such that the perturbation solution remains approximately valid. Therefore, it appears reasonable to consider the case where ε_{co} takes only a constant fraction $z<1$ of the critical strain, i.e.

$$\varepsilon_{co} = z\, n.$$

This coupling of ε_{co} and n allows to put (4.167) into the following form

$$S = ZN(1-\alpha)\,, \tag{4.168}$$

where the definitions

$$Z = \frac{z^{(1-n)/2}}{(1-z)^{3/2}}\,, \qquad N = \frac{1}{n^{n/2}} \frac{1}{n} \tag{4.169}$$

are introduced. In the interval $0<n\leq 1$ the factor N varies in the range $1 \leq N < \infty$.

To get an estimate of Z and N and their product ZN for different hardening exponents n, it is assumed that ε_{co} amounts only up to 10% of the critical strain n, i.e.

$$z = 0.1\,.$$

With this restriction the results are listed in Table 4.2

The increase of the product-term ZN with decreasing hardening exponent n implies that the sensitivity S increases, in spite of the limitation of the strain ε_{co} to a constant fraction $z = 0.1$ of the critical strain n; in fact, this is found also for smaller fractions $z < 0.1$. This trend is apparently in qualitative agreement with the sensitivity variation when the hardening exponent n is decreased but the fractional limitation is given up and the strain ε_{co} is held constant: the sensitivity S increases considerably as shown in Fig.4.8, where only the 1st order perturbation term is included in the $\varepsilon(0,0)/\varepsilon_{co}$ versus β representation. Note that for this plot the sufficiently small constant value 0.13 for the strain ε_{co} was chosen such that $\varepsilon_{co} \leq n$ for all values of n used in Fig.4.8.

The evaluation of the n-dependence of the sensitivity S, Eq.(4.167), under the constant stress condition (i.e. σ_{Ro}/K = const.) and observing the stress-strain relation Eq.(4.151), remains to be pursued.

The influence of the strain gradient term can be made evident also in a more seizable way by representing the results in the form of a stress-strain diagram. Such a representation is a rather natural choice to demonstrate the influence of the size of geometrically similar specimens, especially if spatially local measures of the strain are used; this was pointed out for the fully linear case already in Section 3.1.4.2.

The stress-strain diagram to be shown is the normalized engineering stress σ_{Ro}/K at ξ=0 versus the local engineering strain $\varepsilon_R(0,0)$ at ξ=0, which is obtained from the logarithmic strain $\varepsilon(0,0)$ via

$$\varepsilon_R(0,0) = e^{\varepsilon(0,0)} - 1 .$$

For the construction of these diagrams we proceed as follows: the strain measure $\varepsilon_{co}<n$, which is also a measure for the stress level and which is considered here only as an intermediate variable, is prescribed in discrete steps. With (4.151) the normalized engineering stress σ_{Ro} is given by

$$\frac{\sigma_{Ro}}{K} = \varepsilon_{co}^{n} e^{-\varepsilon_{co}} .$$

The corresponding non-classical logarithmic strain $\varepsilon(0,0) \equiv \varepsilon_o$ is calculated from (4.166). For given values of n, α and β the parameter representations of σ_{Ro}/K and $\varepsilon_R(0,0)$, with ε_{co} as parameter, are obtained. Elimination of ε_{co} yields finally a (σ_{Ro}/K versus $\varepsilon_R(0,0)$)-graph or vice versa. Then, for given values of n and α and varying β within a diagram, the size influence is demonstrated. The calculations were performed for α = 0.0625 & 0.5625 and n = 1/5 & 1/9 and the normalized gradient coefficient β is in the interval $0 \le \beta \le 0.1$. These plots, which include the cross-section reduction influence and which are based on the 2nd order perturbation solution, are shown in Fig.4.9a-d. It should be noted that the graphs are certainly not valid beyond the critical value n of the logarithmic strain $\varepsilon(0,0)$. Thus, the corresponding limits of the engineering strain are indicated in Table 4.3

In Fig 4.9a-d plots covering the whole strain regime are shown but also enlarged details in small strain regions. Inspection of the figures shows that the successive increase of the normalized gradient coefficient β, which is a measure for the increasing gradient parameter l_i or for the decreasing size L^*, yields as successive increase of the normalized flow stress σ_{Ro}/K, provided the strains are sufficiently small. Of course, this expected result corresponds to the common size effect already discussed for the relative strain $\varepsilon(0,0)/\varepsilon_{co}$. As discussed before, in this range of small strains the 2nd order perturbation solution gives reasonable accurate approximations provided the parameter β is not too large. From Fig 4.9a-d it is qualitatively seen that the increase in flow stress with decreasing size is rather small. A specific example will illustrate this. We choose a specimen with a profile as shown in Fig.3.2b, top-right, with the following parameters

$$\alpha = 0.5625, \qquad \frac{D_o}{D_\infty} = 0.75, \qquad \frac{L^*}{D_\infty/2} = 0.188.$$

For the large specimen the normalized gradient parameter is assumed to be

$$\beta = \frac{l_i}{L^*} = \frac{l_i}{D_o}\frac{D_o}{D_\infty}\frac{D_\infty}{L^*} = 0.01 ,$$

which yields

$$\frac{l_i}{D_o} = \beta \frac{D_\infty}{D_o} \frac{L^*}{D_\infty} = 1.2533\ 10^{-3};$$

thus, the above choice implies that the internal length scale l_i is only about the thousandth part of the minimum diameter D_0.

The strain hardening exponent is taken to be

$$n=1/5 .$$

The corresponding engineering stress-strain curves for various parameters β are shown in Fig.4.9a. For the large specimen with β=0.01 and an engineering strain of 2% at the minimum section Fig.4.9a allows to estimate the corresponding normalized engineering stress to be

$$\frac{\sigma_R}{K} = 0.4485 .$$

Decreasing the size proportionally by a factor of 10, the β-parameter becomes β=0.1 and the corresponding engineering stress at a strain of 2% increases to

$$\frac{\sigma_R}{K} = 0.4561,$$

This is a 1.7% change of the flow stress. For an engineering strain level of 4% the increase in flow stress by reducing the specimen size is only slightly larger (1.8%). Results for a larger strain level at the minimum section are difficult to obtain from Fig.4.9a since the 2nd order perturbation solution appears to be not accurate enough.

It is fairly obvious that such small effects on the stress-strain curve are experimentally not detectable: the natural scatter due to other influence would likely mask this size effect.

The internal length-to-minimum diameter ratio and the non-uniformity of the stress distribution need a considerable increase to produce an observable effect. Fig.4.9a-d show that for larger strains, approaching the critical strain limit, an 'inverse' size effect is found for all parameter constellations: the flow stress including the ultimate stress decreases with increasing β-values. This effect is related to the erroneous dominance of the quadratic perturbation term, as already noted for relative strain-versus-β representation even without consideration of the cross-section reduction (Fig.4.2, 4.5 and 4.6). In fact, Fig.4.10 shows engineering strain - engineering stress curves which account only for the 1st order perturbation term: a qualitatively different behavior is obtained which shows no intersection of the curves. However, for large strains these results are equally erroneous. These results demonstrate that an approximate perturbation solution for large strains requires more than just the 1st and the 2nd order perturbation terms. In the following section some results are presented and discussed which include contributions of the 3rd order perturbation term.

4.4.3 On the Contribution of the Third Order Perturbation Term (Power Law Hardening without Cross-Section Reduction)

It is rather noteworthy that, using only the results of Section 4.3.1 and 4.3.2 and Appendix 6, it is possible to determine the 3rd order term $\overset{3}{\varepsilon}(\xi,\eta)$ at $\xi=0$, $\eta=0$, i.e. $\overset{3}{\varepsilon}(0,0)$. This allows the improvement of the maximum strain $\varepsilon(0,0)$ at the minimum cross-section, which is now given by

$$\varepsilon(0,0) = \overset{0}{\varepsilon}(0) + \beta\,\overset{1}{\varepsilon}(0,0) + \beta^2\,\overset{2}{\varepsilon}(0,0) + \beta^3\,\overset{3}{\varepsilon}(0,0). \tag{4.170}$$

Thus, the determination of the distinct value $\overset{3}{\varepsilon}(0,0)$ does not require the inclusion of the 4th order perturbation term. If, however, the function $\overset{3}{\varepsilon}(\xi,\eta)$ were of interest, then the analysis must be extended to include the 4th order term $\overset{4}{\varepsilon}(\xi,\eta)$ followed by the suppression of secular terms as previously. For the present, including the cross-section reduction due to the deformation formally, one gets with Eq.(4.82), (4.83), and (4.85)

$$\left.\begin{aligned} &\overset{3}{\varepsilon}(\xi,\eta) = B_3(\xi)\,e^{-\sqrt{\varphi}\eta} + v_o(\xi)\,e^{-2\sqrt{\varphi}\eta} + w_o(\xi)\,e^{-3\sqrt{\varphi}\eta} \\ &v_o(\xi) = \gamma_2(\xi)/(3\varphi)\,, \qquad w_o(\xi) = \gamma_3(\xi)/(8\varphi)\,, \end{aligned}\right\} \tag{4.171}$$

where $\gamma_2(\xi)$ and $\gamma_3(\xi)$ is given by (A6.12). Thus

$$\overset{3}{\varepsilon}(0,0) = B_3(0) + v_o(0) + w_o(0)\,. \tag{4.172}$$

Here $v_o(0)$ and $w_o(0)$ or $\gamma_2(0)$ and $\gamma_3(0)$ can be determined from the results obtained already. The term $B_3(0)$ can be deduced from the boundary condition $(\text{B.C.II})_4$, Eq.(4.42):

$$\overset{2}{\varepsilon}_\xi + \mu'\,\overset{3}{\varepsilon}_\eta = 0\,, \qquad \text{at } \xi=0,\ \eta=0\,. \tag{4.173}$$

The η-derivative of $(4.171)_1$ at $\xi=0$, $\eta=0$ is found to be

$$\left(\overset{3}{\varepsilon}_\eta\right)_{\substack{\xi=0\\ \eta=0}} = -\sqrt{\varphi}\ [B_3(0) + 2v_o(0) + 3w_o(0)]\,, \tag{4.174}$$

which yields with (4.173)

$$B_3(0) = \frac{1}{\sqrt{\varphi}}\frac{1}{(\mu_o')_0}\left(\overset{2}{\varepsilon}_\xi\right)_0 - 2v_o(0) - 3w_o(0)\,. \tag{4.175}$$

Thus

$$\overset{3}{\varepsilon}(0,0) = \frac{1}{\sqrt{\varphi}}\frac{1}{(\mu_o')_0}\left(\overset{2}{\varepsilon}_\xi\right)_0 - \upsilon_o(0) - 2w_o(0)\,; \tag{4.176}$$

here $\mu'(\xi)$ is given by (4.72) and $\overset{2}{\varepsilon}_\xi(\xi,\eta)$ follows from (4.81). The explicit determination of the various terms is considerably simplified if the cross-section reduction due to the deformation is consistently neglected. Under this simplification and after a lengthy intermediate calculation one obtains finally

$$\left(\overset{3}{\varepsilon}\right)_0 = \overset{3}{\varepsilon}(0,0) = \varepsilon_{co}\left(\frac{\varepsilon_{co}^{1-n}}{n}\right)^{3/2}\left(\frac{1-\alpha}{n}\right)^3\left\{\frac{75n-11}{288}(1-n) - \frac{14+n}{12}\frac{1-n}{1-\alpha}[1-\alpha(1\text{-}n)] - \right.$$

$$\left. - \left(\frac{\alpha}{1-\alpha}\right)^2(1-2n)(1-n) + \frac{\alpha}{(1-\alpha)^2}(1-n)(2-n) - \frac{1}{(1-\alpha)^2}\right\}. \tag{4.177}$$

Thus, with the previous result Eq.(4.147) and (4.177), including cubic terms of β, the relative strain at the minimum cross-section reads

$$\frac{\varepsilon_o}{\varepsilon_{co}} = \frac{\varepsilon(0,0)}{\varepsilon_{co}} = 1 - \beta\left(\frac{\varepsilon_{co}^{1-n}}{n}\right)^{1/2}\frac{1-\alpha}{n} + \beta^2\left(\frac{\varepsilon_{co}^{1-n}}{n}\right)\left(\frac{1-\alpha}{n}\right)^2\left[\frac{17}{12}(1-n) + \frac{n}{1-\alpha}\right] -$$

$$-\beta^3\left(\frac{\varepsilon_{co}^{1-n}}{n}\right)^{3/2}\left(\frac{1-\alpha}{n}\right)^3\left\{\frac{11-75n}{288}(1-n) + \frac{14+n}{12}\frac{1-n}{1-\alpha}[1-\alpha(1\text{-}n)] + \right.$$

$$\left. + \left(\frac{\alpha}{1-\alpha}\right)^2(1-2n)(1-n) - \frac{\alpha}{(1-\alpha)^2}(1-n)(2-n) + \frac{1}{(1-\alpha)^2}\right\}. \tag{4.178}$$

For linear hardening n=1 Eq.(4.178) yields

$$\frac{\varepsilon_o}{\varepsilon_{co}} = 1 - \beta(1-\alpha) + \beta^2(1-\alpha) - \beta^3(1-\alpha)\,. \tag{4.179}$$

This agrees with the exact solution Eq.(4.149) up to the cubic term. For vanishing small hardening $n \to 0$ Eq.(4.178) simplifies to

$$\frac{\varepsilon_o}{\varepsilon_{co}} = \frac{\varepsilon(0,0)}{\varepsilon_{co}} \approx 1 - \beta\left(\frac{\varepsilon_{co}^{1-n}}{n}\right)^{1/2}\frac{1-\alpha}{n} + \beta^2\left(\frac{\varepsilon_{co}}{n}\right)\left(\frac{1-\alpha}{n}\right)^2\frac{17}{12} -$$

$$-\beta^3\left(\frac{\varepsilon_{co}}{n}\right)^{3/2}\left(\frac{1-\alpha}{n}\right)^3\left[\frac{11}{288} + \frac{14}{12} + 1\right]. \tag{4.180}$$

The β-derivative of these two limiting cases gives

$$\frac{d[\varepsilon(0,0)/\varepsilon_{co}]}{d\beta} = -A_1 + 2\beta A_2 - 3\beta^2 A_3 \tag{4.181}$$

with

$$\left.\begin{aligned} A_1 &= \begin{cases} (1-\alpha) & n=1 \\ \left(\dfrac{\varepsilon_{co}}{n}\right)^{1/2}\dfrac{1-\alpha}{n} & n\to 0 \end{cases} \\ A_2 &= \begin{cases} (1-\alpha) & n=1 \\ \left(\dfrac{\varepsilon_{co}}{n}\right)\left(\dfrac{1-\alpha}{n}\right)^2\dfrac{17}{12} & n\to 0 \end{cases} \\ A_3 &= \begin{cases} (1-\alpha) & n=1 \\ \left(\dfrac{\varepsilon_{co}}{n}\right)^{3/2}\left(\dfrac{1-\alpha}{n}\right)^3\left[\dfrac{11}{288}+\dfrac{14}{12}+1\right] & n\to 0 \end{cases} \end{aligned}\right\} \tag{4.182}$$

Then a relative minimum of the $(\varepsilon(0,0)/\varepsilon_{co}$ versus $\beta)$-curve is obtained, if the condition

$$\frac{d[\varepsilon(0,0)/\varepsilon_{co}]}{d\beta} = 0 \tag{4.183}$$

admits a real solution for β. The roots of this quadratic equation are

$$\beta_{1,2} = \frac{1}{3}\frac{A_2}{A_3} \pm \sqrt{\frac{1}{9}\left(\frac{A_2}{A_3}\right)^2 - \frac{1}{3}\frac{A_1}{A_3}} = \frac{1}{3}\frac{A_2}{A_3} \pm \frac{1}{3}\frac{1}{A_3}\sqrt{A_2^2 - 3A_3A_1}\ . \tag{4.184}$$

For both limiting cases (4.182) the radicand of Eq.(4.184) is found to be negative:

$$A_2^2 - 3A_3A_1 < 0\ ; \tag{4.185}$$

thus, a real root does not exist. Therefore, it may be expected that the $(\varepsilon(0,0)/\varepsilon_{co}$ versus $\beta)$-curve does not admit an extremum (minimum) but is a continuously decreasing function not only for the limiting values of the hardening exponent but also in the intermediate range $1>n>0$. This is confirmed by the numerical results shown in the following.

Fig.4.11 shows a comparison of the β-dependence of the exact and the 3rd order perturbation solution for the relative strain assuming linear strain hardening (n=1) and ignoring cross-section reduction. It is seen that the 3rd order approximation generally overestimates the effect of the strain reduction

$$\frac{\varepsilon_{co} - \varepsilon(0,0)}{\varepsilon_{co}}$$

due to the gradient term. Comparing this with the corresponding 2nd order approximation, Fig.4.2 shows a considerable improvement: agreement within less than 10% underestimation in the relative strain is found up to β=0.5 and more, instead of β=0.275 in Fig.4.2.

The dependence of the relative strain on the normalized gradient coefficient is shown in Fig.4.12 for non-linear strain hardening $0<n\leq 1$ and for the parameters α = 0.5625, 0.7225, 0.81 and ε_{co} = 0.01, 0.05, 0.1, 0.3. Depending on the parameters n, α, and ε_{co} the 3rd order approximation exaggerates the gradient effect for larger β-values. This is noted when the magnitude of the derivative $d(\varepsilon(0,0)/\varepsilon_{co})/d\beta$ starts to increase from an initially almost constant value.

The size effect is illustrated using the same parameters as used previously for the 2nd order approximation, i.e. α=0.5625, n=1/9, and ε_{co}=0.05[7], which is well below the critical value ε_{co}=1/9=0.1$\overline{1}$. From Fig.4.12 this yields the strain ratio $\varepsilon(0,0)/\varepsilon_{co}$=0.761$\overline{6}$ if β=0.1[8]. An increase of size by a factor of ten ($\rightarrow\beta$=0.01) gives $\varepsilon(0,0)/\varepsilon_{co}$=0.96$\overline{6}$. Thus, the maximum strain, estimated by a 3rd order perturbation approximation, reduces by about

$$\frac{0.96\overline{6}-0.761\overline{6}}{0.96\overline{6}}\,100 = 21.2\%$$

when the size is reduced by a factor of 10 such that the normalized gradient parameter β is increased from 0.01 to 0.1. This is a sufficient amount of deviation of the rather local axial strain at the minimum cross-section, which certainly should be measurable by appropriate means. However, an important condition is here that the other parameters, especially the measure for the stress level ε_{co}, are the same in both the small and the large specimen.

The choice of the parameters of the above example, in fact, corresponds to a realistic specimen geometry, as shown in Fig.3.2b, top right, with

$$\alpha = 0.5625, \qquad \frac{D_o}{D_\infty} = \sqrt{\alpha} = 0.75, \qquad \frac{L^*}{D_\infty/2} = 0.188\ ;$$

then

$$\frac{D_0}{l_i} = \begin{cases} 797.9 & \text{for } \beta = \dfrac{l_i}{L^*} = 0.01 \quad \text{large specimen} \\ 79.79 & \text{for } \beta = \dfrac{l_i}{L^*} = 0.1 \quad \text{small specimen}. \end{cases}$$

If, for example, we interpret the internal length scale l_i as the grain size, then the above numbers define the number of grains along a specimen diameter; provided D_0=3 mm (2 mm) for the small specimen the grain size would correspond to 37.6 μm (25 μm), which are grain sizes of a realistic magnitude.

Of course, the percentage strain reduction calculated accounts only for the axial strain gradient in the specimen; the effect of the radial strain variations are not captured by this simple uniaxial model.

As previously done in Section 4.4.2, stress-strain diagrams (Fig.4.13a & b, 4.14a & b), relating the local stresses and strains at the minimum cross-sections, have been obtained including the 3rd order perturbation correction; however, the influence of the cross-section reduction is not contained here.

---

[7] This strain level corresponds to the normalized stress level σ_{Ro}/K=0.7169.

[8] As seen in Fig.4.5b, the 2nd order perturbation solution is not accurate enough for this parameter combination.

It is evident from these curves that the instability (relative stress maximum) is not captured; more important, also the 3rd order perturbation approximation fails (backward swing of the curves) for large values of β when the strain is increased beyond a certain limit. Yet for sufficiently small strains and β-values the increase in strength with decreasing size (increase of β) is seen which is just another aspect of the size influence. But the influence of the gradient term on the stress at a given strain is relatively small: for

$$\alpha = 0.5625, \qquad n = 1/9, \qquad \varepsilon_{co} = \varepsilon_R(0,0) = 0.05$$

the normalized stress σ_R/K is increased by only about 3.77% if β is increased from β=0 (very large specimen) to β=0.1 (Fig.4.14a). A somewhat larger strengthening effect is obtained even at a lower strain level if the non-uniformity of strain distribution is increased. For a rather wasp-waisted specimen ($\alpha = 0.0625$, $\sqrt{\alpha} = D_o / D_\infty = 0.25$), the same hardening exponent (n = 1/9), and a smaller local strain $\varepsilon_{co} = \varepsilon_R(0,0) = 0.015$ the normalized engineering stress is increased by about 6.5% when the dimensionless gradient parameter β is again increased from $\beta = 0$ (very large specimen) to $\beta = 0.1$ (Fig.4.14b). With

$$\beta = \frac{l_i}{L^*} = \frac{l_i}{D_o}\frac{D_o}{L^*},$$

one gets

$$\frac{D_o}{l_i} = \frac{1}{\beta}\frac{D_o}{L^*}.$$

The ratio D_o/l_i may be interpreted as the number of grains along the minimum neck diameter, say $D_o/l_i = 50$. Then $L^*/D_o = 0.2$ which represents a very steep transition from the minimum diameter D_o to the largest diameter D_∞, i.e. within a diameter D_o's distance from the minimum section the diameter increases up to 95.3% of the asymptotic value D_∞. The detection of these effects in the percentage range requires very careful specimen preparation and testing to minimize masking influences and pseudo size effects.

5. Three-Point-Bending of a Uniform Beam with Power Law Hardening

5.1 Statement of the Problem

Within the EU-Project REVISA [1.4, 1.5] U-notched beams with rectangular cross-section will be tested quasistatically in three-point-bending using specimens of different sizes. In the following a strength of materials theory for an un-notched beam is formulated accounting for plasticity by using a power law hardening deformation theory which includes a 2nd order strain gradient linearly. Only small deformations will be considered and shear deformation is ignored. This problem is considered as a first step towards understanding the response of the notched beam subjected to hardening. It is shown in the following that, owing to the simplifications, this problem leads to a singular perturbation problem for the beam curvature,

which has the same formal structure as the problem for the tapered rod. Thus, the same solution procedure - multiscale perturbation theory - can be applied. In fact, part of the previously derived equations can be directly used by proper reinterpretation of the variables.

Accounting for tensile and compressive strain in the bending problem, the uniaxial stress-strain law reads

$$\sigma = K|\varepsilon|^n \operatorname{sign}(\varepsilon) - Kl_i^2\nabla^2\varepsilon\ , \qquad 0<n\leq 1. \tag{5.1}$$

With the longitudinal coordinate x and the thickness coordinate y (see Fig.5.1) the strain is given by (Bernoulli hypothesis)

$$\varepsilon(x,y) = k(x)y \tag{5.2}$$

where

$$k(x) = -\frac{d^2w(x)}{dx^2} \text{ : curvature of center line} \tag{5.3}$$

$w(x)$: beam deflection.

The Laplacian of the strain yields

$$\nabla^2\varepsilon = \frac{d^2}{dx^2}\varepsilon + \frac{d^2}{dy^2}\varepsilon = \frac{d^2k}{dx^2}y\ . \tag{5.4}$$

The length of the beam between the simple supports is $2L$ and the central load is denoted by $2P$. Then the bending moment is simply given by

$$M=P(L-x) \qquad 0\leq x\leq L. \tag{5.5}$$

The bending moment is balanced by the moment of the normal stresses in the rectangular cross-section. This yields, together with (5.1),

$$M(x) = b\int_{-h/2}^{h/2}\sigma\, y\, \mathrm{d}y \;=\; 2bK\int_0^{h/2}[k^n y^n - l_i^2\frac{d^2k}{dx^2}y]\, y\, \mathrm{d}y =$$

$$= K\,[J_n k^n - J\, l_i^2\frac{d^2k}{dx^2}] \tag{5.6}$$

where

$$\left.\begin{aligned} J &= J_1 = \frac{bh^3}{12} \\ J_n &= 2b\int_0^{h/2} y^{n+1}\mathrm{d}y = \frac{bh^{2+n}}{(2+n)2^{1+n}}\ . \end{aligned}\right\} \tag{5.7}$$

The following dimensionless variables and parameters are introduced

$$\left.\begin{aligned} &\kappa = Lk \text{ : dimensionless curvature} \\ &\xi = x/L \text{ : dimensionless axial coordinate} \\ &q = \frac{J}{J_n}\frac{1}{L^{1-n}} \text{ : dimensionless parameter} \\ &\beta = l_i/L \text{ : dimensionless internal length scale.} \end{aligned}\right\} \tag{5.8}$$

With

$$q = \frac{J}{J_n}\frac{1}{L^{1-n}} = \frac{J}{L}\frac{L^n}{J_n} = \left(\frac{h}{L}\right)^{1-n}\frac{(2+n)2^{1+n}}{12} \tag{5.9}$$

it is noted that for $h/L<1$, $0<n\leq 1$

$$\frac{1}{3}\frac{h}{L} < q \leq q_{\max} = (q)_{n=1} = 1. \tag{5.10}$$

Consequently, the moment-curvature relation (5.6) reads

$$M = \frac{J_n K}{L^n}\left\{\kappa^n - q\beta^2\frac{d^2\kappa}{d\xi^2}\right\}. \tag{5.11}$$

Combining this with the equilibrium equation (5.5), the following 2nd order differential equation for the curvature is obtained

$$\beta_q^2\frac{d^2\kappa}{d\xi^2} - \kappa^n = -r_B(\xi), \qquad 0<\xi\leq 1 \tag{5.12}$$

where the right-hand side is

$$\left.\begin{aligned} &r_B(\xi) = \Lambda_n(1-\xi) \\ &\Lambda_n = \frac{L^{1+n}P}{KJ_n} = \left(\frac{L}{h}\right)^{1+n}\frac{P}{Kbh}(2+n)2^{1+n} \end{aligned}\right\} \tag{5.13}$$

and the lumped parameter β_q is introduced

$$\beta_q = \sqrt{q}\,\beta. \tag{5.14}$$

The differential equation (5.12) has the same formal structure as for the tapered tensile rod under small deformations, Eq.(4.96). However, the small parameter β_q involves not only the ratio l_i/L but also (h/L), which is a constant for geometrically similar beam specimens, as well as the hardening exponent n.

For a complete mathematical formulation the differential equation (5.12) requires two boundary conditions for the curvature. Before approaching this choice, some remarks concerning the classical solution κ_c are in place. The solution κ_c is obtained from (5.12) by ignoring the gradient effect by setting β_q=0:

$$\left.\begin{aligned} \kappa_c &= (r_B(\xi))^{1/n} = \kappa_{co}(1-\xi)^{1/n}, \qquad 0<\xi\leq 1 \\ \kappa_{co} &= \Lambda_n^{1/n} = \left(\frac{L}{h}\right)^{\frac{1+n}{n}} \left(\frac{P}{bhK}\right)^{1/n} (2+n)^{1/n}\, 2^{\frac{1+n}{n}} \end{aligned}\right\} \qquad (5.15)$$

where κ_{co} is the largest curvature at ξ=0. The first and second derivatives are

$$\left.\begin{aligned} \frac{d\kappa_c}{d\xi} &= -\kappa_{co}\frac{1}{n}(1-\xi)^{\frac{1-n}{n}}, \\ \frac{d^2\kappa_c}{d\xi^2} &= \kappa_{co}\frac{1-n}{n^2}(1-\xi)^{\frac{1-2n}{n}}. \end{aligned}\right\} \qquad 0<\xi\leq 1 \qquad (5.16)$$

At the center cross-section (ξ=0) the classical curvature κ_c has its absolute maximum but its first order spatial derivative is discontinuous.

The distribution of the second order derivative depends strongly on the power exponent n. We find

n=1 : $\frac{d^2\kappa_c}{d\xi^2}$ vanishes identically, 0<ξ≤1

1/2<n<1 : $\frac{d^2\kappa_c}{d\xi^2}$ is a monotonously increasing concave function of ξ starting from a finite value at ξ=0 and approaching infinity at ξ=1.

n=1/2 : $\frac{d^2\kappa_c}{d\xi^2}$ is constant (=$2\kappa_{co}$)

n=1/3 : $\frac{d^2\kappa_c}{d\xi^2}$ is a linearly decreasing function (=$6\kappa_{co}(1-\xi)$)

0<n<1/3 : $\frac{d^2\kappa_c}{d\xi^2}$ is a monotonuously decreasing concave function of ξ starting from the largest finite value at ξ=0 and approaching zero at ξ=1.

For n≤1/3, which is the technologically most interesting regime, the second order derivative of the curvature has its absolute maximum as one approaches the central position ξ=0. Therefore, the largest effect of the gradient term in the differential equation (5.12) is expected around ξ=0. Furthermore, it can be argued that the central force $2P$ is the limiting case of a uniformly distributed loading along some small finite beam section of length s around ξ=0. The

corresponding moment distribution in this section is parabolic and, for n=1, so is the curvature according to the classical theory. Then the second derivative $\frac{d^2\kappa_c}{d\xi^2}$ is proportional to s^{-1} at ξ=0 which yields even an unbounded value for $s\to 0$ and fixed load P. Therefore, the largest influence of the second order gradient term in (5.12) will be at and around ξ=0. For small values of β_q it will be confined to this regime.

Coming back to the choice of the boundary conditions, the prescription of the curvature at ξ=0 for the gradient dependent case is physically unreasonable. We follow here a similar argument as for the tapered rod (Section 3.1.1): it is assumed that

$$\left(\frac{d\varepsilon(x,y)}{dx}\right)_{x=0} = 0 \qquad \forall y$$

which yields with (5.2) the boundary condition

$$\text{B.C. II} \qquad \left(\frac{d\kappa}{d\xi}\right)_{\xi=0} = 0. \tag{5.17}$$

The other boundary condition is prescribed at ξ=1 :

$$\text{B.C. I} \qquad (\kappa)_{\xi=1} = 0. \tag{5.18}$$

This choice reflects the assumption that the gradient influence for small values of β_q is restricted to the central part of the beam and is not sensible at the ends. This assumption and the vanishing of the bending moment at ξ=1 implies condition (5.18).

We consider geometrically similar beam specimens which are scaled up by the geometrical scaling factor λ>1. The geometrical data take the following values.

$$\bar{h} = h\lambda, \quad \bar{b} = b\lambda, \quad \bar{L} = L\lambda. \tag{5.19}$$

If geometrical and physical similarities are required, then the dimensionless characteristic parameters of the differential equation and the boundary conditions must be the same, i.e.

$$\left.\begin{aligned} &\bar{\beta}_q = \beta_q \\ &\bar{n} = n \\ &\left(\frac{\bar{L}}{\bar{h}}\right)^{1+n} \frac{\bar{P}}{\bar{b}\bar{h}} \frac{1}{\bar{K}} = \left(\frac{L}{h}\right)^{1+n} \frac{P}{bh} \frac{1}{K}. \end{aligned}\right\} \tag{5.20}$$

With $(5.20)_2$ and if the strict geometrical similarity (5.19) applies, then

$$\bar{q} = q \tag{5.21}$$

and also

$$\left.\begin{aligned} &\bar{\beta}=\beta \quad \text{or} \quad \frac{\bar{l}_i}{l_i}=\lambda \\ &\text{and} \\ &\frac{\bar{P}}{\bar{b}\bar{h}}\frac{1}{\bar{K}}=\frac{P}{bh}\frac{1}{K} \quad \text{or} \quad \frac{\bar{P}}{P}\frac{K}{\bar{K}}=\lambda^2. \end{aligned}\right\} \tag{5.22}$$

Here conditions (5.22) are formally the same as (4.11). Again similarity cannot be achieved strictly if the gradient term is present and if the material is the same in the small and the large-scale specimen.

However, the situation is, at least theoretically, somewhat relaxed for specimens made of the same material if geometrically distorted specimens are considered. To obtain the same dimensionless curvature at homologous positions $\bar{x}/\bar{L}=x/L$, only the conditions (5.20) have to be satisfied. We introduce the distorted scale factors

$$\lambda=\frac{\bar{L}}{L}\neq\lambda_h=\frac{\bar{h}}{h}\neq\lambda_b=\frac{\bar{b}}{b}. \tag{5.23}$$

Condition $(5.20)_2$ is identically satisfied and $(5.20)_1$ yields

$$\left(\frac{\lambda_h}{\lambda}\right)^{\frac{1-n}{2}}=\lambda \text{ or } \lambda_h=\lambda^{\frac{3-n}{2}}, \quad n\neq 1. \tag{5.24}$$

Condition $(5.20)_3$ implies

$$\frac{\bar{P}}{P}=\left(\frac{\lambda_h}{\lambda}\right)^{1+n}\lambda_h\lambda_b. \tag{5.25}$$

If the cross-section areas are required to scale according to λ^2, i.e.,

$$\frac{\bar{h}\bar{b}}{hb}=\lambda_h\lambda_b=\lambda^2 \tag{5.26}$$

as for the non-distorted case, then

$$\lambda_b=\frac{\lambda^2}{\lambda_h}=\lambda^{\frac{1+n}{2}}, \quad n\neq 1. \tag{5.27}$$

and

$$\frac{\bar{P}}{P}=\left(\frac{\lambda_h}{\lambda}\right)^{1+n}\lambda^2=\lambda^{\frac{5-n^2}{2}}. \tag{5.28}$$

Assuming λ=10, we obtain distorted scale factors λ_h and λ_b as listed in Table 5.1

For a given ratio $\bar{h}/\bar{b}$ of the full scale beam (the "prototype") we obtain with (5.24) and (5.27)

$$\frac{h}{b} = \frac{1}{\lambda^{1-n}} \frac{\overline{h}}{\overline{b}}. \tag{5.29}$$

Thus, increasing the length scale factor λ reduces the depth-to-width ratio h/b of the small-scale model. However, for the linear case n=1 Eq.(5.9) yields $\overline{q} = q$=1 and then $\overline{\beta} = \beta$ implies λ=1: a scaled down distorted model is not possible for the linear case n=1. The result (5.29) implies a very large distortion of the cross-section dimensions. For example, with λ=10, n=1/5 and 1/9 one finds $\lambda^{1-n} = 6.31$ and 7.74, respectively. Formally this is valid for any non-zero internal length scale l_i. On the contrary, if l_i=0 exactly or if $\overline{\beta}$ & β <<1, the conditions (5.20) are either exactly or only approximately satisfied. In these cases similarity, i.e. equality of the dimensionless curvatures, can be achieved exactly or approximately without cross-section distortion but of course with the standard scaling of the applied load

$$\frac{\overline{P}}{P} = \lambda^2 < \lambda^{\frac{5-n^2}{2}} = \left(\frac{\overline{P}}{P}\right)_{\text{distorted}}. \tag{5.30}$$

5.2 Solution of the Linear Problem (n=1)

For the linear case n=1 the lumped parameter β_q reduces to

$$\beta_q = \beta = \frac{l_i}{L} \tag{5.31}$$

and the differential equation (5.12) reduces to a linear one

$$\beta^2 \frac{d^2\kappa}{d\xi^2} - \kappa = -r_{BI}(\xi) \tag{5.32}$$

$$\left.\begin{aligned} r_{BI}(\xi) &= \Lambda_1(1-\xi) \\ \Lambda_1 &= \left(\frac{L}{h}\right)^2 \frac{P}{bhK} 12. \end{aligned}\right\} \tag{5.33}$$

The exact solution, observing the boundary conditions (5.17) and (5.18), is easily obtained

$$\kappa(\xi) = \kappa_c(\xi) - \kappa_{co}\beta\left[\frac{e^{-\xi/\beta}}{1+e^{-2/\beta}} - \frac{e^{\xi/\beta}}{1+e^{2/\beta}}\right] \tag{5.34}$$

$$\left.\begin{aligned} \kappa_c(\xi) &= \kappa_{co}(1-\xi) \\ \kappa_{co} &= \Lambda_1 \end{aligned}\right\} \tag{5.35}$$

where $\kappa_c(\xi)$ is the classical solution without gradient effect.

With (5.3) and (5.8) the differential equation for the dimensionless deflection $w(\xi)/L$ of the centrally loaded simply supported beam is

$$\frac{d^2(w/L)}{d\xi^2} = -Lk = -\kappa(\xi) \tag{5.36}$$

and the associated boundary conditions are

$$\left(\frac{dw}{d\xi}\right)_{\xi=0} = 0\,, \qquad (w)_{\xi=1} = 0\,. \tag{5.37}$$

The solution is

$$\frac{w(\xi)}{L} = \frac{w_c(\xi)}{L} - \Lambda_1\beta^2\left[\frac{1}{1+e^{-2/\beta}} + \frac{1}{1+e^{2/\beta}}\right](1-\xi) + \\ + \Lambda_1\beta^3\left[\frac{e^{-\xi/\beta} - e^{-1/\beta}}{1+e^{-2/\beta}} - \frac{e^{\xi/\beta} - e^{1/\beta}}{1+e^{2/\beta}}\right] \tag{5.38}$$

where w_c/L is the classical solution without gradient effect

$$\frac{w_c(\xi)}{L} = \Lambda_1\left[\frac{1}{3} - \frac{\xi^2}{2} + \frac{\xi^3}{6}\right]. \tag{5.39}$$

5.3 Approximate Analytical Solution by the Method of Multiple Scales for the Non-Linear Case

5.3.1 The Governing System of Perturbation Equations

For small β_q-values, $0 < \beta_q << 1$, an approximate analytical solution is possible using the method of multiple scales of perturbation theory. Because of the mathematical analogy the results of section 4.3.3 can be used when the variables are properly reinterpreted:

$$\varepsilon \to \kappa\,,\ \varepsilon_c \to \kappa_c\,,\ \beta \to \beta_q\,,\ r_R \to r_B; \tag{5.40}$$

of course, the spatial dependence of the right-hand sides of the differential equation are very different, and differences are in the boundary conditions.

The multi-scale expansion of the dimensionless curvature κ is given by

$$\kappa = \hat{\kappa}(\xi;\beta_q) = \tilde{\kappa}(\xi,\eta;\beta_q) = \\ = \overset{0}{\kappa}(\xi,\eta) + \beta_q \overset{1}{\kappa}(\xi,\eta) + \beta_q^2 \overset{2}{\kappa}(\xi,\eta) + \beta_q^3 \overset{3}{\kappa}(\xi,\eta) \tag{5.41}$$

with

$$\left.\begin{aligned} \xi &= \frac{x}{L} \text{ : the "slow" spatial variable} \\ \eta &= \frac{\mu_B(\xi)}{\beta_q} \text{ : the "fast" spatial variable .} \end{aligned}\right\} \qquad (5.42)$$

The development of the differential equations and the boundary conditions in terms of $\overset{i}{\kappa}(\xi,\eta)$ (i=0,1,2,3), $\mu_B(\xi)$ and β_q yields

$$\left.\begin{aligned} \beta_q^0 : \text{DEQ}(0) &\Rightarrow \overset{0}{\kappa}_{\eta\eta} - \frac{\overset{0}{\kappa}^n}{(\mu_B')^2} = -\frac{r_B(\xi)}{(\mu_B')^2} \\ \beta_q^1 : \text{DEQ}(1) &\Rightarrow \overset{1}{\kappa}_{\eta\eta} - \Omega_B^2 \overset{1}{\kappa} = R_{B1}(\overset{0}{\kappa}, \mu_B) \\ \beta_q^2 : \text{DEQ}(2) &\Rightarrow \overset{2}{\kappa}_{\eta\eta} - \Omega_B^2 \overset{2}{\kappa} = R_{B2}(\overset{0}{\kappa}, \overset{1}{\kappa}, \mu_B) \\ \beta_q^3 : \text{DEQ}(3) &\Rightarrow \overset{3}{\kappa}_{\eta\eta} - \Omega_B^2 \overset{3}{\kappa} = R_{B3}(\overset{0}{\kappa}, \overset{1}{\kappa}, \overset{2}{\kappa}, \mu_B) \end{aligned}\right\} \qquad (5.43)$$

where

$$\Omega_B^2(\xi) = \frac{n}{\overset{0}{\kappa}} \frac{\overset{0}{\kappa}^n}{(\mu_B')^2} \qquad (5.44)$$

and R_{Bi}, i=1,2,3 are the differential operators

$$\left.\begin{aligned} R_{B1} &= -\frac{1}{(\mu_B')^2}(2\,\mu_B'\overset{0}{\kappa}_{\xi\eta} + \mu_B''\overset{0}{\kappa}_{\eta}) \\ R_{B2} &= -\frac{1}{(\mu_B')^2}(2\,\mu_B'\overset{1}{\kappa}_{\xi\eta} + \mu_B''\overset{1}{\kappa}_{\eta} + \overset{0}{\kappa}_{\xi\xi}) - \Omega_B^2 \frac{1}{2}(1-n)\frac{1}{\overset{0}{\kappa}}\left(\overset{1}{\kappa}\right)^2 \\ R_{B3} &= -\frac{1}{(\mu_B')^2}(2\,\mu_B'\overset{2}{\kappa}_{\xi\eta} + \mu_B''\overset{2}{\kappa}_{\eta} + \overset{1}{\kappa}_{\xi\xi}) - \Omega_B^2(1-n)\frac{\overset{1}{\kappa}\overset{2}{\kappa}}{\overset{0}{\kappa}} + \\ &\quad + \Omega_B^2 \frac{1}{6}(1-n)(2-n)\frac{\left(\overset{1}{\kappa}\right)^3}{\left(\overset{0}{\kappa}\right)^2} \end{aligned}\right\} \qquad (5.45)$$

where

$$(\bullet)' = \frac{d(\bullet)}{d\xi}.$$

The boundary conditions (5.18) and (5.17) yield

$$\left.\begin{array}{lll} & B.C.\ I\ (\xi=1,\ \eta\to\infty) & B.C.\ II\ (\xi=0,\ \eta=0) \\ \beta_q^{-1}: & - & \overset{0}{\kappa}{}'_{\eta} = 0 \\ \beta_q^{0}: & \overset{0}{\kappa}\to 0 & \overset{0}{\kappa}_{\xi} + \mu_B' \overset{1}{\kappa}_{\eta} = 0 \\ \beta_q^{1}: & \overset{1}{\kappa}\to 0 & \overset{1}{\kappa}_{\xi} + \mu_B' \overset{2}{\kappa}_{\eta} = 0 \\ \beta_q^{2}: & \overset{2}{\kappa}\to 0 & \overset{2}{\kappa}_{\xi} + \mu_B' \overset{3}{\kappa}_{\eta} = 0 \\ \beta_q^{3}: & \overset{3}{\kappa}\to 0 & (\overset{3}{\kappa}_{\xi} = 0). \end{array}\right\} \qquad (5.46)$$

Note that the boundary condition B.C.I at $x=L$, Eq.(5.18), is transformed into conditions at $\xi=1$ but $\eta\to\infty$ in the (ξ,η) space since $\eta=\mu_B(\xi)/\beta_q$ may become large for arbitrary small values of β_q; this argument is different from the reasoning in Section 4.3.

5.3.2 Solution of the Perturbation Equations

Comparison of the perturbation system (5.43) and (5.46) with (4.98) and (4.42) shows that the differences concern only the right-hand sides of the differential equation DEQ(0) and the associated boundary condition B.C.I. Thus, if $\overset{0}{\kappa}$ is found, all higher perturbation functions are fully determined in terms of $\overset{0}{\kappa}$ and n. Since the differential equations and boundary conditions (except the spatial assignment of the B.C.I in the (ξ,η)-space) for the higher order perturbation functions are mathematically the same for the two systems, the solution procedure of section (4.3.3) can be formally transformed to the present problem, the only difference - apart from the 0^{th} order approximation - being the notation.

As previously, the 0^{th} order approximation $\overset{0}{\kappa}$ corresponds to the classical solution κ_c

$$\overset{0}{\kappa}(\xi) = \kappa_c(\xi) = (r_B(\xi))^{1/n} = \Lambda_n^{1/n}(1-\xi)^{1/n} = \kappa_{co}\,(1-\xi)^{1/n} \qquad (5.47)$$

which satisfies the differential equation DEQ(0) and the two associated boundary conditions. Thus

$$\left.\begin{array}{l} \overset{0}{\kappa}_{\xi} = -\,\kappa_{co}\,\dfrac{1}{n}(1-\xi)^{\frac{1-n}{n}} \\ \overset{0}{\kappa}_{\xi\xi} = \kappa_{co}\,\dfrac{1-n}{n^2}(1-\xi)^{\frac{1-2n}{n}} \end{array}\right\} \qquad (5.48)$$

and

$$R_{B1} \equiv 0. \tag{5.49}$$

Then the 1st order perturbation function $\overset{1}{\kappa}(\xi,\eta)$, the solution of DEQ(2), is

$$\overset{1}{\kappa}(\xi,\eta) = B_1(\xi)\, e^{-\Omega_B(\xi)\eta} \tag{5.50}$$

where the boundary condition B.C.I for $\overset{1}{\kappa}$ is observed. Following the procedure of Section 4.3, the secular terms of the particular solution of the 2nd order perturbation $\overset{2}{\kappa}$ can be removed which yields

$$\Omega_B = \pm\sqrt{\varphi} = \text{const.} \tag{5.51}$$

and thus

$$\mu_B{}' = +\left[\frac{1}{\varphi}\frac{n}{\overset{0}{\kappa}{}^{1-n}}\right]^{1/2} \tag{5.52}$$

and

$$\left.\begin{aligned} B_1(\xi) &= D_B\left(\frac{\overset{0}{\kappa}(\xi)^{1-n}}{n}\right)^{1/4} \\ D_B &= \left(\frac{\overset{0}{\kappa}{}^{1-n}}{n}\right)_0^{1/4} (\overset{0}{\kappa_\xi})_0 \\ (\overset{0}{\kappa_\xi})_0 &= -\kappa_{co}\frac{1}{n}\,. \end{aligned}\right\} \tag{5.53}$$

The intermediate result for the 2nd order perturbation $\overset{2}{\kappa}(\xi,\eta)$, analogous to Eq.(4.111), reads

$$\overset{2}{\kappa}(\xi,\eta) = B_2(\xi)e^{-\sqrt{\varphi}\eta} - \frac{\alpha_o(\xi)}{\varphi} + \frac{\alpha_2(\xi)}{3\varphi}e^{-2\sqrt{\varphi}\eta} \tag{5.54}$$

where

$$\left.\begin{aligned}
\alpha_o(\xi) &= -\frac{1}{(\mu_B')^2}\overset{0}{\kappa}_{\xi\xi} = -\varphi\frac{\left(\overset{0}{\kappa}\right)^{1-n}}{n}\overset{0}{\kappa}_{\xi\xi} \\
\alpha_2(\xi) &= -\Omega_B^2\frac{1}{2}(1-n)\frac{1}{\overset{0}{\kappa}}B_1^2 = \\
&= -\varphi\frac{1}{2}(1-n)\left(\frac{\overset{0}{\kappa}^{1-n}}{n}\right)_0^{1/2}\left(\overset{0}{\kappa}_\xi\right)_0^2\frac{1}{\overset{0}{\kappa}(\xi)}\left(\frac{\overset{0}{\kappa}(\xi)^{1-n}}{n}\right)^{1/2}
\end{aligned}\right\} \qquad (5.55)$$

which are formally the same as $(4.56)_{1\&4}$. The removing of the secular term in the particular solution $\overset{3}{\kappa}(\xi,\eta)$ yields, analogous to (4.112), a differential equation for $B_2(\xi)$

$$B_2' + \frac{1}{2}\frac{\mu_B''}{\mu_B'}B_2 = S_B \qquad (5.56)$$

where (compare with (4.113))

$$S_B(\xi) = \frac{1}{2}\frac{1}{\sqrt{\varphi}}\frac{1}{\mu_B'}B_1'' - \frac{1}{2}\frac{1}{\sqrt{\varphi}}\frac{\overset{0}{\kappa}^n}{\mu_B'}\left(\frac{n(1-n)}{\left(\overset{0}{\kappa}\right)^2}\right)\frac{\alpha_o}{\varphi}B_1. \qquad (5.57)$$

With (4.114) the solution of (5.56) is

$$B_2(\xi) = \frac{1}{\nu_B}\int_0^\xi \nu_B S_B\,\mathrm{d}\tau + \frac{(\nu_B)_0}{\nu_B}(B_2)_0 \qquad (5.58)$$

and with (4.115) and (4.116) we get

$$\left.\begin{aligned}
\nu_B &= (\mu_B')^{1/2} = \left(\frac{1}{\varphi}\frac{n}{\left(\overset{0}{\kappa}\right)^{1-n}}\right)^{1/4}, \qquad (\nu_B)_0 = (\mu_B')_0^{1/2} \\
(B_2)_0 &= B_2(0) = \frac{1}{4}\left(\frac{1}{n}\right)^2\frac{1}{\left(\overset{0}{\kappa}\right)_0^n}\left[\frac{7}{3}n(1-n)\right]\left(\overset{0}{\kappa}_\xi\right)_0^2.
\end{aligned}\right\} \qquad (5.59)$$

The function $\mu_B(\xi)$ can be found explicitly by integrating (5.52) using the initial condition $\mu_B(0)=0$. For $n\neq 1/3$ we get

$$\mu_B(\xi) = \left(\frac{n}{\varphi}\right)^{1/2} \kappa_{co}^{-\frac{1-n}{2}} \frac{2n}{1-3n}\left[(1-\xi)^{-\frac{1-3n}{2n}} - 1\right] \tag{5.60}$$

and, provided n=1/3,

$$[\mu_B(\xi)]_{n=1/3} = -\left(\frac{n}{\varphi}\right)^{1/2} \kappa_{co}^{-\frac{1}{3}} \ln(1-\xi). \tag{5.61}$$

The determination of the function $B_2(\xi)$, according to (5.58), can be done analytically for arbitrary hardening exponents n. This somewhat lengthy analysis is given in Appendix (10). The result is for $n \neq 1/3$ (otherwise see Appendix (10))

$$\left.\begin{aligned} B_2(\xi) &= \kappa_{co}^{2-n} \frac{1-n}{n^3} z(\xi)^{\frac{1-n}{4n}} \left\{\frac{7}{12} - \frac{17-21n}{16(1-3n)}\left[1 - z(\xi)^{\frac{1-3n}{2n}}\right]\right\} \\ z(\xi) &= 1-\xi\,. \end{aligned}\right\} \tag{5.62}$$

For a complete representation of the 2nd order perturbation curvature $\overset{2}{\kappa}(\xi,\eta)$, Eq.(5.54), we require $\alpha_o(\xi)$ and $\alpha_2(\xi)$ defined by (5.55). The first function is already determined, Eq.(A10.6)$_6$, and the second is found to be

$$\alpha_2(\xi) = -\frac{1}{2}\varphi\kappa_{co}^{2-n}\frac{1-n}{n^3} z(\xi)^{-\frac{1+n}{2n}}. \tag{5.63}$$

Summarizing we get the following perturbation functions

$$\left.\begin{aligned} \overset{0}{\kappa} &= \kappa_c(\xi) = \kappa_{co}\, z(\xi)^{1/n} \\ \overset{1}{\kappa}(\xi,\eta) &= B_1(\xi)e^{-\sqrt{\varphi}\eta} = -\kappa_{co}^{\frac{3-n}{2}} \frac{1}{n^{3/2}} z(\xi)^{\frac{1-n}{4n}} e^{-\sqrt{\varphi}\eta} \\ \overset{2}{\kappa}(\xi,\eta) &= B_2(\xi)e^{-\sqrt{\varphi}\eta} - \frac{\alpha_o(\xi)}{\varphi} + \frac{\alpha_2(\xi)}{3\varphi} e^{-2\sqrt{\varphi}\eta} = \\ &= \kappa_{co}^{2-n}\frac{1-n}{n^3}\left\{ z(\xi)^{\frac{1-n}{4n}}\left(\frac{7}{12} - \frac{17-21n}{16(1-3n)}\left[1 - z(\xi)^{\frac{1-3n}{2n}}\right]\right) e^{-\sqrt{\varphi}\eta} \right. \\ &\quad \left. + z(\xi)^{\frac{2-3n}{n}} - \frac{1}{6} z(\xi)^{-\frac{1+n}{2n}} e^{-2\sqrt{\varphi}\eta} \right\} \end{aligned}\right\} \tag{5.64}$$

with

$$\sqrt{\varphi}\eta = \sqrt{\varphi}\,\frac{\mu_B(\xi)}{\beta_q} = \frac{1}{\beta_q}\left(\frac{n}{\kappa_{co}^{1-n}}\right)^{1/2}\frac{2n}{1-3n}\left[(1-\xi)^{-\frac{1-3n}{2n}}-1\right]. \tag{5.65}$$

Here $n\neq 1/3$ is implied; otherwise appropriate changes for $B_2(\xi)$ and $\mu_B(\xi)$ have to be made. The above functions define the asymptotic solution

$$\kappa = \hat{\kappa}(\xi;\beta_q) = \tilde{\kappa}(\xi,\eta;\beta_q) = \overset{0}{\kappa}(\xi) + \beta_q \overset{1}{\kappa}(\xi,\eta) + \beta_q^2 \overset{2}{\kappa}(\xi,\eta). \tag{5.66}$$

For the special case $n=1$ we get

$$\left.\begin{aligned} &\overset{0}{\kappa}(\xi) = \kappa_c(\xi) = \kappa_{co}\, z(\xi), \qquad \kappa_{co} = \left(\frac{L}{h}\right)^2 \frac{P}{Kbh}\,12 \\ &\overset{1}{\kappa}(\xi,\eta) = -\,\kappa_{co}\, e^{-\sqrt{\varphi}\eta} \\ &\overset{2}{\kappa}(\xi,\eta) \equiv 0 \end{aligned}\right\} \tag{5.67}$$

and

$$\sqrt{\varphi}\eta = \frac{1}{\beta_q}\xi, \qquad \beta_q = \sqrt{q}\,\beta = \beta. \tag{5.68}$$

Thus, the approximation yields

$$\kappa(\xi) = \kappa_c(\xi) - \kappa_{co}\,\beta\, e^{-\xi/\beta}. \tag{5.69}$$

We note that this result satisfies the boundary condition B.C.II, Eq.(5.17), at the center of the beam exactly; the boundary condition B.C.I, Eq.(5.18), at the end of the beam, is satisfied only for $\beta\to 0$. This is due to the transformed boundary condition B.C.I, Eq.(5.46), where for $x=L$ the fast variable η was required to take very large values ($\eta\to\infty$).

The exact solution (5.34) for the linear case $n=1$ can be approximated for small values $\beta<<1$ such that $e^{-2/\beta}<<1$; this transforms (5.34) into

$$\kappa(\xi) = \kappa_c(\xi) - \kappa_{co}\beta\left\{e^{-\xi/\beta} - e^{-(2+\xi)/\beta} - e^{-(2-\xi)/\beta} + e^{-(4-\xi)/\beta}\right\}. \tag{5.70}$$

For ξ close to zero the dominant gradient contribution is given by the first term in parentheses. For ξ close to unity the terms in parentheses cancel; thus, the boundary condition B.C.I is exactly satisfied. In comparison to Eq.(5.69), note the additional exponential terms in (5.70), which are necessary for an exact satisfaction of the boundary condition at the end of the beam. However, at the center of the beam $\xi=0$ the perturbation solution (5.69) agrees exactly with the dominant term in (5.70).

5.4 Evaluation

5.4.1 The Linear Case (n=1)

The non-classical distribution of the dimensionless curvature is given by Eq.(5.34) and is plotted in Fig.5.2. It consists of the classical part κ_c and a non-classical part depending on β which -for small values of β, e.g. β<0.1 - is a fast decaying contribution close to the center of the beam ξ=0 (boundary layer). For greater values of β the gradient term influence is found over the whole length of the beam.

With Eq.(5.2) the bending strain in the beam is proportional to the curvature. Thus, the maximum tensile strain opposite to the applied central load is

$$\varepsilon_{o\,\max} = (k)_{\xi=0}\,\frac{h}{2} = \frac{h}{2L}(\kappa)_{\xi=0}\,.$$

With ε_c being the classical strain distribution, its maximum value (at ξ=0) is

$$\varepsilon_{co\,\max} = \frac{h}{2L}\kappa_{co}\,;$$

then the ratio of the maximum strain of the non-classical and the classical solution is given by

$$\frac{\varepsilon_{o\max}}{\varepsilon_{co\max}} = \frac{(\kappa)_o}{\kappa_{co}}\,.$$

Fig.5.2 shows the rather strong reduction of the maximum strain (~curvature) at the center ξ=0. In explicit terms the relative strain is given by

$$\frac{\varepsilon_{o\max}}{\varepsilon_{co\max}} = \frac{(\kappa)_o}{\kappa_{co}} = 1-\beta\,\frac{2\sinh(2/\beta)}{1+2\cosh(2/\beta)} \tag{5.71}$$

which is plotted in Fig.5.3. For small values β (~≤0.1) this can be approximated by

$$\frac{\varepsilon_{o\max}}{\varepsilon_{co\max}} = \frac{(\kappa)_o}{\kappa_{co}} = 1-\beta\,. \tag{5.72}$$

The upper limit of $\beta = l_i/L = 1$ is a purely mathematical construct if the internal length scale l_i is somehow related to the microstructure of the material. Then the limit

$$\frac{l_i}{h/2} = \beta\,\frac{L}{h}2 \le 1$$

appears to be more reasonable but is still exaggerated. This gives the upper bound

$$\beta < \frac{h}{2L}\,.$$

If the shear deflection is required to be less than 5% of the bending deflection to be negligible in steel (Szabó 1958, [5.1], p.125), then $h/L<0.227$ and this implies

$$\beta<0.11 \tag{5.73}$$

in the linear case.

A change in the parameter β reflects a change in the material (l_i) or a change in size (L). Thus, Fig.5.3 visualizes the size dependence of the bending strain at the beam center since β is inversely proportional to the size. With the subscript (p) denoting a large specimen ("prototype") and (m) denoting a small specimen ("model") we have

$$\beta_p = \frac{l_i}{L_p} = \frac{l_i}{L_m}\frac{L_m}{L_p} = \beta_m \frac{1}{\lambda} \tag{5.74}$$

and

$$\frac{(\varepsilon_{o\max})_p}{(\varepsilon_{o\max})_m} = \frac{1-\beta_p}{1-\beta_m} = \frac{1-\beta_m/\lambda}{1-\beta_m}\,. \tag{5.75}$$

Assuming β_m to be given by the limit value

$$\beta_m = 0.11 \tag{5.76}$$

as described above, Eq.(5.75) yields

$$\frac{(\varepsilon_{o\max})_p}{(\varepsilon_{o\max})_m} = 1.1236 - 0.1236\,\lambda^{-1}. \tag{5.77}$$

Comparing a very large specimen ($\lambda\to\infty$) and the smallest specimen satisfying the limit value (5.76), Eq.(5.77) shows that at the most a difference of 12% in the maximum strain of the bending specimens is predicted.

The results of Section (5.1) allow also to illustrate the size influence on a dimensionless force-deformation relation. The maximum bending stress opposite to the applied central load is, according to the classical theory,

$$\sigma_{co\,\max} = \frac{PL}{bh^3/12}\frac{h}{2}. \tag{5.78}$$

With (5.15) and n=1 we get

$$\kappa_{co} = \left(\frac{L}{h}\right)^2 \frac{P}{Kbh}12 = 2\frac{L}{h}\frac{\sigma_{co\,\max}}{K} = 2\frac{L}{h}\varepsilon_{co\,\max}$$

and thus Eq.(5.71) yields

$$\left.\begin{aligned} \tilde{P} &= \frac{\sigma_{co\,\max}}{K} = C(\beta)\varepsilon_{o\,\max} \\ C(\beta) &= \left[1-\beta\,\frac{2\sinh(2/\beta)}{1+2\cosh(2/\beta)}\right]^{-1} . \end{aligned}\right\} \qquad (5.79)$$

The left-hand side of Eq.$(5.79)_1$ is a dimensionless stress calculated using the classical theory -a measure for the loading- and $\varepsilon_{o\,\max}$ is the maximum local strain according to the non-classical solution. The stiffness C is size dependent via the parameter β and is bounded from below and above by

$$1 \le C(\beta) \le 1.1216 \le 6.7086$$

$$\text{with } 0 \le \beta = \frac{l_i}{L} \le 0.11 \le 1$$

where the very large specimen yields the value C_o=1 and the reasonable smallest specimen (β=0.11) yields the stiffness $C_{\beta=0.11}$=1.1216. In this range, to a first approximation,

$$C(\beta)=1+\beta \qquad (5.80)$$

when the exponential term in (5.79) is approximated by "1". Thus the relative change in stiffness is proportional to β:

$$\frac{C(\beta)-C_o}{C_o} \sim \beta .$$

It is fairly obvious that the qualitative trends are very similar to those obtained for the linear case of the tapered tensile rod (Section (3.1.4)).

5.4.2 The Non-Linear Case ($n\neq1$)

The approximate perturbation solution for the gradient enhanced deformation plasticity law is given by (5.64) to (5.66). Naturally, it consists of the classical solution κ_c (the 0th order approximation $\overset{0}{\kappa}$) and the non-classical part (the 1st and 2nd order terms) depending on β_q. The latter are exponentially decaying contributions close to the center of the beam. For ξ<<1 the exponent $\sqrt{\varphi\eta}$, Eq.(5.65), simplifies to

$$\sqrt{\varphi\eta} \approx \frac{1}{\beta_q}\left(\frac{n}{\kappa_{co}^{1-n}}\right)^{1/2}\xi . \qquad (5.81)$$

The decay rate d, defined by

$$d = \frac{1}{\beta_q}\left(\frac{n}{\kappa_{co}^{1-n}}\right)^{1/2}, \tag{5.82}$$

is not only depending on β_q and the hardening exponent n but also on κ_{co}, defined by $(5.15)_2$,

$$\kappa_{co} = \left(\frac{L}{h}\right)^{\frac{1+n}{n}}\left(\frac{P}{Kbh}\right)^{1/n}(2+n)^{1/n}\,2^{\frac{1+n}{n}} = \frac{L}{h}\left(\frac{4PL}{Kbh^2}\right)^{1/n}\left(1+\frac{n}{2}\right)^{1/n}2 \tag{5.83}$$

which is the maximum dimensionless curvature at ξ=0 according to the classical solution. It is a nonlinear measure for the loading P. Thus, by increasing κ_{co} the decay rate (d) is reduced. For example, if n=1/5 and 1/9, then

$$d \sim \left(\frac{P}{Kbh}\right)^{-2} \text{ and } \left(\frac{P}{Kbh}\right)^{-4}.$$

This is in contrast to the linear case (n=1), Eq.(5.68), where the decay is not depending on the loading level but given by

$$(d)_{n=1} = \frac{1}{\beta_q} = \frac{1}{\beta}.$$

It appears necessary to estimate the expected admissible range of the dimensionless shear force

$$\tilde{P} = \frac{P}{Kbh} \tag{5.84}$$

using realistic material response data K, n and others, for example for the ferritic reactor pressure vessel steel A533-B and stainless steel 304 at room or low temperatures. Kumar et al. (1981, [5.2]) used the Ramberg-Osgood stress-strain relationship

$$\frac{\varepsilon}{\varepsilon_o} = \frac{\sigma}{\sigma_o} + \alpha\left(\frac{\sigma}{\sigma_o}\right)^m, \quad m \geq 1 \tag{5.85}$$

for the interpolation of uniaxial tensile test results less than 30% strain. An alternative form of (5.85) is

$$\varepsilon = \frac{1}{E}\sigma + \left(\frac{\sigma}{K}\right)^{\frac{1}{n}}, \quad n \leq 1 \tag{5.86}$$

where

$$E=\frac{\sigma_o}{\varepsilon_o},\qquad n=\frac{1}{m}\le 1,\qquad K=\frac{\sigma_o}{(\varepsilon_o\alpha)^{1/m}} \tag{5.87}$$

The corresponding material data are listed in Table 5.2

Ignoring the elastic strain σ/E in Eq.(5.86) yields the classical deformation plasticity model used in this section. Within this model the maximum bending stress at $\xi=0$ is

$$\sigma_{co\,\max}=K\left(\frac{K_{co}}{L}\frac{h}{2}\right)^n=K\left(\frac{P}{Kbh}\right)\left(\frac{L}{h}\right)(2+n)\,2=$$

$$=K\left(\frac{4PL}{Kbh^2}\right)\left(1+\frac{n}{2}\right). \tag{5.88}$$

For h/L=0.2 and the A533-B steel this gives

$$\sigma_{co\,\max}=21.03\,K\left(\frac{P}{Kbh}\right)=16.32\,10^3\left(\frac{P}{Kbh}\right)\text{[MPa]}$$

and for the stainless steel we get

$$\sigma_{co\,\max}=21.84\,K\left(\frac{P}{Kbh}\right)=14.67\,10^3\left(\frac{P}{Kbh}\right)\text{[MPa]}.$$

If the load P is assumed to be very large such that

$$\tilde{P}=\left(\frac{P}{Kbh}\right)\ge 1,$$

then the maximum bending stress is out of the range of validity of the power law hardening model; a reasonable upper limit is estimated to be 100ksi ≈ 690MPa (see ref. [5.2]). Thus, an acceptable range for the variable $\tilde{P}$ is

$$\left.\begin{aligned}&\tilde{P}=\frac{P}{Kbh}\le 0.042<\frac{690}{16.32\,10^3}\\ \text{or}\qquad&\\ &\tilde{\tilde{P}}=\frac{4PL}{Kbh^2}\le 1.0\end{aligned}\right\}\quad \frac{h}{L}\sim 0.2 \tag{5.89}$$

For smaller values h/L<0.2 the variable $\tilde{P}$ is restricted to even smaller values. If, however, h/L>0.2, then $\tilde{P}$ may take somewhat larger values than given by $(5.89)_1$. In any case it is concluded that

$$\tilde{P}=\frac{P}{Kbh}<<1. \tag{5.90}$$

The quantity $\tilde{\tilde{P}}$ and the condition $(5.89)_2$ may be given a simple interpretation. The bending moment at ξ=0 is M_o=PL. Assuming that the bending stress distribution in the cross-section is piecewise constant as in ideal plasticity, then the corresponding bending stress, which balances M_o, is given by

$$\sigma_F = \frac{4PL}{bh^2}. \tag{5.91}$$

Thus, Eq.$(5.89)_2$ implies

$$\frac{\sigma_F}{K} \leq 1. \tag{5.92}$$

In fact, in the limit $n \to 0$ the power law hardening model (without gradient enhancement) yields

$$\sigma = \pm K,$$

the rigid ideal-plastic stress-strain relation. Therefore, an ideal plastic bending stress distribution is obtained at the center of the beam if the limit load, defined by

$$\tilde{\tilde{P}} = \frac{4PL}{Kbh^2} = 1, \tag{5.93}$$

is reached. Thus, Eq.$(5.89)_2$ is a rather natural restriction although strictly valid only for n=0.

The normalized curvature distribution along the beam is obtained from equations (5.64) ÷ (5.66) and $(5.15)_2$. It is shown for the specific values n=0.2, $\tilde{P}$ =P/Kbh=0.035 and h/L=0.2 in Fig.5.4 for several 2nd order strain gradient parameters β. The boundary layer effect of the strain gradient term (β>0) is clearly seen. Compared to the linear case (n=1, Fig 5.2) and for 0<β<0.05 it is evident that the non-linearity increases the reduction of the relative maximum curvature at ξ=0, because it becomes load-dependent. It is also exemplified by Eq.(5.15) & (5.16) that the power law hardening produces a very different classical curvature distribution (β=0): The non-linearity shifts the normalized curvature κ_c/κ_{co} towards the center of the beam.

Now attention is put to the curvature and relative strain at ξ=0. With $\xi \to 0$, $\eta \to 0$ we get in general terms

$$\kappa(0,0) = \overset{0}{\kappa}(0) + \beta_q \overset{1}{\kappa}(0,0) + \beta_q^2 \overset{2}{\kappa}(0,0)$$

where

$$\overset{0}{\kappa}(0) = \kappa_{co}$$

$$\overset{1}{\kappa}(0,0) = B_1(0) = \left(\frac{\kappa_{co}^{1-n}}{n} \right)^{1/2} (\overset{0}{\kappa_\xi})_0$$

$$\overset{2}{\kappa}(0,0) = B_2(0) - \frac{\alpha_o(0)}{\varphi} + \frac{\alpha_2(0)}{3\varphi} =$$

$$= \frac{7}{12}\frac{1-n}{n}\kappa_{co}^{-n}\,\overset{0}{(\kappa\xi)_0^2} + \left(\frac{\kappa_{co}^{1-n}}{n}\right)\overset{0}{(\kappa\xi\xi)_0} - \frac{1-n}{6}\left(\frac{\kappa_{co}^{1-n}}{n}\right)\kappa_{co}^{-1}\,\overset{0}{(\kappa\xi)_0^2}$$

such that

$$\kappa(0,0) = \kappa_{co} + \beta_q\left(\frac{\kappa_{co}^{1-n}}{n}\right)^{1/2}\overset{0}{(\kappa\xi)_0}$$

$$+ \beta_q^2\left\{\frac{5}{12}\frac{1-n}{n}\kappa_{co}^{-n}\,\overset{0}{(\kappa\xi)_0^2} + \frac{\kappa_{co}^{1-n}}{n}\overset{0}{(\kappa\xi\xi)_0}\right\}$$

and the relative curvature and bending strain is

$$\frac{\varepsilon_{o\max}}{\varepsilon_{co\max}} = \frac{\kappa(0,0)}{\kappa_{co}} = 1 + \beta_q\left(\frac{\kappa_{co}^{1-n}}{n}\right)^{1/2}\frac{\overset{0}{(\kappa\xi)_0}}{\kappa_{co}} +$$

$$+\beta_q^2\frac{\kappa_{co}^{1-n}}{n}\left\{\frac{5}{12}(1-n)\left(\frac{\overset{0}{(\kappa\xi)_0}}{\kappa_{co}}\right)^2 + \frac{\overset{0}{(\kappa\xi\xi)_0}}{\kappa_{co}}\right\}. \qquad (5.94)$$

Recalling the analogous procedure in section (4), this result is generally valid irrespective of the specific load distribution along the beam, provided it is symmetric with respect to ξ=0 and the boundary conditions (5.17&18) apply. Of course the specific values $\overset{0}{(\kappa)_0}$, $\overset{0}{(\kappa\xi)_0}$, $\overset{0}{(\kappa\xi\xi)_0}$ depend on the load distribution and its magnitude. Especially if $\overset{0}{(\kappa\xi)_0}$=0, which is the case when the bending moment distribution is smooth around ξ=0, then the term linear in β_q drops out and (5.94) simplifies to

$$\frac{\varepsilon_{o\max}}{\varepsilon_{co\max}} = \frac{\kappa(0,0)}{\kappa_{co}} = 1 + \beta_q^2\frac{1}{n\kappa_{co}^n}\overset{0}{(\kappa\xi\xi)_0}\,. \qquad (5.95)$$

Thus, the relative strain reduction $(1 - \varepsilon_{o\max}/\varepsilon_{co\max})$ is only quadratically affected by the small parameter β_q due to the non-classical 2nd order strain gradient extension of the deformation law. This is a result that is reasonably expected.

With (5.48) the curvature at $\xi\to 0$ is in explicit terms

$$\kappa(0,0) = \kappa_{co} - \beta_q\left(\frac{\kappa_{co}^{1-n}}{n}\right)^{1/2}\frac{\kappa_{co}}{n} + \beta_q^2\left(\frac{\kappa_{co}^{1-n}}{n}\right)\frac{17}{12}\frac{1-n}{n^2}\kappa_{co} \qquad (5.96)$$

and the relative strain (5.94) reads

$$\frac{\varepsilon_{o\max}}{\varepsilon_{co\max}} = 1 - \beta_q \left(\frac{\kappa_{co}^{1-n}}{n}\right)^{1/2} \frac{1}{n} + \beta_q^2 \left(\frac{\kappa_{co}^{1-n}}{n}\right) \frac{1-n}{n^2} \frac{17}{12}. \tag{5.97}$$

Using the decay rate parameter (d), Eq.(5.82), this ratio takes the form

$$\frac{\varepsilon_{o\max}}{\varepsilon_{co\max}} = 1 - \frac{1}{nd} + \left(\frac{1}{nd}\right)^2 (1-n) \frac{17}{12}\ ; \tag{5.98}$$

thus, an increase in the decay rate (d) is connected with a decrease of the relative strain reduction $(1 - \varepsilon_{o\max} / \varepsilon_{co\max})$.

The relative strain is plotted versus $\beta = l_i/L$ in Fig.5.5. As in Section 4, it is seen that, depending on the magnitude of the hardening exponent n, the relation (5.97) becomes erroneous when β approaches ~0.1 from below because a monotonous decrease of the relative strain is expected, as found for the linear case (n=1) (Fig.5.3). This is due to the dominance of the quadratic β-term for large β-values. For example, for n=1/9 the result appears to be reasonable up to β=0.03. Thus, Fig.5.5 shows also that a decrease in the hardening exponent n will reduce the range of validity of the 2nd order perturbation approximation to smaller values of β. An extension of the range of validity can be obtained by including higher order terms in β_q in the approximation.

For the purpose of comparison the relative strain versus β is also shown without the quadratic term (Fig.5.6). The results show that for a given loading P/Kbh, geometry h/L, and $\beta=l_i/L$ a decrease of the hardening exponent n down to 1/9 produces an increase in the relative strain reduction $(1 - \varepsilon_{o\max} / \varepsilon_{co\max})$. In other words, the importance of the 2nd order strain gradient influence and thus the size influence on the relative strain increases with a decrease of the hardening exponent n. However, because of the mathematical similarity of the tension rod problem (Section 4) and the beam bending problem, a similar behavior, especially for varying hardening exponents n, is evident. Concerning the classical solution, Eq.(5.15), (5.16), (5.47) & (5.48), a decrease in the hardening exponent n yields a shift of the relative curvature κ_c/κ_{co} and its 1st and 2nd order derivative, $\kappa_{c\xi}/\kappa_{co}$ and $\kappa_{c\xi\xi}/\kappa_{co}$, respectively, towards the center of the beam. Thus, the 'relative non-uniformity' of the curvature distribution at $\xi = 0^+$ is increased. For very small values of n, their maximum at $\xi = 0^+$ behave according to

$$(\kappa_{c\xi})_0 / \kappa_{co} = -\frac{1}{n}, \qquad (\kappa_{c\xi\xi})_0 / \kappa_{co} = \frac{1-n}{n^2}$$

with

$$\kappa_{co} \approx \left[\tilde{\tilde{P}}\right]^{1/n} e^{1/2} \frac{2L}{h}, \qquad \tilde{\tilde{P}} = \frac{4PL}{Kbh^2} < 1, \qquad \lim_{n\to 0}(1+\frac{n}{2})^{1/n} = e^{1/2}.$$

In Section 4.4.1 this increase of the relative non-uniformity with decreasing hardening exponent was called 'relative localization'.

Keeping the geometry, the loading P, and the parameters K and β constant but decreasing the hardening exponent n, the maximal deformation measures κ_{co}, $(\kappa_{c\xi})_0$, $(\kappa_{c\xi\xi})_0$ decrease and their limit values vanish:

$$\lim_{n\to 0}\kappa_{co}=\lim_{n\to 0}(\kappa_{c\xi})_0=\lim_{n\to 0}(\kappa_{c\xi\xi})_0=0.$$

In this limit state the beam does not suffer any deformation as long as $\tilde{\tilde{P}}<1$.

Thus, opposing effects are obviously contained in the general equation (5.94) when the hardening exponent is decreased. These qualitative findings, already discussed in the context of the tapered tensile rod, suggest that the relative strain, Eq.(5.97), will show a peculiar dependence on the hardening exponent n, i.e. some optimal influence when all other parameters and variables are held constant. These results are confirmed in Fig.5.7 and Fig.5.8. Fig.5.7 shows the dependence of the maximum bending strain (non-classical solution) on the hardening exponent. For a certain range of small hardening exponents almost no deformation is obtained but for larger values of n a strong, almost linear increase in deformation is seen.

Fig.5.8, the relative strain versus n, is of special interest: for a fixed set of parameters, especially the dimensionless shear load $\tilde{P}$, there exists a specific value of the hardening exponent for which the 2nd order gradient influence on the relative strain is largest, i.e. at the minimum of the plots in Fig.5.8. For the chosen parameters the characteristic exponents are close to actual hardening exponents of structural materials (Table 5.1). Obviously, the stoutness h/L and the loading level $\tilde{P}$ or $\tilde{\tilde{P}}$ have a strong influence on the relative strain. We note that the range of stoutness data in Fig.5.8a corresponds to the following range of the load parameter $\tilde{\tilde{P}}$

$$0.48\le \tilde{\tilde{P}}=\tilde{P}\frac{L}{h}4\le 0.8.$$

Further, the range of the shear load parameter $\tilde{P}$ in Fig.5.8b is equivalent to

$$0.5\le \tilde{\tilde{P}}\le 0.9.$$

The dependence of the relative strain on the load parameter $\tilde{P}$ can be obtained from (5.97) using (5.83). It is shown in Fig.5.9 for fixed parameters n=0.2, h/L=0.2 but β varying between 0.01 and 0.04 and the load parameter restricted to $0\le \tilde{P}\le 0.04$ ($0\le \tilde{\tilde{P}}\le 0.8$).

For β=0.01 and h/L=0.2 the internal length l_i is 5% of the depth of the beam and the relative strain reduction is about 7% for the maximal load parameter $\tilde{P}$=0.04. Decreasing the size of the beam by a factor of four, the internal length corresponds to 20% of the beam depth and the strain reduction is almost 20%. In any case it is obvious that the 2nd order gradient influence to be effectively detectable, the internal length should amount to several hundredth of half-length of the beam. Of course, some other parameters, e.g. the stoutness h/L, can be changed to increase its influence.

Analogous to Section 5.4.1, Eq.(5.97) is used to determine the bending strain ratio of two geometrically similar beam specimens of different size -the model (m) and the prototype (p)- made of the same material and under scaled loading, i.e. P/bh = const.

With (5.74) we get from (5.97)

$$\frac{(\varepsilon_{o\max})_p}{(\varepsilon_{o\max})_m} = \frac{1-\sqrt{q}\beta_p\left(\frac{\kappa_{co}^{1-n}}{n}\right)^{1/2}\frac{1}{n}+q\beta_p^2\left(\frac{\kappa_{co}^{1-n}}{n}\right)\frac{1-n}{n^2}\frac{17}{12}}{1-\sqrt{q}\beta_m\left(\frac{\kappa_{co}^{1-n}}{n}\right)^{1/2}\frac{1}{n}+q\beta_m^2\left(\frac{\kappa_{co}^{1-n}}{n}\right)\frac{1-n}{n^2}\frac{17}{12}}$$

$$= \frac{1-B_m\lambda^{-1}+B_m^2\lambda^{-2}(1-n)\frac{17}{12}}{1-B_m+B_m^2(1-n)\frac{17}{12}}, \tag{5.99}$$

where

$$B_m = \sqrt{q}\beta_m\left(\frac{\kappa_{co}^{1-n}}{n}\right)^{1/2}\frac{1}{n} = \frac{1}{nd_m}. \tag{5.100}$$

The quantity B_m is determined by the shape and the material properties of the beam and the loading but especially by the absolute size L_m of the beam model via the parameter $\beta_m=l_i/L_m$. To obtain a typical value for B_m the following example is considered:

We take h/L=0.2 and n=1/9. This yields q=0.043. The load parameter $\tilde{\tilde{P}}$ is assumed to be quite large

$$\tilde{\tilde{P}} = \frac{4PL}{Kbh^2} = 0.8$$

which gives with (5.83)

$$\kappa_{co} = 2.183$$

and thus

$$B_m = 7.9267\ \beta_m.$$

According to Fig.5.5, it is estimated that the perturbation approximation is appropriate up to β=0.03 if n=1/9. This β-value defines the minimum size (length) of the beam, which can be treated with the present perturbation approximation. Thus we assume

$$\beta_m = 0.03;$$

this implies that the internal length amounts to 15% of the beam depth h. Consequently

$$B_m = 0.2378.$$

With these data Eq.(5.99) gives

$$\frac{(\varepsilon_{o\max})_p}{(\varepsilon_{o\max})_m} = \frac{1.000 - 0.238\lambda^{-1} + 0.0712\lambda^{-2}}{0.833} = 1.200 - 0.285\,\lambda^{-1} + 0.085\,\lambda^{-2}\,.$$

For λ=10 we get

$$\frac{(\varepsilon_{o\max})_p}{(\varepsilon_{o\max})_m} = 1.172.$$

Increasing λ indefinitely yields the upper bound

$$\left[\frac{(\varepsilon_{o\max})_p}{(\varepsilon_{o\max})_m}\right]_{\lambda\to\infty} = \frac{1}{1 - B_m + B_m^2(1-n)\dfrac{17}{12}} = 1.200\,. \qquad (5.101)$$

For the purpose of comparison we consider the linear case n=1. Then B_m=β_m and Eq.(5.75) or (5.99) gives for the very large specimens

$$\left[\frac{(\varepsilon_{o\max})_p}{(\varepsilon_{o\max})_m}\right]_{\substack{n=1\\ \lambda\to\infty}} = \frac{1}{1-\beta_m} = 1.031. \qquad (5.102)$$

Eq.(5.101) compared with (5.102) illustrates again the enhancement of the strengthening effect of gradient plasticity in small specimens when non-linear hardening (n<1) is involved.

Of course the strain ratio Eq.(5.101) increases with a rise of the load level $\tilde{\tilde{P}}$. Table 5.3 shows the strong non-linear dependence for a set of discrete load levels. For small values of B_m this non-linearity follows the power law relation

$$\left(\frac{\varepsilon_{o\max}}{\varepsilon_{co\max}}\right)_{\lambda\to\infty} \sim \left(\tilde{\tilde{P}}\right)^{\frac{1-n}{2n}};$$

for n =1/9 the exponent is 4. For values of $\tilde{\tilde{P}}$ approaching 1 the solution Eq.(5.101) becomes erroneous.

The result (5.96) for the maximum curvature at ξ=0 allows to demonstrate the size influence on a dimensionless force-deformation relation. Fig.5.10 zooms in on the relation between the non-classical local bending strain at ξ=0 and the load parameter $\tilde{P}$ =P/Kbh (dimensionless shear stress) for h/L=0.2, n=1/5, and with β as a parameter. It is seen that the bundle of dimensionless stress strain curves fans out and, with increasing β-values (decreasing size L), smaller specimens suffer less strain under the same scaled loading. We recall that all curves would collapse into one curve if no size effect were involved (l_i≡0). In principle such qualitative trends can be tested by scaled experiments since both quantities can be determined easily. However, it is evident that the theory is very simple. Several effects (e.g. large deformations, shear deformation, multiaxiality) are ignored and some of them may not only produce quantitative but also qualitative effects. Therefore, the fitting of the internal length

parameter l_i to a set of experiments may be a delicate task since the result may be sensitive to the simplifications of the theoretical model.

6. Summarizing Discussion and Conclusions

6.1 Scope of the Section

The enhancement of elastic-plastic and damage models by higher order gradient or non-local (integral) terms in the stress-strain relations, yield condition, or evolution equations for the internal variables has been introduced to limit 'pathological' strain localization and mesh dependence occuring in finite element solutions of conventional boundary value problems which do not involve an internal material length. Thus the above models were developed, in part, to cope with the non-well-posedness of the classical material models, which arises when material softening comes into play. Generally, the advanced theories implicate gradient or non-local terms which, in turn, can be associated with internal length scales that have the status of material parameters. Although several authors introduced these terms motivated by computational arguments, we emphasize here the more physical point of view that the internal length scales are somehow characteristic of the material microstructure. As a consequence of the gradient generalization, the interaction between the geometric length of a specimen and the internal length causes a size-dependent response of the theoretical model. Physically, this is quite plausible since the microstructure may influence the response; for example, when the sizes of domains with rather non-uniform strain distributions become comparable with typical length scales of the microstructure.

As mentioned in the Introduction of Part I [1.1] and of Part II, the general objectives of the theoretical work described in Part II 'Applications' are to exemplify the extent strain gradient plasticity captures the size influence on the deformation behavior. This, of course, requires the choice of specific gradient plasticity models and therefore any qualitative and quantitative results will be model-dependent.

Generally, gradient enhanced plasticity models do not allow easy analytical solutions of the corresponding boundary value problems. Therefore, depending on the model, numerical procedures have been developed, for example as sketched in Part I, Section 3. However, instead of the development or adoption of a purely numerical solution procedure and its realization in a computer program, a direct approach was chosen to be more appropriate at the present development state: Simple loading configurations are selected and relatively simple gradient plasticity models are used such as proposed by Aifantis (1984, [6.1]); i.e. extensions of the usual yield condition of classical plasticity by terms proportional to the norm of the strain gradient and the Laplacian of the strain, which are amenable to relatively easy theoretical treatment. At most one-dimensional problems are considered which belong to two different categories:

1st *Group: Algebraic problems*

The size dependence of the yield initiation in pure bending and pure torsion is treated using a conventional elasticity model in the elastic regime and a conventional yield condition enhanced by a 1st and a 2nd order strain gradient term. No boundary value problem needs to be solved. Fitting of the strain gradient solutions to available experimental data is performed.

2nd *Group: One-dimensional boundary value problems*

The size dependence is systematically studied for geometrically similar specimens of the same material and the relative influence of the strain gradient terms is determined. Ignoring elastic effects, a deformation type plasticity law with power law hardening is assumed, which is extended by the Laplacian of the strain. Spatially one-dimensional boundary value problems are considered, i.e. tension of tapered rods and three-point bending of uniform beams. Exact solutions are obtained for the linear cases and approximate analytical solutions are developed for the non-linear problems using the method of multiple scales of singular perturbation theory. Appropriate experimental data are presently not available for comparison.

In the following we will discuss these two different task groups and extract related conclusions.

6.2 First Group: Algebraic Problems

The literature survey (Part I, Section 2) on the size effect of the initiation of yielding under non-uniform stress in geometrically similar specimens of the same material (especially steel with pronounced lower and upper yield stress) revealed, for various types of specimens, a quasi-exponential decrease of the yield stress when the size is increased.

Two relatively simple specimen families, i.e.

- torsion of circular rods (Morisson 1939, [1.2])
- pure bending of smooth rectangular beams (Richards 1958, [1.3]),

were selected to assess the interpretative capability of gradient plasticity models. In the context of small deformation theory the yield condition is taken to be of the form

$$\sigma = \sigma_o - c_1(\nabla\varepsilon \cdot \nabla\varepsilon)^{1/2} - c_2\nabla^2\varepsilon\,, \tag{6.1}$$

where σ and ε are scalar stress and strain measures, ∇ is the Nabla-operator and $\nabla^2=\nabla\cdot\nabla$ the Laplace-operator, and σ_o (=const.) is the tensile yield stress under homogeneous stress conditions for the case of ideal plasticity (no hardening). In the elastic region Hooke's law is assumed to apply. It is important to note that the strain ε in the enriched yield condition is the elastic strain at the instant of yielding which is also linearly related to the stress according to Hooke's law. Thus, in a certain sense, the strain gradient terms in the enriched yield condition can also be interpreted as 1st and 2nd order spatial stress gradients.

Definitely, this model cannot predict any size effect if the macroscopic strain or stress gradients vanish identically, i.e. for a homogeneous state. Therefore, the interpretation of geometrically scaled experiments under non-uniform stress states with this model is reasonable only if homogeneous tensile tests with the same material do not reveal a size effect on the initiation of yielding.

In fact, for the material (plain carbon steel) used by Morrison for the torsion tests, several scaled tension and compression tests with a scale factor of only up to 3.55 have been performed, which showed neither a size dependence of the yield nor of the ultimate stress.

On the other hand, for the mild steel used by Richards (1958, [1.3]) for his scaled bending tests, no accompanying tensile tests were performed. However, Richards carried out a

large number of tensile tests for a mild steel not identified to be the same to that used for the bending tests; these tensile tests demonstrate a definite decrease of the yield stress with increasing size and a considerable scatter.

However, frequently the opinion is expressed that true size effects in ordinary tensile tests of ductile engineering materials are so small that they are difficult to detect (see Shearin, Ruark and Trimble (1948, [6.2])). The literature survey performed on this topic and described in Part I shows that the yield stress, the 0.2%-proof stress or the stress at 0.5% strain are frequently found to be not affected by the change in size. However, there are definite exceptions where a decrease of these quantities is observed when the diameter is increased. Also, experimental evidence obtained by Plechanova and Ratner (1954, [6.3]) supports the suggestion that this size dependence may not only be generated by surface hardening induced by the machining of the specimens; possibly it is an inherent material property related to the heterogeneity of the microstructure.

The adaption of the gradient plasticity model to Morrison's torsion tests implied a least squares fitting of three parameters: the two gradient parameters c_1/G and c_2/G (where G is the elastic shear modulus) and the parameter Λ, which is the ratio of the yield stress in shear and tension, i.e. $\Lambda = \tau_o / \sigma_o$.

The size effect formula, Eq.(2.4), may also be written in the form

$$\frac{Y(\alpha)}{\sigma_o} = \frac{\Lambda}{1-(l_1/\alpha)+(l_2/\alpha)^2} \quad , \tag{6.2}$$

where Y is the yield stress at the surface of the circular torsion rod, α is its radius and where the two internal length parameters

$$l_1 = -\frac{\bar{c}_1}{G} = -\frac{c_1}{G}\Lambda^2, \qquad l_2 = \sqrt{\frac{\bar{c}_2}{G}} = \sqrt{\frac{c_2}{G}}\Lambda \tag{6.3}$$

are the coefficients of the radius dependent terms.

The fitting procedure yielded

$$c_1/G = -1.427 \text{ mm}, \quad c_2/G = 0.85 \text{ mm}^2, \tag{6.4}$$

or alternatively

$$\left.\begin{array}{l} l_1 = 0.38\text{mm}\,, \quad l_2 = 0.476\text{mm} \\ \text{with} \\ \Lambda = 0.516\,. \end{array}\right\} \tag{6.5}$$

The ratio Λ is between 0.577 (von Mises yield condition) and 0.5 (Tresca yield condition) and is comparable to values found in the literature on carbon steel.

The fitting shown in Fig.2.1 is remarkably close to the experimental results, which show a rather small scatter[9]. It is obvious that the internal length parameters l_1 and l_2 are fairly

[9] Some of the scatter has been eliminated by normalizing the yield stress with respect to the tensile yield stresses of the various specimens.

comparable in magnitude but the effect of the corresponding terms in Eq.(6.2) is opposite: the first order term is dominant not only in magnitude but more important, the proper trend to capture the experimentally observed size dependence is contained in the 1st order term because of the sign of c_1/G. It appears that the inclusion of only the 2nd order gradient term in the gradient enhanced deformation plasticity model would not suffice to obtain an acceptable fit.

For comparison, the minimum radius of the smallest torsion specimen is 1.293 mm and the grain size is less than 0.042mm. Thus, the internal length parameters l_1 and l_2 (Eq.(6.5)) are considerably less than the minimum dimension of the torsion specimens and both are about 10 times larger than the grain size. This is a fairly reasonable result. With some caution one may interpret qualitatively this result that the 'joint action of several crystal grains' determines an internal length scale responsible for the size dependence of the yield initiation. This is in line with suggestions by Morrison (1939, [1.2] and Part I). Morrison proposed a simple theory of yield for the case of non-uniform stressing. He suggested for a bending test that 'yield cannot occur in an individual crystal surrounded by unyielded material but only in a number of crystals which occupy a sufficient thickness to permit of the complicated readjustment (of the crystals) which must take place before movement can occur, it is unreasonable to expect to find yield before a stress equal to yield stress in uniform tension is applied to a depth of this magnitude. It seems reasonable to suppose that the depth might be of the order of a few crystal diameters.'

The adaption of the gradient plasticity model to Richards' pure bending tests, was also done by applying a least squares fit. It is important to note that for this loading configuration, the 2nd order gradient term involving the gradient parameter c_2 vanishes identically and thus only the 1st order term remains. The two parameters σ_o and c_1/E were determined by the fitting procedure. Eq.(2.7) with the data from Section 2.2 can be written in the form

$$\frac{Y(h)}{\sigma_o} = \frac{1}{1-\left(\frac{l}{h/2}\right)}\,, \tag{6.6}$$

with

$$\left.\begin{aligned} l &= -\frac{c_1}{E} = -\frac{c_1}{G}\frac{1}{2(1+\nu)} = 1.125 \text{ mm} \\ \frac{c_1}{G} &= -2.97 \text{ mm} \\ \sigma_o &= 225.6 \text{ Mpa}\,. \end{aligned}\right\} \tag{6.7}$$

The internal length parameter l is found to be well below the half-depth ($h/2$ = 3.19 mm) of the smallest beam specimen accounted for in the fitting process; this is, of course, a necessary requirement for a reasonable quasi-hyperbolic fit of the size effect model.

The obtained fit (Fig.2.2) with only two parameters, covering a scale range of 3.84, is comforting, but it refers to the mean values of the relatively large scatter bands associated with each specimen size. Also the experimental results are somewhat masked by the observed non-uniformity of the yield stress along the radius of the circular stock bar that the specimens

were taken from (Part I, Richards (1958, [1.3])). A comparison of the internal length scale with the grain size is not possible since these data are not reported.

It is interesting to compare the two corresponding internal length parameters (c_1/G), Eq.(6.4) and Eq.(6.7), associated to the first order strain gradient term. It is noted that the internal length parameter for the bending case is two times larger than the one obtained for the torsion data. This difference may possibly be attributed to a difference in composition and microstructure of the two steels used. Of course, it may also be an indication that the proposed gradient terms are not capable to catch the two size effects uniformly if the materials were the same.

The conclusions may be stated as follows:

(a) The two separate fitting processes of a simple gradient plasticity model, including 1st and 2nd order strain gradient terms, gave comforting agreement of the fitted models with the mean values of experimental data in torsion and pure bending experiments. Evidently, these phenomenological models are useful means to interpret these observed size effects although a physical interpretation of the gradient term was not used.

(b) The results indicate that it is important to include a 1st order strain gradient term in the enhanced yield condition and it suffices to use a linear dependence on the strain gradient only. The 2nd order strain term is of no importance for the case of pure bending and of a minor one in the case of torsion; here it introduces an opposing compensating size effect compared to the 1st order term.

(c) The 1st order strain gradient parameters obtained in the two different tests with different materials differ by only a factor of two. Whether this is accidentally so or due to the difference in material cannot be decided.

(d) For the case of torsion, the 1st order strain gradient coefficient was found to be about 10 time larger than the grain size. Possibly this may be an indication to interpret the existence of an internal length scale by the 'collective action of several crystal grains' in the yielding process, a suggestion already made by Morrison and others.

(e) The enhancement of the classical ideal plastic yield condition by 1st and 2nd order strain gradient terms may be viewed as being equivalent to an enhancement by 1st and 2nd order stress gradients.

(f) Finally, further comparison between gradient theory and mechanical tests of geometrically scaled specimen families of the same material is necessary which really allows assessing the predictive capabilities of the theoretical models. This requires testing of scaled specimens to identify conventional material parameters and especially the gradient coefficients (internal length scales) but also independent scaled tests, using the same material to verify the predictive capabilities of the phenomenological model.

At the present state we do not have recourse to such experimental data, neither from the open literature nor from the experimental part of the REVISA project. This is partly due to the delay of the project but also due the complexity of the specimen geometry, which requires elaborated numerical solution of the non-classical boundary value problems.

6.3 Second Group: One-Dimensional Boundary Value Problems

In the 2nd group one-dimensional boundary value problems were solved and parameter calculations were performed by changing the specimen size or the internal length scale to assess the influence of the strain gradient term in comparison to the classical part of the constitutive equation.

In contrast to the first group, elasticity and the existence of a yield condition were ignored. Instead, a linear or power law hardening deformation type plasticity law was assumed for the classical part; also for the gradient term, only the 2nd order strain gradient (Laplacian) was used. For a uniaxial state of stress, this model reads[10]

$$\sigma = K\varepsilon^n - K\, l_i^2 \frac{d^2\varepsilon}{dX^2}, \qquad 0 < n \leq 1\,; \tag{6.8}$$

for the case of large strains, σ is the applied Cauchy stress, ε is the logarithmic strain and X the material (Lagrangian) coordinate. This form is related to early proposals of Aifantis and coworkers (1987, [6.5], 1988, [6.6]); the gradient term can also be considered as an approximation to a certain non-local (integral) formulation (Appendix 1).

The following cases were analyzed:

- tension of tapered rods under different assumptions,
- three-point bending of smooth beams.

Under the assumptions of a uniaxial state of stress the governing equilibrium equation can be trivially solved independently of the constitutive relation. This 'uncoupling' allows a direct integration of the constitutive equation which takes the form of a 2nd order differential equation for the strain. The required non-conventional boundary conditions, which typically have to be introduced for gradient models, are defined. The most important condition is the assumed vanishing of the strain gradient at the center of the tapered rods and of the beams. For smooth specimens this follows from the symmetry but not for the non-smooth exponentially tapered rod. Under simplifying assumptions it is shown in a separate analysis (Appendix (1)) that a 2nd order strain gradient model may be a valid approximation for a non-local (integral) model far from boundaries or geometric discontinuities, if the internal length l_i is appropriately interpreted. However, in a small region close to the boundary a gradient approximation should also include a 1st order strain gradient. But more important, the boundary condition obtained from the non-local model may differ significantly from the assumed vanishing of the strain gradient at the center of the specimen. Thus, the gradient model and its non-classical boundary condition generally require a different motivation.

(i) Tension of Tapered Rods: Linear Case

First we considered a linear stress-strain relation without allowing a cross-section area reduction (small strains). Thus, under the assumption of small strains and linear hardening two fully linear tapered rod problems are analyzed and discussed:

- an exponentially tapered rod under tension,
- a U-notched rod under tension.

[10] K and l_i are material constants, with l_i determining the gradient influence. An alternative gradient formulation is obtained by the use of spatial (Eulerian) coordinates (Eringen 1962, [6.4]). We did not follow this assumption.

Exact solutions were obtained which allow a qualitative insight easily. A comparison of the classical and the non-classical solution ε_c and ε, respectively, for the exponentially tapered rod at the same stress level shows that the inclusion of a 2nd order strain gradient in the constitutive model together with the non-classical boundary condition yields

- a reduction of the maximum strain at the minimum cross-section and
- a smoothing-out of the strain peaks, i.e. the discontinuities of the 1st order strain gradient.

The importance of the non-classical boundary condition to obtain these effects is emphasized. The qualitative findings are in line with results obtained by Altan and Aifantis (1992, [6.7]), Ru and Aifantis (1993, [6.8]) and Vardoulakis, Exadaktylos and Aifantis (1996, [6.9]) by using strain gradient-dependent elasticity theories, i.e. modifications of Hooke's law, to account for excessively high strain gradients developed in the neighborhood of a crack-tip (singular stress and strain field). These modifications dispense with the crack-tip strain singularity.

With L^* being the transition length (a characteristic measure for the size of the specimen) of the exponentially tapered rod and l_i being the internal length, a non-dimensional gradient parameter $\beta = l_i / L^* < 1$ is defined. With D_o being the minimum diameter (at $\xi = 0$) and D_∞ the largest diameter (at $\xi \to \infty$) one obtains

$$\beta = \frac{l_i}{L^*} = \frac{l_i}{D_o}\frac{D_o}{D_\infty}\frac{D_\infty}{L^*} = \frac{l_i}{D_o}\sqrt{\alpha}\frac{D_\infty}{L^*}, \tag{6.9}$$

where

$$\alpha = \frac{A_o}{A_\infty} = \frac{D_o^2}{D_\infty^2} . \tag{6.10}$$

For geometrically similar specimens the dimensionless factors α and D_∞ / L^* remain constant, whereas only the ratio l_i / D_o changes if the size is changed and the material is the same. A change of shape is obtained by varying at least one of the three quantities D_o, D_∞ and L^*, or holding the ratio of two dimensions constant (e.g. $\sqrt{\alpha}$) and varying independently the third one. Since l_i is assumed to be related to the microstructure, the ratio l_i / D_o should be clearly less than '1'.

The exact non-classical solution ε depends on the parameter β and, of course, on the geometry of the specimen. For the relative strain $\varepsilon_o / \varepsilon_{co}$[11] at the minimum cross-section one obtains, Eq.(3.22), for the purely linear case

$$\frac{\varepsilon_o}{\varepsilon_{co}} = \frac{1+\alpha\beta}{1+\beta} \tag{6.11}$$

which decreases monotonically with increasing β-value (decreasing size) and approaches '1' for very large specimens ($\beta \to 0$); the rate of decrease $d(\varepsilon_o / \varepsilon_{co})/d\beta$ is largest for $\beta \to 0$. For example, for a wasp-waisted specimen with $\alpha = 0.0625$ ($D_o / D_\infty = \sqrt{\alpha} = 0.25$) and a large β-value ($\beta = 0.2$)[12] the relative strain reduction, i.e. $(\varepsilon_{co} - \varepsilon_o)/\varepsilon_{co}$, is about 19% (Fig.3.5). The non-classical strain distribution is found to consist of two contributions: a part that essentially

[11] $\varepsilon_o \equiv$ non-classical strain and $\varepsilon_{co} \equiv$ classical strain at minimum cross-section.

[12] Note that with Eq.(6.9) the values $\sqrt{\alpha} = 0.25$ and $\beta = 0.2$ corresponds to $(l_i / D_o) = 0.8(L^* / D_\infty) = 0.2(L^* / D_o)$; thus for a small value of l_i / D_o, say 0.02, a wasp-waisted neck with $L^* / D_o = 0.1$ is required.

represents the classical strain distribution and another part which for small values of β and increasing distance from the strain maximum is a fast decaying contribution; in fact, it represents for $\beta << 1$ a boundary layer effect which is entirely due to the gradient term. This is also the region where the first and the second order derivatives of the classical strain solution are largest. Thus, the 2nd order strain gradient influence is largest where the classical solution shows a large variation, i.e. inhomogeneity.

The size dependence of the deformation behavior of the linear model can also be represented by determining dimensionless load-displacement or dimensionless stress-strain graphs. For example, the plot of the local dimensionless stress-strain relation at the minimum cross-section (where the gradient effect is largest), which is a linear relation, yields the largest stiffness for the smallest specimen ($\beta \rightarrow 1$). Of course, for very large specimens ($\beta \rightarrow 0$) the classical relation is obtained.

With the obtained solutions also a fairly obvious fact is demonstrated: the size influence is more readily detectable in dimensionless force-deformation graphs when a local strain – related to a region of intensive strain non-uniformity – is used as a deformation measure than in approaches which use a strain average on an extended spatial domain.

The combination of the linear 2nd order strain gradient deformation model with two common engineering fracture criteria, i.e.

- a critical local stress, or
- a critical local strain,

which are assumed to be size independent material data, yields a theoretical assertion about the size dependence of fracture. However, the reader should recognize that the authors do not expect that the combination of a relatively simple size-dependent deformation law and a size-independent local failure criterion will yield qualitatively correct trends for the failure stress and failure strain.

Assuming the validity of the size invariant local critical stress criterion, the combination with the gradient model yields, of course, a size-independent normalized failure load, whereas the normalized deformation measures are size-dependent: scaled-up specimens have larger local and average strains at fracture. It is noted that this qualitative trend is not in agreement with trends observed experimentally: frequently the normalized fracture load and strain decrease with an increase in size (e.g. Brown et al. 1947, [3.1], Shearin et. al. 1948, [6.2]).

Provided a size invariant critical local strain criterion holds, then, of course, the local fracture strain at the minimum cross-section is size invariant. However, the associated normalized fracture load decreases with an increase in size. This last trend is in qualitative accordance with experimental observations.

On the other hand from the knowledge of these normalized fracture loads one may determine the associated average strains for different specimen sizes. Although the maximum local strains at fracture are assumed to be the same, the average strains are size dependent, i.e. they are larger for small specimens than for large ones.

With the parameter $\beta = l_i/L^*$ being the governing parameter for the size dependence, it is obvious that the influence of size will decrease with increasing dimensions. Furthermore, if two size dependent quantities are compared, for example the normalized fracture loads obtained from a critical strain criterion, then the ratio of the normalized fracture loads, Eq.(3.37), is not only depending on the geometrical scale factor λ but also on the absolute size. Therefore, keeping λ = const., but increasing the size of the small and the large specimen proportionally, will lead to an equalization of these normalized fracture loads.

(ii) Tension of Tapered Rods: Non-Linear Case

Next we considered a non-linear stress-strain relation (power law hardening) and allowed for cross-section area reduction during loading. Although the purely linear problem of the exponentially tapered tension rod provides rather valuable qualitative information, the consideration of the non-linearities due to power law hardening ($n<1$) and large strains (allowance for cross-section reduction due to volume conservation) is an important step towards a more realistic deformation model. The governing nonlinear differential equation, Eq.(4.7), is

$$\left.\begin{aligned} &\beta^2 \frac{d^2\varepsilon}{d\xi^2} - \varepsilon^n = -r_R(\xi)\, e^{\varepsilon} \\ &\text{where} \\ &r_R(\xi) = \frac{\sigma_R(\xi)}{K} \end{aligned}\right\} \qquad (6.12)$$

is proportional to the engineering tension stress $\sigma_R(\xi)$ in the rod.

It is noted that the two non-linear effects imply instability in the classical case ($\beta = 0$) when the local logarithmic strain ε becomes equal to the hardening exponent n. At this instant the increase in load due to hardening is balanced by the 'geometric softening' due to cross-section reduction. Thus, a hardening before and a softening phase after the load maximum are to be distinguished in the classical case.

An exact solution for the non-linear gradient enhanced deformation model, Eq.(6.12), appears not to be possible. However, for small β-values and a bounded 2nd order strain derivative the gradient term represents a perturbation in Eq.(6.12). The exact linear solution proved that essentially two types of spatial dependencies are involved: a part, which essentially represents the classical solution, and a second part, which is a boundary layer contribution controlled by the parameter β. For $\beta = 0$ the differential equation (6.12) reduces to an algebraic problem, its solution being the classical solution ε_c which satisfies the boundary condition at $\xi \to \infty$ but not at $\xi = 0$ (minimum cross-section). Thus, Eq.(6.12) together with its boundary conditions (4.9) signals a singular perturbation problem. An approximate asymptotically valid analytical solution was obtained using a generalized version of the method of multiple scales by Nayfeh (1973, [4.3]). A 'slow' and a 'fast' variable,

$$\xi = \frac{x}{L^*} \quad \text{and} \quad \eta = \frac{\mu(\xi)}{\beta}, \qquad (6.13)$$

were introduced and a uniformly valid expansion

$$\tilde{\varepsilon}(\xi,\eta;\beta) = \overset{0}{\varepsilon}(\xi,\eta) + \beta \overset{1}{\varepsilon}(\xi,\eta) + \beta^2 \overset{2}{\varepsilon}(\xi,\eta) + \beta^3 \overset{3}{\varepsilon}(\xi,\eta)\,. \qquad (6.14)$$

was assumed to be applicable, where the two-scale functions $\overset{k}{\varepsilon}(\xi,\eta)$, $k = 0, 1, 2, 3$ as well as $\mu(\xi)$ remain to be determined. By developing and arranging according to powers of the small parameter β, the differential equation (6.12) and its boundary conditions transform to a system of ordinary differential equations of 2nd order in the η-variable for the $\overset{k}{\varepsilon}(\xi,\eta)$ and associated

boundary conditions, where the ξ-variable is silent. The system must be solved in successive steps since the right-hand side of the k^{th} equation depends on the solutions of the previous differential equations. This system of differential equations is characterized by the fact that the nonlinearity is restricted to the 0^{th} order equation for $\overset{0}{\varepsilon}(\xi,\eta)$; but fortunately, it allows a simple solution, namely,

$$\overset{0}{\varepsilon}(\xi,\eta) = \varepsilon_c(\xi), \tag{6.15}$$

the classical solution being independent of the 'fast' variable η. The successive equations for $\overset{k}{\varepsilon}(\xi,\eta)$, k = 1, 2, 3, are linear differential equations; their solutions involve 'integration constants' which, of course, are functions of ξ. They are determined partly by the boundary conditions. Further conditions in the form of differential equations are obtained for the remaining 'integration constants' and for the yet unknown function $\mu(\xi)$ by suppressing 'secular terms' which make the ratio $\overset{k+1}{\varepsilon} / \overset{k}{\varepsilon}$ unbounded in the (ξ,η)-domain; this is an essential part at the heart of the singular perturbation method. This yields, among others, the function $\mu(\xi)$, which determines the 'fast' variable η as a functional of the classical strain distribution:

$$\mu(\xi) = \int_0^{\xi} \left(\frac{1}{\varphi} \frac{[n - \overset{0}{\varepsilon}(\tau)]}{[\overset{0}{\varepsilon}(\tau)]^{1-n}} \right)^{1/2} d\tau; \tag{6.16}$$

the constant φ may be chosen as convenient. Since a closed form representation for the classical solution $\varepsilon_c(\xi) = \overset{0}{\varepsilon}(\xi)$ does not exist, the above integral and others of the general solution need numerical integration. It is noted that the derived asymptotic solution for the logarithmic strain distribution, Eq.(4.91), does not explicitly depend on the spatial variation of the cross-section area. This geometric quantity is solely contained in the function $\overset{0}{\varepsilon} = \varepsilon_c$ and the obtained solution is applicable to any smooth cross-section variation in the region $0 \le \xi < \infty$ satisfying the properties at $\xi \to \infty$.

If the perturbation solution of the fully non-linear problem is reduced to the case of small strains (neglect of the cross-section reduction), an explicit analytical solution for the classical strain distribution is trivially obtained

$$\varepsilon_c = \left(\frac{\sigma_R}{K} \right)^{1/n} = \overset{0}{\varepsilon} \tag{6.17}$$

and the integral in Eq.(6.16) simplifies to

$$\mu_R = \int_0^{\xi} \left(\frac{1}{\varphi} \frac{n}{[\overset{0}{\varepsilon}(\tau)]^{1-n}} \right)^{1/2} d\tau; \tag{6.18}$$

Furthermore, for the exponentially tapered rod a closed form solution for odd integer values of $1/n$ is derived for μ_R and other integrals such that an analytical representation of the non-classical strain distribution along the tension rod and especially in the boundary layer close to $\xi = 0$ is obtained.

Although the perturbation solution of the fully non-linear problem requires numerical integrations, important results can be derived without recourse to numerical methods. These refer to the maximum strain $\varepsilon(0,0)$ at the minimum cross-section ($\xi = 0$) and its dependence on the size and shape of the tension rod and the constitutive parameters. Thus, closed form approximate analytical solutions are obtained which allow direct insight into the essential response characteristics.

With ε_{co} being the maximum strain at $\xi = 0$ of the classical solution, one obtains the maximum $\varepsilon(0,0)$ of the non-classical strain in normalized form (relative strain ratio), up to terms quadratic in β, as follows (Eq.(4.158)):

$$\frac{\varepsilon(0,0)}{\varepsilon_{co}} = 1 + \beta \left\{ \left[n - \underset{===}{\left(\overset{0}{\varepsilon}\right)_0} \right] \left(\overset{0}{\varepsilon}\right)_0^{1+n} \right\}^{-1/2} \left(\overset{0}{\varepsilon}_{\xi} \right)_0 +$$

$$+ \beta^2 \left(\left[n - \underset{===}{\left(\overset{0}{\varepsilon}\right)_0} \right] \left(\overset{0}{\varepsilon}\right)_0^{1+n} \right)^{-1} \left\{ \left(\overset{0}{\varepsilon}_{\xi\xi} \right)_0 \left(\overset{0}{\varepsilon}\right)_0 + \right.$$

$$\left. + \left(\overset{0}{\varepsilon}_{\xi} \right)_0^2 \left(n - \underset{===}{\left(\overset{0}{\varepsilon}\right)_0} \right)^{-1} \left[\frac{5}{12} n(1-n) + \underset{=====}{\frac{n}{4} \left(\overset{0}{\varepsilon}\right)_0} + \underset{=====}{\frac{1}{6} \left(\overset{0}{\varepsilon}\right)_0^2} \right] \right\}, \qquad (6.19)$$

where $\varepsilon_c \equiv \overset{0}{\varepsilon}$ is the solution of

$$\varepsilon_c^n = \frac{\sigma_R}{K} e^{\varepsilon_c} \; ; \qquad (6.20)$$

here $\left(\overset{0}{\varepsilon}\right)_0$, $\left(\overset{0}{\varepsilon}_{\xi}\right)_0$ and $\left(\overset{0}{\varepsilon}_{\xi\xi}\right)_0$ are the classical solution and its 1st and 2nd order derivative at the minimum cross-section ($\xi = 0$).

The explicit representation of the relative strain for the exponentially tapered tensile rod with a sharp neck[13] and for the fully non-linear case is

$$\frac{\varepsilon(0,0)}{\varepsilon_{co}} = 1 - \beta \left[\frac{\left(\overset{0}{\varepsilon}\right)_0^{1-n}}{n - \underset{==}{\left(\overset{0}{\varepsilon}\right)_0}} \right]^{1/2} \frac{1-\alpha}{n - \underset{==}{\left(\overset{0}{\varepsilon}\right)_0}} +$$

[13]The term 'sharp neck' is used to indicate the shape of the initial profile of the tapered rod at hand. This in contrast to the localized neck due to usual geometric softening of initially smooth specimens.

$$+\beta^2\frac{\overset{0}{(\varepsilon)_0}^{1-n}}{n-\overset{0}{(\varepsilon)_0}}\left[\frac{1-\alpha}{n-\overset{0}{(\varepsilon)_0}}\right]^2\frac{1}{n-\overset{0}{(\varepsilon)_0}}\left\{\frac{\alpha}{1-\alpha}\left(n-\overset{0}{(\varepsilon)_0}\right)^2+n\right.$$

$$\left.+\frac{5}{12}n(1-n)+\underline{\frac{n}{4}\overset{0}{(\varepsilon)_0}}+\underline{\frac{1}{6}\overset{0}{(\varepsilon)_0^2}}\right\}; \qquad (6.21)$$

in the purely linear case ($n = 1$ and deletion of the underlined terms) this simplifies to

$$\frac{\varepsilon(0,0)}{\varepsilon_{co}}=1-\beta(1-\alpha)+\beta^2(1-\alpha)\,. \qquad (6.22)$$

The following observations and qualitative conclusions can be made, concerning the properties of the approximate solution and its limitations and including the trends imposed by a change of material parameters, the specimen size and shape, and specific assumptions:

(a) For a tension rod with a sharp neck one finds for $\xi = 0^+$

$$(\varepsilon_{c\xi})_0 = \overset{0}{(\varepsilon_\xi)_0} < 0, \qquad (\varepsilon_{c\xi\xi})_0 = \overset{0}{(\varepsilon_{\xi\xi})_0} > 0\,,$$

since the classical strain $\varepsilon_c \equiv \overset{0}{\varepsilon}$ is essentially a function of the inverse of the cross-section distribution. Thus, the dominant term of the relative strain approximation, Eq.(6.19), linear in the parameter β, is negative. This implies for sufficiently small β-values a reduction of the maximum non-classical strain $\varepsilon(0,0)$ compared to the classical value ε_{co}. Provided the tensile load is properly scaled and the specimens are geometrically similar and of the same material, the size influence is entirely contained in the parameter β: if the size is decreased, then L^* decreases and β increases, which implies a decrease of the relative strain. Within the present context, this is the most important aspect of the size effect for the tensile rod.

(b) The singular perturbation solution for the fully non-linear and non-uniform tension problem, Eq.(6.19), is not valid close to instability. Then $\overset{0}{(\varepsilon)_0} = \varepsilon_{co}$ approaches the hardening exponent n and the derivatives $\overset{0}{(\varepsilon_\xi)_0}$ and $\overset{0}{(\varepsilon_{\xi\xi})_0}$ grow beyond bounds. Thus, a prerequisite of the perturbation solution for the differential equation Eq.(6.12), i.e. boundedness of $d^2\varepsilon/d\xi^2$, is not assured for large strains approaching instability.

(c) The underlined terms in Eq.(6.19) are due to the allowance for cross-section reduction induced by the assumed volume conservation during plastic deformation. If this is ignored (small strain assumption), Eq.(6.19) simplifies to

$$\frac{\varepsilon(0,0)}{\varepsilon_{co}} = 1 + \beta \left[\frac{1}{n \overset{0}{(\varepsilon)}_0^{1+n}} \right]^{1/2} \left(\overset{0}{\varepsilon}_\xi \right)_0 +$$

$$+ \beta^2 \left[\frac{1}{n \overset{0}{(\varepsilon)}_0^{1+n}} \right] \left\{ \left(\overset{0}{\varepsilon}_{\xi\xi} \right)_0 \left(\overset{0}{\varepsilon} \right)_0 + \frac{5}{12}(1-n) \left(\overset{0}{\varepsilon}_\xi \right)_0^2 \right\} \tag{6.23}$$

and $\overset{0}{\varepsilon}$ is simply given by

$$\overset{0}{\varepsilon}(\xi) = \varepsilon_c(\xi) = \left(\frac{\sigma_R(\xi)}{K} \right)^{1/n} . \tag{6.24}$$

(d) For the case of a smooth neck at $\xi = 0$, the strain $\varepsilon_c(\xi) = \overset{0}{\varepsilon}(\xi)$ has a relative maximum at $\xi = 0$

$$(\overset{0}{\varepsilon}_\xi)_0 = 0, \qquad (\overset{0}{\varepsilon}_{\xi\xi})_0 < 0 \tag{6.25}$$

and Eq.(6.19) simplifies to

$$\frac{\varepsilon(0,0)}{\varepsilon_{co}} = 1 - \beta^2 \left(\left[n - \underline{\underline{\overset{0}{(\varepsilon)}_0}} \right] \left(\overset{0}{\varepsilon}_0^n \right)^{-1} \left| \overset{0}{\varepsilon}_{\xi\xi} \right|_0 < 1. \right. \tag{6.26}$$

This reflects the quadratic dependence of the gradient enhanced constitutive equation on the internal length l_i. The sign of the quadratic term shows that the strain gradient term implies a reduction of the strain maximum compared to the classical solution. If only the specimen size is reduced but the stress level $\sigma_R(\xi)$ is kept constant by proper scaling of the load, then the parameter β increases and the maximum strain $\varepsilon(0,0)$ as well as the relative strain are shifted to smaller values.

Clearly, the size effect is not restricted to a sharp neck but is, of course, also present for a smooth neck. However, it is only quadratically depending on the normalized gradient parameter β. Therefore, the smoothness of the neck as defined by Eq.(6.25)[14] determines a 'switch' from a linear to a quadratic dependence on β. Obviously, the smooth minimum section of the neck may be a rather 'local affair' which needs a 'magnification' to be detectable. This shows that the relative strain reduction at the minimum neck section, i.e. a local value at $\xi = 0$, may be rather sensible to the local geometric properties.

The relative strain of a smooth neck can be given a lucid interpretation if the cross-section reduction is ignored. The Eq.(6.26) simplifies to

[14]Note: these conditions do not define a 'degree' of smoothness

$$\frac{\varepsilon(0,0)}{\varepsilon_{co}} = 1 - \beta^2 \frac{1}{n} \left(\overset{0}{\varepsilon}\right)_0^{1-n} \frac{\left|\overset{0}{\varepsilon}_{\xi\xi}\right|_0}{\left(\overset{0}{\varepsilon}\right)_0} \tag{6.27}$$

with

$$\left(\overset{0}{\varepsilon}\right)_0 = \varepsilon_{co} = \left(\frac{\sigma_{Ro}}{K}\right)_0^{1/n} . \tag{6.28}$$

With D_o being the minimum neck diameter and R_o the radius of curvature of the meridional profile at the minimum section one obtains (Eq.(4.140))

$$\frac{\varepsilon_{co} - \varepsilon(0,0)}{\varepsilon_{co}} = (\varepsilon_{co})^{1-n} \frac{4}{n^2} \left(\frac{l_i}{D_o}\right)\left(\frac{l_i}{R_o}\right) = \left(\frac{\sigma_{Ro}}{K}\right)^{\frac{1-n}{n}} \frac{4}{n^2} \left(\frac{l_i}{D_o}\right)\left(\frac{l_i}{R_o}\right) . \tag{6.29}$$

Thus, this result for a smooth neck demonstrates that the internal length scale 'l_i' in relation to the minimum geometrical length scales D_o and R_o determines the relative strain reduction, i.e. the gradient effect. The ratio l_i/R_o is of special importance since for very uniform necks, i.e. R_o/D_o very large, the gradient effect vanishes.

Also, the form of Eq.(6.29) and the assumption that 'l_i' is related to a microstructural length scale suggest that both ratios l_i/D_o and l_i/R_o should be clearly less than '1' such that the model remains reasonable. Thus, the limit of Eq.(6.29) for $R_o \rightarrow 0$, which formally gives a singular result, should be excluded. Geometrically this limit represents a sharp neck and here the non-smooth solution applies.

In addition, Eq.(6.29) proofs the importance of the hardening exponent n for the relative strain reduction. If the classical strain level ε_{co} is controlled by increasing the loading such that

$$\varepsilon_{co} = \left(\frac{\sigma_{Ro}}{K}\right)^{1/n} = \text{const.} ,$$

for decreasing values n, then the relative strain reduction may decrease, pass through a minimum and is very sensitive especially for small values of n, because it increases beyond bounds for $n \rightarrow 0$. If, however, the normalized stress σ_{Ro}/K is required to be constant

$$\frac{\sigma_{Ro}}{K} = \varepsilon_{co}^{n} = \text{const.} < 1 ,$$

then the strain ε_{co} decreases monotonously towards zero with decreasing n but the relative strain reduction shows a maximum for a finite n-value (Fig.4.1). It is shown that this is due to two opposing effects, i.e. the above mentioned decrease of ε_{co} and the increase of the 'relative localization'

$$\left|\frac{(\varepsilon_{c\xi\xi})_0}{\varepsilon_{co}}\right| = \frac{1}{n}\left(\frac{A_R''}{A_R}\right)_0 ,$$

with decreasing hardening exponent.

(e) For a non-smooth tension rod with a sharp neck at $\xi = 0$ the relative strain depends also linearly on the normalized gradient parameter β although only a second order strain gradient is assumed in the constitutive model. Observing the previous statement, this is due to the non-smooth cross-section distribution around $\xi = 0$ which induces non-smoothness in the tension stress $\sigma_R(\xi)$.

(f) The derivatives $(\overset{0}{\varepsilon}_\xi)_0$ and $(\overset{0}{\varepsilon}_{\xi\xi})_0$, given by Eq.(4.160), are determined by the initial geometry of the tension rod at $\xi = 0$, the strain level $\varepsilon_{co} = (\overset{0}{\varepsilon})_0$ (or engineering stress level σ_{Ro}) and especially by the distance $(n - \varepsilon_{co})$ from instability. This applies also to the relative strain $\varepsilon(0,0) / \varepsilon_{co}$.

For a prescribed engineering stress level σ_{Ro} the corresponding classical strain $\varepsilon_{co} = (\overset{0}{\varepsilon})_0$ is larger when the cross-section reduction is accounted for, compared to the case without this geometric non-linearity. The same trend is valid for the derivatives $(\overset{0}{\varepsilon}_\xi)_0$ and $(\overset{0}{\varepsilon}_{\xi\xi})_0$. Thus, it follows from Eq.(6.19) that the relative strain reduction $(\varepsilon_{co}-\varepsilon(0,0))/\varepsilon_{co}$ is increased when the cross-section reduction due to plastic deformation is accounted for.

(g) When all parameters and the tensile loading σ_R/K are held constant but the hardening exponent n is decreased ($1 \geq n \rightarrow 0$), then the classical strain ε_{co} decreases. Under the small strain assumption its derivatives $(\varepsilon_{c\xi})_0$ and $(\varepsilon_{c\xi\xi})_0$ decrease in magnitude and in the limit $n \rightarrow 0$ no deformation is obtained. However, the 'relative localization' for a sharp neck, i.e.

$$\left|\frac{(\varepsilon_{c\xi})_0}{\varepsilon_{co}}\right| = \frac{1}{n}\left(\frac{A_R'}{A_R}\right)_0 ,$$

increases with decreasing n. These two opposing effects generate a peculiar n-dependence of the sensitivity (Fig.4.7)

$$S = \left|\frac{d\varepsilon(0,0)/\varepsilon_{co}}{d\beta}\right|_{\beta\rightarrow 0}$$

and of the relative strain reduction $(\varepsilon_{co}-\varepsilon(0,0))/\varepsilon_{co}$: a maximum at a finite n-value.

(h) For β increasing towards '1' (i.e. very small specimens of a family of geometrically similar probes) the parabolic character of the asymptotic solution becomes dominant and strongly erroneous: the exact solution for the relative strain, Eq.(6.11), of the purely linear case is a monotonously decreasing function of the normalized gradient parameter β;

however, the perturbation solution, Eq.(6.22), has a relative minimum at $\beta = 0.5$ and underestimates the gradient effect for large β values (small sizes).

For the non-linear case this minimum is shifted to β values less than 0.5 and thus, the range of validity of the quadratic perturbation approximation reduces to very small values of β (i.e. large specimen sizes).

(i) The range of validity of the perturbation approximation can be extended by accounting for higher order terms in β. This has been done by including terms cubic in β, but neglecting the cross section reduction. By comparison with the exact solution for the linear case, a definite extension of the validity of the perturbation approximation to larger values of β is observed. However, for β becoming too large, this 3rd order approximation overestimates the gradient effect and thus becomes also erroneous.

The validity of the perturbation solution can be extended to larger β-values by including even higher-order powers of β but this becomes yet more laborious. This extends also the strain range wherein the perturbation approximation is reasonably applicable. However, close to instability the approximation fails in any case since the terms of the power series representation are not affected by a series extension and they become singular.

(k) Aside from demonstrating the size influence via a graph of the relative strain reduction versus β, which is a mathematically very convenient way, the results can also be used to prepare engineering stress-strain diagrams. This representation is a rather natural choice since it simulates the size influence in a tensile test with a tapered specimen. As pointed out previously, spatially local measures of the strain should be used instead strain averages over extended domains. Therefore, the engineering stress σ_{Ro} and the corresponding gradient affected engineering strain $\varepsilon_R(0,0)$ at the minimum neck section, where the main gradient effect is located, were plotted in the same diagram by eliminating the intermediate variable $\varepsilon_{co} = \overset{0}{(\varepsilon)}_0$ from the governing equations.

This has been done for the fully non-linear case (Section 4.2.2) using the 2nd order perturbation solution (Fig.4.9) and also for a 3rd order approximation (Fig.4.13 & 4.14) but without the effect of the cross-section reduction (Section 4.3.3). For large strains and large β-values (small sizes) the results are, as mentioned before, not sufficiently accurate. Nevertheless, for sufficiently small strains and β-values, valid approximations are obtained which show the increase in flow stress with decreasing size (increase of β); this is just another aspect of the size influence.

An example may illustrate this. For a rather wasp-waisted specimen ($\alpha = 0.0625$, $\sqrt{\alpha} = D_o / D_\infty = 0.25$) low hardening exponent (n =1/9, ferritic steel), and a small local stain $\varepsilon_{co} = \varepsilon_R(0,0) = 1.5\%$ the normalized engineering stress is increased by about 6.5% if the dimensionless gradient parameter β is increased from $\beta = 0$ (very large specimen) to $\beta = 0.1$ (Fig.4.14b). With Eq.(6.9) and with D_o / l_i interpreted as the number of grains along the minimum diameter, say $D_o / l_i = 50$, one gets $L^* / D_o = 0.2$. This is a very steep transition from the minimum diameter D_o to the largest diameter D_∞: within a diameter D_o's distance from the minimum section the diameter has increased up to 95% of the asymptotic value D_∞. An experimental detection of a flow stress increase in the percentage range requires a very homogeneous material, careful specimen preparation and testing to minimize masking influences and pseudo size effects (e.g., macroscopic material inhomogeneity, surface hardening due to machining).

(ℓ) It should be realized that the exponentially tapered tensile rod was treated as a uniaxial stress problem. Under a multiaxial stress state and using a classical material model, a sharp neck induces a stress and strain singularity, i.e. locally much larger stress and strain gradients are generated than in the uniaxial stress model. Thus, the quantitative size effects of the simple model presented here may possibly underestimate the influence of the 2nd order strain gradient term generated in a fully three-dimensional state.

(iii) Bending of Smooth Beams

The parametric size effect studies were also performed for the problem of quasistatic bending of smooth beams (length: $2L$) with rectangular cross-section under a single load $2P$ at the center and simply supported at the ends. Again the validity of a power law hardening deformation type plasticity theory was supposed which includes a 2nd order strain gradient. Only small deformations were considered, shear deformation was ignored and a linear strain distribution (Bernoulli's hypotheses) across the depth of the beam was assumed. This problem yields a 2nd order differential equation for the beam curvature. It is especially noteworthy that it represents a singular perturbation problem of boundary layer type, which has the same formal structure as the problem for the tapered rod. Thus, the same solution procedure – multiscale method for singular perturbation boundary value problems – was applicable such that a very large part of the previously derived equations was transferable to the new problem by proper reinterpretation of the variables.

The governing dimensionless differential equation, Eq.(5.12) is

$$\beta_q^2 \frac{d^2\kappa}{d\xi^2} - \kappa^n = -r_B(\xi), \qquad 0 < \frac{x}{L} = \xi \le 1\,, \tag{6.30}$$

where $\kappa = Lk$ is the dimensionless curvature, $r_B(\xi)$ is proportional to the bending moment and the small lumped parameter β_q is defined by

$$\beta_q = \sqrt{q}\,\beta\,, \tag{6.31}$$

with the dimensionless gradient parameter

$$\beta = \frac{l_i}{L}\,, \tag{6.32}$$

and the parameter q

$$\frac{1}{3}\frac{h}{L} \le q = \left(\frac{h}{L}\right)^{1-n} \frac{(2+n)2^{1+n}}{12} \le 1 \tag{6.33}$$

L: half length of beam
h: depth of beam
} $\frac{h}{L} < 1.$

In contrast to the tapered tension rod problem, the dimensionless perturbation parameter β_q has a more complex structure: a shape factor h/L and the constitutive parameter n are involved. Boundary conditions are assumed, Eq.(5.17) & (5.18), with the essential assumption being the vanishing of the 1st order derivative κ_ξ at the center of the beam ($\xi = 0$); this is analogous to the tension rod.

For the linear case $n = 1$ (implying $\beta_q = \beta$), the governing equation (6.30) admits an exact solution. With κ_{co} being the maximum dimensionless curvature of the classical solution at the center of the beam (Eq.5.67), i.e.

$$\kappa_{co} = \left(\frac{L}{h}\right)^2 \frac{P}{Kbh}\, 12 \tag{6.34}$$

and $\kappa(0) \equiv (\kappa)_0$ denoting the maximum value of the non-classical solution, the relative strain in the tension side at the center of the beam is found to be

$$\frac{\varepsilon_{o\max}}{\varepsilon_{co\max}} = \frac{(\kappa)_0}{\kappa_{co}} = 1 - \beta \frac{2\sinh(2/\beta)}{1 + 2\cosh(2/\beta)}\ ; \tag{6.35}$$

for small β-values this can be approximated by

$$\frac{\varepsilon_{o\max}}{\varepsilon_{co\max}} = \frac{(\kappa)_0}{\kappa_{co}} = 1 - \beta\ . \tag{6.36}$$

For the non-linear case $0 < n < 1$ and small β_q-values an approximate analytical solution was developed by applying mathematical analogy with the tapered tension rod problem and transferring the essentials of the tapered tension rod solution.

With

$$\kappa_c(\xi) = \overset{0}{\kappa}(\xi) \tag{6.37}$$

being the classical solution and identical with the 0th order perturbation solution, the dimensionless curvature at the center of the beam ($\xi = 0$) of the classical solution is (see Eq.(5.83))

$$\kappa_c(0) = \kappa_{co} = \overset{0}{\kappa}(0) = \left(\overset{0}{\kappa}\right)_0 = \frac{L}{h}\left(\frac{4PL}{Kbh^2}\right)^{1/n}\left(1 + \frac{n}{2}\right)^{1/n} 2\ . \tag{6.38}$$

The determination of the maximum $\kappa(0,0)$ of the non-classical curvature in normalized form (Eq.(5.94)) yields

$$\frac{\kappa(0,0)}{\kappa_{co}} = 1 + \beta_q \left(\frac{\kappa_{co}^{1-n}}{n}\right)^{1/2} \frac{\overset{0}{(\kappa_\xi)_0}}{\kappa_{co}} +$$

$$+\beta_q^2 \frac{\kappa_{co}^{1-n}}{n}\left\{\frac{\overset{0}{(\kappa_{\xi\xi})_0}}{\kappa_{co}}+\frac{5}{12}(1-n)\left[\frac{\overset{0}{(\kappa_{\xi})_0}}{\kappa_{co}}\right]^2\right\}=\frac{\varepsilon_{o\max}}{\varepsilon_{co\max}}\,, \tag{6.39}$$

which is equivalent to the relative strain at the tension side of the beam at $\xi = 0$. In explicit terms one obtains

$$\frac{\varepsilon_{o\max}}{\varepsilon_{co\max}}=\frac{\kappa(0,0)}{\kappa_{co}}=1-\beta_q\left(\frac{\kappa_{co}^{1-n}}{n}\right)^{1/2}\frac{1}{n}+\beta_q^2\left(\frac{\kappa_{co}^{1-n}}{n}\right)\frac{1-n}{n^2}\frac{17}{12}. \tag{6.40}$$

Clearly, for the linear case $n = 1$ it simplifies to

$$\frac{\varepsilon_{o\max}}{\varepsilon_{co\max}}=\frac{\kappa(0,0)}{\kappa_{co}}=1-\beta\,. \tag{6.41}$$

The following observation and qualitative conclusions can be made which reflect, to a considerable extent, results obtained for the tapered tension rod:

(a) For the case of three-point-bending with a single load $2P$ at the center of the beam, the moment distribution is non-smooth at $\xi=0$. Thus one finds for $\xi = 0^+$

$$\overset{0}{(\kappa_{c\xi})_0}=\overset{0}{(\kappa_{\xi})_0}<0, \qquad \overset{0}{(\kappa_{c\xi\xi})_0}=\overset{0}{(\kappa_{\xi\xi})_0}>0\,.$$

Thus, the dominant term, linear in β_q, of the relative strain, Eq.(6.39), is negative which implies a reduction of the maximum non-classical strain $\varepsilon_{o\max}$ compared to the classical value $\varepsilon_{co\max}$. For geometrical similar specimens of the same material and for scaled loading,

$$\frac{\overline{P}}{P}=\lambda^2 \tag{6.42}$$

λ : geometrical scale factor $\lambda \geq 1$
$\overline{P}$: load for large scale specimen
P : load for small scale specimen

similarity cannot be achieved but a size effect is present which is entirely contained in the parameter $\beta = l_i/L$, which is part of the lumped parameter $\beta_q = \sqrt{q}\,\beta$: if the size decreases, β increases and the relative curvature or strain decreases.

(b) In contrast to the tapered tension rod similarity of the curvature distribution (but not the strain distribution) can be achieved theoretically, if specimens with geometrically distorted cross-sections are considered. Different geometric scale factors for the length L, the depth h and the width b are assumed, i.e.

$$\lambda = \frac{\bar{L}}{L} \neq \lambda_h = \frac{\bar{h}}{h} \neq \lambda_b = \frac{\bar{b}}{b}. \tag{6.43}$$

If the cross-section areas are required to scale according to λ^2, then $\lambda_h \lambda_b = \lambda^2$ and for a given ratio $\bar{h}/\bar{b}$ of the large scale beam, one obtains for the small scale distorted beam

$$\frac{h}{b} = \frac{1}{\lambda^{1-n}} \frac{\bar{h}}{\bar{b}} \tag{6.44}$$

and the loading is required to scale according to

$$\frac{\bar{P}}{P} = \lambda^{\frac{5-n^2}{2}}. \tag{6.45}$$

Thus, increasing the length scale factor $\lambda > 1$ reduces the depth-to-width ratio h/b of the small-scale beam and its loading P has to be smaller than geometrical scaling ($\bar{P}/P = \lambda^2$) requires. However, for the linear case $n = 1$ a distorted small-scale beam obeying the similarity conditions for the curvature is not possible. Also for the non-linear case the result Eq.(6.44) implies a large distortion of the cross-section dimensions, which is difficult to realize.

(c) For the case of a uniform load distribution along the beam the moment distribution around $\xi = 0$ is smooth and has a relative maximum such that

$$\overset{0}{(\kappa_\xi)}_0 = 0, \qquad \overset{0}{(\kappa_{\xi\xi})}_0 < 0$$

and Eq.(6.39) simplifies to

$$\frac{\varepsilon_{o\max}}{\varepsilon_{co\max}} = \frac{\kappa(0,0)}{\kappa_{co}} = 1 - \beta_q^2 \frac{\kappa_{co}^{1-n}}{n} \left| \frac{\overset{0}{(\kappa_{\xi\xi})}_0}{\kappa_{co}} \right|. \tag{6.46}$$

It reflects the quadratic dependence of the gradient enriched constitutive equation on the internal length l_i. Again a decrease of size of geometrically similar specimens of the same material reduces the relative curvature $\kappa(0,0)/\kappa_{co}$ and the relative strain $\varepsilon_{o\max}/\varepsilon_{co\max}$.

Clearly, the smoothness of the load distribution determines a dominantly linear or quadratic dependence on β_q: a smooth load (moment) distribution implies only a quadratic dependence of the relative curvature on the β_q-parameter, whereas a non-smooth load (moment) distribution triggers also a linear dependence on β_q. This is entirely analogous to the results of the tension rod problem. Thus, evidently non-smoothness in the load or geometry increases the non-uniformity of the strain distribution and gives rise also to first order contributions to the size effect induced by a second order gradient plasticity model.

(d) For increasing β_q-values (β-values), i.e. decreasing size, the parabolic character of the asymptotic solution becomes dominant and erroneous: the size effect is underestimated.

Further, a decrease in the hardening exponent n will reduce the range of validity of the 2nd order perturbation approximation to smaller values of β.

(e) When the geometry, the single force loading P ($\tilde{\tilde{P}} = 4Pl / Kbh^2 < 1$) and the constitutive parameters K and l_i are held constant but only the hardening exponent n is decreased, then the maximal measures of the classical curvature κ_{co}, $(\kappa_{c\xi})_0$ and $(\kappa_{c\xi\xi})_0$ decrease and their limit values for $n \to 0$ vanish. In this limit state the beam is undeformed. However, the distribution of the relative curvature κ_c/κ_{co} and its 1st and 2nd order derivative $\kappa_{c\xi}/\kappa_{co}$ and $\kappa_{c\xi\xi}/\kappa_{co}$ are shifted towards the center of the beam. This trend of a 'relative localization' of the deformation can be quantified by measures for the 'relative non-uniformity' of the curvature distribution at $\xi = 0$, i.e.

$$\left|\frac{(\kappa_{c\xi})_0}{\kappa_{co}}\right| = \frac{1}{n}, \qquad \left|\frac{(\kappa_{c\xi\xi})_0}{\kappa_{co}}\right| = \frac{1-n}{n}, \tag{6.47}$$

which for $n \to 0$ increase and become unbounded. In the general expression for the relative curvature Eq.(6.39) an opposing trend is caused by the decrease of the term $\kappa_{co}^{(1-n)/2}$ towards zero. These opposing trends create a special n-dependence of the relative curvature or relative strain when the hardening exponent n is varied but the dimensionless loads $\tilde{P}$ or $\tilde{\tilde{P}}$ and all other parameters are held constant: a minimum of the relative strain (maximum of the relative strain reduction) at a small but finite n-value (Fig.5.8); this effect becomes more pronounced for larger applied loadings $\tilde{P} = P / Kbh$.

(f) The perturbation solution for the beam curvature consists of the gradient-unaffected classical solution and 1st and 2nd order contributions due to the gradient plasticity terms. The two gradient plasticity affected terms are exponentially decaying contributions close to the center of the beam (boundary layer terms), the 1st order contribution $\beta_q \overset{1}{\kappa}(\xi,\eta)$ being proportional to $e^{-\sqrt{\varphi}\eta}$. The 'fast' spatial variable $\sqrt{\varphi}\eta$ in the neighborhood of the center is given by (Eq.(5.81))

$$\sqrt{\varphi}\eta \approx \xi d = \frac{x}{L} d \tag{6.48}$$

where

$$d = \frac{1}{\beta_q}\left(\frac{n}{\kappa_{co}^{1-n}}\right)^{1/2} = \frac{1}{\delta} \tag{6.49}$$

is the dimensionless decay rate. Its inverse $1/d = \delta$ is a dimensionless measure for the length of the decay (width of the boundary layer) which is proportional to β_q.

It can be shown that the relative strain or curvature is closely related to decay rate d or decay length measure δ (Eq.(5.98)):

$$\frac{\varepsilon_{o\max}}{\varepsilon_{co\max}} = \frac{\kappa(0,0)}{\kappa_{co}} = 1 - \frac{\delta}{n} + \left(\frac{\delta}{n}\right)^2 (1-n)\,\frac{17}{12}\,. \tag{6.50}$$

Thus, an increase of the decay length measure δ increases the relative strain reduction $(\varepsilon_{co\max}-\varepsilon_{o\max})/\varepsilon_{co\max}$. Fig.5.4 visualizes the obvious trend and qualitatively the same behavior is found for the tapered tension rod (Fig.3.3, 3.4, 4.4).

(g) A quantitative estimate of the size effect on the maximum bending strain of two geometrically similar specimens - (m) denoting the model and (p) the prototype - of different sizes but under scaled loading has been determined in general terms (Eq.(5.99)). If a very large specimen is compared with the small-scale specimen such that $\lambda = L_p / L_m = h_p / h_m \to \infty$, an upper bound estimate for the size effect on the bending strain ratio is obtained

$$\left[\frac{(\varepsilon_{o\max})_p}{(\varepsilon_{o\max})_m}\right]_{\lambda\to\infty} = \frac{1}{1 - B_m + B_m^2 (1-n)\dfrac{17}{12}}\,, \tag{6.51}$$

where

$$\left.\begin{aligned} B_m &= \sqrt{q}\,\beta_m \left(\frac{\kappa_{co}^{1-n}}{n}\right)^{1/2} \frac{1}{n} = \frac{1}{d_m}\frac{1}{n} = \frac{\delta_m}{n} \\ \beta_m &= l_i / L_m \end{aligned}\right\} \tag{6.52}$$

refer to the small scale model and d_m is the decay rate and δ_m the decay length of the small- scale model.

The size independent quantities are

$$\left.\begin{aligned} \kappa_{co} &= \frac{L}{h}\left(\tilde{\tilde{P}}\right)^{1/n}\left(1+\frac{n}{2}\right)2 = \text{const.} \\ \tilde{\tilde{P}} &= \frac{4PL}{Kbh^2} = \text{const.} \\ q &= \left(\frac{h}{L}\right)^{1-n} \frac{(2+n)2^{1+n}}{12} = \text{const.} \end{aligned}\right\} \tag{6.53}$$

For sufficiently small values of $B_m < 1$ Eq.(6.51) allows the rough estimate

$$\left[\frac{(\varepsilon_{o\max})_p}{(\varepsilon_{o\max})_m}\right]_{\lambda\to\infty} = 1 + B_m = 1 + \frac{1}{d_m}\frac{1}{n} = \frac{\delta_m}{n}\,. \tag{6.54}$$

For a typical set of data the upper bound strain ratio is found as follows. A beam depth-to-length ratio h/L = 0.2, a hardening exponent n = 1/9 (characteristic for a ferritic reactor

vessel steel), and a fairly large load factor $\tilde{\tilde{P}} = 4PL/Kbh^2 = 0.8 < 1$ were assumed. For the normalized gradient coefficient a value of $\beta_m = l_i/L_m = 0.03$ was used for the small-scale beam specimen; this represents the maximum value for which the approximate perturbation solution remains appropriate when $n = 1/9$. With these data the internal length l_i amounts to 15% of the beam depth h_m of the small specimen. This yields

$$B_m = 0.2378$$

and from Eq.(6.51) one obtains

$$\left[\frac{(\varepsilon_{o\max})_p}{(\varepsilon_{o\max})_m}\right]_{\lambda\to\infty} = 1.20\,,$$

i.e., in comparison to the small specimen a 20% higher bending strain in the very large specimen under scaled loading $\tilde{\tilde{P}}_m = \tilde{\tilde{P}}_p = 0.8$. Of course, the strain ratio Eq.(6.51) is strongly dependent on the load level $\tilde{\tilde{P}}$ and increases with its rise; e.g., for $\tilde{\tilde{P}} = 0.7$ and 0.9 one obtains for the strain ratio 1.13 and 1.25, respectively. However, for large load levels $\tilde{\tilde{P}}$, the estimate becomes erroneous because of the dominance of the quadratic term of B_m.

(h) The results of the perturbation solution have been used to demonstrate the size influence on a dimensionless load versus maximum bending strain diagram (Fig.5.10). As mentioned before for the tapered tension rod, this representation of the size effect is a rather natural choice since it simulates directly experimental conditions. It is found that a bundle of dimensionless curves fans out and, with increasing β-values (decreasing size L), smaller specimens show a higher flow stress at the same strain. However, the size influence on the stress becomes effective in the percentage range only for β-values of 0.01 and larger.

6.4 Recommendations for Further Theoretical Work

(1) A quantitative estimate of the accuracy of the singular perturbation solution can, of course, be given if an exact solution is available for the purpose of comparison; this luxury is restricted to the exception of a fully linear problem. In the non-linear case one has to include in the power series approximation at least one additional term beyond the order of the required approximation. For example, if a perturbation approximation up to 2nd order (i.e. β^2-term) is required, this solution requires, in any case, also the 3rd order contribution for the suppression of the secular terms in the 2nd order contribution, but a complete presentation of the 3rd order contribution is not necessary.

This may suffice to determine the 3rd order contribution at distinct positions (Section 4.4.3) which then allows to estimate the accuracy of the second order approximation at this position. If an extended comparison is of interest, then the complete 3rd order contribution is necessary. This, in fact, requires the inclusion of the 4th order contribution to suppress the secular terms in the 3rd order contribution. Thus, the amount

of algebra to obtain higher order approximations may be discouraging. The objective of the derivation is, of course, to get a non-numerical solution which contains the parameters in the problem; thus, attention should be given to computerized symbolic manipulations, using symbolic languages like 'Maple', 'Mathematica' or others.

(2) For the fully non-linear case the evaluation of the sensitivity

$$S = \left(\frac{d\varepsilon(0,0)/\varepsilon_{co}}{d\beta} \right)_{\beta=0}$$

for varying hardening exponents n and with the stress level being constant (σ_{Ro}/K = const.) remains to be done.

(3) The developed analytical perturbation solution is not valid close to instability and beyond. However, the influence of a gradient term in the plasticity law and of a change of specimen size on the ultimate stress and on the response in the softening region, especially the formation of deformation patterns, are important questions. A first step towards these questions should be a review of the related literature.

(4) The simple linear non-local (integral) model approximated in Appendix (1) by a gradient model and associated boundary conditions should be solved analytically and should be compared with the standard gradient model, to obtain further insight into the importance of the non-classical boundary condition.

(5) The gradient enhanced plasticity law should include also a first order strain gradient term which implies that two different internal length scales are operative. Thus, there exists the possibility of mode transitions in deformation and failure when the size is changed. Also, the development or application of an appropriate singular perturbation solution appears to be a challenging task.

(6) The gradient plasticity model used in this report did not include rate dependence (viscoplasticity) or damage. Especially in the softening regime the damage evolution is important for the modeling of failure (fracture) and its size dependence. First steps towards this direction have been done by Aifantis and coworkers.

(7) The develpment of numerical solution procedures and computer programs for gradient plasticity models are required for more complex geometries than those treated in this study. Of course, this development depends largely on the physical effects included in the model and its mathematical structure. Some concepts are presented in Part I.

Acknowledgement: It is gratefully recognized that this work was financially supported by the EU under the project 'Reactor Vessel Integrity in Severe Accidents (REVISA)', contract FI4S-CT96-0024. The authors also express their gratitude to B. Dolensky, G. Hailfinger and Dr. T. Jordan (all FZK-IRS) for the preparation of first versions of a part of the numerous figures and Dr. T. Jordan, Dr. R. Krieg and Dr. B. Göller (FZK-IRS) for their enduring engagement in the proofreading of the final version.

References Part II, Section 1

[1.1] Malmberg T., Tsagrakis I., Eleftheriadis I. and Aifantis E.C.: On the gradient plasticity approach to size effects, Part I: Reviews, Technical Report INV-REVISA (99)-P011, June 1999; Revised Version: Milestone Report INV-REVISA (00)-P006, March 2001; *Forschungszentrum Karlsruhe, Scientific Report FZKA 6321*, March 2001.

[1.2] Morrison J.L.M.: The yield of mild steel with particular reference to the effect of size of specimen, *Proc. of the Inst. of Mech. Eng. 142*, pp. 193-223, 1939

[1.3] Richards C.W.: Effect of size on the yielding of mild steel beams, *Proc. Am. Soc. Testing Mats. 58*, pp. 955-970, 1958

[1.4] Devos J., Ritter B., Auerkari P., Dupas P. and Malmberg T.: Reactor vessel integrity in severe accidents (REVISA), in *Proc. of the FISA-97 Symposium on EU-Research on Severe Accidents*, eds. Van Goethem G., Keinhorst G., Martin Bermejo J., Zurita A., Luxembourg, 17-19 November 1997, pp. 113-122, EUR 18258 EN, 1998

[1.5] Devos J., Le Ber L., Nicolas L., Bhandari S., Messelier-Gouze C., Auerkari P., Santaoja K., Caroli C., Fokkens J., Lämmer H., Malmberg T., Krompholz K., Solomos G., Aifantis E.C., Eisert P.: Reactor vessel integrity in severe accidents (REVISA), *Proc. FISA99-EU Research in Reactor Safety, Conclusion Symposium on Shared-Cost and Concerted Actions*, Nov. 29 – Dec.1, 1999, Luxemburg.

References Part II, Section 2

[2.1] Stach T.: *Zur Skalierung von Modellversuchen zum Aufprall fluessiger Massen auf deformierbare Strukturen*, Forschungszentrum Karlsruhe, Scientific Report FZKA 5903, 1997

[2.2] Jordan T. and Malmberg T.: Size effect on liquid impact and resulting structured response, *1998 ASME / JSME Joint Pressure Vessel and Piping Conference*, San Diego, California, July 26-30, 1998

[2.3] Malmberg T., Aktaa J., Schlossmacher P.: Personal communications, Forschungszentrum Karlsruhe, 1999.

[2.4] Malmberg T.: Aspects of similitude theory in solid mechanics, Part I: Deformation behavior, *Forschungszentrum Karlsruhe, Scientific Report FZKA 5657*, 1995

References Part II, Section 3

[3.1] Brown W.F., Lubahn J.D., Ebert L.J.: Effect of section size on the static notch bar tensile properties of mild steel plate, *Welding J. 26*, pp. 554_{-s}-559_{-s}, 1947

[3.2] Hildebrand F.B.: *Advanced calculus for applications*, Prantice-Hall, Inc., Englwood Cliff., New Jersey, 1962

[3.3] Dwight H.B.: *Tables of integrals and other mathematical data*, The Macmillan Comp., New York, 1967

References Part II, Section 4

[4.1] Hollomon J.H.: Tensile deformation, *Trans. Metallurgical Soc. ASME 16*, pp. 268-290, 1949

[4.2] O'Malley R.E.: *Singular perturbation methods of ordinary differential equations*, Springer Verlag, New York, 1991
[4.3] Nayfeh A.: *Perturbation methods*, John Wiley & Sons, New York, 1973
[4.4] Nayfeh A.: *Introduction to perturbation techniques*, John Wiley & Sons, New York, 1981
[4.5] Kervorkian J. and Cole F.D.: *Perturbation methods in applied mathematics*, Springer Verlag, New York, 1981
[4.6] Holmes M.H., *Introduction to perturbation methods*, Springer Verlag, New York, 1995
[4.7] Simmonds J.G. and Mann J.E., *A first look at perturbation theory*, R.E. Krieger Publ. Comp. Malabar Florida, 1986

References Part II, Section 5

[5.1] Szabó J.: *Einführung in die Technische Mechanik*, Springer Verlag, 1958
[5.2] Kumar V., German M.D., Shih C.F.: An engineering approach for elastic-plastic fracture analysis, *Electric Power Research Institute, EPRI NP-1931, Research Project 1237-1*, Topical Report, July 1981

References Part II, Section 6

[6.1] Aifantis E.C.: On the microstructural origin of certain inelastic models, *J. Mat. Engng. Tech. 106*, pp. 326-330,1984
[6.2] Shearin P.E., Ruark A.E. and Trimble R.M.: Size effects in steels and other metals from slow notch bend tests, *Fracturing of Metals*, A.S.M. Cleveland, pp. 167-188, 1948
[6.3] Plechanova N.G. and Ratner S.J.: Size influence on plastic materials, (in Russian), *Zhur. Tekh. Fiz. 23*, 3, pp.445-453, 1954
[6.4] Eringen, *Nonlinear theory of continuous media*, McGraw-Hill, New York, San Francisco, Toronto, London, 1962
[6.5] Aifantis E.C.: The physics of plastic deformation, *Int. J. Plasticity 3*, pp. 211-247, 1987
[6.6] Zbib H.M. and Aifantis E.C.: On the localization and postlocalization behavior of plastic deformation, I, II and III, *Res. Mechanica, Int. J. Struct. Mech. Mater. Sci. 23*, pp. 261-277, 279-292 and 293-305, 1988
[6.7] Altan B.S. and Aifantis E.C.: On the structure of the mode III crack-tip in gradient elasticity, *Scripta Met. Mater. 26*, pp. 319-324, 1992
[6.8] Ru C.Q. and Aifantis E.C.: A simple approach to solve boundary value problems in gradient elasticity, *Acta Mechanica 101*, pp. 59-68, 1993
[6.9] Vardoulakis I., Exadaktylos G. and Aifantis E.C.: Gradient elasticity with surface energy: Mode III crack problem, *Int. J. Struct. 33*, pp. 4531-4559, 1996

Tables

Table 4.1: Limit strains at instability.

m	$\varepsilon = n$	ε_R	$\frac{(\sigma_R)_{max}}{K} = \frac{n^n}{e^n}$
1	1	1.718	0.368
3	0.333	0.3956	0.497
5	0.2	0.2214	0.593
9	0.11	0.1175	0.701
13	0.077	0.08	0.760

Table 4.2: Influence of hardening exponent n on the sensitivity $S \sim ZN$ under the constraint z=0.1

n	Z	N	ZN
1	1.1712	1	1.1712
1/3	0.5436	3.6028	1.9586
1/5	0.4663	5.8731	2.7384
1/9	0.4209	10.1685	4.2800
1/13	0.4047	14.3479	5.8061
$\rightarrow 0$	$\rightarrow 0.3704$	$\rightarrow \infty$	$\rightarrow \infty$

Table 4.3: Critical strain limits

$\varepsilon(0,0) = n$	$\varepsilon_R(0,0)$
1/5 = 0.2	0.2214
1/9 = 0.1111	0.1175

Table 5.1: Distorted scale factors λ_h and λ_b for λ=10.

n =	1/3	1/5	1/9
λ_h =	21.54	25.12	27.83
λ_b=	4.64	3.98	3.594

Table 5.2: Ramberg-Osgood Material Parameters

Material	σ_o [MPa]	ε_o	α	m	E [MPa]	n	K [MPa]
A533-B (93°C) (ref. [5.2] pp. 6-14)	414	0.002	1.12	9.71	$207\ 10^3$	0.103	776.05
SS 304 (R.T.) (ref. [5.2] pp. 6-23)	207	0.001	1.691	5.421	$207\ 10^3$	0.184	671.88

Table 5.3: Influence of load level $\tilde{\tilde{P}}$ on upper bound strain ratio $(\varepsilon_{o\max}/\varepsilon_{co\max})_{\lambda\to\infty}$ ($h/L = 0.2$, $n = 1/9$, $\beta_m = 0.03$)

$\tilde{\tilde{P}}$	B_m	$\left(\frac{\varepsilon_{o\max}}{\varepsilon_{co\max}}\right)_{\lambda\to\infty}$
0.4	0.01486	1.0148
0.5	0.03285	1.0359
0.6	0.07524	1.0731
0.7	0.1394	1.1299
0.8	0.2378	1.200
0.9	0.3809	1.2472

Figures

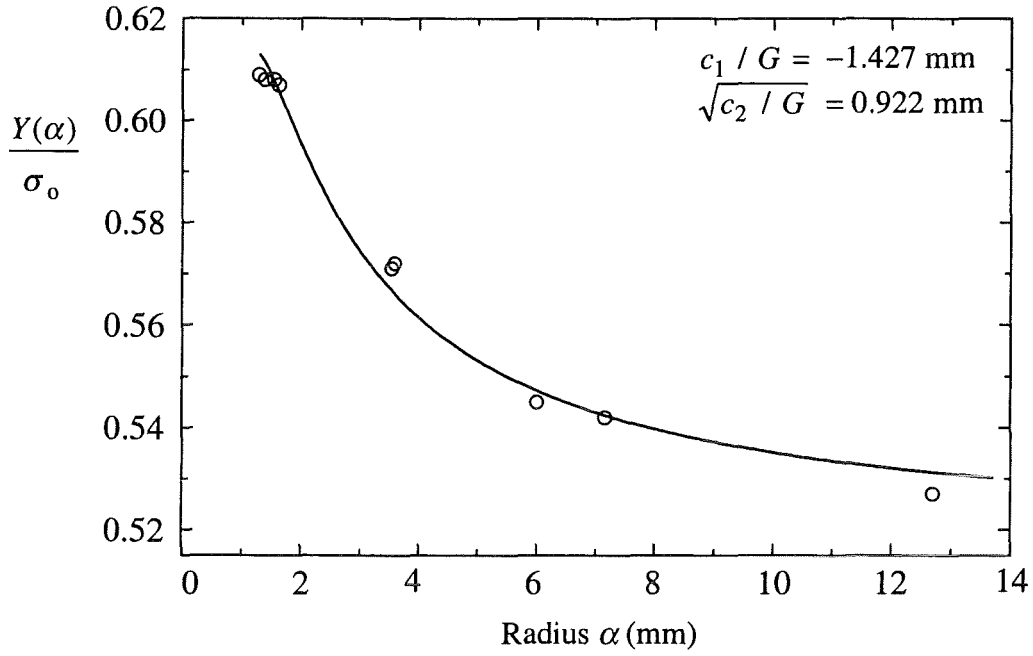

Fig. 2.1 Morrison's experimental data of the size-dependent yielding in torsion of mild steel and fitting of a gradient plasticity model.

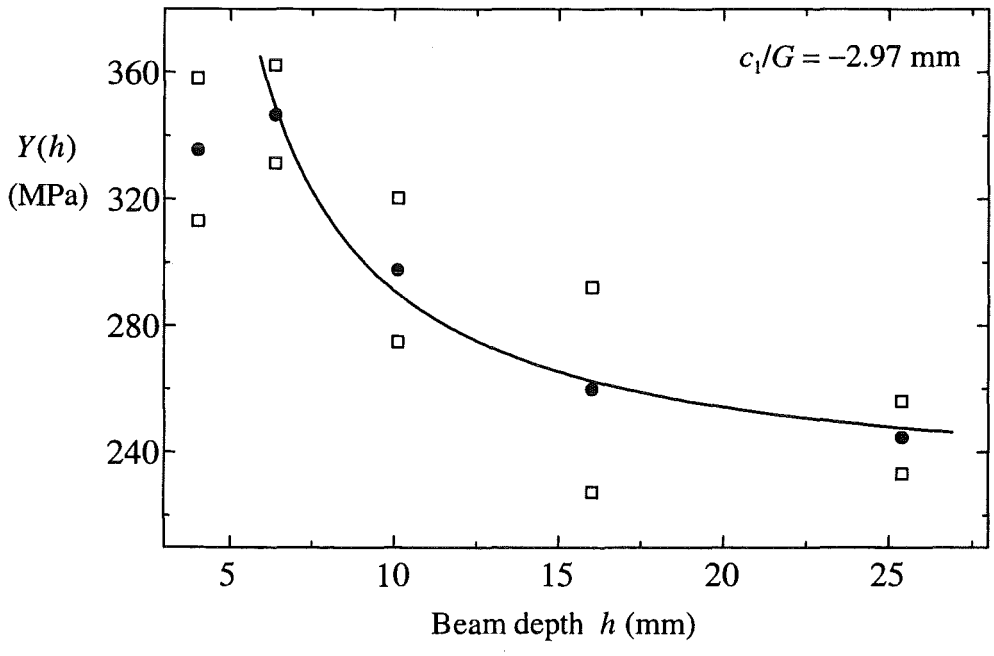

Fig. 2.2 Richards' experimental data of the size-dependent yielding in pure bending of mild steel and fitting of a gradient plasticity model.

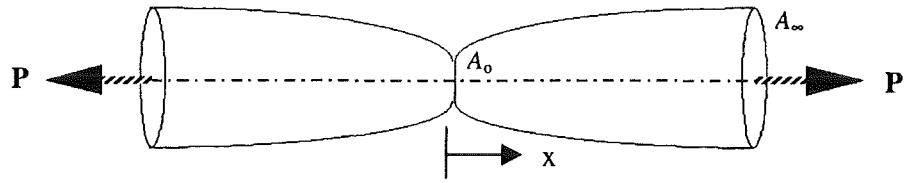

Fig. 3.1 An exponentially tapered tensile rod.

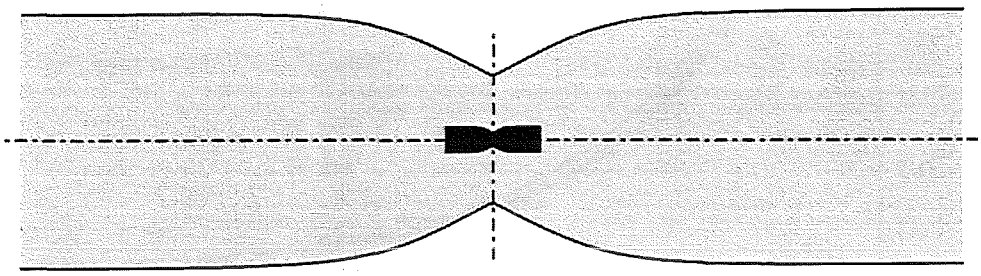

(a) Large and small scale exponentially tapered tensile specimen (scale factor 1:10)

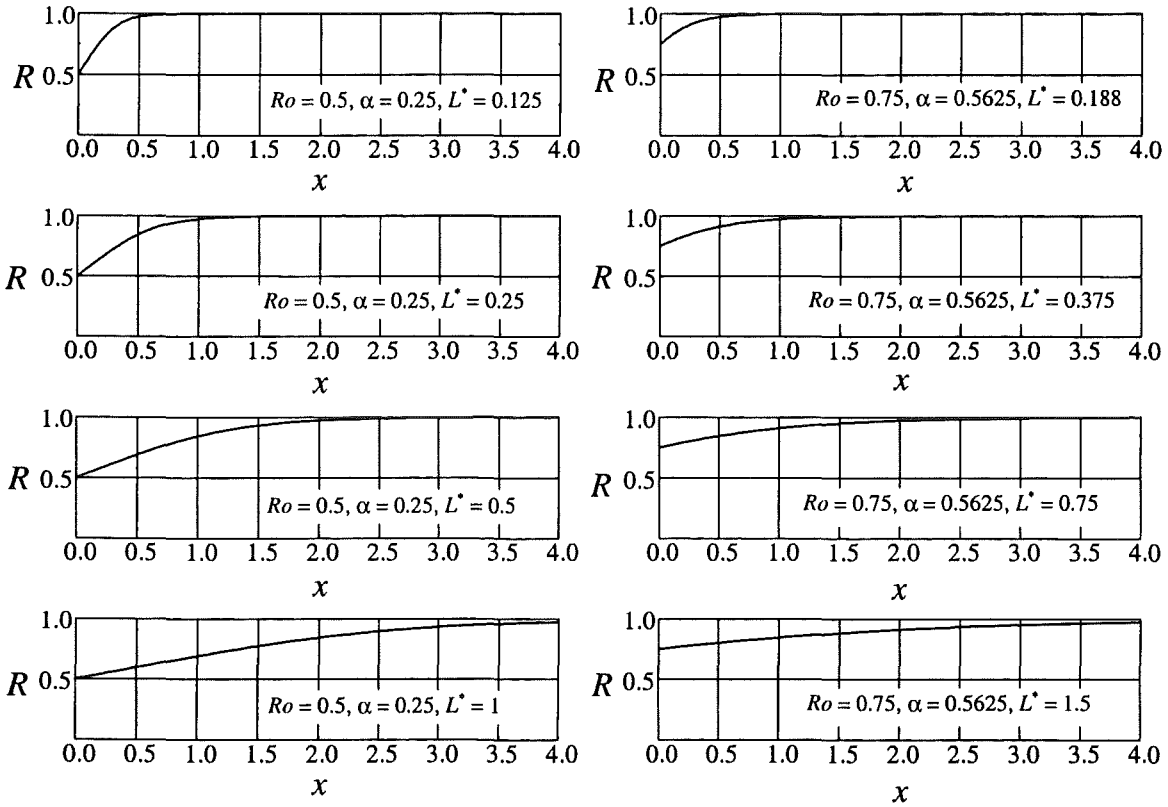

(b) Contours of exponentially tapered tensile rods.

Fig. 3.2 Profiles of exponentially tapered tensile rods.

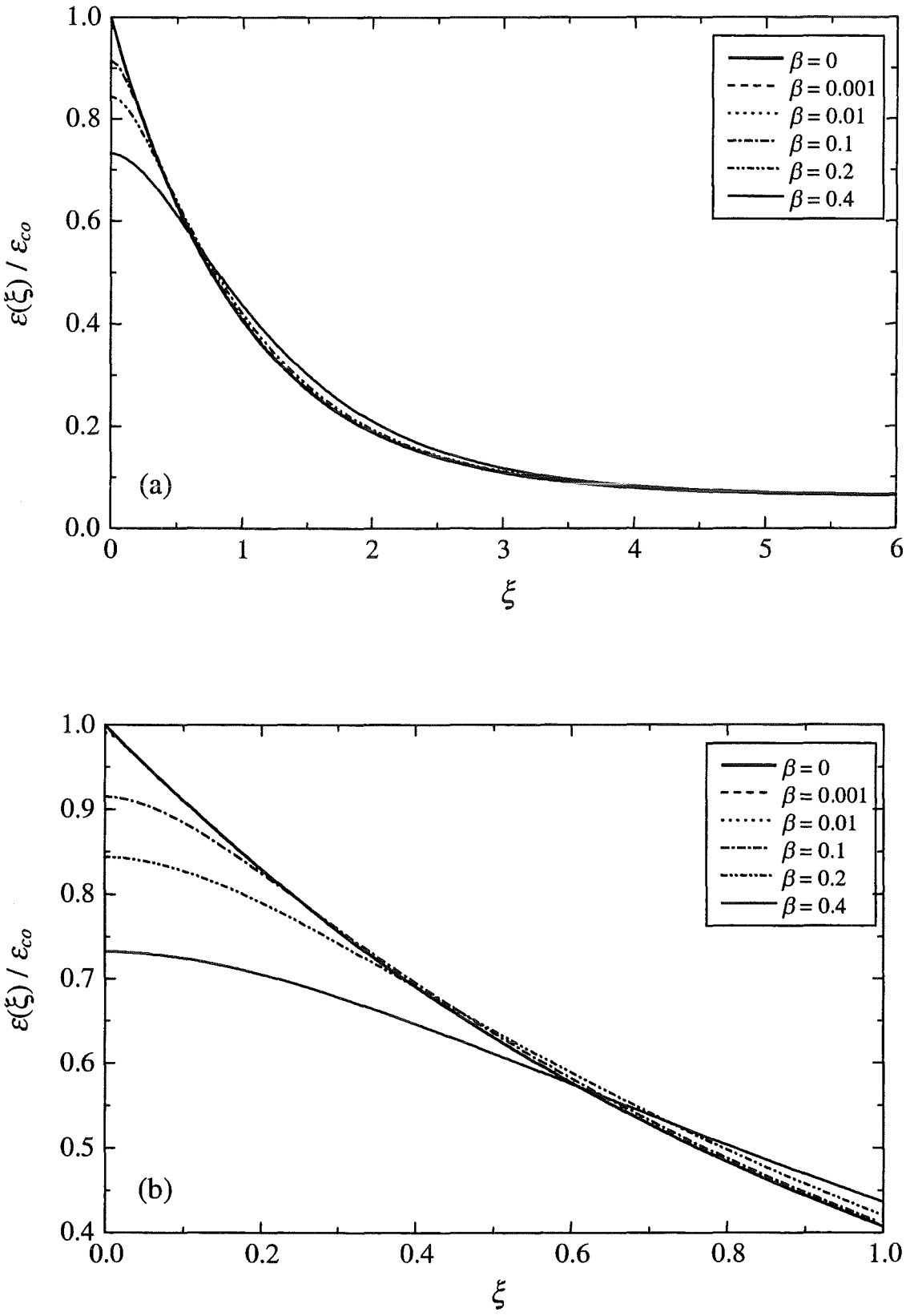

Fig. 3.3 Relative strain distribution in an exponentially tapered rod ($\alpha = 0.0625$; linear case $n = 1$, classical theory $\beta = 0$, gradient theory $\beta \neq 0$).

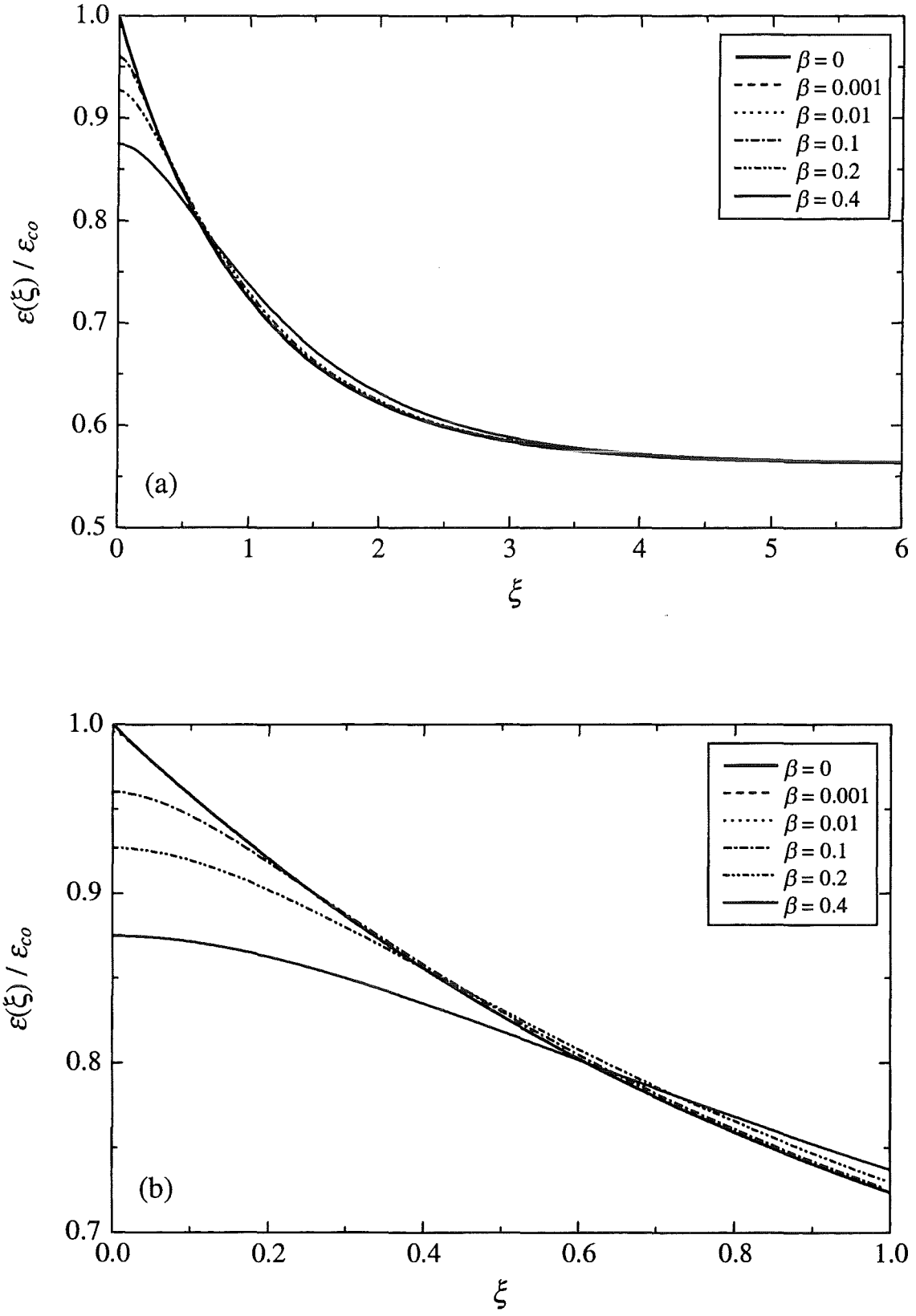

Fig. 3.4 Relative strain distribution in an exponentially tapered rod ($\alpha = 0.5625$; linear case $n = 1$, classical theory $\beta = 0$, gradient theory $\beta \neq 0$).

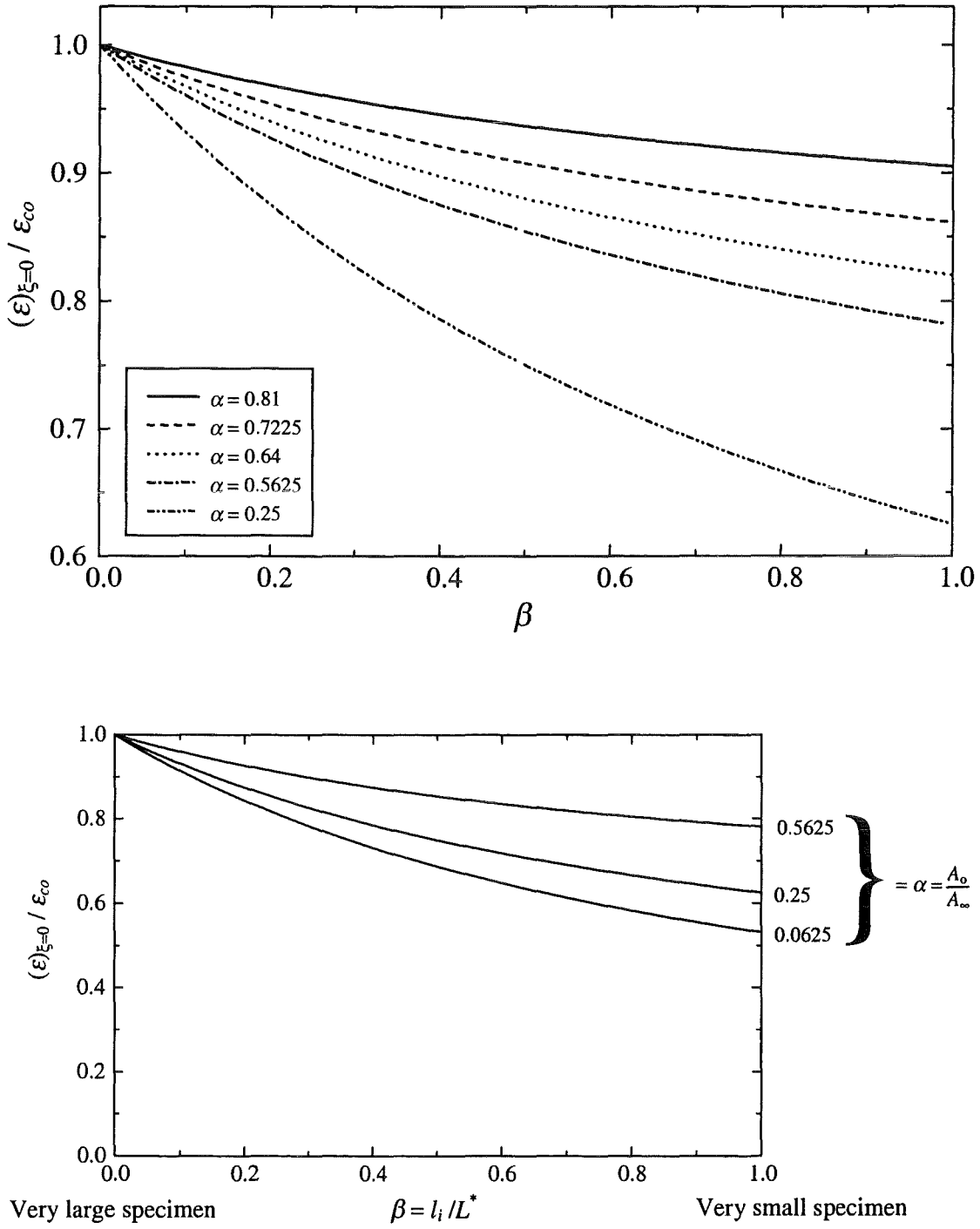

Fig. 3.5 Relative strain at minimum cross-section of an exponentially tapered rod versus β (linear case $n = 1$, classical theory $\beta = 0$, gradient theory $\beta \neq 0$).

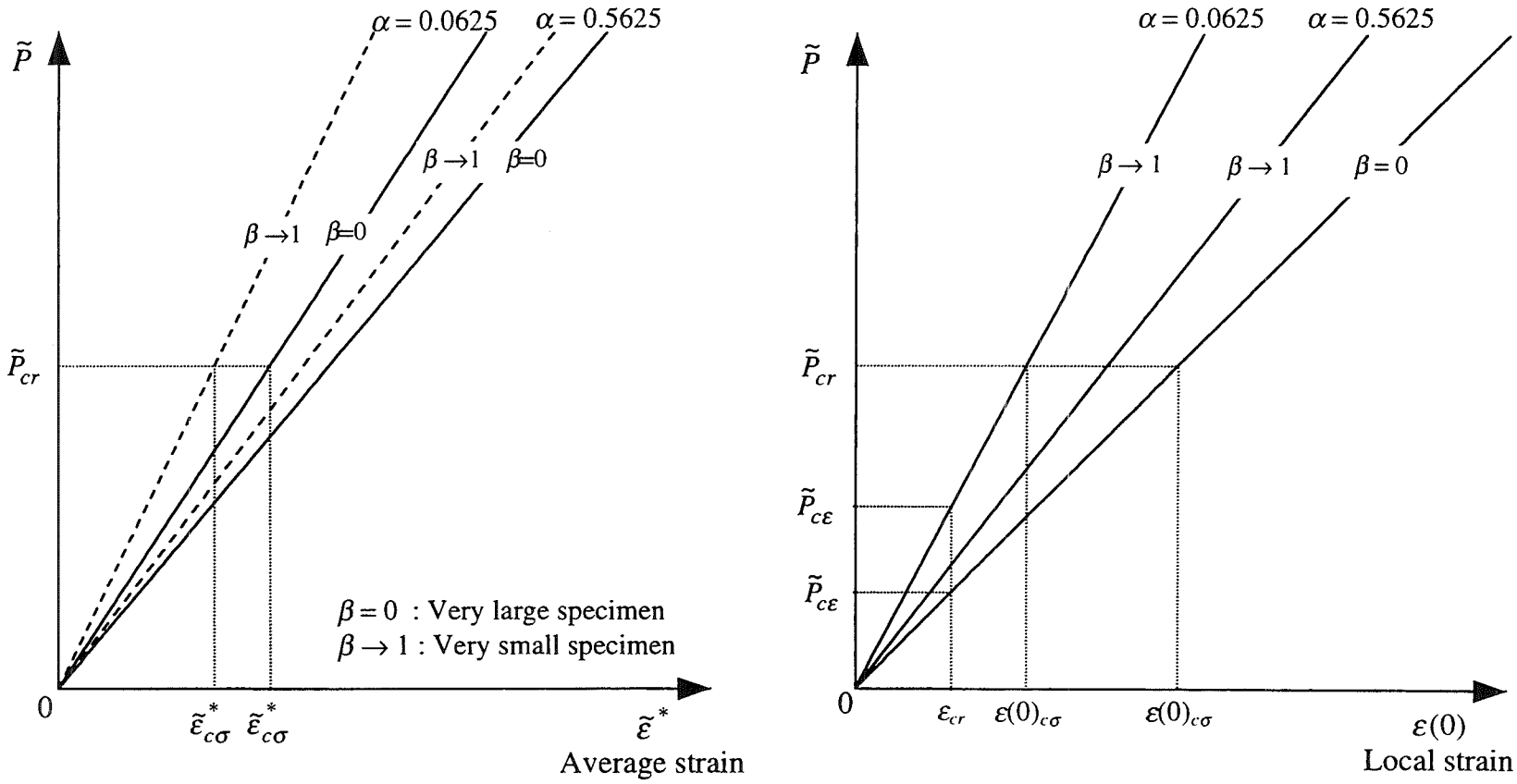

Fig. 3.6 Normalized load - displacement curves for the linear case (n = 1). Limiting cases of size influence for two cross-section ratios α.
(a) Consequence of a critical stress fracture criterion.
(b) Consequences of a critical stress or a critical strain fracture criterion.

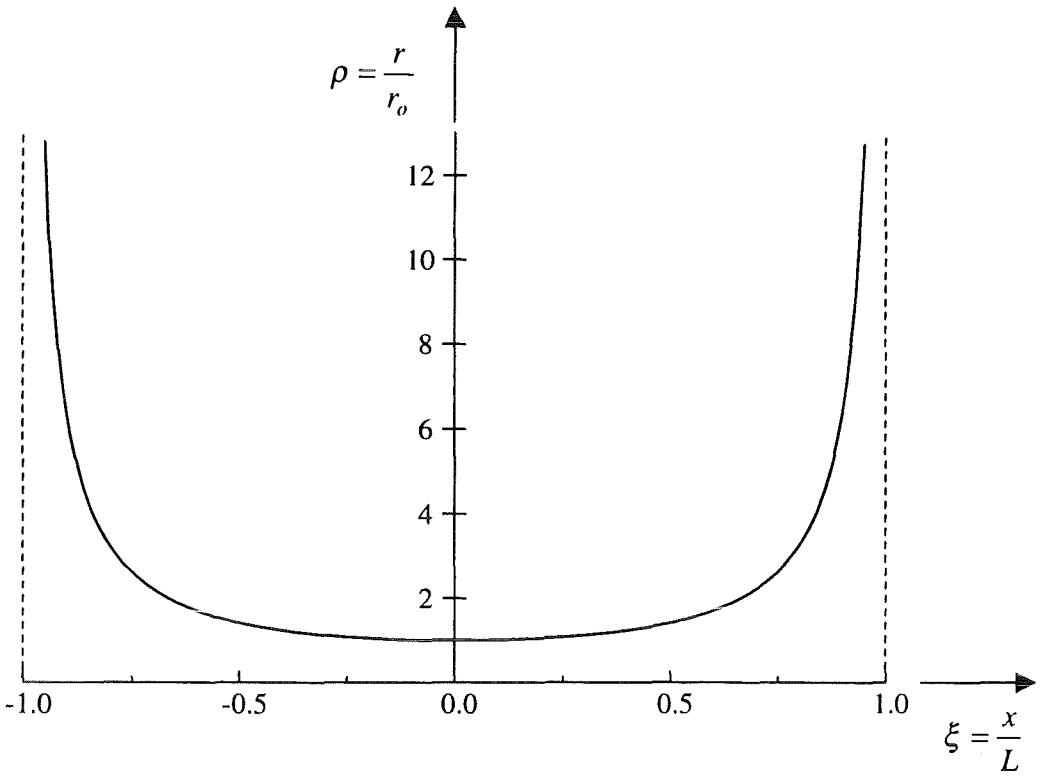

Fig. 3.7 Geometry of idealized U-notch.

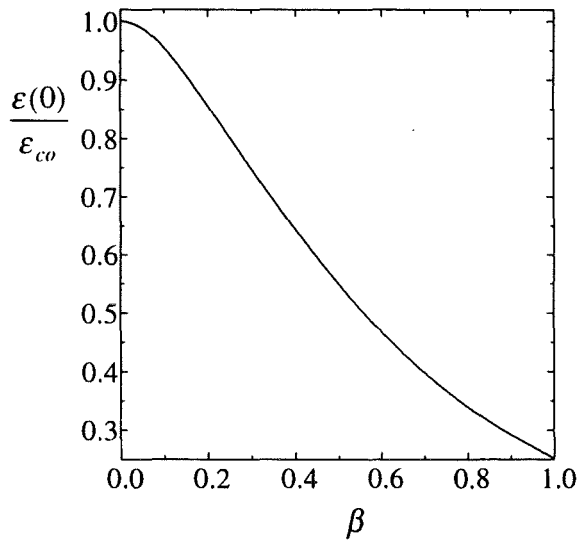

Fig. 3.8 Relative strain at $\xi = 0$ versus β.

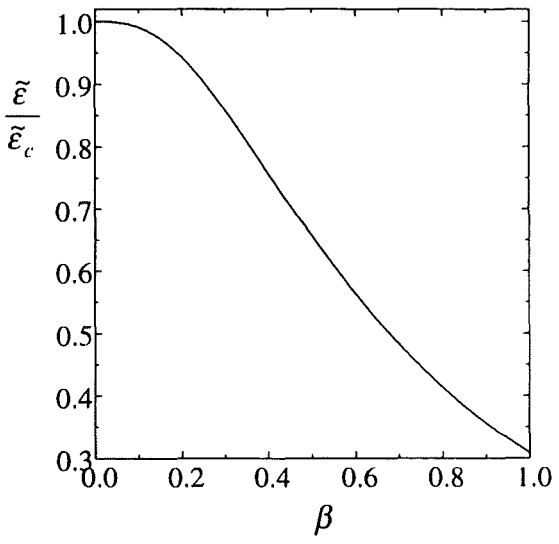

Fig. 3.9 Relative strain at $\xi = 0$ versus β. (U-notched rod, linear case $n = 1$, classical theory $\beta = 0$, gradient theory $\beta \neq 0$).

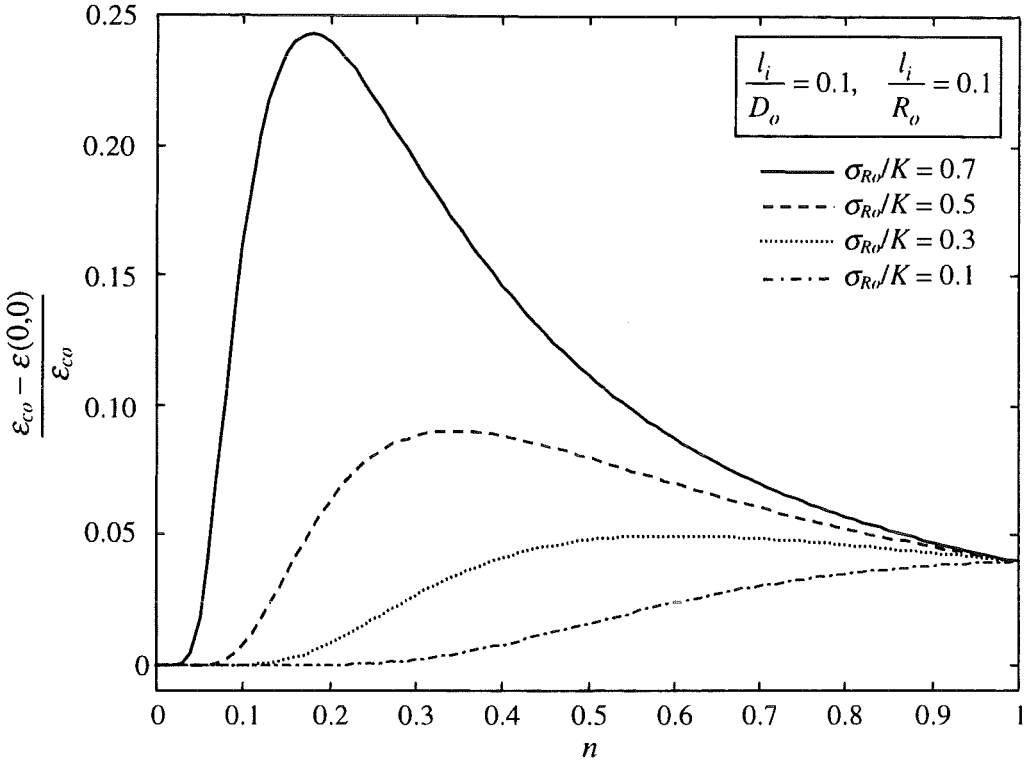

Fig. 4.1 Relative strain reduction versus hardening exponent n; tapered tension rod with smooth neck.

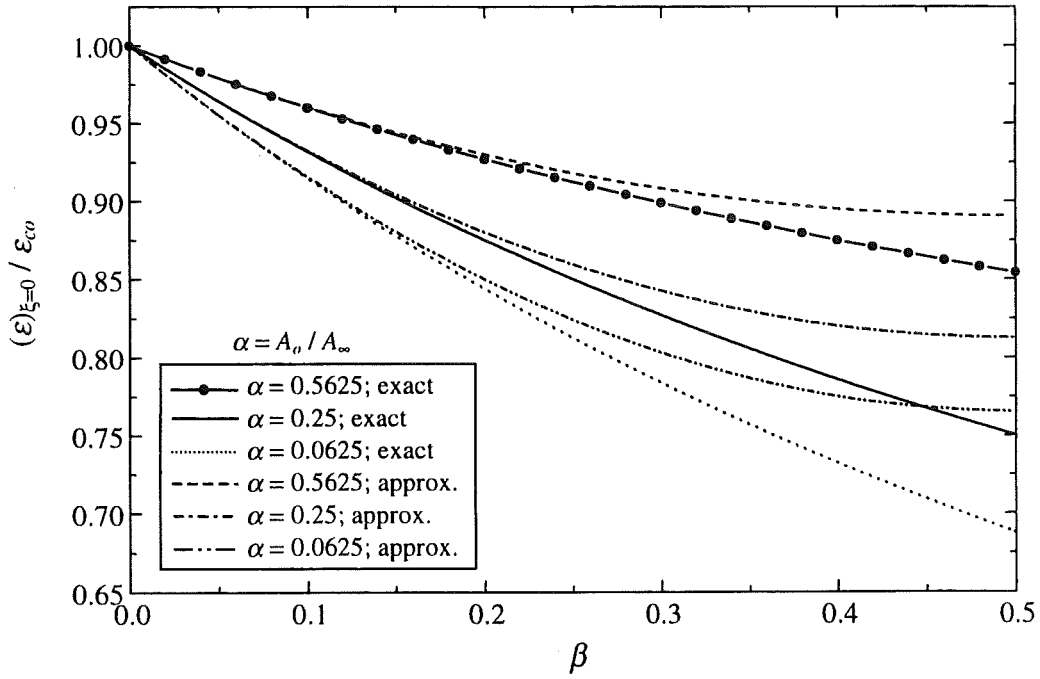

Fig. 4.2 Relative strain $\varepsilon(0,0)/\varepsilon_{co}$ versus normalized strain gradient coefficient β: reduction of the maximum strain due to gradient plasticity in the tapered rod problem; comparison of exact and 2nd order perturbation solution for linear hardening (n=1), without cross-section reduction.

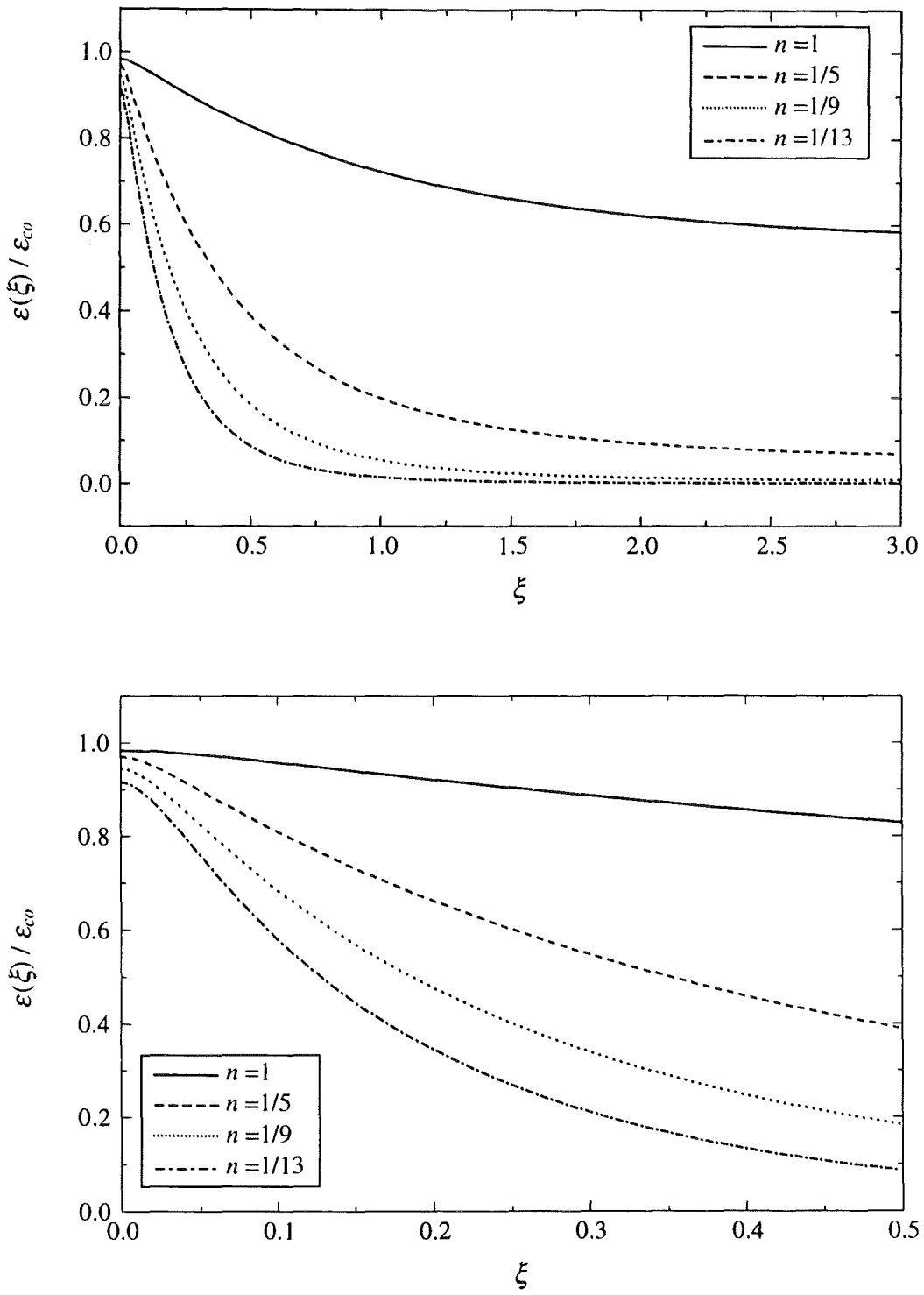

Fig. 4.3 Relative strain distribution for various strain hardening exponents; exponentially tapered rod with power law strain hardening, without cross-section reduction (α=0.5625, ε_{co}=0.01, β=0.02), 2[nd] order perturbation solution.

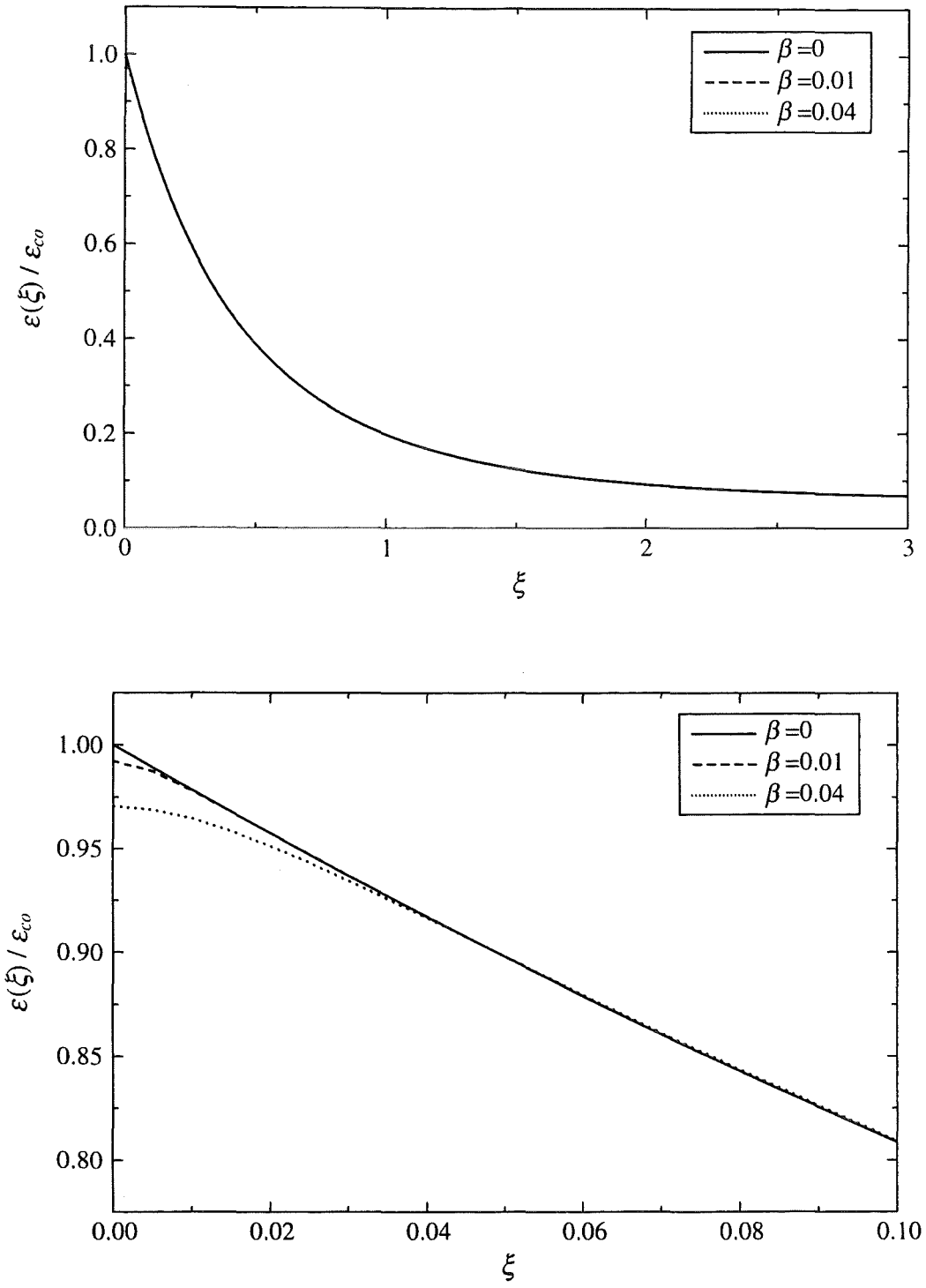

Fig. 4.4 Relative strain distribution for various normalized gradient coefficients β; exponentially tapered rod with power law strain hardening, without cross-section reduction (α=0.5625, ε_{co}=0.01, n=1/5), 2nd order perturbation solution.

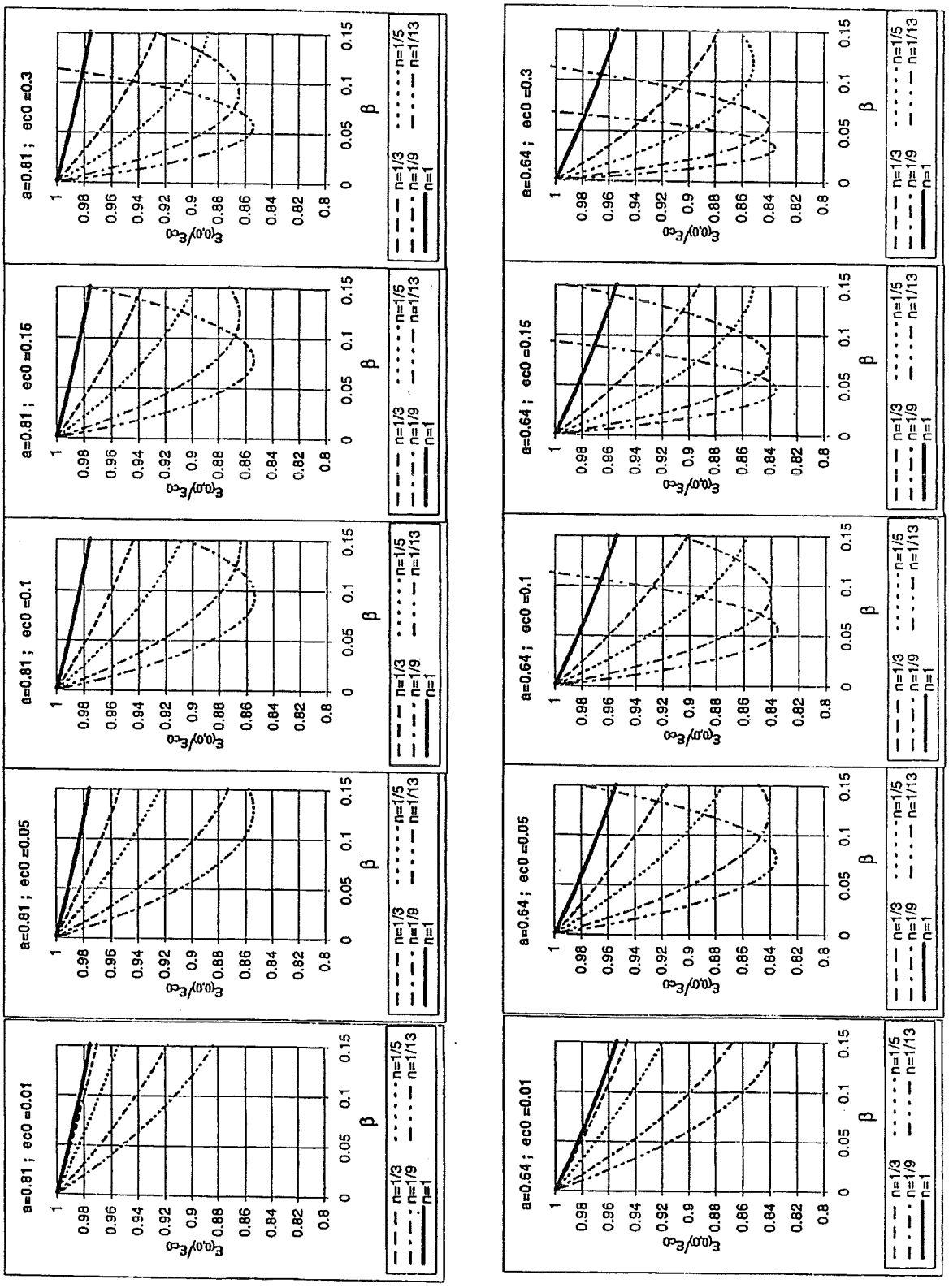

Fig.4.5a Relative strain $\varepsilon(0,0)/\varepsilon_{co}$ versus normalized gradient coefficient β: reduction of maximum strain due to gradient plasticity in the tapered rod problem; 2nd order perturbation solution for non-linear strain hardening ($n \leq 1$) without cross-section reduction.

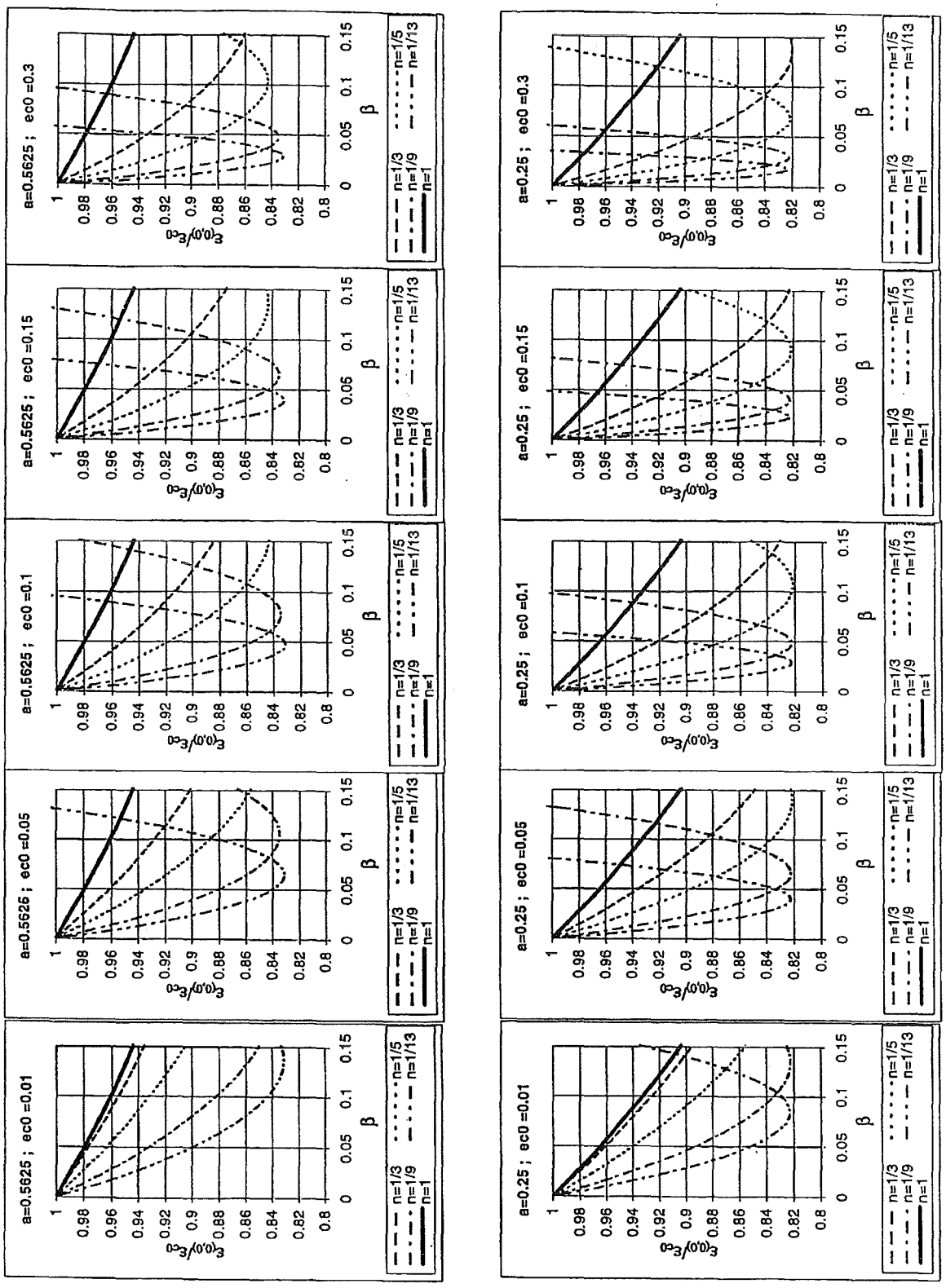

Fig.4.5b Relative strain $\varepsilon(0,0)/\varepsilon_{co}$ versus normalized gradient coefficient β: reduction of maximum strain due to gradient plasticity in the tapered rod problem; 2nd order perturbation solution for non-linear strain hardening ($n \leq 1$) without cross-section reduction.

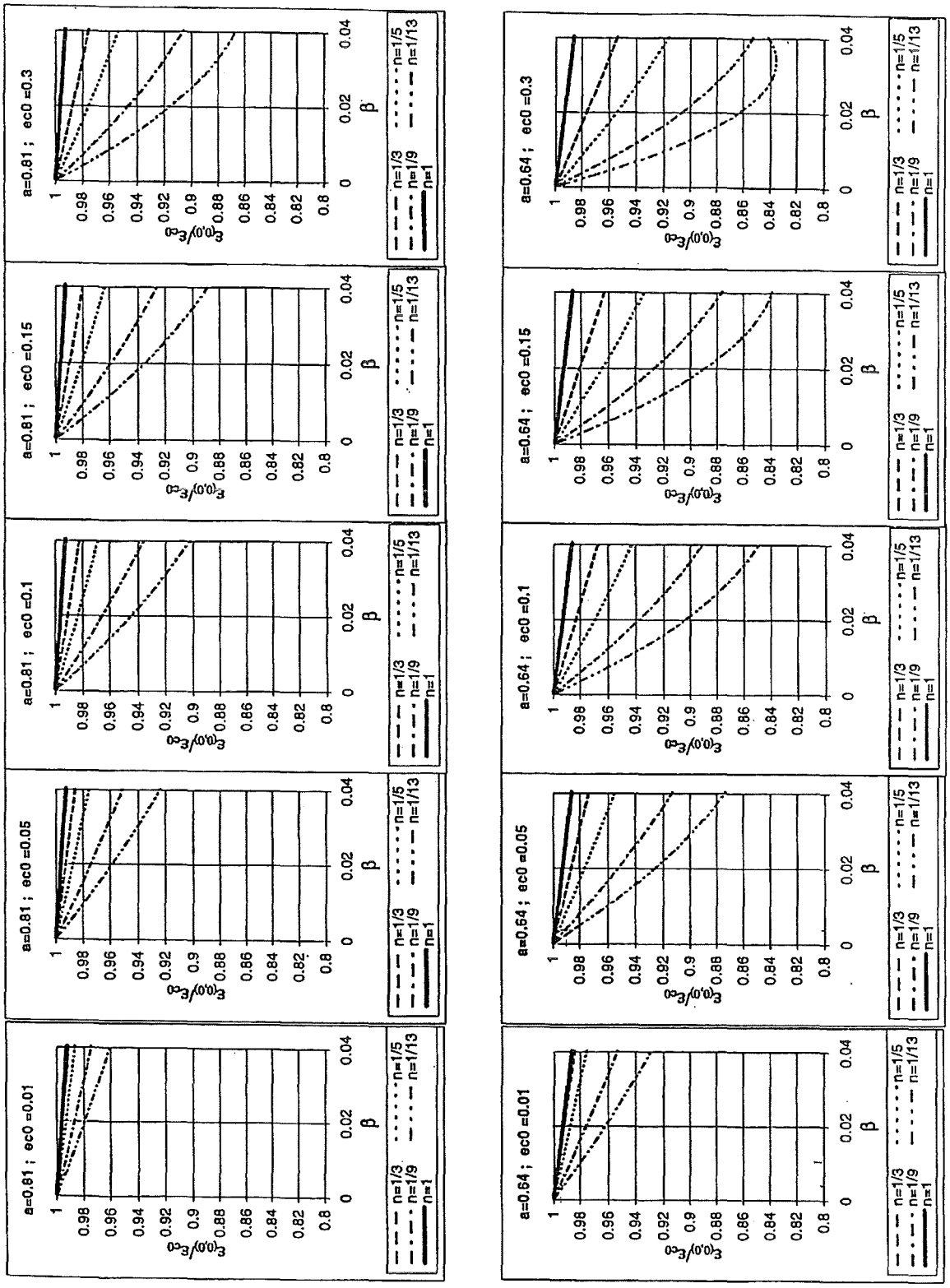

Fig.4.6a Relative strain $\varepsilon(0,0)/\varepsilon_{co}$ versus normalized gradient coefficient β: reduction of maximum strain due to gradient plasticity in the tapered rod problem; 2nd order perturbation solution for non-linear strain hardening ($n \leq 1$) without cross-section reduction.

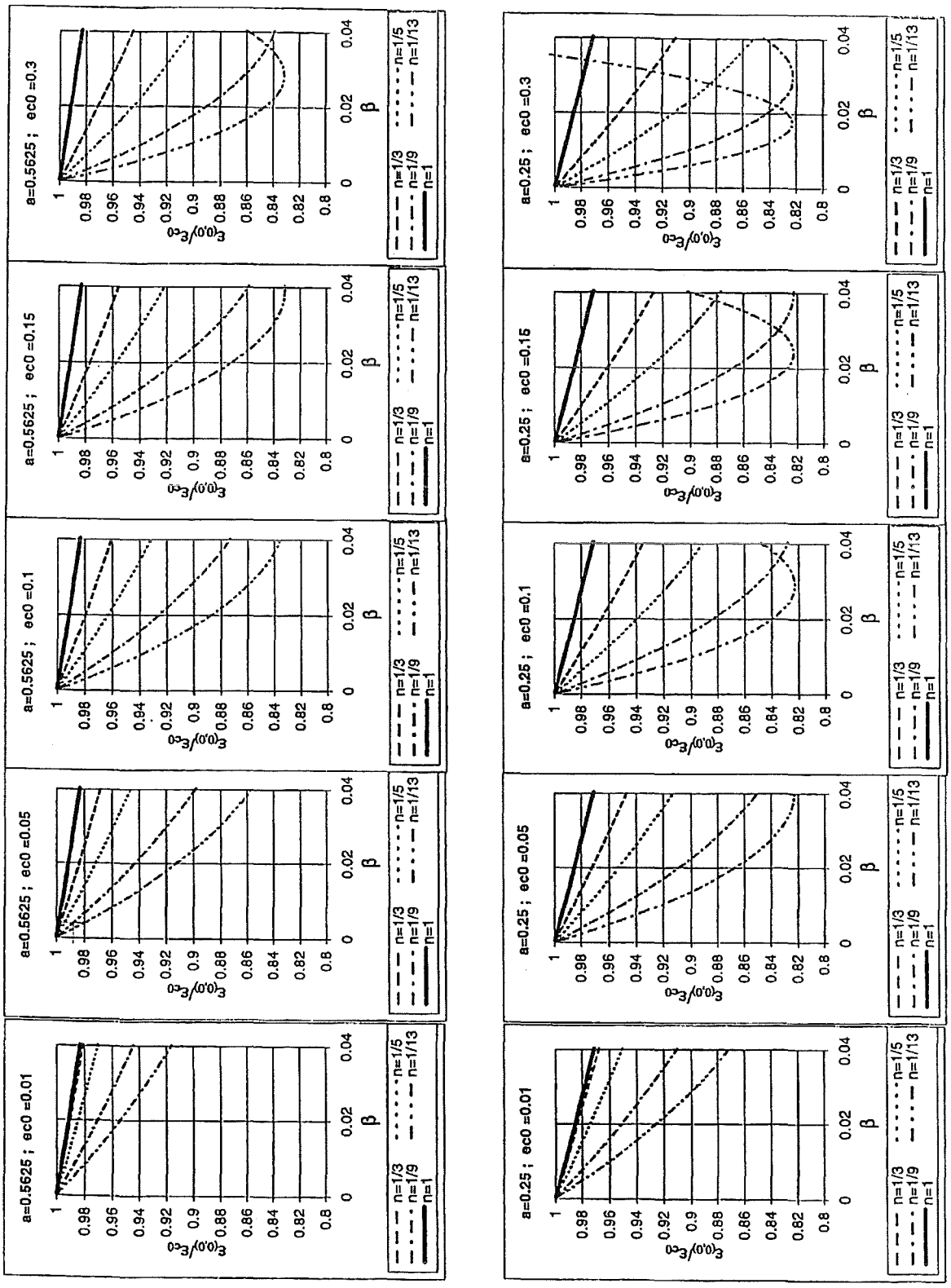

Fig.4.6b Relative strain $\varepsilon(0,0)/\varepsilon_{c0}$ versus normalized gradient coefficient β: reduction of maximum strain due to gradient plasticity in the tapered rod problem; 2nd order perturbation solution for non-linear strain hardening ($n \leq 1$) without cross-section reduction.

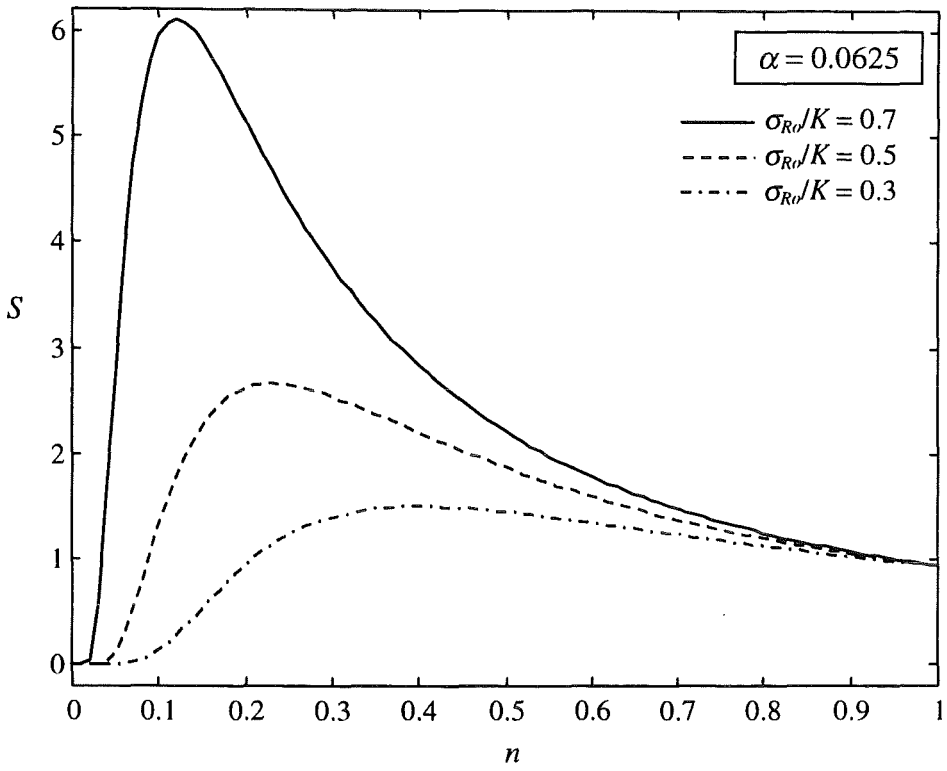

Fig. 4.7 Magnitude of the sensitivity S of the relative strain versus hardening exponent n for different normalized stress levels σ_{R0}/K; exponentially tapered tension rod with sharp neck ($\alpha = 0.0625$).

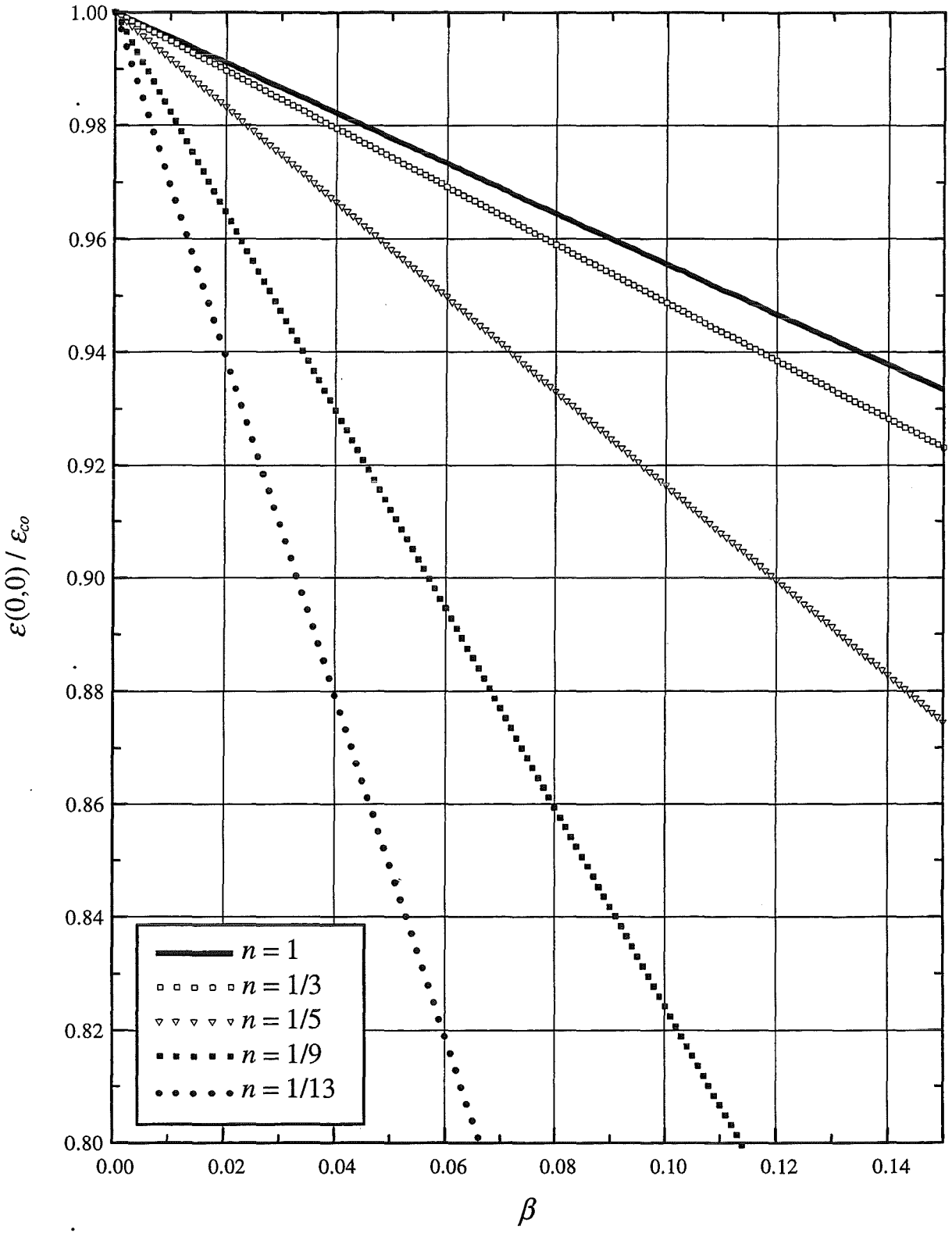

Fig. 4.8 Relative strain $\varepsilon(0,0)/\varepsilon_{co}$ versus normalized strain gradient coefficient β; exponentially tapered tension rod; linear and non-linear strain hardening ($n \leq 1$) including cross-section reduction; perturbation solution up to 1st order ($\alpha = 0.5625$, $\varepsilon_{co} = 0.01$).

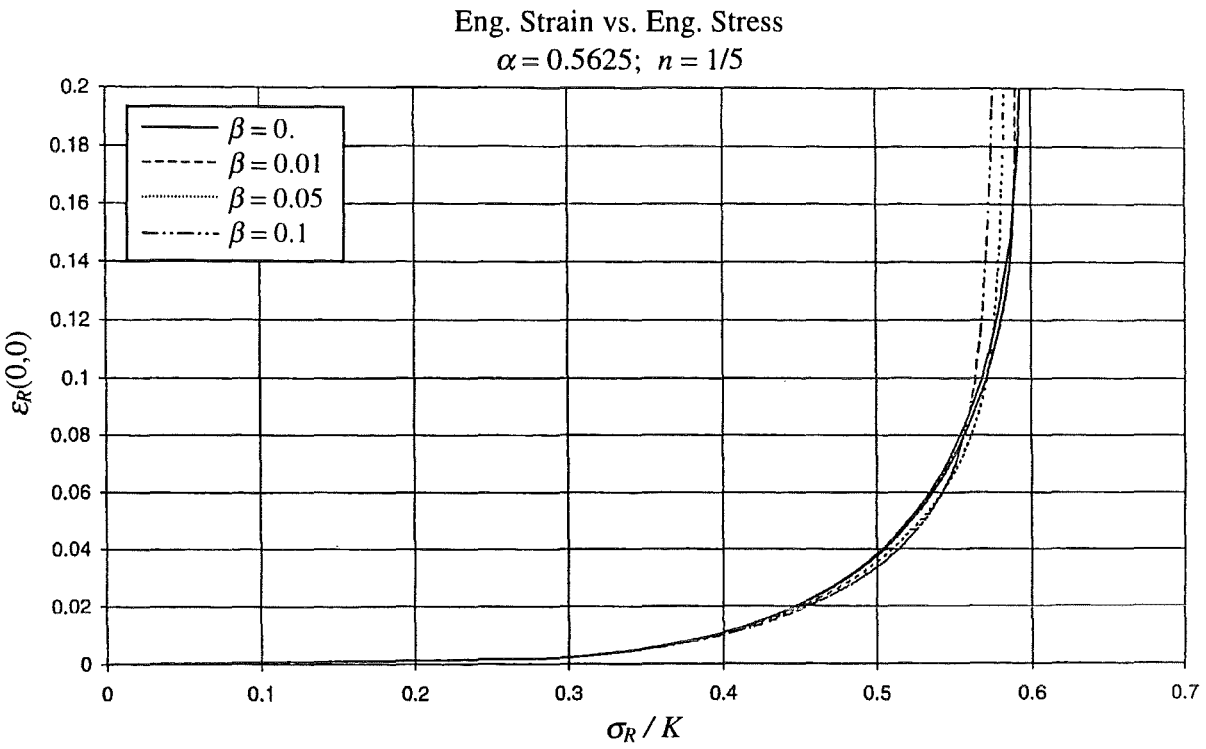

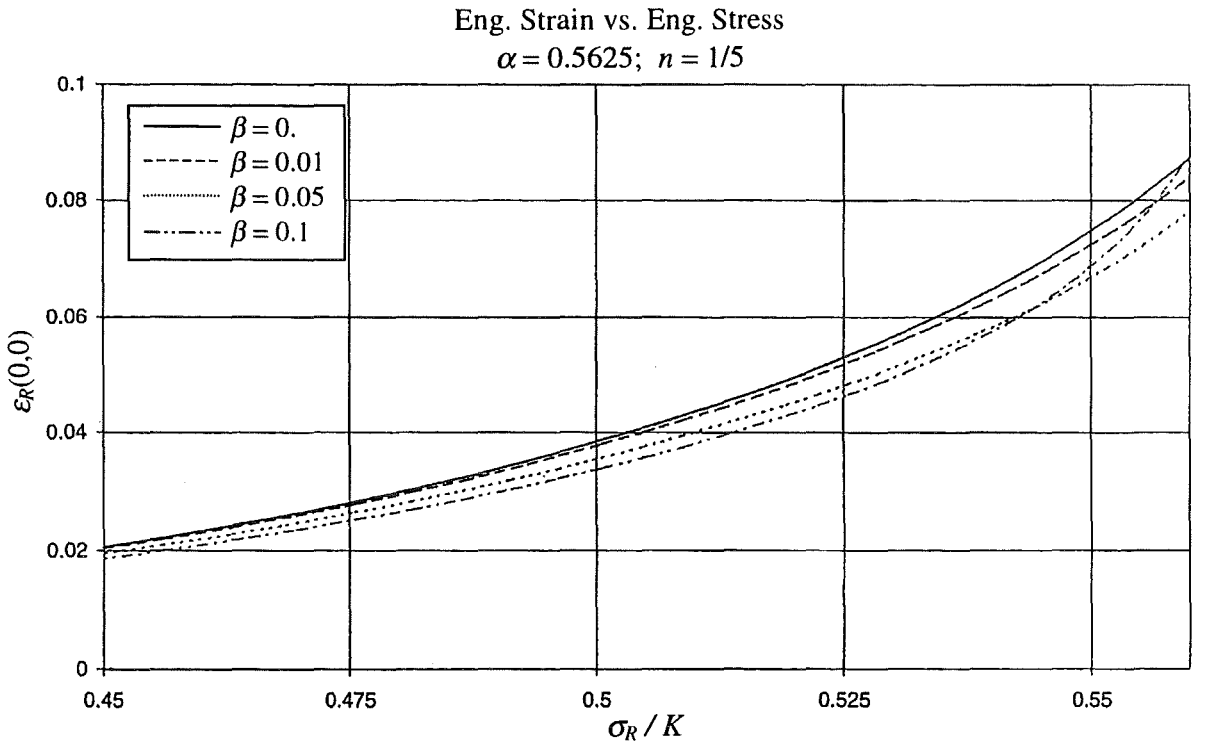

Fig. 4.9a Effect of specimen size on the local eng. strain-eng. stress diagram at the minimum cross-section; exponentially tapered tensile rod with power law strain hardening, gradient plasticity and cross-section reduction; 2nd order perturbation solution.

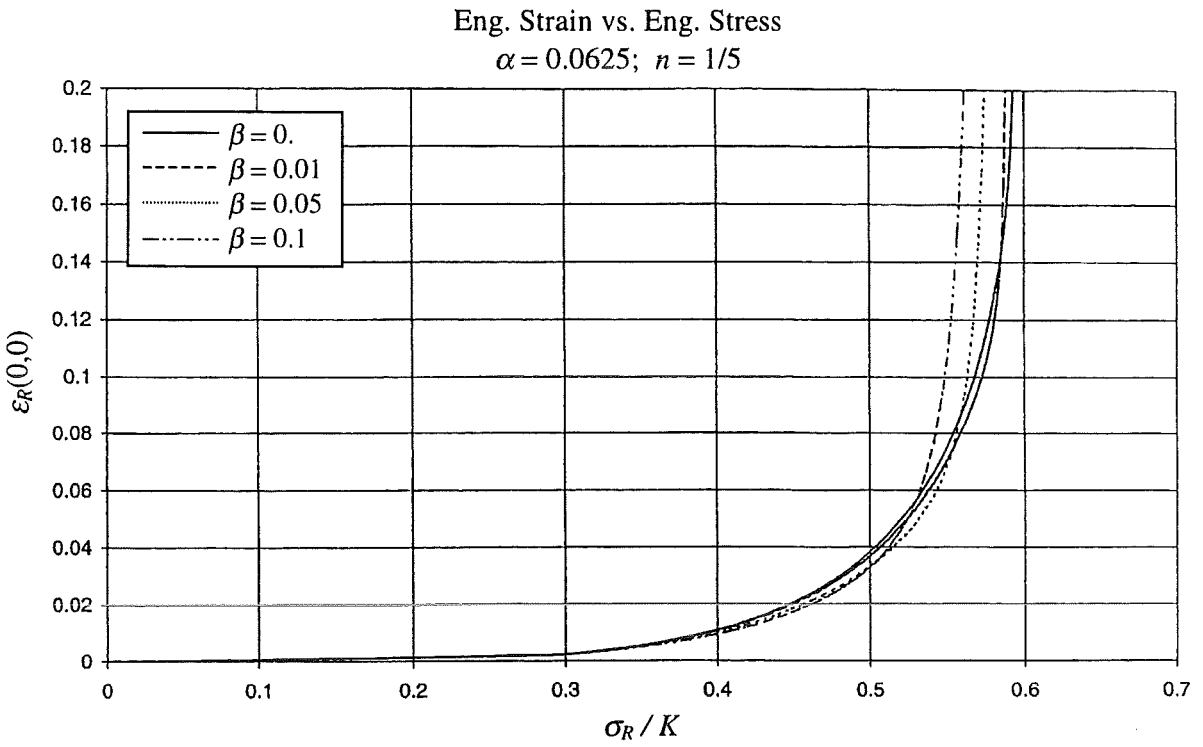

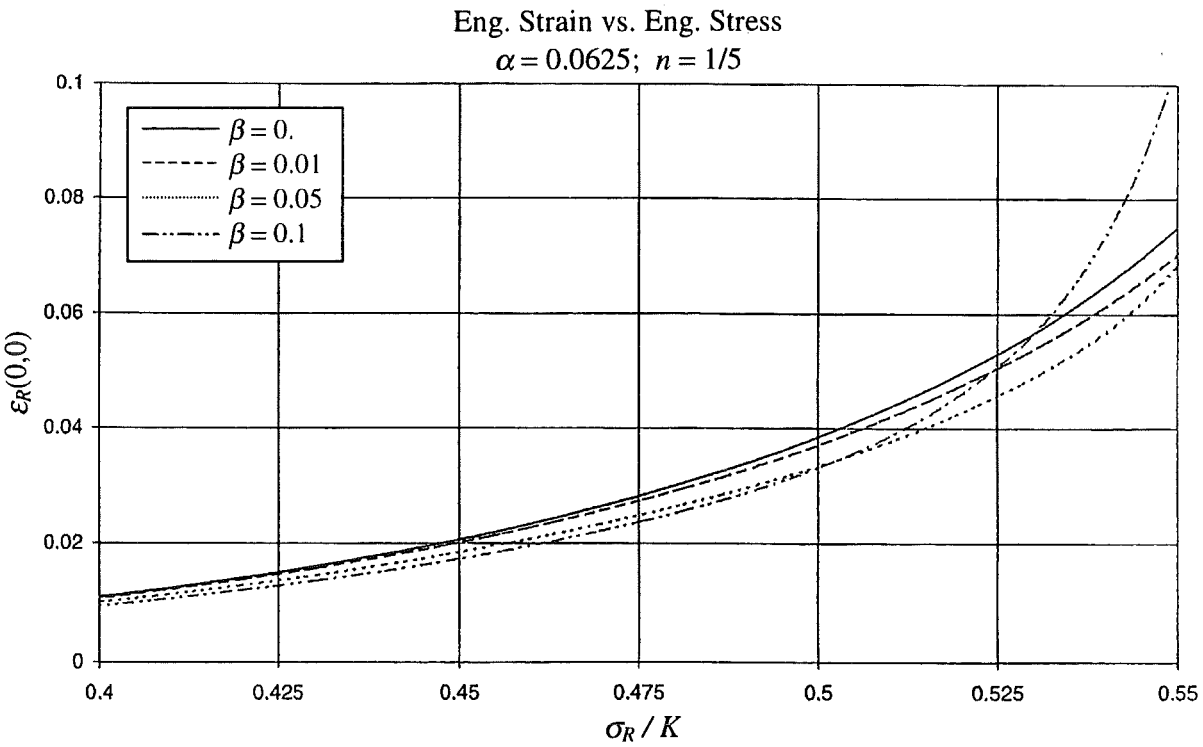

Fig. 4.9b Effect of specimen size on the local eng. strain-eng. stress diagram at the minimum cross-section; exponentially tapered tensile rod with power law strain hardening, gradient plasticity and cross-section reduction; 2nd order perturbation solution.

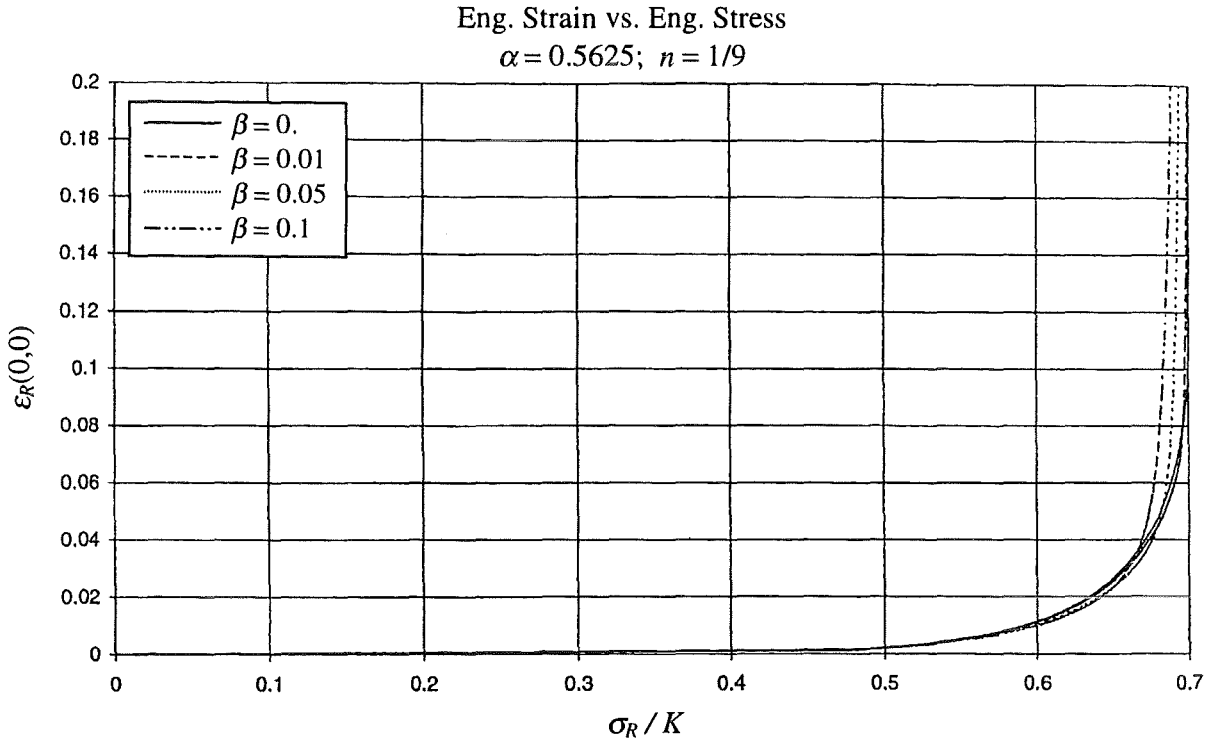

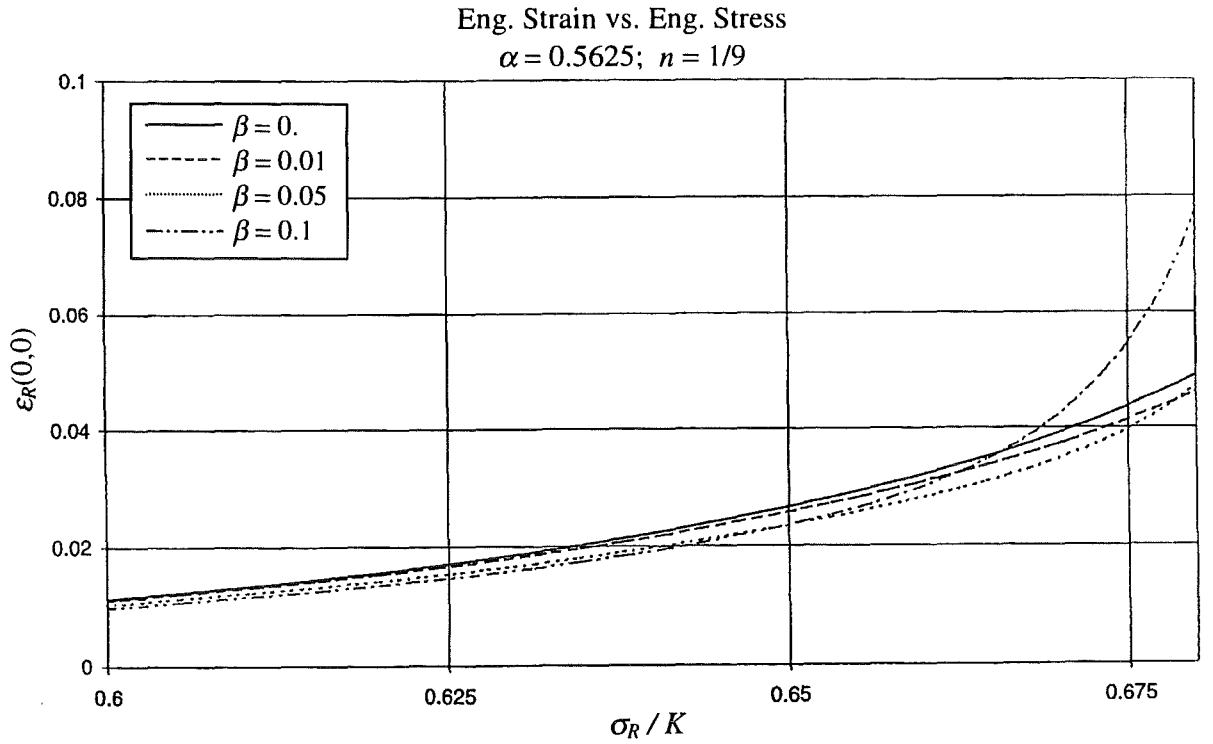

Fig. 4.9c Effect of specimen size on the local eng. strain-eng. stress diagram at the minimum cross-section; exponentially tapered tensile rod with power law strain hardening, gradient plasticity and cross-section reduction; 2nd order perturbation solution.

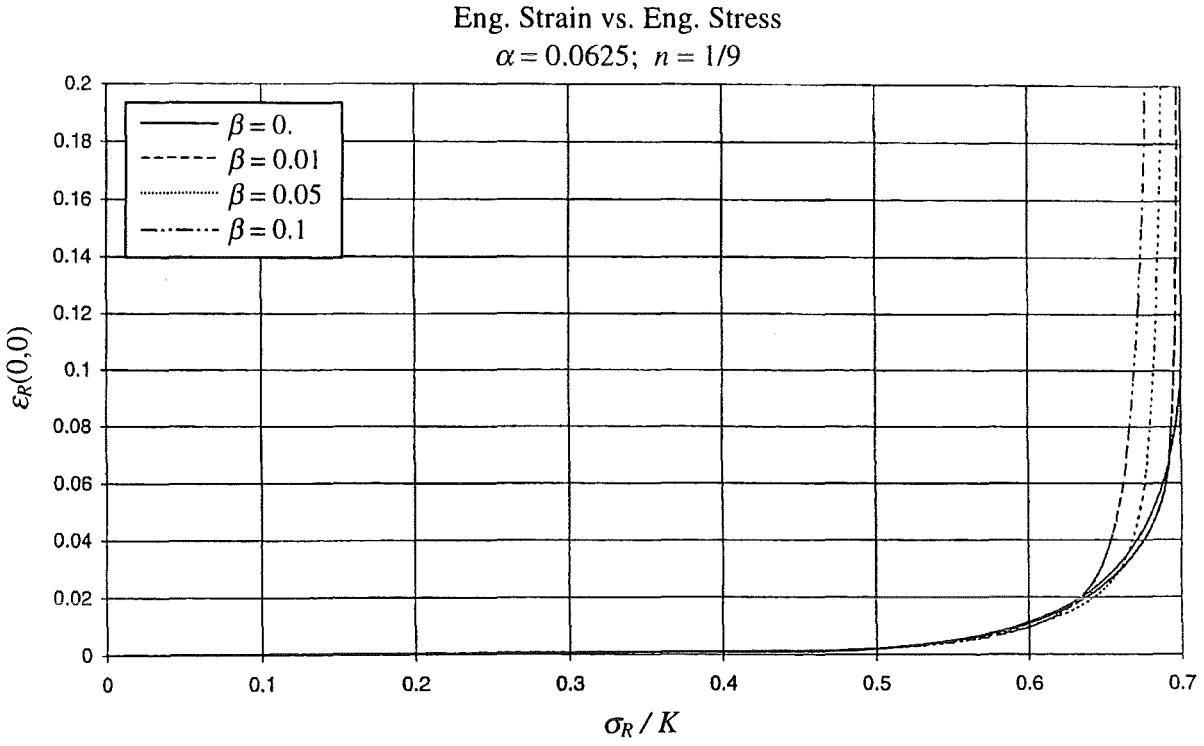

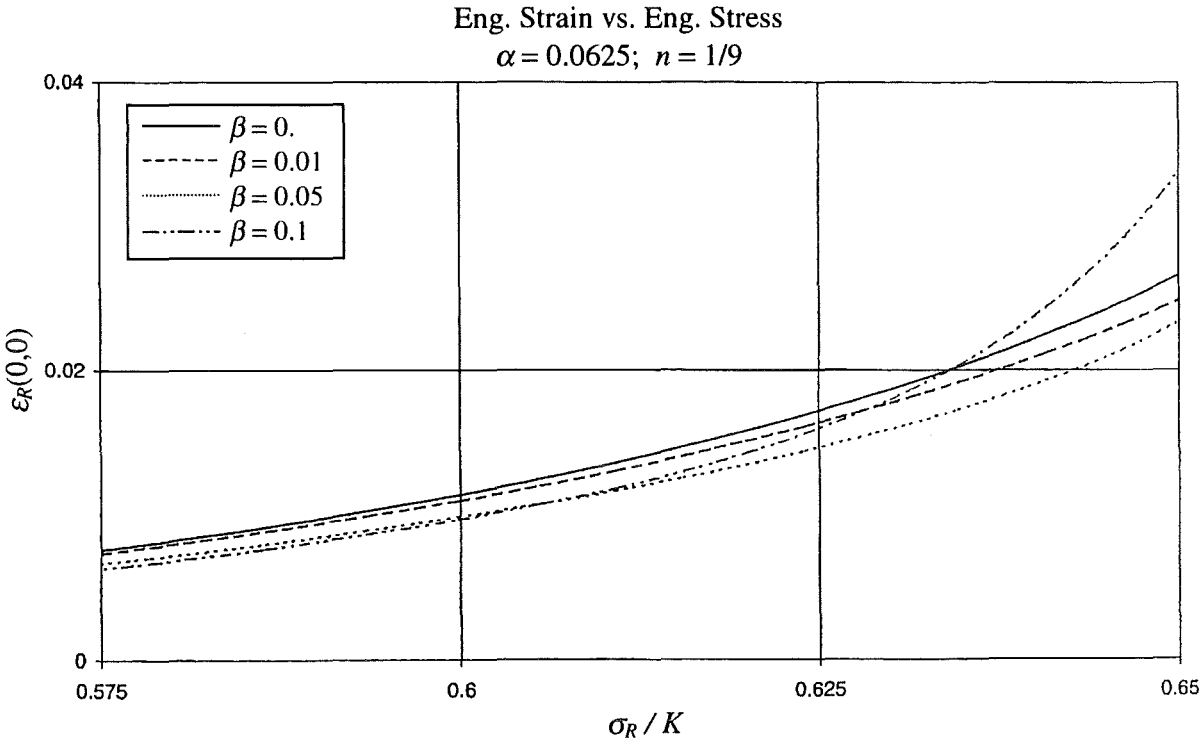

Fig. 4.9d Effect of specimen size on the local eng. strain-eng. stress diagram at the minimum cross-section; exponentially tapered tensile rod with power law strain hardening, gradient plasticity and cross-section reduction; 2nd order perturbation solution.

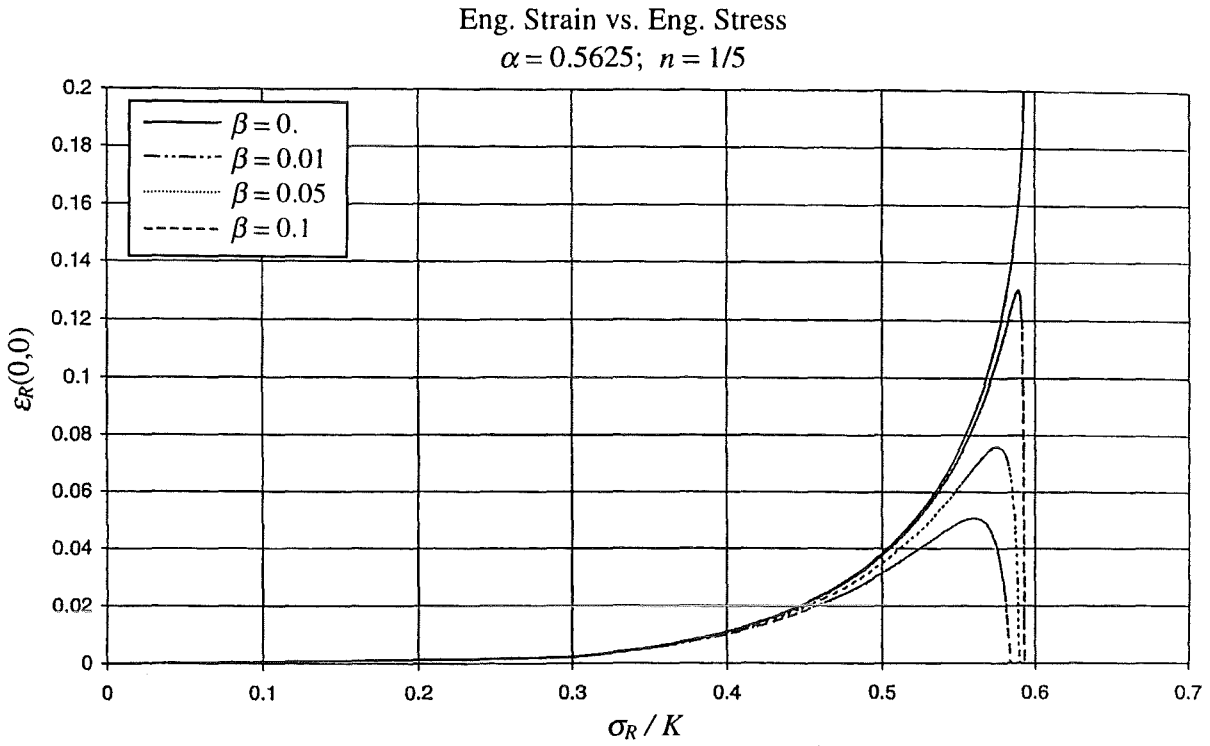

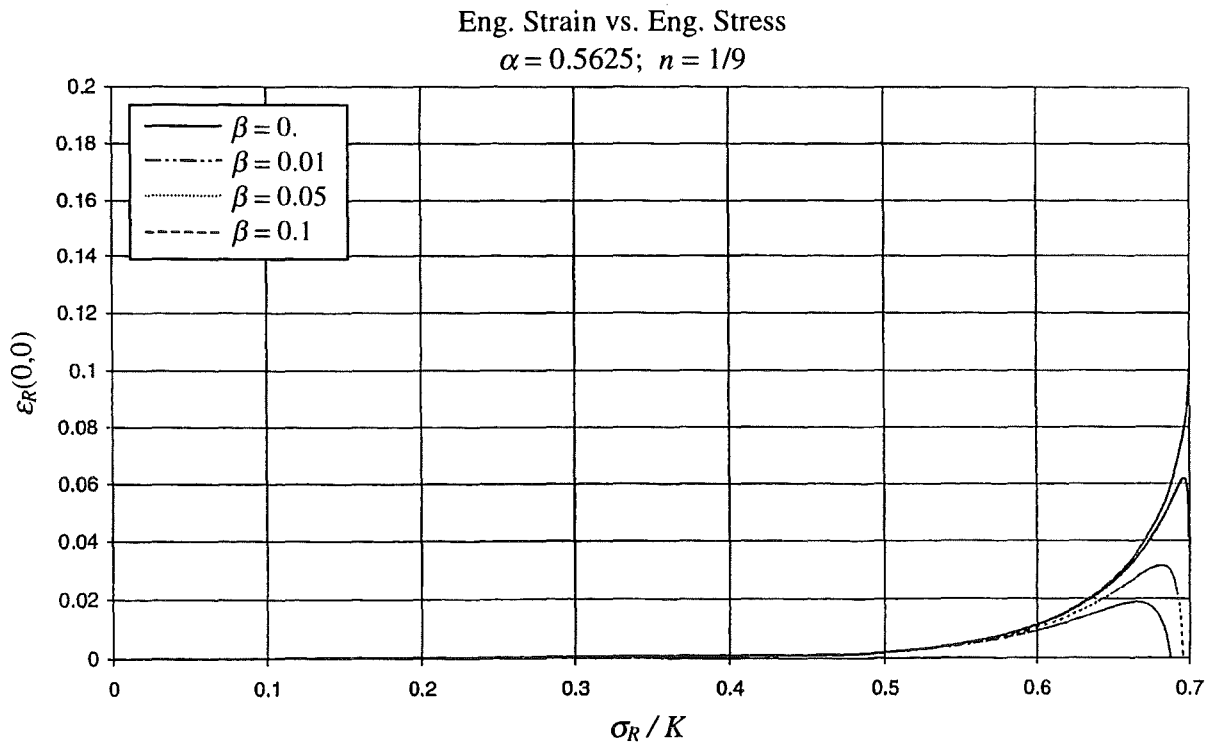

Fig. 4.10 Local eng. strain-eng. stress diagram at the minimum cross-section; 1st order perturbation solution for exponentially tapered tensile rod with power law strain hardening, gradient plasticity and cross-section reduction.

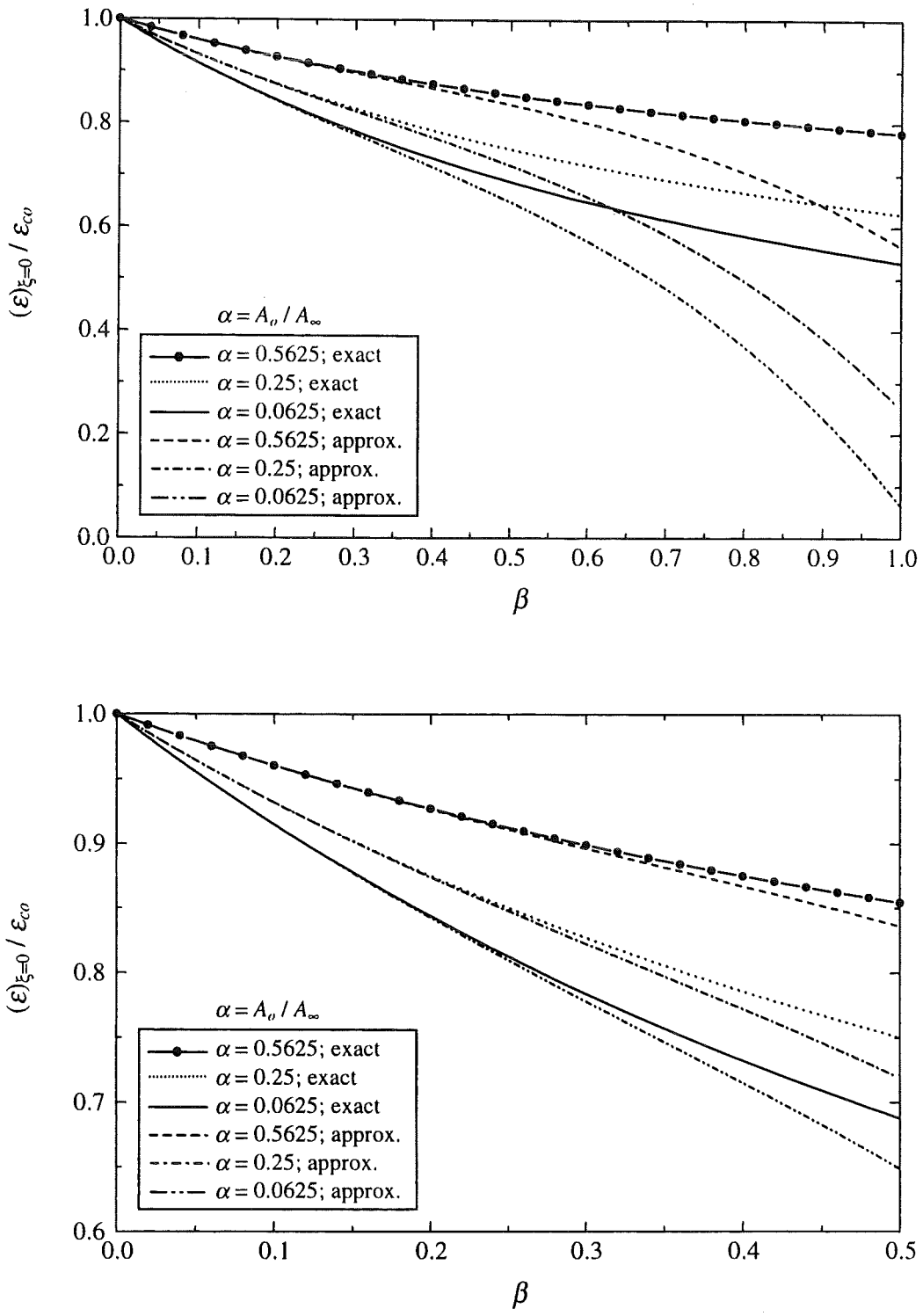

Fig. 4.11 Relative strain $\varepsilon(0,0)/\varepsilon_{co}$ versus normalized strain gradient coefficient β: reduction of the maximum strain gradient plasticity in the tapered rod problem; comparison of exact and 3rd order perturbation solution for linear hardening (n=1), without cross-section reduction.

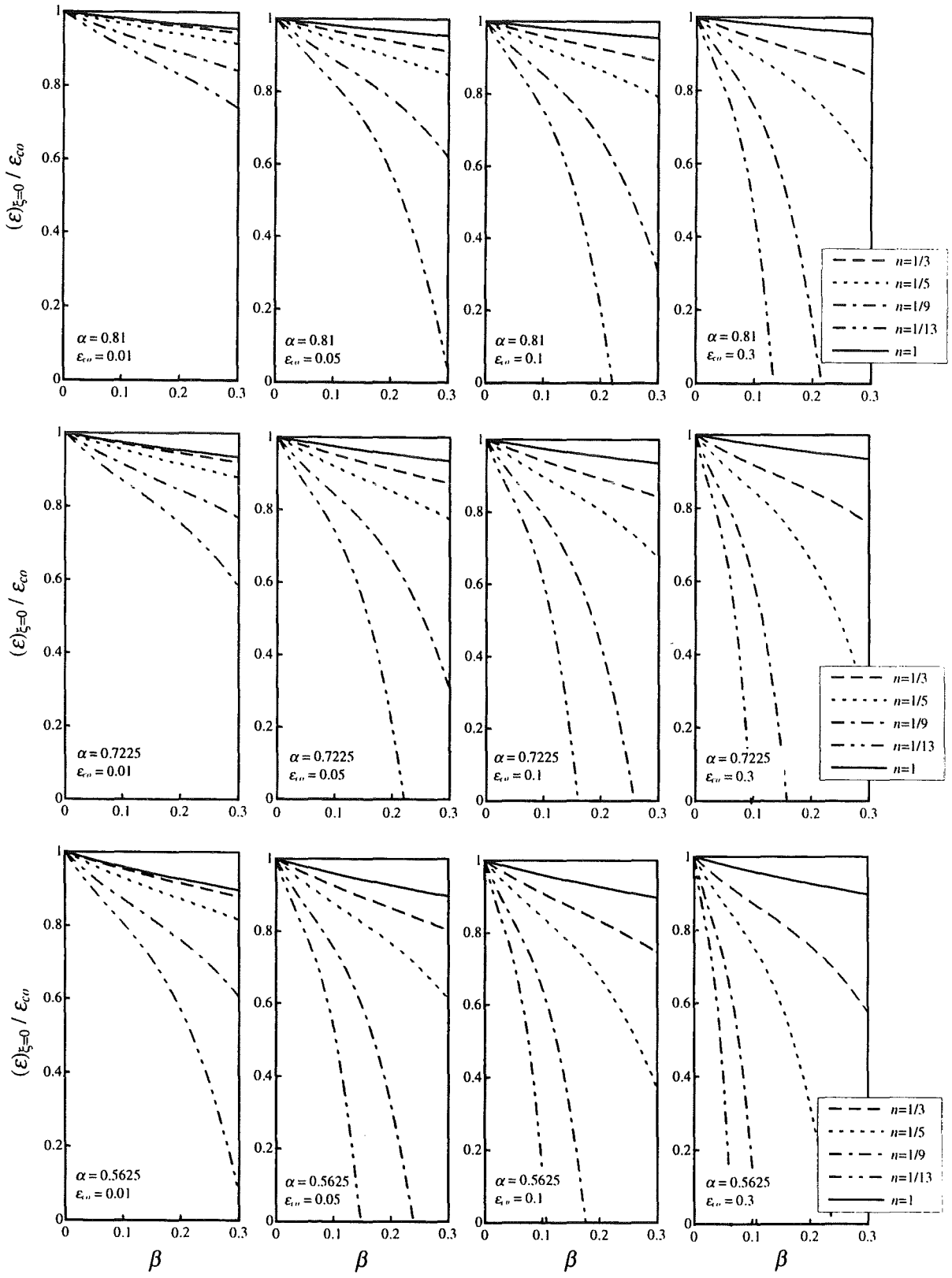

Fig. 4.12 Relative strain $\varepsilon(0,0)/\varepsilon_{co}$ versus normalized strain gradient coefficient β: reduction of the maximum strain gradient plasticity in the tapered rod problem; 3rd order perturbation solution for non-linear strain hardening ($n \leq 1$), without cross-section reduction.

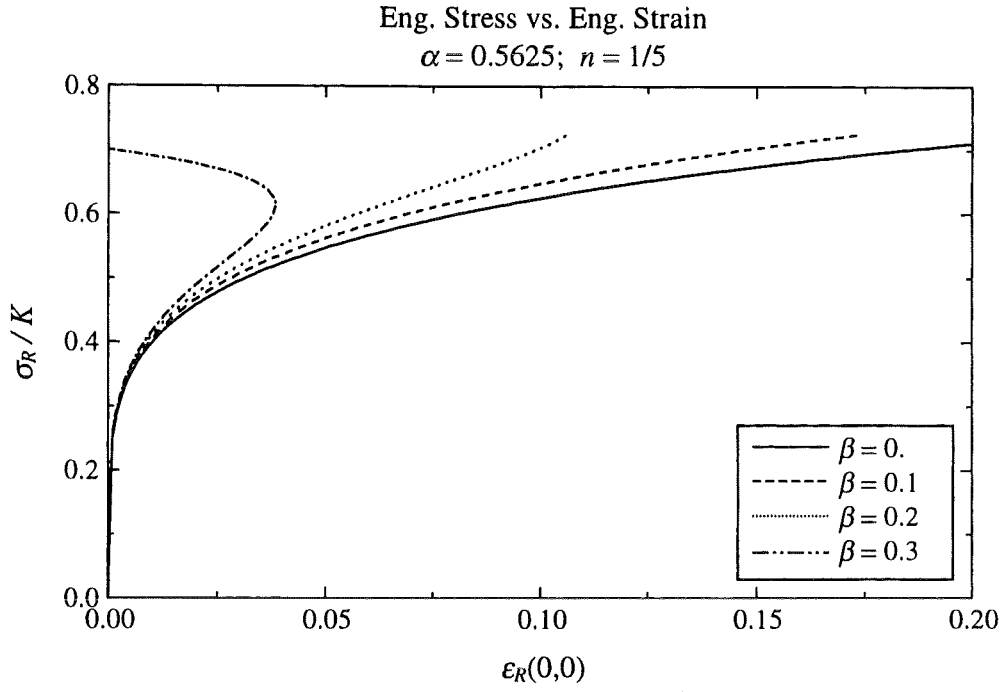

Fig. 4.13a Effect of specimen size on the local eng. stress-eng. strain diagram at the minimum cross-section; exponentially tapered tensile rod with power law strain hardening and gradient plasticity, without cross-section reduction; 3rd order perturbation solution.

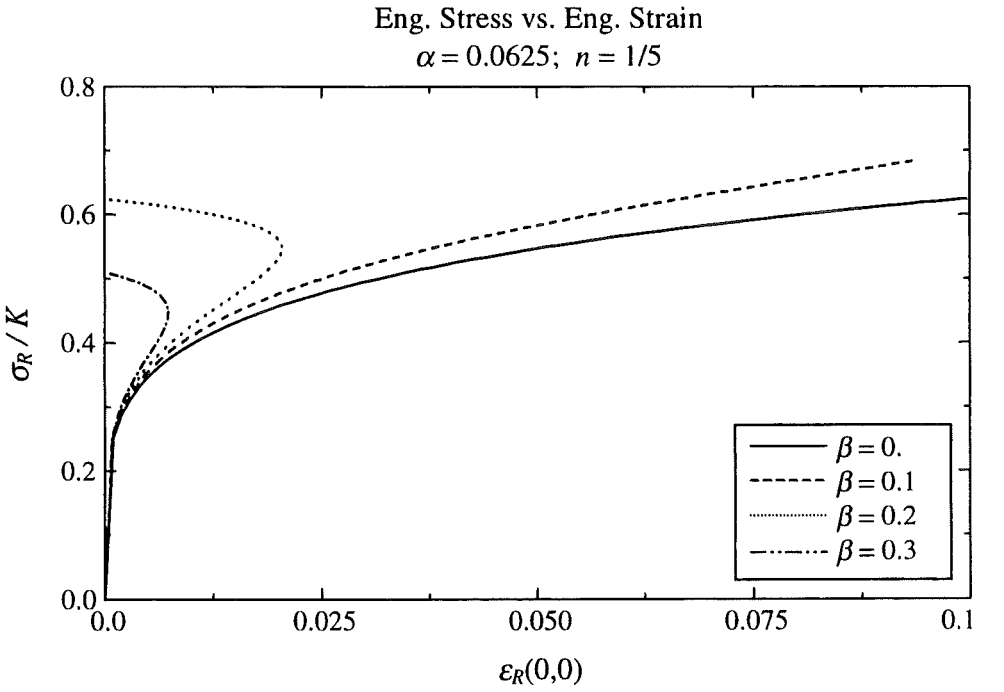

Fig. 4.13b Effect of specimen size on the local eng. stress-eng. strain diagram at the minimum cross-section; exponentially tapered tensile rod with power law strain hardening and gradient plasticity, without cross-section reduction; 3rd order perturbation solution.

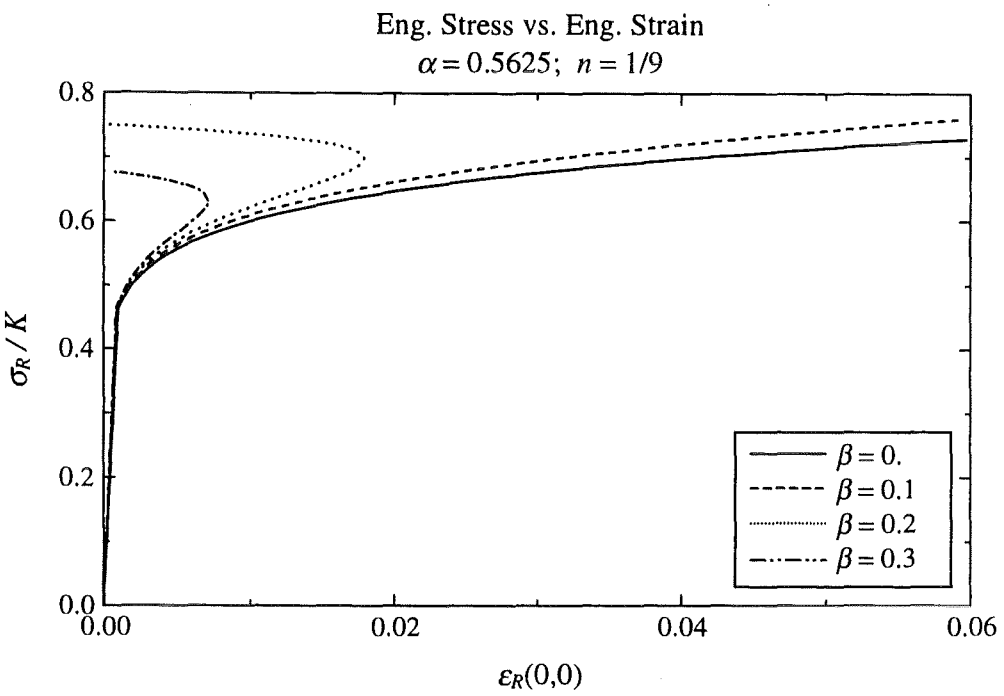

Fig. 4.14a Effect of specimen size on the local eng. stress-eng. strain diagram at the minimum cross-section; exponentially tapered tensile rod with power law strain hardening and gradient plasticity, without cross-section reduction; 3rd order perturbation solution.

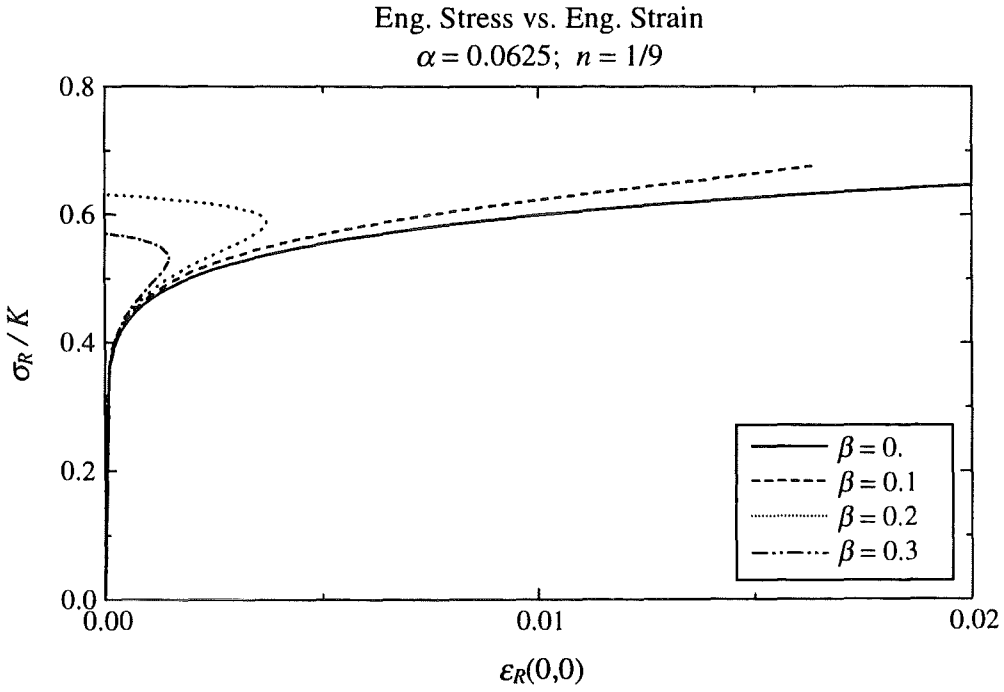

Fig. 4.14b Effect of specimen size on the local eng. stress-eng. strain diagram at the minimum cross-section; exponentially tapered tensile rod with power law strain hardening and gradient plasticity, without cross-section reduction; 3rd order perturbation solution.

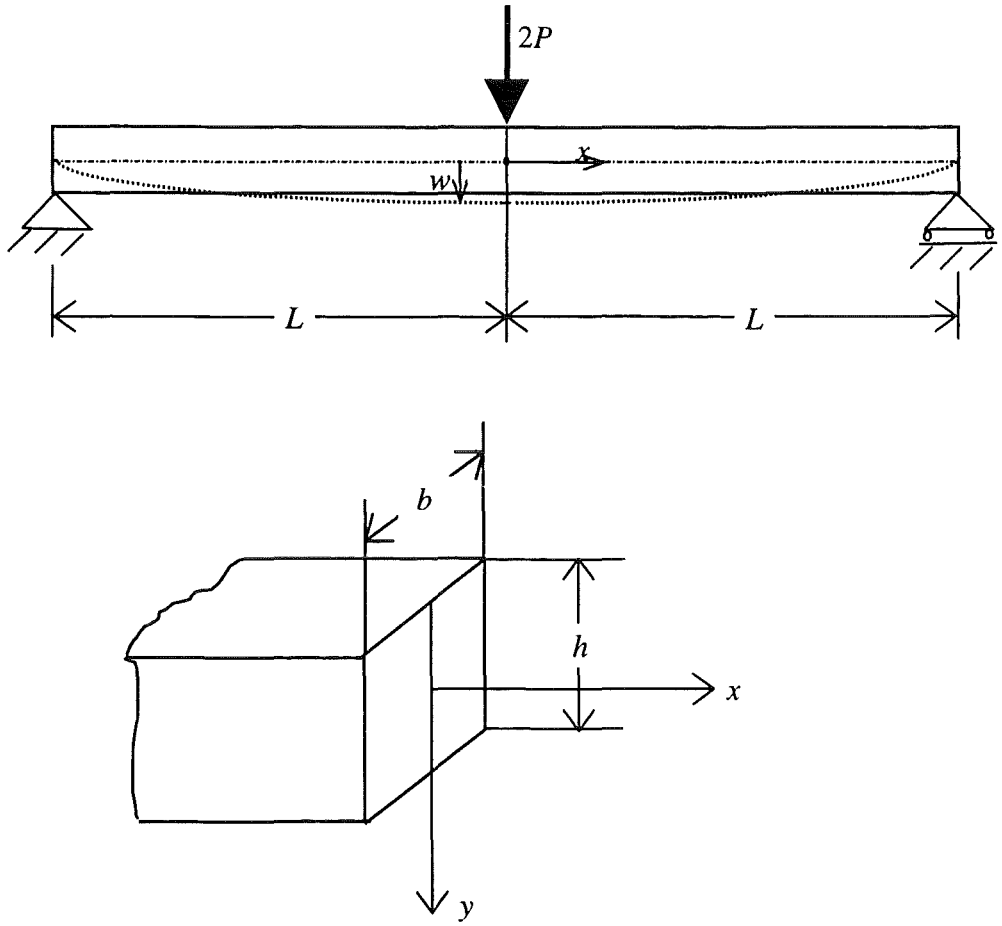

Fig. 5.1 Dimensions and coordinate system for the three-point bending of a rectangular beam.

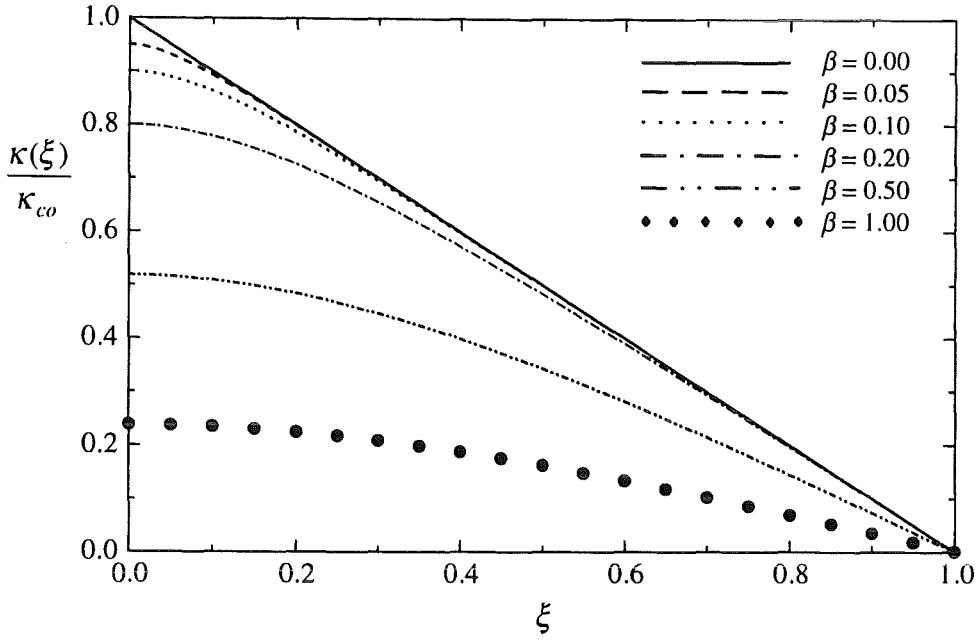

Fig. 5.2 Normalized curvature distribution along half-length of beam. Exact non-classical solution (linear case (n=1), β=l_i/L: 2nd order strain gradient parameter).

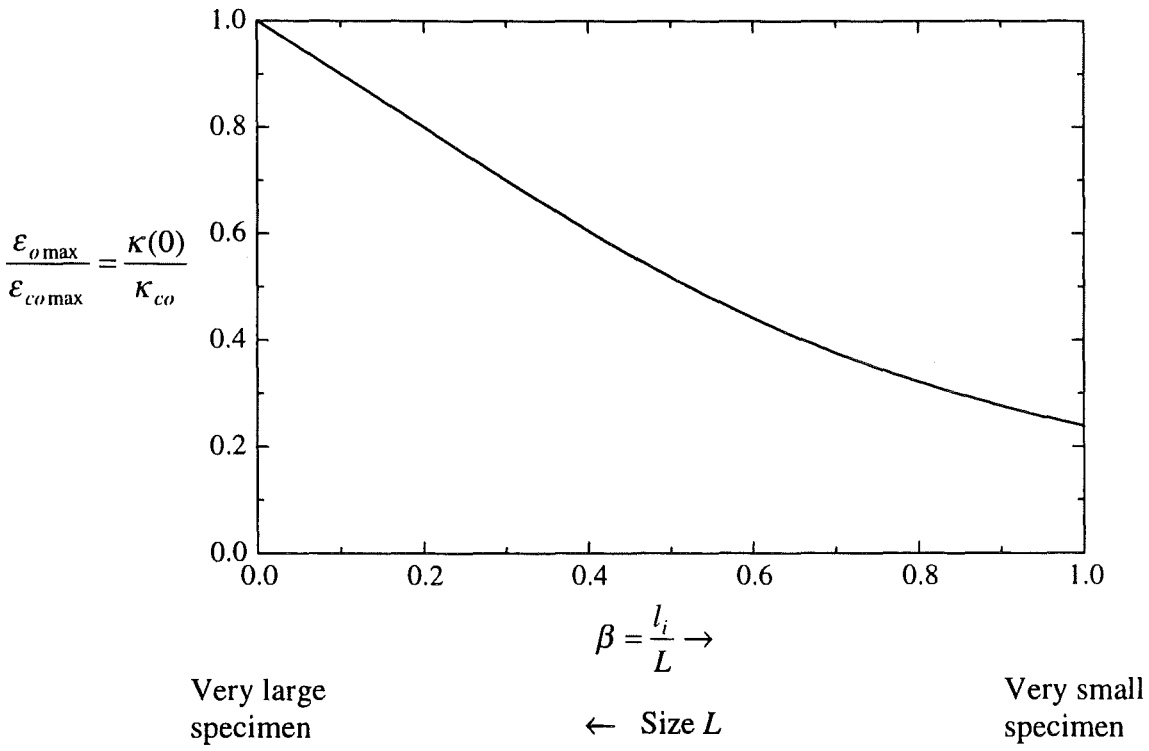

Fig. 5.3 Maximum relative bending strain (curvature) at beam center versus β (exact non-classical solution, linear case (n=1)).

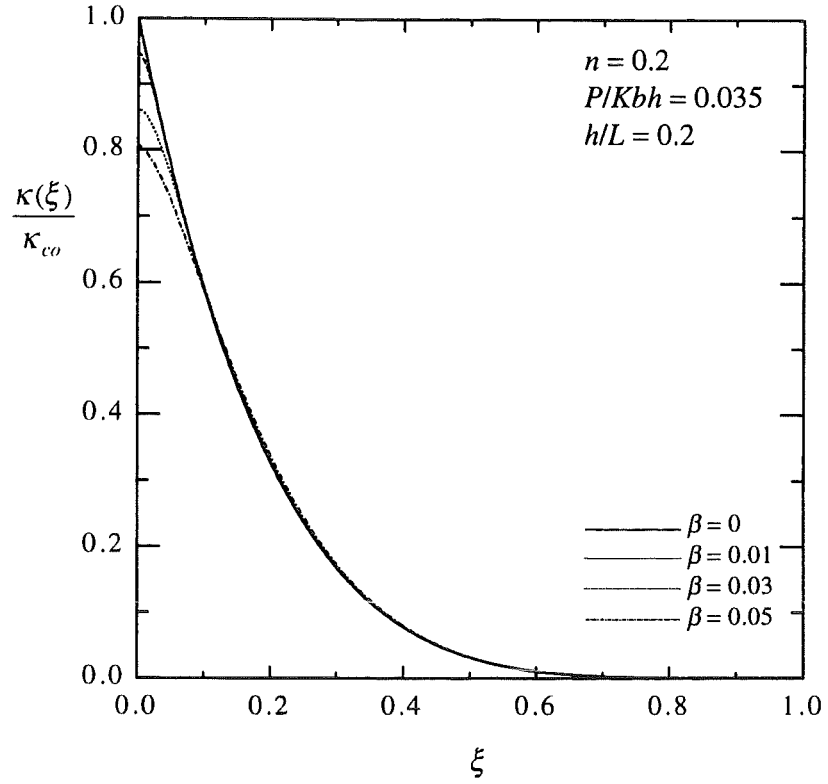

(a)

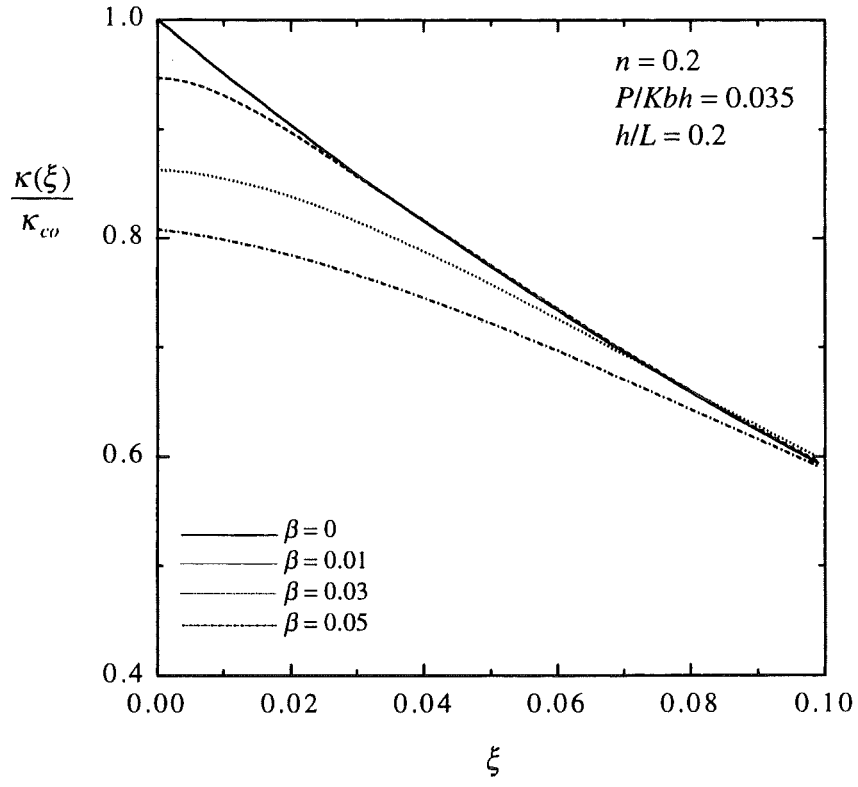

(b)

Fig. 5.4 Normalized curvature distribution along half length of beam; approximate perturbation solution (non-linear case (n=0.2), $\beta=l_i/L$: 2nd order strain gradient parameter).

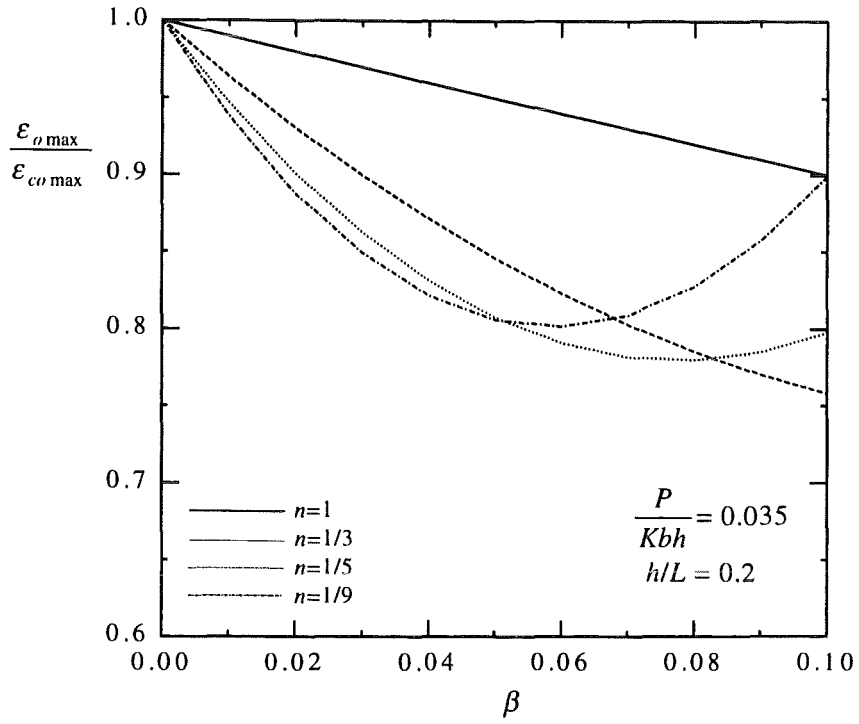

Fig. 5.5 Relative bending strain (curvature) at beam center versus $\beta=l_i/L$; second order approximate perturbation solution.

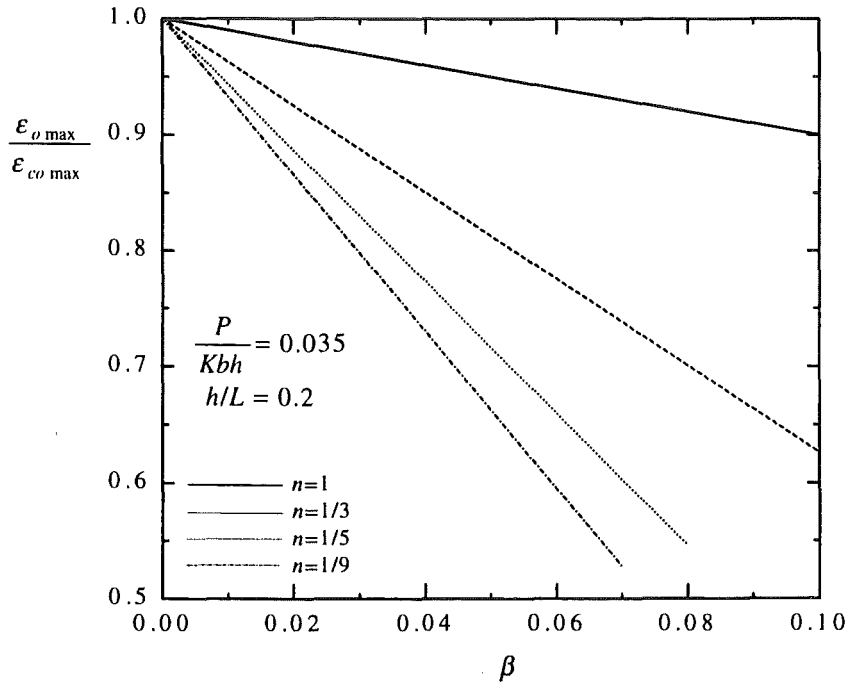

Fig. 5.6 Maximum relative bending strain at beam center versus $\beta=l_i/L$; first order approximate perturbation solution.

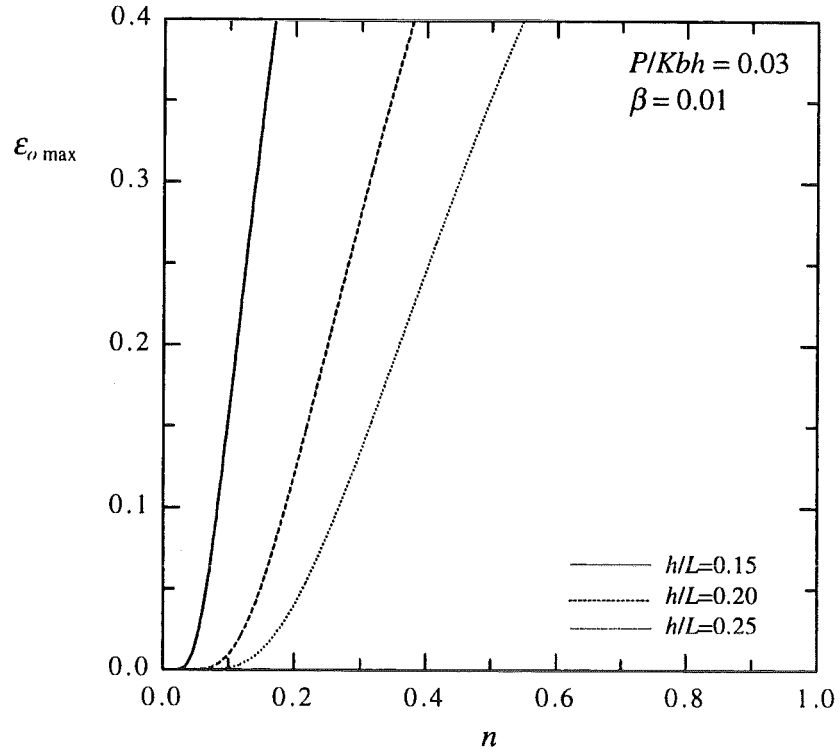

(a)

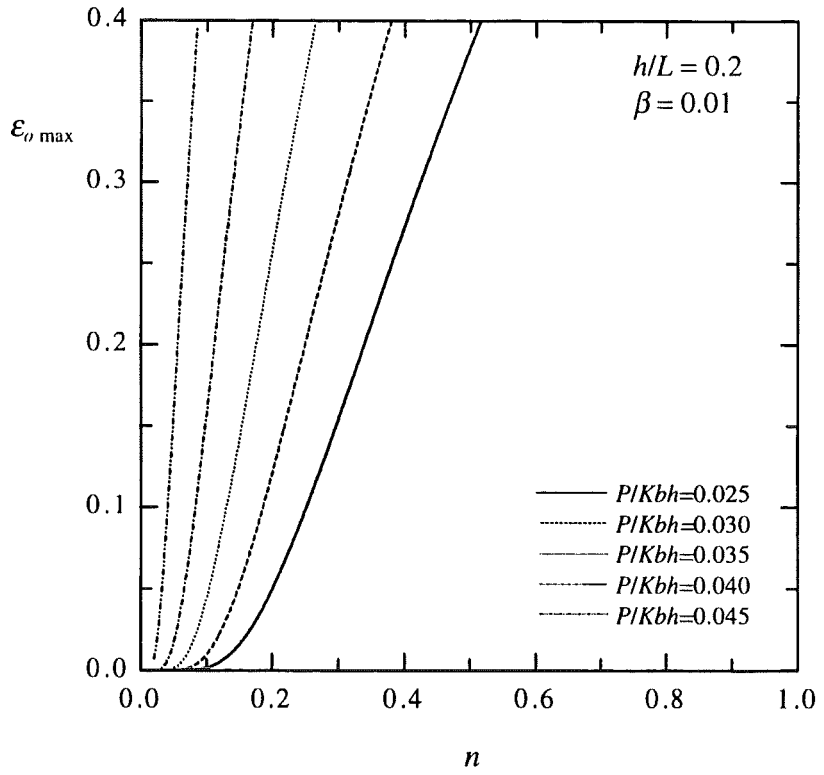

(b)

Fig. 5.7 Maximum non-classical bending strain at center of beam versus hardening exponent.

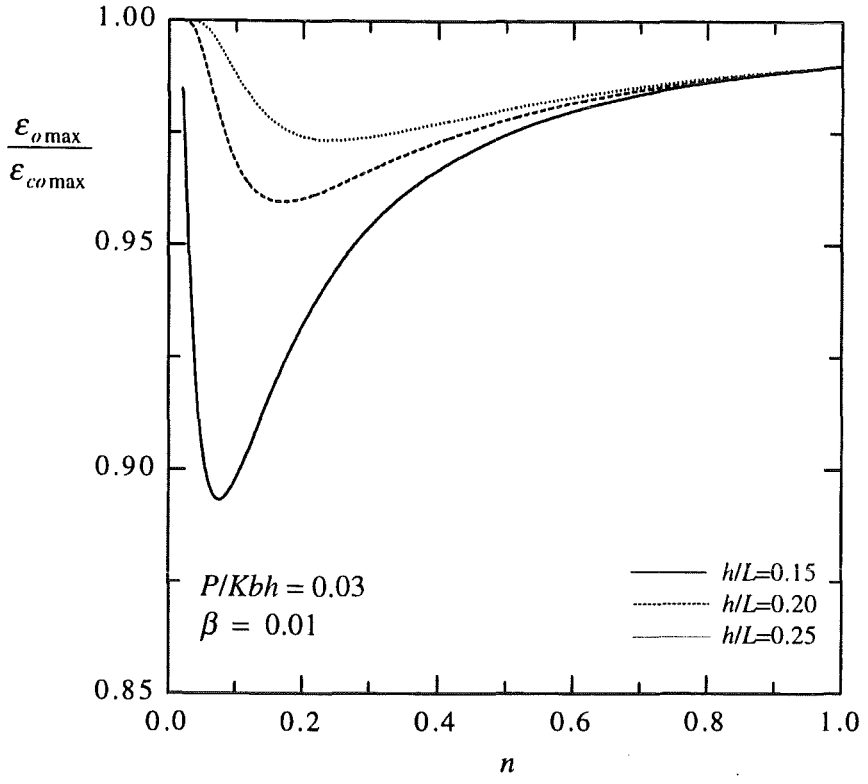

(a)

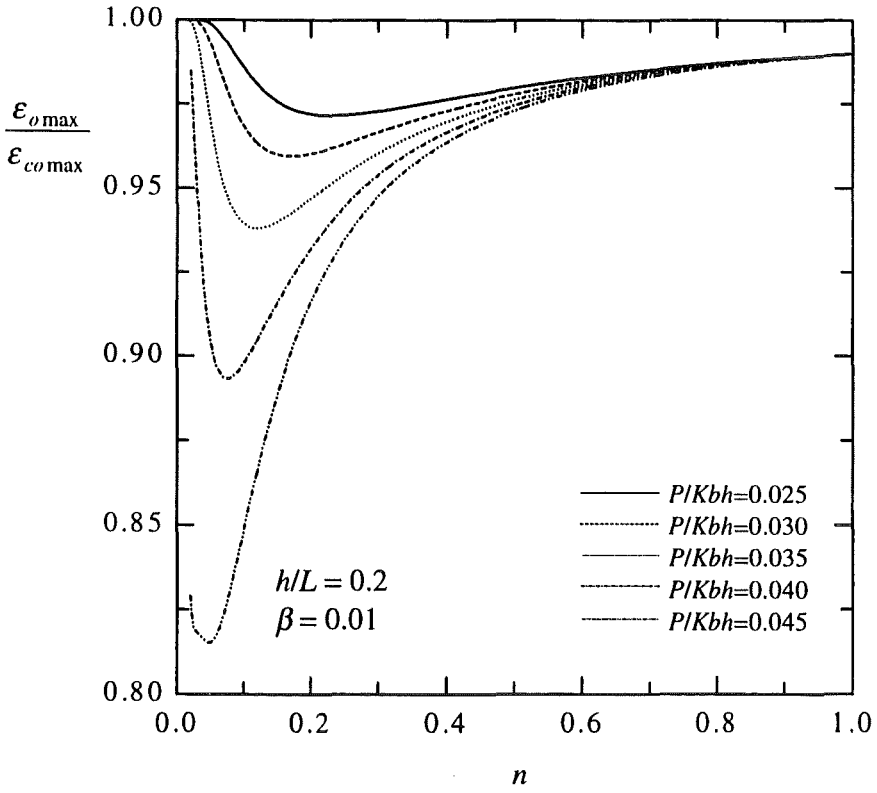

(b)

Fig. 5.8 Maximum relative bending strain (curvature) at beam center versus hardening exponent.

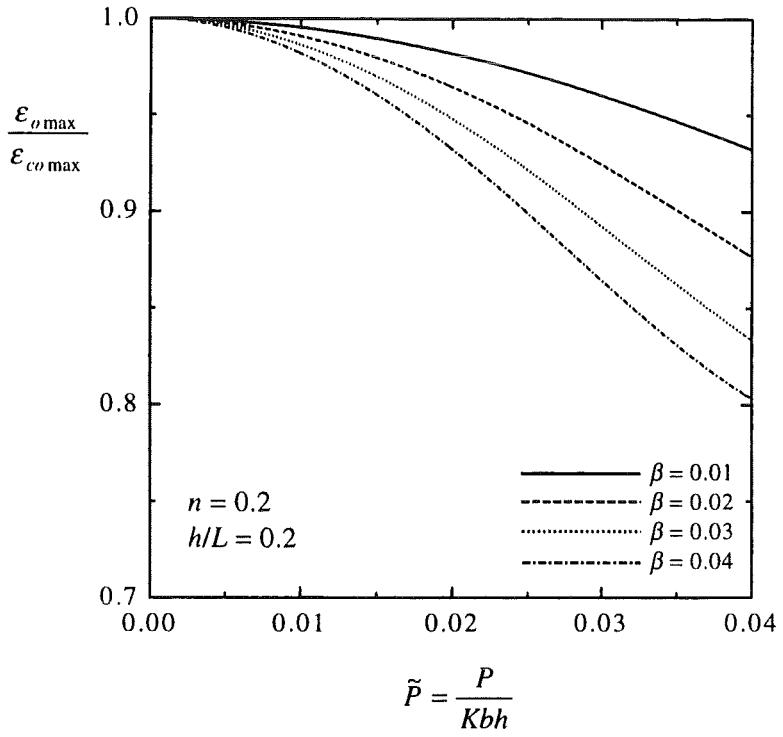

Fig. 5.9 Maximum relative bending strain (curvature) at center of beam versus load parameter $\tilde{P}$ (dimensionless shear force).

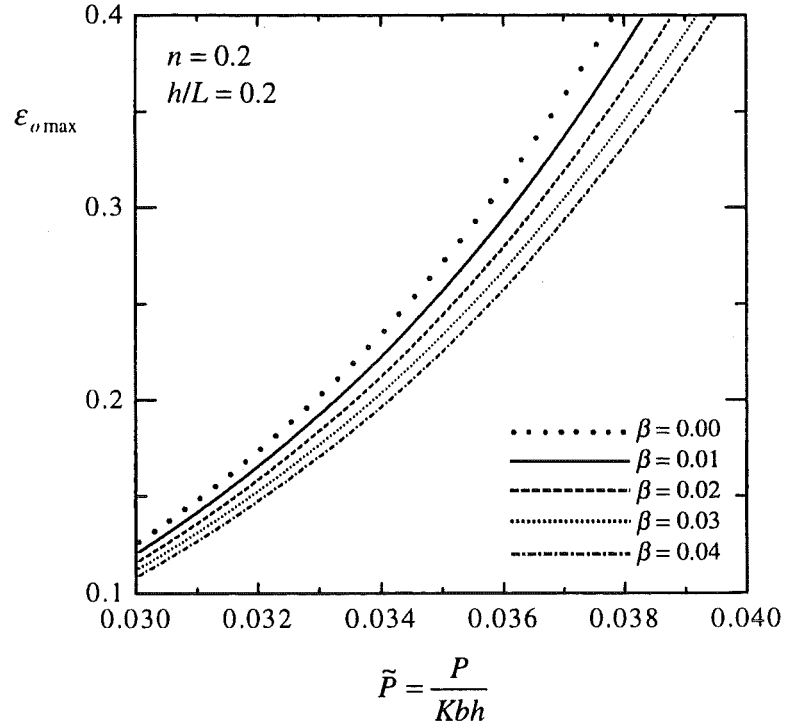

Fig. 5.10 Maximum bending strain at center of beam versus load parameter $\tilde{P}$ (dimensionless shear force).

Appendix (1): On the Non-Classical Boundary Condition B.C. II

In the following we compare the linear 2nd order gradient model (3.1) and its associated non-classical boundary condition (3.10) with a simple non-local (integral) model. To realize this comparison the non-local model is approximated by a differential constitutive equation and corresponding boundary conditions.

Several authors (e.g. Mühlhaus & Aifantis [A1.1], Zbib [A1.2], Peerlings et al. [A1.3]) have used non-local models of integral type, which involved an average strain or the average of an other variable (e.g. damage) in some neighborhood of the material point at x in the interior of the body, to motivate higher order gradients in the constitutive equations (see also Bazant & Chen [A1.4]). However, these considerations did not include points at or close to the boundaries or geometric discontinuities. This question will be discussed here to some extend within an one-dimensional setting.

The uniaxial non-local model is taken to be of the form

$$\sigma = \overset{v}{K}\varepsilon - \frac{C}{\mu^+ + \mu^-}\int_{-\mu^-}^{\mu^+} \varepsilon(x+y)dy\,, \tag{A1.1}$$

where $\overset{v}{K}$ and C are material constants and μ^+ and μ^- define the size on a small material neighborhood of the material point x.

If the strain distribution is uniform, then (A1.1) reduces to

$$\sigma = K\varepsilon\,,$$

where

$$K = \overset{v}{K} - C > 0 \tag{A1.2}$$

is required. Provided the material point is far from any boundary or discontinuity, then

$$\mu^+ = \mu^- = \mu\,, \tag{A1.3}$$

μ being a material constant with the dimension of a length and Eq.(A1.1) takes the following form

$$\sigma = \overset{v}{K}\varepsilon - \frac{C}{2\mu}\int_{-\mu}^{\mu} \varepsilon(x+y)dy\,; \tag{A1.4}$$

The second term is simply proportional to the average strain in a small one-dimensional "volume" of size 2μ.

The lower and upper integration limit μ^- and μ^+ need further definition close to and at the left boundary x=0. Since the constitutive equation is non-local, some decision about the influence of physical constitution beyond the boundary, i.e. in the interval $-\mu \le x<0$, on the behavior in the regime $0\le x$ has to be made.

We consider two simple cases treated consecutively

Case I: The exponentially tapered rod is attached to a rigid solid at x_L=0. Thus, there is no deformation in the regime x<0.

Case II: The tapered rod consists of two deformable parts of the same material symmetrically arranged. Thus, the strain field is perfectly symmetric with the center of symmetry at x=0.

Case I : Non-Symmetric Case

As long as the material point x is not too close to the boundary, the form of the Eq.(A1.4) does not change. If the averaging integral in (A1.4) encloses the boundary at x=0 such that the center (x) of the integration regime in (A1.4) has a distance from the boundary less than μ, then the relation (A1.1) applies instead of (A1.4) with

$$\left.\begin{aligned} \mu^+ &= \mu, \\ \mu^- &= x \le \mu, \quad x \ge 0 \end{aligned}\right\} \qquad \text{(A1.5)}$$

and

$$\mu^+ + \mu^- = \mu + x\,; \qquad \text{(A1.6)}$$

thus the lower integration limit is at the boundary.

As previously, we assume that for very large values x the strain distribution approaches the uniform distribution of a rod with constant cross-section. These conditions completely describe the problem if the stress distribution is given by prescribing the longitudinal force and the variation of the cross-section. No other conditions, especially at the boundaries, are necessary. In fact the problem is to solve a very special kind of one-dimensional integral equation.

Aside from the integral formulation there is a major difference to the gradient model of section (3.1.1): The non-local model involves the three distinct material parameters $\overset{\nu}{K}$ or K, C and μ instead of the two parameters K and l_i.

A numerical solution could be obtained by discretizing the range between the boundaries[1] such that the discrete values of the strains ε_i (i=1,2,...n) are the unknowns and the integral is evaluated numerically. This discretized form of (A1.1) is then to be satisfied at all nodal points which finally yields a system of linear equations for the discrete ε_i.

It is generally known that some types of one-dimensional integral equations can be transformed exactly into equivalent ordinary differential equations with associated boundary conditions. It is conjectured that this is not possible (or not easily possible) for the present case. However, the approximate reduction of the non-local problem to the solution of differential equations with associated boundary conditions is feasible and will be derived in the following. This approximate formulation is then compared with the gradient model of section (3.1.1).

[1] The right boundary has to be set at some fixed large value x=x_R.

Using the Taylor series approximation of the strain distribution[2] around x up to quadratic terms

$$\varepsilon(x+y) = \varepsilon(x) + \frac{1}{1!}\varepsilon'(x)\,y + \frac{1}{2!}\,\varepsilon''(x)\,y^2 + \ldots\,, \tag{A1.7}$$

the integral in (A1.1) is approximated by

$$\frac{C}{\mu^+ + \mu^-}\int_{-\mu^-}^{\mu^+} \varepsilon(x+y)dy =$$

$$= \frac{C}{\mu^+ + \mu^-}\left\{\varepsilon(x)\,(\mu^+ + \mu^-) + \varepsilon'(x)\frac{1}{2}[(\mu^+)^2 - (\mu^-)^2] + \varepsilon''(x)\frac{1}{6}[(\mu^+)^3 + (\mu^-)^3]\right\}$$

$$= C\varepsilon(x) + C\left\{\varepsilon'(x)\frac{1}{2}(\mu^+ - \mu^-) + \varepsilon''(x)\frac{1}{6}[(\mu^+)^2 - \mu^+\mu^- + (\mu^-)^2]\right\}. \tag{A1.8}$$

Thus (A1.1) takes the form

$$\sigma(x) = K\varepsilon(x) - C\,\frac{1}{2}(\mu^+ - \mu^-)\,\varepsilon'(x) - C\,\frac{1}{6}[(\mu^+)^2 - \mu^+\mu^- + (\mu^-)^2]\,\varepsilon''(x). \tag{A1.9}$$

If the material point x and the dragged along averaging integral are far from the boundary $x=x_L=0$, then (A1.3) applies and (A1.8) simplifies to

$$\sigma(x) = K\varepsilon(x) - \frac{1}{6}C\mu^2\varepsilon''(x). \tag{A1.10}$$

We note that the inclusion of a 3rd order term in the Taylor series (A1.7) would have dropped out in (A1.10). This relation corresponds fully to the higher order gradient model (3.1) if instead of the length scale μ the length scale l_i is introduced.

$$l_i = \sqrt{\frac{1}{6}\frac{C}{K}}\,\mu < \mu. \tag{A1.11}$$

Close to the boundary $x=x_L=0$ limits of integration are given by (A1.5). Consequently (A1.9) takes the following form

$$\sigma(x) = K\varepsilon(x) - C_I(x)\,\varepsilon'(x) - C_{II}(x)\varepsilon''(x)\,, \tag{A1.12}$$

where

[2] Continuity and sufficient differentiability of $\varepsilon(x)$ is presumed.

$$C_I(x) = C\frac{1}{2}(\mu - (x - x_L))$$

$$C_{II}(x) = C\frac{1}{6}(\mu^2 - \mu(x - x_L) + (x - x_L)^2). \qquad \text{(A1.13)}$$

We note here explicitly that 3rd order derivatives, if they were included in the Taylor expansion (A1.7), would not drop out in (A1.12).

$C_I(x)$ is a linear function in the interval $x_L \leq x \leq x_L + \mu$. At $x = x_L + \mu = \mu$ it vanishes and thus agrees with the derived fact that 1st order gradients of the strain are not effective in the interior. Its largest value is at the boundary $x = x_L = 0$,

$$(C_I)_{\max} = C_I(x_L) = \frac{1}{2}C\mu, \qquad \text{(A1.14)}$$

which shows that the 1st order gradient term in (A1.12) is given the largest importance at the boundary.

The function $C_{II}(x)$ is a parabola in the interval $x_L \leq x \leq x_L + \mu$. At the boundary $x = x_L = 0$ and at $x = x_L + \mu = \mu$ it takes the same value as the constant coefficient of the 2nd order gradient term in the interior of the body:

$$C_{II}(x = x_L) = C_{II}(x = x_L + \mu) = \frac{1}{6}C\mu^2. \qquad \text{(A1.15)}$$

Its minimum is

$$(C_{II})_{\min} = \frac{3}{4}\frac{1}{6}C\mu^2, \qquad \text{(A1.16)}$$

which is located at the center of the interval. The average value of $C_{II}(x)$ in the boundary interval is

$$(C_{II})_{\text{average}} = \frac{5}{6}\frac{1}{6}C\mu^2. \qquad \text{(A1.17)}$$

Thus, except for a small dip close to the boundary the coefficient of the 2nd order strain gradient is constant everywhere and equal to $\frac{1}{6}C\mu^2$.

In the interior of the body and close to the boundary $x = x_L = 0$ the integral model has been approximated by the two different differential equations of 2nd order, (A1.10) and (A1.12), which differ mainly in the presence of the 1st order-strain derivative in the equation close to the boundary. A solution of these DEQ's require a boundary condition at $x = x_L = 0$. From the theory of ordinary DEQ's this can involve the strain and/or its 1st derivative but no higher order derivatives. This condition is found as follows.

At the boundary $x = x_L = 0$ the differential equation (A1.12) yields the relation

$$\sigma(x_L) = K\varepsilon(x_L) - \frac{1}{2} C\mu\varepsilon'(x_L) - \frac{1}{6} C\mu^2\varepsilon''(x_L)\,, \tag{A1.18}$$

which still involves the 2nd order derivative. The general integral of (A1.1) may be written in the form

$$\sigma = \overset{v}{K}\varepsilon(x) - \frac{C}{\mu^+ + \mu^-} \int_{-\mu^-}^{\mu^+} \varepsilon(x+y)dy = \overset{v}{K}\varepsilon(x) - \frac{C}{\mu^+ + \mu^-} \int_{x-\mu^-}^{x+\mu^+} \varepsilon(z)dz =$$

$$= \overset{v}{K}\varepsilon(x) - \frac{C}{\mu^+ + \mu^-} [F(x+\mu^+) - F(x-\mu^-)]\,, \tag{A1.19}$$

where $F(z)$ is the integral of $\varepsilon(z)$. The derivative of (A1.19) is

$$\sigma'(x) = \overset{v}{K}\varepsilon'(x) - \frac{C}{\mu^+ + \mu^-} [\varepsilon(x+\mu^+) - \varepsilon(x-\mu^-)] +$$

$$+ \frac{(\mu^+ + \mu^-)'}{(\mu^+ + \mu^-)^2} C[F(x+\mu^+) - F(x-\mu^-)]\,. \tag{A1.20}$$

The integral function F may be eliminated from (A1.20) by using (A1.19) which yields the exact relation

$$\sigma'(x) = \overset{v}{K}\varepsilon'(x) - \frac{C}{\mu^+ + \mu^-} [\varepsilon(x+\mu^+) - \varepsilon(x-\mu^-)]$$

$$+ \frac{(\mu^+ + \mu^-)'}{\mu^+ + \mu^-} [\overset{v}{K}\varepsilon(x) - \sigma(x)]\,. \tag{A1.21}$$

Close to the boundary $x=x_L=0$ we have

$$\mu^+ + \mu^- = \mu + x, \qquad (\mu^+ + \mu^-)' = 1.$$

Using the Taylor series approximation (A1.7), we get

$$\varepsilon(x+\mu^+) - \varepsilon(x-\mu^-) = \varepsilon'(x)\,(\mu^+ + \mu^-) + \frac{1}{2!}\varepsilon''(x)\,[(\mu^+)^2 - (\mu^-)^2]. \tag{A1.22}$$

If x approaches the boundary $x_L=0$, then (A1.21) takes the form

$$\sigma'(x_L) = K\varepsilon'(x_L) - \frac{1}{2} C\mu\varepsilon''(x_L) + \frac{1}{\mu} [\overset{v}{K}\varepsilon(x_L) - \sigma(x_L)]\,. \tag{A1.23}$$

Combining (A1.18) and (A1.23) allows to eliminate the 2nd order derivative:

$$\sigma'(x_L) = K\varepsilon'(x_L) - \frac{1}{2}[\frac{6K}{\mu}\varepsilon(x_L) - 3C\varepsilon'(x_L) - \frac{6}{\mu}\sigma(x_L)] + \frac{1}{\mu}[\overset{\nu}{K}\varepsilon(x_L) - \sigma(x_L)],$$

or more compact

$$\sigma' - \frac{2}{\mu}\sigma = (K + \frac{3}{2}C)\varepsilon' - \frac{1}{\mu}(2K - C)\varepsilon, \qquad x = x_L = 0. \tag{A1.24}$$

This is the required boundary condition at $x_L=0$ where the left side is a prescribed quantity. The r.h.s. contains the strain ε as well as its 1st gradient ε' and all three material parameters of the non-local model are involved. Ignoring the non-local effect, i.e.

$$C \to 0, \quad \mu \to 0,$$

(A1.24) simply reduces to the trivial classical result

$$\sigma = \overset{\nu}{K}\varepsilon \text{ at } x = x_L = 0.$$

From (A1.24) an important conclusion can be drawn for the case that the cross-section $A(x)$ of the rod has a relative minimum at $x = x_L = 0$. Then

$$A'(x) = 0 \text{ at } x = x_L = 0$$

and thus

$$\sigma' = 0 \text{ at } x = x_L = 0.$$

For the classical case without non-locality the strain gradient at the boundary is then

$$\varepsilon_c' = 0 \text{ at } x = x_L = 0.$$

However, accounting for non-locality we obtain from (A1.24)

$$\frac{2}{\mu}\sigma = \frac{1}{\mu}(2K - C)\varepsilon - (K + \frac{3}{2}C)\varepsilon',$$

which is still a complex boundary condition including both the strain and its gradient.

Summarizing, the non-local model is approximated by the following DEQ's and boundary conditions:

DEQ's:

$$\left.\begin{aligned} x \geq \mu: \quad & \sigma(x) = K\varepsilon(x) - \frac{1}{6}C\mu^2\varepsilon''(x). \\ 0 < x < \mu: \quad & \sigma(x) = K\varepsilon(x) - C_I(x)\varepsilon'(x) - C_{II}(x)\varepsilon''(x). \end{aligned}\right\} \tag{A1.25}$$

B.C.'s:

$$\left.\begin{array}{l} x=0:\ \sigma' - \dfrac{2}{\mu}\,\sigma = (K+\dfrac{3}{2}C)\,\varepsilon' - \dfrac{1}{\mu}(2K-C)\,\varepsilon \\ x=\mu:\ \text{Continuity of } \varepsilon \text{ and } \varepsilon' \\ x\to\infty:\ \varepsilon = \varepsilon_\infty = \dfrac{P}{A_\infty}\dfrac{1}{K}, \end{array}\right\} \qquad \text{(A1.26)}$$

where the functions $C_I(x)$ and $C_{II}(x)$ are defined by (A1.13). Following the discussion of their properties and assuming that μ is small compared to L^*

$$\mu << L^*,$$

it appears possible to ignore the first order term in $(A1.25)_2$ and to use the approximation

$$C_{II}(x) \approx \frac{1}{6}C\mu^2,$$

such that the form of the differential equation is the same in the whole domain $0<x$. However, the boundary conditions $(A1.26)_{1+3}$ should not be affected by this approximation. The validity of this simplification needs further analysis.

Case II : Symmetric Case

In the interior of the rod, far from the boundary $x= x_L=0$, the non-local model (A1.1) can be approximated by the same 2nd order differential equation (A1.10) as for the non-symmetric case. However, close to the boundary $x= x_L=0$ the deformable material on the left side of the boundary affects the response on the right side $x_L=0<x$. Because of the assumed perfect symmetry of the strain distribution around $x=0$ the non-local model (A1.1) takes now the following form:

$$\sigma = \overset{v}{K}\,\varepsilon(x) - \frac{C}{2\mu}\left\{\int_{-x}^{\mu}\varepsilon(x+y)\mathrm{d}y + \int_{-x}^{\mu-2x}\varepsilon(x+y)\mathrm{d}y\right\} =$$

$$= \overset{v}{K}\,\varepsilon(x) - \frac{C}{2\mu}\left\{\int_{0}^{x+\mu}\varepsilon(z)\mathrm{d}z + \int_{0}^{\mu-x}\varepsilon(z)\mathrm{d}z\right\}. \qquad \text{(A1.27)}$$

Using the Taylor series approximation (A1.7), the integrations in (A1.27) are performed and one obtains

$$\sigma(x) = \overset{v}{K}\,\varepsilon(x) - \frac{C}{2\mu}\left\{\varepsilon(x)\left([\mu+x] + [\mu-2x+x]\right) +\right.$$

$$+\frac{1}{2}\varepsilon'(x)\left([\mu^2-x^2]+[(\mu-2x)^2-x^2]\right)+\frac{1}{6}\varepsilon''(x)\left([\mu^3+x^3]+[(\mu-2x)^3+x^3]\right)\}$$

More compactly the governing differential equation is now given by

$$\sigma(x)=K\varepsilon(x)-\tilde{C}_I(x)\,\varepsilon'(x)-\tilde{C}_{II}(x)\,\varepsilon''(x). \tag{A1.28}$$

with

$$\left.\begin{aligned} K &= \overset{v}{K}-C \\ \tilde{C}_I(x) &= C\frac{1}{2}\left[\mu-2x+\frac{x^2}{\mu}\right] \\ \tilde{C}_{II}(x) &= C\frac{1}{6}\left[\mu^2-3\mu x+6x^2-3\frac{x^3}{\mu}\right]. \end{aligned}\right\} \tag{A1.29}$$

The largest values of $\tilde{C}_I$ is at the boundary $x=x_L=0$

$$(\tilde{C}_I)_{\max}=\frac{1}{2}C\mu, \tag{A1.30}$$

followed by a parabolic decay towards zero at the relative minimum at $x=\mu$. The cubic function $\tilde{C}_{II}$ takes the same value at the boundary and at $x=\mu$ as the constant coefficient of the 2nd order gradient term in the interior of the rod ($\mu\leq x$):

$$(\tilde{C}_{II})_{x=x_L=0}=(\tilde{C}_{II})_{x=\mu}=\frac{1}{6}C\mu^2. \tag{A1.31}$$

The above values (A1.30) and (A1.31) agree with the corresponding values of the non-symmetric case. The relative minimum of $\tilde{C}_{II}$ is

$$(\tilde{C}_{II})_{\min}=\frac{5}{9}\frac{1}{6}C\mu^2, \tag{A1.32}$$

which is positioned at $x=\mu/3$. Compared to the non-symmetric case this minimum is shifted towards the boundary. The relative maximum is at $x=\mu$. Its mean value in the interval $0\leq x\leq\mu$ is

$$(\tilde{C}_{II})_{\text{mean}}=\frac{3}{4}\frac{1}{6}C\mu^2. \tag{A1.33}$$

The required boundary condition at $x=x_L=0$ is found analogously to the previous approach. Approaching the boundary $x=x_L=0$, Eq.(A1.28) reduces to

$$\sigma(x_L) = K\varepsilon(x_L) - \frac{1}{2}\, C\mu\, \varepsilon'(x_L) - \frac{1}{6}\, C\mu^2\, \varepsilon''(x_L)\,,$$

which is the same as for the non-symmetric case. The formal integration in $(A1.27)_2$ yields

$$\sigma(x) = \overset{v}{K}\ \varepsilon(x) - \frac{C}{2\mu}\ \left\{(F(z))_{z=x+\mu} - (F(z))_{z=0} + (F(z))_{z=\mu-x} - (F(z))_{z=0}\right\}\,, \tag{A1.34}$$

where $F(z)$ is the integral of $\varepsilon(z)$. The first derivative with respect to x is

$$\begin{aligned}\sigma'(x) &= \overset{v}{K}\ \varepsilon'(x) - \frac{C}{2\mu}\ \left\{\varepsilon(x+\mu) - \varepsilon(\mu-x)\right\} = \\ &= \overset{v}{K}\ \varepsilon'(x) - \frac{C}{2\mu}\ \left\{\varepsilon(x+\mu) - \varepsilon(x+(\mu-2x))\right\}.\end{aligned} \tag{A1.35}$$

Using the Taylor series approximation (A1.7) yields

$$\begin{aligned}\sigma'(x) = \overset{v}{K}\ \varepsilon'(x) - \frac{C}{2\mu}\ \Big\{\ &\varepsilon(x) + \varepsilon'(x)\mu + \frac{1}{2}\varepsilon''(x)\mu^2 - \\ &- \left(\varepsilon(x) + \varepsilon'(x)\,(\mu-2x) + \frac{1}{2}\varepsilon''(x)\,(\mu-2x)^2\right)\Big\} = \\ = \overset{v}{K}\ \varepsilon'(x) - C\frac{x}{\mu}\ \varepsilon'(x) &+ C\left(x - \frac{x^2}{\mu}\right)\varepsilon''(x).\end{aligned} \tag{A1.36}$$

If x approaches the boundary $x=x_L=0$, then (A1.36) reduces to the simple condition

$$\sigma'(x_L) = \overset{v}{K}\ \varepsilon'(x_L). \tag{A1.37}$$

This is the required boundary condition which represents only a condition on the strain gradient; in contrast to the previous result (A1.24) the strain is not involved. Also only a single material parameter, that of the classical part of the constitutive relation, is of importance. Ignoring the non-local effect, i.e.

$$C\to 0\,,\ \mu\to 0\,,$$

does not affect condition (A1.37) which is then simply a consequence of the classical linear stress-strain relation. However, clearly this observation does not imply that in the non-local case the local strain at the boundary is determined by the stress, i.e.

$$\sigma(x_L) \neq \overset{v}{K}\ \varepsilon(x_L).$$

An important result follows from the boundary condition (A1.37). If the cross-section variation is smooth, i.e. $A'(x)=0$ and thus $\sigma'(x)=0$ at $x=x_L=0$, then (A1.37) implies the vanishing of the strain gradient

$$\varepsilon'(x_L) = 0. \tag{A1.38}$$

This is a rather obvious result implied by symmetry and smoothness. Only under these conditions the non-local model yields the vanishing of the 1st order gradient at this boundary.

As for the non-symmetric case it appears conceivable to replace the differential equation (A1.28), valid in the regime $x_L = 0 < x < \mu$, by the simpler form (A1.10) such that (A1.10) is applicable in the whole regime $x_L = 0 < x$. However, the boundary condition (A1.37) should still apply.

Conclusions:

The 2nd order linear gradient model

$$\sigma = K\varepsilon - K l_i^2 \frac{\mathrm{d}^2\varepsilon}{\mathrm{d}x^2} \tag{A1.39}$$

and its non-classical boundary condition

$$\frac{\mathrm{d}\varepsilon}{\mathrm{d}x} = 0 \quad \text{at } x=x_L=0 \tag{A1.40}$$

generally cannot be considered as an approximate representation of a non-local model such as (A1.1), first of all because of the smaller number of material parameters (two instead of three). However, far from boundaries or geometric discontinuities the 2nd order gradient model is a valid approximation if the internal length (l_i) is appropriately interpreted. However, in a small region (size less than μ) close to the boundary (A1.39) differs from the non-local model by a first order strain gradient term which is missing in (A1.39). The importance of a first order gradient close to the boundary has also been pointed out by Pijaudier-Cabot et al. [A1.5]. But more important, the boundary conditions obtained from the non-local model for the non-symmetric and the symmetric case differ significantly from (A1.40). However, for the case of perfect symmetry and smoothness of the cross-section variation at the boundary, Eq.(A1.39), ignoring additional terms in the interval $x_L=0<x<\mu$, and the boundary condition (A1.40) agree with the appropriate representation of the non-local model (A1.1). Thus, aside from this exception, the gradient model (A1.39) and its non-classical boundary condition (A1.40) need another motivation than a non-local integral model.

References

[A1.1] H.B. Mühlhaus and E.C. Aifantis, A variational principle for gradient plasticity, *Int. J. Solids & Struct. 28*, 845-857, (1991).

[A1.2] H.M. Zbib, Strain gradients and size effects in non-homogeneous plastic deformation, *Script. Metall. Mat. 30*, 1223-1226, (1994).

[A1.3] R.H.J. Peerlings, R. de Borst, W.A.M Brekelmans and J.H.P de Vree, Gradient enhanced damage for quasi-brittle materials, *Int. J. for Num. Meth. In Eng. 39*, 3391-3403, (1996).

[A1.4] Z.P. Bazant and E-P. Chen, Scaling of structural failure, *Appl. Mech. Rev. 50*, 593-627 (1997).

[A1.5] G. Pijaudier-Cabot , Z.P. Bazant and M. Tabarra, Comparison of various models for strain-softening, *Eng. Comput. 5*, 141-150 (1988).

Appendix (2): Derivation of the Exact Solution for the Linear Problem of an Exponentially Tapered Rod

The homogeneous solution of (3.14) is

$$\varepsilon_{\text{hom}} = C_1 e^{\zeta} + C_2 e^{-\zeta} \tag{A2.1}$$

and a particular solution is chosen to be of the form

$$\varepsilon_{\text{part}} = D_0 + D_1 e^{-\beta\zeta} \; ; \tag{A2.2}$$

here $\beta<1$ is required. Then

$$\frac{d^2\varepsilon_{\text{part}}}{d\zeta^2} = D_1\beta^2 e^{-\beta\zeta}$$

and the left side of (3.14) reads

$$-(D_1(1-\beta^2)\, e^{-\beta\zeta} + D_0).$$

Comparison with the right side of (3.14) yields

$$D_o = \frac{P}{A_o}\frac{1}{K}\alpha, \qquad D_1 = \frac{1}{1-\beta^2}\frac{P}{A_o}\frac{1}{K}(1-\alpha). \tag{A2.3}$$

Therefore

$$\varepsilon_{\text{part}} = \varepsilon_{co}\left[\alpha + \frac{1-\alpha}{1-\beta^2} e^{-\beta\zeta}\right] \tag{A2.4}$$

where

$$\varepsilon_{co} = \frac{P}{A_o}\frac{1}{K} \tag{A2.5}$$

is the maximum strain of the classical solution at the minimum cross-section area. The general solution is

$$\varepsilon(\zeta) = \varepsilon_{\text{hom}} + \varepsilon_{\text{part}}. \tag{A2.6}$$

The boundary condition B.C.I, Eq.$(3.16)_1$, implies

$$C_1 \equiv 0 \tag{A2.7}$$

and $\varepsilon_{co}\alpha = \varepsilon_\infty$ which is trivially satisfied. The boundary condition B.C.II, Eq.$(3.16)_2$, yields

$$C_2 = -\varepsilon_{co}\frac{1-\alpha}{1-\beta^2}\beta \ . \qquad \text{(A2.8)}$$

Thus the complete solution for the non-classical strain distribution, using ξ again as the independent variable and with $\beta<1$, is given by

$$\varepsilon(\xi) = \varepsilon_{co}\left\{ \left[\alpha + \frac{1-\alpha}{1-\beta^2}\, e^{-\xi}\right] - \frac{1-\alpha}{1-\beta^2}\beta\, e^{-\xi/\beta} \right\}. \qquad \text{(A2.9)}$$

Appendix (3): Derivation of the Governing System of Perturbation Equations

The partial derivatives in Eq.(4.35) and (4.36) are expressed in terms of the polynomial presentation (4.37) and a collection according to powers of β is done. This yields

$$\beta^2\frac{d^2\hat{\varepsilon}}{d\xi^2} = \beta^2 \left\{ \left[\overset{0}{\varepsilon}_{\xi\xi} + \beta \overset{1}{\varepsilon}_{\xi\xi} + \beta^2 \overset{2}{\varepsilon}_{\xi\xi} + \beta^3 \overset{3}{\varepsilon}_{\xi\xi} \right] + \right.$$

$$+ 2\frac{\mu'}{\beta}\left[\overset{0}{\varepsilon}_{\xi\eta} + \beta \overset{1}{\varepsilon}_{\xi\eta} + \beta^2 \overset{2}{\varepsilon}_{\xi\eta} + \beta^3 \overset{3}{\varepsilon}_{\xi\eta} \right] +$$

$$+ \left(\frac{\mu'}{\beta}\right)^2 \left[\overset{0}{\varepsilon}_{\eta\eta} + \beta \overset{1}{\varepsilon}_{\eta\eta} + \beta^2 \overset{2}{\varepsilon}_{\eta\eta} + \beta^3 \overset{3}{\varepsilon}_{\eta\eta} \right] +$$

$$\left. + \frac{\mu''}{\beta}\left[\overset{0}{\varepsilon}_{\eta} + \beta \overset{1}{\varepsilon}_{\eta} + \beta^2 \overset{2}{\varepsilon}_{\eta} + \beta^3 \overset{3}{\varepsilon}_{\eta} \right] \right\}$$

$$= \beta^3 \left[\overset{1}{\varepsilon}_{\xi\xi} + 2\mu' \overset{2}{\varepsilon}_{\xi\eta} + (\mu')^2 \overset{3}{\varepsilon}_{\eta\eta} + \mu'' \overset{2}{\varepsilon}_{\eta} \right] +$$

$$+ \beta^2 \left[\overset{0}{\varepsilon}_{\xi\xi} + 2\mu' \overset{1}{\varepsilon}_{\xi\eta} + (\mu')^2 \overset{2}{\varepsilon}_{\eta\eta} + \mu'' \overset{1}{\varepsilon}_{\eta} \right] +$$

$$+ \beta^1 \left[2\mu' \overset{0}{\varepsilon}_{\xi\eta} + (\mu')^2 \overset{1}{\varepsilon}_{\eta\eta} + \mu'' \overset{0}{\varepsilon}_{\eta} \right] +$$

$$+ \beta^0 \left[(\mu')^2 \overset{0}{\varepsilon}_{\eta\eta} \right]. \qquad \text{(A3.1)}$$

The power law term $\tilde{\varepsilon}^n$, $0<n\leq 1$, and the exponential term $e^{\tilde{\varepsilon}}$ are approximated in terms of powers of β. Thus

$$\tilde{\varepsilon}^n = \left(\overset{0}{\varepsilon} + \beta \overset{1}{\varepsilon} + \beta^2 \overset{2}{\varepsilon} + \beta^3 \overset{3}{\varepsilon} \right)^n =$$

$$= \overset{0}{\varepsilon}^n \left(1 + \beta \overset{1}{\varepsilon}/\overset{0}{\varepsilon} + \beta^2 \overset{2}{\varepsilon}/\overset{0}{\varepsilon} + \beta^3 \overset{3}{\varepsilon}/\overset{0}{\varepsilon} \right)^n$$

$$= \overset{0}{\varepsilon}^n \left\{ 1 + \beta \left[n \overset{1}{\varepsilon}/\overset{0}{\varepsilon} \right] + \beta^2 \left[n \overset{2}{\varepsilon}/\overset{0}{\varepsilon} - \frac{1}{2} n(1-n) \left(\overset{1}{\varepsilon}/\overset{0}{\varepsilon} \right)^2 \right] + \right.$$

$$\left. + \beta^3 \left[n \overset{3}{\varepsilon}/\overset{0}{\varepsilon} - \frac{1}{2} n(1-n) 2 \left(\overset{1}{\varepsilon}/\overset{0}{\varepsilon} \right) \left(\overset{2}{\varepsilon}/\overset{0}{\varepsilon} \right) + \frac{1}{6} n(1-n)(2-n) \left(\overset{1}{\varepsilon}/\overset{0}{\varepsilon} \right)^3 \right] + \ldots \right\}. \qquad \text{(A3.2)}$$

With

$$\tilde{\varepsilon} = \overset{0}{\varepsilon} + \nu$$

$$\nu = \beta \overset{1}{\varepsilon} + \beta^2 \overset{2}{\varepsilon} + \beta^3 \overset{3}{\varepsilon}$$

one finds

$$e^{\tilde{\varepsilon}} = e^{\overset{0}{\varepsilon}} e^{\nu} = e^{\overset{0}{\varepsilon}} \left\{ 1 + \frac{\nu}{1!} + \frac{\nu^2}{2!} + \frac{\nu^3}{3!} + \ldots \right\}$$

where

$$\nu^2 = \beta^2 (\overset{1}{\varepsilon})^2 + 2[\beta^3 \overset{1}{\varepsilon}\, \overset{2}{\varepsilon}] + \ldots$$

$$\nu^3 = \beta^3 (\overset{1}{\varepsilon})^3 + \ldots \quad ;$$

here terms higher than cubic in β are excluded. Then

$$e^{\tilde{\varepsilon}} = e^{\overset{0}{\varepsilon}} \left\{ 1 + \beta \overset{1}{\varepsilon} + \beta^2 \left(\overset{2}{\varepsilon} + \frac{1}{2} (\overset{1}{\varepsilon})^2 \right) + \beta^3 \left(\overset{3}{\varepsilon} + \overset{1}{\varepsilon}\, \overset{2}{\varepsilon} + \frac{1}{6} (\overset{1}{\varepsilon})^3 \right) \right\}. \qquad \text{(A3.3)}$$

Inserting (A3.1), (A3.2) and (A3.3) into the differential equation (4.7) and ordering according to powers in β one obtains

$$\begin{aligned}
&\beta^0 \left[(\mu')^2 \overset{0}{\varepsilon}_{\eta\eta} - \overset{0}{\varepsilon}^n + r_R(\xi)\, e^{\overset{0}{\varepsilon}} \right] + \\
&+ \beta^1 \left[(\mu')^2 \overset{1}{\varepsilon}_{\eta\eta} - n \overset{0}{\varepsilon}^n \left(\overset{1}{\varepsilon} / \overset{0}{\varepsilon} \right) + 2\mu' \overset{0}{\varepsilon}_{\xi\eta} + \mu'' \overset{0}{\varepsilon}_{\eta} + r_R(\xi)\, e^{\overset{0}{\varepsilon}} \overset{1}{\varepsilon} \right] + \\
&+ \beta^2 \left[(\mu')^2 \overset{2}{\varepsilon}_{\eta\eta} - n \overset{0}{\varepsilon}^n \left(\overset{2}{\varepsilon} / \overset{0}{\varepsilon} \right) + \overset{0}{\varepsilon}_{\xi\xi} + 2\mu' \overset{1}{\varepsilon}_{\xi\eta} + \mu'' \overset{1}{\varepsilon}_{\eta} + \right. \\
&\qquad \left. + \overset{0}{\varepsilon}^n \frac{1}{2} n(1-n) \left(\overset{1}{\varepsilon} / \overset{0}{\varepsilon} \right)^2 + r_R(\xi) e^{\overset{0}{\varepsilon}} \left(\overset{2}{\varepsilon} + \frac{1}{2} (\overset{1}{\varepsilon})^2 \right) \right] + \\
&+ \beta^3 \left[(\mu')^2 \overset{3}{\varepsilon}_{\eta\eta} - n \overset{0}{\varepsilon}^n \left(\overset{3}{\varepsilon} / \overset{0}{\varepsilon} \right) + \overset{1}{\varepsilon}_{\xi\xi} + 2\mu' \overset{2}{\varepsilon}_{\xi\eta} + \mu'' \overset{2}{\varepsilon}_{\eta} + \right. \\
&\qquad + \overset{0}{\varepsilon}^n \frac{1}{2} n(1-n) 2 \left(\overset{1}{\varepsilon} / \overset{0}{\varepsilon} \right) \left(\overset{2}{\varepsilon} / \overset{0}{\varepsilon} \right) - \overset{0}{\varepsilon}^n \frac{1}{6} n(1-n)(2-n) \left(\overset{1}{\varepsilon} / \overset{0}{\varepsilon} \right)^3 + \\
&\qquad \left. + r_R(\xi) e^{\overset{0}{\varepsilon}} \left(\overset{3}{\varepsilon} + \overset{1}{\varepsilon}\, \overset{2}{\varepsilon} + \frac{1}{6} (\overset{1}{\varepsilon})^3 \right) \right] = 0
\end{aligned} \qquad \text{(A3.4)}$$

The bracketed terms in (A3.4) are independent of β. Then, following the "Fundamental Theorem of Perturbation Theory" (Simmonds & Mann (1986, [4.7])), for small and positive but otherwise arbitrary values of β each bracketed term must vanish. This yields the following system of differential equations:

$$\left.\begin{aligned}
&\beta^0 : \mathrm{DEQ}(0) \Rightarrow \overset{0}{\varepsilon}_{\eta\eta} - \frac{\overset{0}{\varepsilon}^{\,n}}{(\mu')^2} = -\frac{r_R(\xi)\overset{0}{e^{\varepsilon}}}{(\mu\square)^2} \\
&\beta^1 : \mathrm{DEQ}(1) \Rightarrow \overset{1}{\varepsilon}_{\eta\eta} - \Omega^2(\xi)\ \overset{1}{\varepsilon} = R_1(\overset{0}{\varepsilon}, \mu) \\
&\beta^2 : \mathrm{DEQ}(2) \Rightarrow \overset{2}{\varepsilon}_{\eta\eta} - \Omega^2(\xi)\ \overset{2}{\varepsilon} = R_2(\overset{0}{\varepsilon}, \overset{1}{\varepsilon}, \mu, r_R) \\
&\beta^3 : \mathrm{DEQ}(3) \Rightarrow \overset{3}{\varepsilon}_{\eta\eta} - \Omega^2(\xi)\ \overset{3}{\varepsilon} = R_3(\overset{0}{\varepsilon}, \overset{1}{\varepsilon}, \overset{2}{\varepsilon}, \mu, r_R)
\end{aligned}\right\} \qquad \text{(A3.5)}$$

where

$$\left.\begin{aligned}
&\Omega^2(\xi) = \Omega_R^2(\xi) - \underline{\underline{\frac{\overset{0}{\varepsilon}^{\,n}}{(\mu')^2}}} \\
&\Omega_R^2(\xi) = \frac{n}{\overset{0}{\varepsilon}}\,\frac{\overset{0}{\varepsilon}^{\,n}}{(\mu')^2}
\end{aligned}\right\} \qquad \text{(A3.6)}$$

such that

$$\Omega^2(\xi) = \frac{1}{(\mu')^2}\left(\underline{\underline{\frac{n}{\overset{0}{\varepsilon}} - 1}}\right)\overset{0}{\varepsilon}^{\,n}, \qquad 0<n\leq 1. \qquad \text{(A3.7)}$$

The right sides R_i, i=1,2,3 are differential operators defined as follows:

$$\left.\begin{aligned}
&R_1 = -\frac{1}{(\mu')^2}\left(2\,\mu'\,\overset{0}{\varepsilon}_{\xi\eta} + \mu''\,\overset{0}{\varepsilon}_{\eta}\right) \\
&R_2 = R_{R2} - \underline{\underline{\frac{r_R\overset{0}{e^{\varepsilon}}}{(\mu\square)^3}\,\frac{1}{2}(\overset{1}{\varepsilon})^2}} \\
&R_{R2} = -\frac{1}{(\mu')^2}\left(2\,\mu'\,\overset{1}{\varepsilon}_{\xi\eta} + \mu''\,\overset{1}{\varepsilon}_{\eta} + \overset{0}{\varepsilon}_{\xi\xi}\right) - \Omega_R^2\,\frac{1}{2}(1-n)\,\frac{1}{\overset{0}{\varepsilon}}\,(\overset{1}{\varepsilon})^2 \\
&R_3 = R_{R3} - \underline{\underline{\frac{r_R\overset{0}{e^{\varepsilon}}}{(\mu\square)^3}\left(\overset{1}{\varepsilon}\,\overset{2}{\varepsilon} + \frac{1}{6}(\overset{1}{\varepsilon})^3\right)}} \\
&R_{R3} = -\frac{1}{(\mu')^2}\left(2\,\mu'\,\overset{2}{\varepsilon}_{\xi\eta} + \mu''\,\overset{2}{\varepsilon}_{\eta} + \overset{1}{\varepsilon}_{\xi\xi}\right) - \Omega_R^2\,(1-n)\,\frac{\overset{1}{\varepsilon}\,\overset{2}{\varepsilon}}{\overset{0}{\varepsilon}} + \\
&\qquad\qquad + \Omega_R^2\,\frac{1}{6}(1-n)(2-n)\,\frac{(\overset{1}{\varepsilon})^3}{(\overset{0}{\varepsilon})^2}\ .
\end{aligned}\right\} \qquad \text{(A3.8)}$$

The terms underlined in (A3.6) to (A3.8) represent the contribution due to the cross-section reduction. A similar procedure is applied to the two boundary conditions (4.36). Ordering according to powers of β gives

$$
\left.
\begin{array}{lll}
 & \text{B.C. I } (\xi,\ \eta \to \infty) & \text{B.C. II } (\xi,\ \eta = 0) \\
\beta^{-1}: & - & \mu' \overset{0}{\varepsilon}_{\eta} = 0 \\
\beta^{0}: & \overset{0}{\varepsilon} \to \varepsilon_{\infty} & \overset{0}{\varepsilon}_{\xi} + \mu' \overset{1}{\varepsilon}_{\eta} = 0 \\
\beta^{1}: & \overset{1}{\varepsilon} \to 0 & \overset{1}{\varepsilon}_{\xi} + \mu' \overset{2}{\varepsilon}_{\eta} = 0 \\
\beta^{2}: & \overset{2}{\varepsilon} \to 0 & \overset{2}{\varepsilon}_{\xi} + \mu' \overset{3}{\varepsilon}_{\eta} = 0 \\
\beta^{3}: & \overset{3}{\varepsilon} \to 0 & (\overset{3}{\varepsilon}_{\xi} = 0).
\end{array}
\right\} \qquad \text{(A3.9)}
$$

Note that the condition B.C.II for β^3 is not accurate since 4th order terms in the development of $\tilde{\varepsilon}$ were not included; it will be seen that this condition is not required.

Appendix (4): The Particular Solution of DEQ(2)

For the particular solution of the perturbation equation DEQ(2), Eq.$(4.38)_3$, with the right side R_2 given by (4.58), the choice

$$\overset{2}{\varepsilon}_{\text{part}} = -\frac{\alpha_o(\xi)}{\Omega^2(\xi)} + f(\xi,\eta)\, e^{-\Omega(\xi)\eta} + h(\xi,\eta)\, e^{-2\Omega(\xi)\eta} \tag{A4.1}$$

is used where f and h have to be determined. Then

$$\left.\begin{aligned} \frac{\partial}{\partial\eta}\overset{2}{\varepsilon}_{\text{part}} &= (\dot f - \Omega f)\, e^{-\Omega\eta} + (\dot h - 2\Omega h)\, e^{-2\Omega\eta} \\ \frac{\partial^2}{\partial\eta^2}\overset{2}{\varepsilon}_{\text{part}} &= (\ddot f - 2\Omega\dot f + \Omega^2 f)\, e^{-\Omega\eta} + (\ddot h - 4\Omega\dot h + 4\Omega^2 h) e^{-2\Omega\eta}\,, \end{aligned}\right\} \tag{A4.2}$$

where

$$(\dot{}) = \frac{\partial}{\partial\eta}.$$

Inserting (4.1) and $(A4.2)_2$ into DEQ(2) and observing the structure of R_2, Eq.(4.58), one obtains the following condition:

$$(\ddot f - 2\Omega\dot f) e^{-\Omega\eta} + (\ddot h - 4\Omega\dot h + 3\Omega^2 h)\, e^{-2\Omega\eta} = (\alpha_1 + \bar\alpha_1\eta) e^{-\Omega\eta} + \alpha_2^* e^{-2\Omega\eta}. \tag{A4.3}$$

Equating the corresponding exponential terms, two linear ordinary differential equations in the η-space for the functions f and h are obtained:

$$\left.\begin{aligned} \ddot f - 2\Omega\dot f &= \alpha_1 + \bar\alpha_1\eta \\ \ddot h - 4\Omega\dot h + 3\Omega^2 h &= \alpha_2^* \end{aligned}\right\} \tag{A4.4}$$

Obviously

$$f = f_1(\xi)\eta + f_2(\xi)\,\eta^2 \tag{A4.5}$$

and so $Eq.(A4.4)_1$ gives

$$2f_2 - 2\Omega^2(f_1 + 2f_2\,\eta) = \alpha_1 + \bar\alpha_1\eta\,,$$

which implies

$$2f_2 - 2\Omega f_1 = \alpha_1$$

$$-4\Omega f_2 = \bar\alpha_1\,.$$

Thus

$$\left.\begin{aligned} f_1(\xi) &= -\left(\frac{\alpha_1}{2\Omega} + \frac{\overline{\alpha}_1}{4\Omega^2}\right) \\ f_2(\xi) &= -\frac{\overline{\alpha}_1}{4\Omega} \ . \end{aligned}\right\} \qquad \text{(A4.6)}$$

Eq.(A4.4)$_2$ implies that (h) is independent of the variable η; one gets

$$h = h_o(\xi) = \frac{\alpha_2{}^*}{3\Omega^2} . \qquad \text{(A4.7)}$$

And the particular solution is

$$\overset{2}{\varepsilon}_{\text{part}} = -\frac{\alpha_0}{\Omega^2} + (f_1\eta + f_2\,\eta^2)\ \mathrm{e}^{-\Omega\eta} + h_0\mathrm{e}^{-2\Omega\eta} \ , \qquad \text{(A4.8)}$$

where α_o, Ω , f_1, f_2 and h_o are functions of ξ.

Appendix(5): Determination of the Function $B_1(\xi)$

The solution of the differential equation (4.75)

$$B_1' + \frac{1}{2}\frac{\mu''}{\mu'} B_1 = 0 , \tag{A5.1}$$

which is a consequence of the suppression of the secular terms, is found as follows. With

$$\frac{1}{2}\frac{\mu''}{\mu'} = \frac{1}{2}\frac{\mathrm{d}}{\mathrm{d}\xi} \ln \mu' = \frac{\mathrm{d}}{\mathrm{d}\xi} \ln(\mu')^{1/2} \tag{A5.2}$$

and

$$\nu = (\mu')^{1/2} \tag{A5.3}$$

we get

$$\frac{1}{2}\frac{\mu''}{\mu'} = \frac{\nu'}{\nu}.$$

Then Eq.(A5.1) takes the form

$$\nu B_1' + \nu' B_1 = (\nu B_1)' = 0 \tag{A5.4}$$

and the general solution is

$$B_1(\xi) = \frac{c}{\nu} = \frac{c}{(\mu')^{1/2}} , \tag{A5.5}$$

where c is an integration constant. With μ' given by (4.72) the function B_1 reads

$$B_1(\xi) = D \left(\frac{\overset{0}{\varepsilon}(\xi)^{1-n}}{n - \overset{0}{\varepsilon}(\xi)} \right)^{1/4} , \tag{A5.6}$$

where the constants c and φ have been lumped into a new constant D:

$$D = c\varphi^{1/4}. \tag{A5.7}$$

This integration constant is determined from the boundary condition for $\overset{1}{\varepsilon}$ at ξ,η=0, Eq.(4.42):

$$\overset{0}{\varepsilon}_\xi + \mu' \overset{1}{\varepsilon}_\eta = 0 ; \qquad \xi,\eta=0. \tag{A5.8}$$

With $(4.54)_1$ one gets

$$(\overset{0}{\varepsilon}_\xi)_o - (\mu')_o \Omega (B_1)_o = 0 ,$$

such that

$$(B_1)_o = B_1(0) = \frac{c}{(\mu')_o^{1/2}} = \frac{1}{\Omega(\mu')_o}(\overset{0}{\varepsilon}_\xi)_o \tag{A5.9}$$

and consequently

$$D = c\varphi^{1/4} = \left(\frac{\overset{0}{\varepsilon}^{1-n}}{n - \overset{0}{\varepsilon}} \right)_o^{1/4} (\overset{0}{\varepsilon}_\xi)_o . \tag{A5.10}$$

Appendix (6): The Particular Solution of DEQ(3)

The differential equation DEQ(3), Eq.$(4.38)_4$, reads

$$\beta^3 : \text{DEQ(3)} \Rightarrow \overset{3}{\varepsilon}_{\eta\eta} - \Omega^2(\xi)\,\overset{3}{\varepsilon} = R_3(\overset{0}{\varepsilon},\overset{1}{\varepsilon},\overset{2}{\varepsilon},\mu,r_R) = \tilde{R}_3(\overset{0}{\varepsilon},\overset{1}{\varepsilon},\overset{2}{\varepsilon},\mu)\,, \tag{A6.1}$$

where $\tilde{R}_3$ is defined by $(4.47)_3$ and $(4.41)_5$

$$\tilde{R}_3(\overset{0}{\varepsilon},\overset{1}{\varepsilon},\overset{2}{\varepsilon},\mu) = R_{R3}(\overset{0}{\varepsilon},\overset{1}{\varepsilon},\overset{2}{\varepsilon},\mu) - \frac{\overset{0}{\varepsilon}^{\,n}}{(\mu')^2}\left(\overset{1}{\varepsilon}\,\overset{2}{\varepsilon} + \frac{1}{6}\left(\overset{1}{\varepsilon}\right)^3\right). \tag{A6.2}$$

$$R_{R3} = -\frac{1}{(\mu')^2}(2\,\mu'\,\overset{2}{\varepsilon}_{\xi\eta} + \mu''\,\overset{2}{\varepsilon}_{\eta} + \overset{1}{\varepsilon}_{\xi\xi}) - \Omega_R^2\,\frac{1}{2}(1-n)\,2\frac{\overset{1}{\varepsilon}\,\overset{2}{\varepsilon}}{\overset{0}{\varepsilon}} +$$

$$+\,\Omega_R^2\frac{1}{6}(1-n)(2-n)\,\frac{\left(\overset{1}{\varepsilon}\right)^3}{\left(\overset{0}{\varepsilon}\right)^2}. \tag{A6.3}$$

With

$$\begin{aligned}\overset{2}{\varepsilon} &= B_2(\xi)\mathrm{e}^{-\sqrt{\varphi}\eta} - \frac{\alpha_o(\xi)}{\varphi} + h_o(\xi)\mathrm{e}^{-2\sqrt{\varphi}\eta} \\ &= B_2(\xi)\mathrm{e}^{-\sqrt{\varphi}\eta} - \frac{\alpha_o(\xi)}{\varphi} + \frac{\alpha_2^*(\xi)}{3\varphi}\mathrm{e}^{-2\sqrt{\varphi}\eta}\,,\end{aligned} \tag{A6.4}$$

we get

$$\left.\begin{aligned}\overset{2}{\varepsilon}_{\eta} &= -\sqrt{\varphi}\;B_2\mathrm{e}^{-\sqrt{\varphi}\eta} - 2\sqrt{\varphi}\,\frac{\alpha_2^*}{3\varphi}\mathrm{e}^{-2\sqrt{\varphi}\eta} \\ \overset{2}{\varepsilon}_{\xi\eta} &= -\sqrt{\varphi}\;B_2'\mathrm{e}^{-\sqrt{\varphi}\eta} - 2\sqrt{\varphi}\,\frac{(\alpha_2^*)'}{3\varphi}\mathrm{e}^{-2\sqrt{\varphi}\eta}\,;\end{aligned}\right\} \tag{A6.5}$$

further

$$\overset{1}{\varepsilon} = B_1(\xi)\mathrm{e}^{-\sqrt{\varphi}\eta}\,, \qquad \overset{1}{\varepsilon}_{\xi\xi} = B_1''(\xi)\mathrm{e}^{-\sqrt{\varphi}\eta}\,, \tag{A6.6}$$

as well as

$$\left.\begin{aligned} \overset{1}{\varepsilon}\,\overset{2}{\varepsilon} &= -B_1\,\frac{\alpha_o}{\varphi}\,e^{-\sqrt{\varphi}\eta} + B_1\,B_2\,e^{-2\sqrt{\varphi}\eta} + B_1\frac{\alpha_2^*}{3\varphi}e^{-3\sqrt{\varphi}\eta} \\ (\overset{1}{\varepsilon})^3 &= (B_1)^3 e^{-3\sqrt{\varphi}\eta}\ . \end{aligned}\right\} \qquad \text{(A6.7)}$$

Using the results for $\overset{1}{\varepsilon}$ and $\overset{2}{\varepsilon}$ and their derivatives, R_{R3} takes the following explicit form

$$R_{R3} = \gamma_{R1}(\xi)e^{-\sqrt{\varphi}\eta} + \gamma_{R2}(\xi)e^{-2\sqrt{\varphi}\eta} + \gamma_{R3}(\xi)e^{-3\sqrt{\varphi}\eta}\ , \qquad \text{(A6.8)}$$

where

$$\left.\begin{aligned} \gamma_{R1}(\xi) &= \frac{2}{\mu'}\sqrt{\varphi}\ B_2' + \frac{\mu''}{(\mu')^2}\sqrt{\varphi}\ B_2 - \frac{1}{(\mu')^2}\ B_1'' + \Omega_R^2\ \frac{1}{2}(1-n)\,2\frac{1}{\overset{0}{\varepsilon}}\ \frac{\alpha_0}{\varphi}\ B_1 \\ \gamma_{R2}(\xi) &= \frac{2}{\mu'}\,\frac{2}{3}\,\frac{(\alpha_2^*)'}{\sqrt{\varphi}} + \frac{\mu''}{(\mu')^2}\,\frac{2}{3}\,\frac{\alpha_2^*}{\sqrt{\varphi}} - \Omega_R^2\ \frac{1}{2}(1-n)\,2\frac{1}{\overset{0}{\varepsilon}}\ B_1\,B_2 \\ \gamma_{R3}(\xi) &= -\left\{\ \Omega_R^2\ \frac{1}{2}(1-n)\,2\frac{1}{\overset{0}{\varepsilon}}\ \frac{\alpha_2^*}{3\varphi}B_1 - \Omega_R^2\ \frac{1}{6}(1-n)(2-n)\ \frac{1}{\left(\overset{0}{\varepsilon}\right)^2}(B_1)^3\right\} \end{aligned}\right\} \qquad \text{(A6.9)}$$

and

$$\frac{\overset{0}{\varepsilon}^n}{(\mu')^2}\left(\overset{1}{\varepsilon}\,\overset{2}{\varepsilon} + \frac{1}{6}(\overset{1}{\varepsilon})^3\right) =$$

$$= \frac{\overset{0}{\varepsilon}^n}{(\mu')^2}\left\{-B_1\,\frac{\alpha_0}{\varphi}\,e^{-\sqrt{\varphi}\eta} + B_1\,B_2\,e^{-2\sqrt{\varphi}\eta} + \left(B_1\frac{\alpha_2^*}{3\varphi} + \frac{1}{6}(B_1)^3\right)e^{-3\sqrt{\varphi}\eta}\ \right\}. \qquad \text{(A6.10)}$$

Combining all terms on the right side of (A6.2), we obtain

$$R_3 = \gamma_1(\xi)e^{-\sqrt{\varphi}\eta} + \gamma_2(\xi)e^{-2\sqrt{\varphi}\eta} + \gamma_3(\xi)e^{-3\sqrt{\varphi}\eta}\ , \qquad \text{(A6.11)}$$

where

$$\gamma_1 = \frac{2}{\mu'}\sqrt{\varphi}\,B_2' + \frac{\mu''}{(\mu')^2}\sqrt{\varphi}\,B_2 - \frac{1}{(\mu')^2}B_1'' +$$

$$+\left(\Omega_R^2\,\frac{1}{2}(1-n)\,2\frac{1}{\overset{0}{\varepsilon}} + \frac{\overset{0}{\varepsilon}{}^n}{(\mu')^2}\right)\frac{\alpha_0}{\varphi}\,B_1$$

$$= \frac{2}{\mu'}\sqrt{\varphi}\,B_2' + \frac{\mu''}{(\mu')^2}\sqrt{\varphi}\,B_2 - \frac{1}{(\mu')^2}B_1'' +$$

$$+\frac{\overset{0}{\varepsilon}{}^n}{(\mu')^2}\left(\frac{n(1-n)}{\overset{0}{(\varepsilon)^2}} + 1\right)\frac{\alpha_0}{\varphi}\,B_1$$

$$\gamma_2 = \frac{2}{\mu'}\frac{2}{3}\frac{(\alpha_2^*)'}{\sqrt{\varphi}} + \frac{\mu''}{(\mu')^2}\frac{2}{3}\frac{\alpha_2^*}{\sqrt{\varphi}} -$$

$$-\left(\Omega_R^2\,\frac{1}{2}(1-n)\,2\frac{1}{\overset{0}{\varepsilon}} + \frac{\overset{0}{\varepsilon}{}^n}{(\mu')^2}\right)B_1\,B_2 =$$

$$= \frac{2}{\mu'}\frac{2}{3}\frac{(\alpha_2^*)'}{\sqrt{\varphi}} + \frac{\mu''}{(\mu')^2}\frac{2}{3}\frac{\alpha_2^*}{\sqrt{\varphi}} - \frac{\overset{0}{\varepsilon}{}^n}{(\mu')^2}\left(\frac{n(1-n)}{\overset{0}{(\varepsilon)^2}} + 1\right)B_1\,B_2$$

$$\gamma_3 = -\Omega_R^2\left\{\frac{1}{2}(1-n)\,2\frac{1}{\overset{0}{\varepsilon}}\,\frac{\alpha_2^*}{3\varphi}B_1 - \frac{1}{6}(1-n)(2-n)\,\frac{1}{\overset{0}{(\varepsilon)^2}}(B_1)^3\right\} -$$

$$-\frac{\overset{0}{\varepsilon}{}^n}{(\mu')^2}\left\{\underset{=\!=\!=\!=\!=}{\frac{\alpha_2^*}{3\varphi}B_1} + \underset{=\!=\!=\!=\!=}{\frac{1}{6}(B_1)^3}\right\} =$$

$$= -\frac{\overset{0}{\varepsilon}{}^n}{(\mu')^2}\left\{\left(\frac{n(1-n)}{\overset{0}{(\varepsilon)^2}} + 1\right)\frac{\alpha_2^*}{3\varphi}B_1 - \left(\frac{n(1-n)(2-n)}{\overset{0}{6(\varepsilon)^3}} - \frac{1}{\overset{=}{6}}\right)(B_1)^3\right\}.$$

(A6.12)

Thus the DEQ(3), Eq.(A6.1), reads with Eq.(4.71)

$$\overset{3}{\varepsilon}{}_{\eta\eta} - \varphi\,\overset{3}{\varepsilon} = \gamma_1(\xi)e^{-\sqrt{\varphi}\eta} + \gamma_2(\xi)e^{-2\sqrt{\varphi}\eta} + \gamma_3(\xi)e^{-3\sqrt{\varphi}\eta}. \qquad \text{(A6.13)}$$

With the boundary condition (4.42), $\eta\to\infty$, $\overset{3}{\varepsilon}\to 0$, the solution has the form

$$\overset{3}{\varepsilon} = \overset{3}{\varepsilon}_{\text{hom}} + \overset{3}{\varepsilon}_{\text{part}} = B_3(\xi)\mathrm{e}^{-\sqrt{\varphi}\eta} + \overset{3}{\varepsilon}_{\text{part}} .$$

The function $B_3(\xi)$ is not of interest here since accuracy only up to 2nd order perturbation terms is required. The unknown function $B_2(\xi)$ is contained in the two functions γ_1 and γ_2 but its derivative B_2' is included only in γ_1. As previously, the particular solution has to be analyzed to remove the secular terms in $\overset{3}{\varepsilon}$; this gives an additional condition for the determination of B_2.

The following formulation is used

$$\left.\begin{aligned}
&\overset{3}{\varepsilon}_{\text{part}} = u(\xi,\eta)\mathrm{e}^{-\sqrt{\varphi}\eta} + \upsilon(\xi,\eta)\mathrm{e}^{-2\sqrt{\varphi}\eta} + w(\xi,\eta)\mathrm{e}^{-3\sqrt{\varphi}\eta} \\
&(\overset{3}{\varepsilon}_{\text{part}})_\eta = \dot{u}\,\mathrm{e}^{-\sqrt{\varphi}\eta} + \dot{\upsilon}\,\mathrm{e}^{-2\sqrt{\varphi}\eta} + \dot{w}\,\mathrm{e}^{-3\sqrt{\varphi}\eta} - \\
&\qquad\qquad - \sqrt{\varphi}\,(u\mathrm{e}^{-\sqrt{\varphi}\eta} + 2\upsilon\,\mathrm{e}^{-2\sqrt{\varphi}\eta} + 3w\mathrm{e}^{-3\sqrt{\varphi}\eta}) \\
&(\overset{3}{\varepsilon}_{\text{part}})_{\eta\eta} = \ddot{u}\,\mathrm{e}^{-\sqrt{\varphi}\eta} + \ddot{\upsilon}\,\mathrm{e}^{-2\sqrt{\varphi}\eta} + \ddot{w}\,\mathrm{e}^{-3\sqrt{\varphi}\eta} - \\
&\qquad\qquad - 2\sqrt{\varphi}\,(\dot{u}\,\mathrm{e}^{-\sqrt{\varphi}\eta} + 2\dot{\upsilon}\,\mathrm{e}^{-2\sqrt{\varphi}\eta} + 3\dot{w}\,\mathrm{e}^{-3\sqrt{\varphi}\eta}) + \\
&\qquad\qquad + \varphi\,(u\mathrm{e}^{-\sqrt{\varphi}\eta} + 4\upsilon\,\mathrm{e}^{-2\sqrt{\varphi}\eta} + 9w\mathrm{e}^{-3\sqrt{\varphi}\eta}).
\end{aligned}\right\} \qquad \text{(A6.14)}$$

Then Eq.(A6.13) reads

$$(\ddot{u} - 2\sqrt{\varphi}\,\dot{u})\mathrm{e}^{-\sqrt{\varphi}\eta} + (\ddot{\upsilon} - 4\sqrt{\varphi}\,\dot{\upsilon} + 3\varphi\,\upsilon)\mathrm{e}^{-2\sqrt{\varphi}\eta} + (\ddot{w} - 6\sqrt{\varphi}\,\dot{w} + 8\varphi\,w)\,\mathrm{e}^{-3\sqrt{\varphi}\eta} =$$

$$= \gamma_1(\xi)\mathrm{e}^{-\sqrt{\varphi}\eta} + \gamma_2(\xi)\mathrm{e}^{-2\sqrt{\varphi}\eta} + \gamma_3(\xi)\mathrm{e}^{-3\sqrt{\varphi}\eta} . \qquad \text{(A6.15)}$$

Comparison of the corresponding exponential terms yields

$$\left.\begin{aligned}
\ddot{u} - 2\sqrt{\varphi}\,\dot{u} &= \gamma_1(\xi) \\
\ddot{\upsilon} - 4\sqrt{\varphi}\,\dot{\upsilon} + 3\varphi\,\upsilon &= \gamma_2(\xi) \\
\ddot{w} - 6\sqrt{\varphi}\,\dot{w} + 8\varphi\,w &= \gamma_3(\xi) ,
\end{aligned}\right\} \qquad \text{(A6.16)}$$

which implies (only particular solutions are required!)

$$\left.\begin{aligned} u(\xi,\eta) &= u_1(\xi)\eta = -\frac{\gamma_1(\xi)}{2\sqrt{\varphi}}\eta\,, \\ \upsilon\,(\xi,\eta) &= \upsilon_o(\xi) = \frac{\gamma_2(\xi)}{3\varphi} \\ w(\xi,\eta) &= w_o(\xi) = \frac{\gamma_3(\xi)}{8\varphi} \end{aligned}\right\} \qquad \text{(A6.17)}$$

and thus

$$\overset{3}{\varepsilon}_{\text{part}}(\xi,\eta) = u_1(\xi)\eta\,\mathrm{e}^{-\sqrt{\varphi}\eta} + \upsilon_o(\xi)\,\mathrm{e}^{-2\sqrt{\varphi}\eta} + w_o(\xi)\,\mathrm{e}^{-3\sqrt{\varphi}\eta}\,. \qquad \text{(A6.18)}$$

Appendix (7): Determination of the Function $B_2(\xi)$

The solution of the differential equation (4.86)

$$B_2' + \frac{1}{2}\frac{\mu''}{\mu'} B_2 = S \tag{A7.1}$$

where

$$S(\xi) = \frac{1}{2}\frac{1}{\sqrt{\varphi}}\frac{1}{\mu'} B_1'' - \frac{1}{2}\frac{1}{\sqrt{\varphi}}\frac{\overset{0}{\varepsilon}{}^{n}}{\mu'}\left(\frac{n(1-n)}{\overset{0}{(\varepsilon)}{}^{2}}+1\right)\frac{\alpha_o}{\varphi} B_1 \tag{A7.2}$$

is derived as follows. Applying the approach used in Appendix (5), we get

$$B_2' + \frac{\nu'}{\nu} B_2 = S,$$

or

$$\nu B_2' + \nu' B_2 = (\nu B_2)' = \nu S, \tag{A7.3}$$

with

$$\nu = (\mu')^{1/2} = \left(\frac{1}{\varphi}\frac{n-\overset{0}{\varepsilon}}{\overset{0}{(\varepsilon)}{}^{1-n}}\right)^{1/4}. \tag{A7.4}$$

Thus the solution is, in general terms,

$$B_2 = \frac{1}{\nu}\int_0^{\xi} \nu S \, d\tau + \frac{c}{\nu},$$

with the integration constant c or

$$B_2 = \frac{1}{\nu}\int_0^{\xi} \nu S \, d\tau + \frac{(\nu)_0}{\nu}(B_2)_0, \tag{A7.5}$$

where

$$(\nu)_0 = (\mu')_0^{1/2}, \qquad (B_2)_0 = B_2(0) \tag{A7.6}$$

are boundary values at ξ=0. $(B_2)_0$ is determined from the boundary condition B.C. II, Eq.$(4.42)_3$,

$$\overset{1}{\varepsilon}_{\xi} + \mu' \overset{2}{\varepsilon}_{\eta} = 0 \quad \text{at} \quad \xi,\eta=0\,. \tag{A7.7}$$

With

$$\overset{1}{\varepsilon} = B_1(\xi)\mathrm{e}^{-\sqrt{\varphi}\eta}\,.$$

$$\overset{2}{\varepsilon} = B_2(\xi)\mathrm{e}^{-\sqrt{\varphi}\eta} - \frac{\alpha_o(\xi)}{\varphi} + \frac{\overset{*}{\alpha_2}(\xi)}{3\varphi}\mathrm{e}^{-2\sqrt{\varphi}\eta}$$

one obtains from (A7.7)

$$(B_1')_0 - (\mu')_0\sqrt{\varphi}\ \left[(B_2)_0 + \frac{2}{3}\frac{(\alpha_2^*)_0}{\varphi}\right] = 0$$

which yields

$$(B_2)_0 = \left(\frac{B_1'}{\mu'}\right)_0 \frac{1}{\sqrt{\varphi}} - \frac{2}{3}\frac{(\alpha_2^*)_0}{\varphi}\,. \tag{A7.8}$$

The right side is explicitly determined as follows. With (4.57) and $(4.39)_2$ the term $(\alpha_2^*)_0$ is

$$(\alpha_2^*)_0 = -\frac{1}{2}\varphi \left[\frac{n(1-n)}{\overset{0}{(\varepsilon)}_0^2} + 1 \underset{=}{=}\right] \left(\frac{\overset{0}{\varepsilon}}{n-\overset{0}{\varepsilon}}\right)_0 (B_1)_0^2$$

where (4.72) is used. Observing (4.77) and (4.78) gives

$$(B_1)_0 = B_1(0) = \left(\frac{\overset{0}{\varepsilon}^{1-n}}{n-\overset{0}{\varepsilon}}\right)_0^{1/2} (\overset{0}{\varepsilon}_{\xi})_0\,. \tag{A7.9}$$

Consequently

$$(\alpha_2^*)_0 = -\frac{1}{2}\varphi\ \left[n(1-n) + \underset{===}{(\overset{0}{\varepsilon})_0^2}\right] \frac{1}{\left(n-\underset{===}{(\overset{0}{\varepsilon})_0}\right)^2} \frac{1}{\overset{0}{(\varepsilon)}_0^n} (\overset{0}{\varepsilon}_{\xi})_0^2 \tag{A7.10}$$

Further

$$B_1'(\xi) = D\,\frac{1}{4}\left(\frac{\overset{0}{\varepsilon}^{1-n}}{n-\overset{0}{\varepsilon}}\right)^{-3/4} \frac{(1-n)(n-\overset{0}{\varepsilon})\overset{0}{\varepsilon}^{-n} + \overset{0}{\varepsilon}^{1-n}}{\overset{0}{(n-\varepsilon)^2}} (\overset{0}{\varepsilon}_{\xi})$$

and thus,

$$\left(\frac{B_1'}{\mu'}\right)_0 = \frac{1}{4}\sqrt{\varphi}\left[\frac{(1-n)}{\overset{0}{(n-\varepsilon)_0}\overset{0}{(\varepsilon)_0^n}} + \frac{\overset{0}{(\varepsilon}\,)_0^{1-n}}{\left(n-\overset{0}{\varepsilon}\right)_0^2}\right]\left(\overset{0}{\varepsilon_\xi}\right)_0^2 . \tag{A7.11}$$

Combining (A7.10) and (A7.11) finally yields

$$(B_2)_0 = \frac{1}{4}\frac{1}{\left(n-\overset{0}{(\varepsilon)}_0\right)^2}\frac{1}{\overset{0}{(\varepsilon)_0^n}}\left[\frac{7}{3}n(1-n)+n\overset{0}{(\varepsilon)}_0+\frac{4}{3}\overset{0}{(\varepsilon)_0^2}\right]\left(\overset{0}{\varepsilon_\xi}\right)_0^2 . \tag{A7.12}$$

Note that the constant φ has canceled. An explicit integration of the integral in (A7.5) needs - in the first place- an explicit expression for the zero order approximation $\overset{0}{\varepsilon}(\xi)$ which is equivalent to the classical solution $\varepsilon_c(\xi)$. Even then it appears that an integration must make use of numerical methods.

Appendix (8): Analytical Solution for the μ_R-Function (Exponentially Tapered Tensile Rod, Cross-Section Reduction Neglected)

With the cross-section reduction neglected, the μ_R-function, Eq.(4.100), reads

$$\mu_R = \left(\frac{n}{\varphi}\right)^{1/2} \int_0^{\xi} \left(\overset{0}{\varepsilon}\right)^{-\frac{1-n}{2}} \mathrm{d}\tau, \tag{A8.1}$$

where $\overset{0}{\varepsilon}$ is given by

$$\overset{0}{\varepsilon}(\xi) = \varepsilon_c(\xi) = \left(\frac{\sigma_R(\xi)}{K}\right)^{1/n} = \left(\frac{P}{A_o}\frac{1}{K}\right)^{1/n} \left(g(\xi)\right)^{1/n} = (\varepsilon_c)_0 \left(g(\xi)\right)^{1/n}, \tag{A8.2}$$

with

$$\left.\begin{aligned} (\varepsilon_c)_0 &= \varepsilon_c(0) = \left(\frac{P}{A_o}\frac{1}{K}\right)^{1/n} \\ g(\xi) &= \alpha + (1-\alpha)\, \mathrm{e}^{-\xi} \quad . \end{aligned}\right\} \tag{A8.3}$$

Thus

$$\mu_R = \left(\frac{n}{\varphi}\right)^{1/2} (\varepsilon_c)_0^{-\frac{1-n}{2}} \int_0^{\xi} g(\tau)^{-\frac{1-n}{2n}} \mathrm{d}\tau \ . \tag{A8.4}$$

Using the transformations

$$p = \frac{1-n}{2n}, \qquad \frac{1}{n} = m = 2p+1 \tag{A8.5}$$

and

$$\mathrm{d}g = (\alpha - g)\mathrm{d}\tau,$$

we get

$$G(g(\xi);p) = \int_0^{\xi} g(\tau)^{-\frac{1-n}{2n}} \mathrm{d}\tau = \int_1^{g(\xi)} \frac{\mathrm{d}g}{g^p(\alpha - g)} \ . \tag{A8.6}$$

For integer values of p, Table A8.1, the right hand integral can be obtained from standard tables of integrals (e.g. Dwight [3.4]). With $g(\xi)$ given by (A8.4), the G-functions are listed in Table A8.2. Then the μ_R-functions for odd exponents m=2p+1 are given by

$$\mu_R = \left(\frac{n}{\varphi}\right)^{1/2} (\varepsilon_c)_0^{-\frac{1-n}{2}} G(g(\xi); \frac{1-n}{2n}) . \qquad \text{(A8.7)}$$

Table A8.1: Relations between power exponents.

p	0	1	2	3	4	5	6
$m = 1/n$	1	3	5	7	9	11	13
n	1	0.333	0.2	0.143	0.111	0.091	0.077

Table A8.2: μ_R- Function for the exponentially tapered rod, $g(\xi) = \alpha + (1-\alpha)\ e^{-\xi}$; $0 < \alpha \leq 1$; cross-section reduction neglected.

p	$m=1/n$	$G(g(\xi); p) = \mu_R / [(n/\varphi)^{1/2} (\varepsilon_C)_0^{-\frac{1-n}{2}}]$
0	1	ξ
1	3	$\frac{1}{\alpha}(\xi + \ln g(\xi))$
2	5	$\frac{1}{\alpha}(1-[g(\xi)]^{-1}) + \frac{1}{\alpha^2}(\xi + \ln g(\xi))$
3	7	$\frac{1}{2\alpha}(1-[g(\xi)]^{-2}) + \frac{1}{\alpha^2}(1-[g(\xi)]^{-1}) + \frac{1}{\alpha^3}(\xi + \ln g(\xi))$
4	9	$\frac{1}{3\alpha}(1-[g(\xi)]^{-3}) + \frac{1}{2\alpha^2}(1-[g(\xi)]^{-2}) + \frac{1}{\alpha^3}(1-[g(\xi)]^{-1}) + \frac{1}{\alpha^4}(\xi + \ln g(\xi))$
5	11	$\frac{1}{4\alpha}(1-[g(\xi)]^{-4}) + \frac{1}{3\alpha^2}(1-[g(\xi)]^{-3}) + \frac{1}{2\alpha^3}(1-[g(\xi)]^{-2}) + \frac{1}{\alpha^4}(1-[g(\xi)]^{-1}) + \frac{1}{\alpha^5}(\xi + \ln g(\xi))$
6	13	$\frac{1}{5\alpha}(1-[g(\xi)]^{-5}) + \frac{1}{4\alpha^2}(1-[g(\xi)]^{-4}) + \frac{1}{3\alpha^3}(1-[g(\xi)]^{-3}) + \frac{1}{2\alpha^4}(1-[g(\xi)]^{-2}) + \frac{1}{\alpha^5}(1-[g(\xi)]^{-1}) + \frac{1}{\alpha^6}(\xi + \ln g(\xi))$

Appendix (9): Analytical Solution for the Function $B_2(\xi)$ (Exponentially Tapered Tensile Rod, Cross-Section Reduction Neglected)

The integral representation of the function $B_2(\xi)$ is given by (4.114):

$$B_2(\xi) = \frac{1}{\nu_R}\left\{\int_0^{\xi} \nu_R\, S_R\, \mathrm{d}\tau + (\nu_R)_0 (B_2)_0\right\}, \tag{A9.1}$$

where

$$\left.\begin{aligned}
&S_R = \frac{1}{2}\frac{1}{\sqrt{\varphi}}\frac{1}{\mu_R'}\quad B_1'' - \frac{1}{2}\frac{1}{\sqrt{\varphi}}\frac{\overset{0}{\varepsilon}{}^{n}}{\mu_R'}\left(\frac{n(1-n)}{\overset{0}{(\varepsilon)}{}^{2}}\right)\frac{\alpha_0}{\varphi}\, B_1 \\
&\nu_R = (\mu_R')^{1/2}, \qquad (\nu_R)_0 = (\mu_R')_0^{1/2} \\
&\mu_R' = \frac{1}{\sqrt{\varphi}}\left(\frac{n}{\overset{0}{\varepsilon}{}^{1-n}}\right)^{1/2} \\
&B_1(\xi) = D\left(\frac{\overset{0}{\varepsilon}{}^{1-n}}{n}\right)^{1/4}, \qquad D = \left(\frac{\overset{0}{\varepsilon}{}^{1-n}}{n}\right)_0^{1/4} \overset{0}{(\varepsilon_\xi)_0} \\
&\alpha_o = -\frac{1}{(\mu_R')^2}\,\overset{0}{\varepsilon}_{\xi\xi}
\end{aligned}\right\} \tag{A9.2}$$

and from (4.90) neglecting the underlined terms,

$$(B_2)_0 = \frac{1}{4}\frac{1}{n^2}\frac{1}{\overset{0}{(\varepsilon)}{}_0^{n}}\frac{7}{3}n(1-n)\left(\overset{0}{\varepsilon}_{\xi}\right)_0^2. \tag{A9.3}$$

With (4.93) and (4.99)

$$\overset{0}{\varepsilon}(\xi) = \varepsilon_c(\xi) = (\varepsilon_c)_0\,[g(\xi)]^{1/n} \tag{A9.4}$$

one gets

$$\left.\begin{aligned} \overset{0}{\varepsilon}_{\xi} &= (\varepsilon_c)_0 \frac{1}{n} g^{\frac{1-n}{n}} (\alpha-g) \\ \overset{0}{\varepsilon}_{\xi\xi} &= (\varepsilon_c)_0 \frac{1}{n} \left\{ \frac{1-n}{n} g^{\frac{1-2n}{n}} (\alpha-g)^2 - g^{\frac{1-n}{n}} (\alpha-g) \right\}; \end{aligned}\right\} \qquad \text{(A9.5)}$$

here the property

$$g' = \frac{dg}{d\xi} = (\alpha-g) \qquad \text{(A9.6)}$$

is used. Further

$$\left.\begin{aligned} B_1' &= \frac{D}{n^{1/4}} \frac{1-n}{4} \overset{0}{\varepsilon}^{-\frac{3+n}{4}} \overset{0}{\varepsilon}_{\xi} \\ B_1'' &= \frac{D}{n^{1/4}} \frac{1-n}{4} \left\{ -\frac{3+n}{4} \overset{0}{\varepsilon}^{-\frac{3+n}{4}-1} (\overset{0}{\varepsilon}_{\xi})^2 + \overset{0}{\varepsilon}^{-\frac{3+n}{4}} \overset{0}{\varepsilon}_{\xi\xi} \right\}. \end{aligned}\right\} \qquad \text{(A9.7)}$$

The integrand in (A9.1) takes the form

$$\nu_R S_R = I + J, \qquad \text{(A9.8)}$$

with

$$I = \frac{1}{2} \frac{1}{\sqrt{\varphi}} \frac{B_1''}{(\mu_R')^{1/2}} = \frac{1}{2} \frac{1}{\varphi^{1/4}} \frac{D}{4} \frac{1-n}{n^{1/2}} \left\{ -\frac{3+n}{4} \overset{0}{\varepsilon}^{-\frac{3+n}{2}} (\overset{0}{\varepsilon}_{\xi})^2 + \overset{0}{\varepsilon}^{-\frac{1+n}{2}} \overset{0}{\varepsilon}_{\xi\xi} \right\}. \qquad \text{(A9.9)}$$

and

$$J = \frac{1}{2} \frac{1}{\sqrt{\varphi}} \frac{n(1-n)}{\overset{0}{(\varepsilon)}^{2-n}} \frac{\overset{0}{\varepsilon}_{\xi\xi}}{(\mu_R')^{5/2}} \frac{B_1}{\varphi} = \frac{1}{2} \frac{1}{\varphi^{1/4}} D \frac{1-n}{n^{1/2}} \overset{0}{\varepsilon}^{-\frac{1+n}{2}} \overset{0}{\varepsilon}_{\xi\xi}. \qquad \text{(A9.10)}$$

Observing (A9.4) and (A9.5) and with the transformation

$$d\xi = dg/(\alpha-g), \qquad \text{(A9.11)}$$

we obtain, omitting the lengthy algebraic manipulations ,

$$\int_0^{\xi} I\,d\tau = \int_1^{g} I\,\frac{dg}{\alpha - g} =$$

$$= \frac{1}{2}\frac{1}{\varphi^{1/4}}\frac{D}{4}\frac{1-n}{n^{5/2}}(\varepsilon_c)_0^{\frac{1-n}{2}}\int_1^{g}\left\{\frac{1-5n}{4}\,g^{\frac{1-5n}{2n}}(\alpha-g) - n\,g^{\frac{1-3n}{2n}}\right\}dg \qquad \text{(A9.12)}$$

and

$$\int_0^{\xi} J\,d\tau = \int_1^{g} J\,\frac{dg}{\alpha - g} =$$

$$= \frac{1}{2}\frac{1}{\varphi^{1/4}}D\frac{1-n}{n^{5/2}}(\varepsilon_c)_0^{\frac{1-n}{2}}\int_1^{g}\left\{(1-n)\,g^{\frac{1-5n}{2n}}(\alpha-g) - n\,g^{\frac{1-3n}{2n}}\right\}dg\ . \qquad \text{(A9.13)}$$

These integrals allow exact integration in terms of elementary functions. For n ≠ 1/3 the result is

$$\int_0^{\xi} (I+J)d\tau =$$

$$= D\frac{1-n}{\varphi^{1/4}\,n^{3/2}}(\varepsilon_c)_0^{\frac{1-n}{2}}\left\{\frac{\alpha}{16}\frac{17-21n}{1-3n}\left(g^{\frac{1-3n}{2n}}-1\right) - \frac{1}{16}\frac{17-n}{1-n}\left(g^{\frac{1-n}{2n}}-1\right)\right\}. \qquad \text{(A9.14)}$$

With (A9.2) and (A9.3) and

$$(g)_{\xi=0} = 1$$

we get

$$\left.\begin{aligned}
(\nu_R)_0\,(B_2)_0 &= \frac{1}{\varphi^{1/4}}\frac{7}{12}\frac{1-n}{n^{3/2}}\left(\frac{1-\alpha}{n}\right)^2(\varepsilon_c)_0^{\frac{7-3n}{4}} \\
\nu_R^{-1} &= \left(\frac{\varphi}{n}\right)^{1/4}(\varepsilon_c)_0^{\frac{1-n}{4}}\,g^{\frac{1-n}{4n}} \\
D &= -\frac{1}{n^{1/4}}\frac{1-\alpha}{n}(\varepsilon_c)_0^{\frac{5-n}{4}}
\end{aligned}\right\} \qquad \text{(A9.15)}$$

and the function $B_2(\xi)$ takes the following form

$$B_2(\xi) = \nu_R^{-1} \{ \int_0^{\xi} (I + J) d\tau + (\nu_R)_0 (B_2)_0 \}$$

$$= (\varepsilon_c)_0^{2-n} (1-\alpha) \frac{1-n}{n^3} g(\xi)^{\frac{1-n}{4n}} \{ \frac{1}{16} [\alpha \frac{17-21n}{1-3n} \left(1 - g(\xi)^{\frac{1-3n}{2n}} \right) -$$

$$- \frac{17-n}{1-n} \left(1 - g(\xi)^{\frac{1-n}{2n}} \right)] + \frac{7}{12} (1-\alpha) \}. \quad \text{(A9.16)}$$

Note that the constant (φ) has dropped out. Also it is emphasized that for linear hardening (n=1) the function $B_2(\xi)$ vanishes identically

$$\left(B_2(\xi) \right)_{n=1} \equiv 0 \ . \quad \text{(A9.17)}$$

Furthermore, if n=1/3 the right-hand sides (rhs) of (A9.14) and (A9.16) have indeterminate forms. Thus, (A9.16) is to be interpreted as

$$\left[B_2(\xi) \right]_{n=1/3} = \lim_{n \to 1/3} [\text{rhs(A 9.16)}] =$$

$$= (\varepsilon_c)_o^{5/3} (1-a) \frac{3}{2} g(\xi)^{1/2} \left\{ \frac{15}{4} \left[-3\alpha \ln g(\xi) - 5\left(1 - g(\xi)\right) \right] + 7(1-\alpha) \right\} \quad \text{(A9.18)}$$

by L' Hospital's rule.

Appendix (10): Analytical Solution for the Function $B_2(\xi)$ (Three-Point-Bending of Uniform Beam)

The function $B_2(\xi)$ is given by (5.58)

$$B_2(\xi) = \frac{1}{\nu_B}\int_0^{\xi} \nu_B\, S_B\, \mathrm{d}\tau + \frac{(\nu_B)_0}{\nu_B}(B_2)_0\,, \tag{A10.1}$$

Where, analogous to (A9.2) and (A9.3),

$$S_B = \frac{1}{2}\frac{1}{\sqrt{\varphi}}\frac{1}{\mu_B{}'}\, B_1'' - \frac{1}{2}\frac{1}{\sqrt{\varphi}}\frac{\overset{0}{\kappa}{}^{n}}{\mu_B{}'}\left(\frac{n(1-n)}{\overset{0}{\kappa}{}^{2}}\right)\frac{\alpha_o}{\varphi}\, B_1 \tag{A10.2}$$

$$\left.\begin{aligned}
&\nu_B = (\mu_B{}')^{1/2}, \qquad (\nu_B)_0 = (\mu_B{}')_0^{1/2}\\
&\mu_B{}' = \frac{1}{\sqrt{\varphi}}\left(\frac{n}{\overset{0}{\kappa}{}^{1-n}}\right)^{1/2}\\
&B_1(\xi) = D_B\left(\frac{\overset{0}{\kappa}{}^{1-n}}{n}\right)^{1/4}, \qquad D_B = \left(\frac{\overset{0}{\kappa}{}^{1-n}}{n}\right)_0^{1/4}(\overset{0}{\kappa}{}_{\xi})_0\\
&\alpha_0 = -\frac{1}{(\mu_B{}')^2}\overset{0}{\kappa}{}_{\xi\xi}\\
&(B_2)_0 = \frac{1}{4}\frac{1}{n^2}\frac{1}{\overset{0}{\kappa}{}_0^{n}}\frac{7}{3}n(1-n)\left(\overset{0}{\kappa}{}_{\xi}\right)_0^2.
\end{aligned}\right\} \tag{A10.3}$$

With

$$z = 1-\xi \tag{A10.4}$$

and (5.15) and (5.16) the 0th order approximation reads

$$\left.\begin{aligned}
&\overset{0}{\kappa} = \kappa_c = \kappa_{co}\, z^{1/n}.\\
&\overset{0}{\kappa}{}_{\xi} = \kappa_{c\xi} = -\kappa_{co}\,\frac{1}{n}\, z^{\frac{1-n}{n}}\\
&\overset{0}{\kappa}{}_{\xi\xi} = \kappa_{c\xi\xi} = \kappa_{co}\,\frac{1-n}{n^2}\, z^{\frac{1-2n}{n}}
\end{aligned}\right\} \tag{A10.5}$$

and the terms (A10.3) take the following form

$$\left.\begin{aligned}
\mu_B' &= \left(\frac{n}{\varphi}\right)^{1/2} \kappa_{co}^{-\frac{1-n}{2}} z^{-\frac{1-n}{2n}} \\
\nu_B &= \left(\frac{n}{\varphi}\right)^{1/4} \kappa_{co}^{-\frac{1-n}{4}} z^{-\frac{1-n}{4n}} \\
(\nu_B)_0 &= \left(\frac{n}{\varphi}\right)^{1/4} \kappa_{co}^{-\frac{1-n}{4}} \\
D_B &= -\frac{1}{n^{5/4}} \kappa_{co}^{\frac{5-n}{4}} \\
B_1 &= -\frac{1}{n^{3/2}} \kappa_{co}^{\frac{3-n}{2}} z^{\frac{1-n}{4n}} \\
\alpha_o &= -\frac{\varphi}{n}\frac{1-n}{n^2} \kappa_{co}^{2-n} z^{\frac{2-3n}{n}} \\
(B_2)_0 &= \frac{7}{12}\frac{1-n}{n^3} \kappa_{co}^{2-n} .
\end{aligned}\right\} \qquad \text{(A10.6)}$$

The derivatives of B_1 are

$$\left.\begin{aligned}
B_1' &= \frac{1-n}{4nn^{3/2}} \kappa_{co}^{\frac{3-n}{2}} z^{\frac{1-5n}{4n}} \\
B_1'' &= -\frac{(1-n)}{4nn^{3/2}}\frac{(1-5n)}{4n} \kappa_{co}^{\frac{3-n}{2}} z^{\frac{1-9n}{4n}} .
\end{aligned}\right\} \qquad \text{(A10.7)}$$

The integrand of (A10.1) is

$$\nu_B S_B = I + J , \qquad \text{(A10.8)}$$

with

$$\left.\begin{aligned}
I &= \frac{1}{2}\frac{1}{\sqrt{\varphi}}\frac{1}{(\mu_B')^{1/2}} B_1'' \\
J &= -\frac{1}{2}\frac{1}{\sqrt{\varphi}}\frac{\overset{0}{\kappa}{}^n}{(\mu_B')^{1/2}}\left(\frac{n(1-n)}{\overset{0}{\kappa}{}^2}\right)\frac{\alpha_o}{\varphi} B_1 .
\end{aligned}\right\} \qquad \text{(A10.9)}$$

Using (A10.6) and (A10.7) we obtain explicitly

$$I = -\frac{1}{2}\,\frac{1}{\varphi^{1/4}}\,\frac{(1-n)(1-5n)}{16n^2n^{7/4}}\,\kappa_{co}^{\frac{7-3n}{4}}\,z^{\frac{1-5n}{2n}}$$

$$J = -\frac{1}{2}\,\frac{1}{\varphi^{1/4}}\,\frac{(1-n)^2}{n^2n^{7/4}}\,\kappa_{co}^{\frac{7-3n}{4}}\,z^{\frac{1-5n}{2n}}\,. \qquad \text{(A10.10)}$$

The integration is straightforward

$$\int_0^{\xi} v_B\, S_B\, \mathrm{d}\tau = \int_0^{\xi} (I+J)\,\mathrm{d}\tau = -\int_1^{z} \big(I(z)+J(z)\big)\mathrm{d}z =$$

$$= \frac{1}{\varphi^{1/4}}\,\frac{(1-n)(17-21n)}{16(1-3n)nn^{7/4}}\,\kappa_{co}^{\frac{7-3n}{4}}\left[z^{\frac{1-3n}{2n}}-1\right] \qquad \text{(A10.11)}$$

provided $n \neq 1/3$. Then the function $B_2(\xi)$ takes finally the following form:

$$B_2(\xi) = (\kappa_{co})^{2-n}\,\frac{1-n}{n^3}\,z(\xi)^{\frac{1-n}{4n}}\left\{\frac{7}{12}-\frac{17-21n}{16(1-3n)}\left[1-z(\xi)^{\frac{1-3n}{2n}}\right]\right\}. \qquad \text{(A10.12)}$$

If $n=1/3$ the right hand side of (A10.12) is indeterminate. Using L'Hospital's rule, we get

$$\left[B_2(\xi)\right]_{n=1/3} = \lim_{n\to 1/3} B_2(\xi) = (\kappa_{co})^{5/3}\,\frac{3}{2}\,z(\xi)^{1/2}\left\{7+\frac{45}{4}\ln z(\xi)\right\}. \qquad \text{(A10.13)}$$